Institut für Chemie – Polymerchemie

# Bio-sourced Adsorbing Poly(2-oxazoline)s Mimicking Mussel Glue Proteins for Antifouling Applications

Zur Erlangung des akademischen Grades

„doctor rerum naturalium"

(Dr. rer. nat.)

in der wissenschaftlichen Disziplin „Polymerchemie"

Eingereicht an der

Mathematisch-Naturwissenschaftlichen Fakultät

der Universität Potsdam


**Nils Lüdecke**

Potsdam, Dezember 2021

Published online on the
Publication Server of the University of Potsdam:
https://doi.org/10.25932/publishup-54983
https://nbn-resolving.org/urn:nbn:de:kobv:517-opus4-549836

„Das schwerste Urteil, ist das Vorurteil. Schau genau in die Welt."

Rüdiger Nehberg

„Wenn man nicht zwei Füße hat, braucht man nur einen Socken auszuziehen."

4-jähriges Kind

## Declaration

The enclosed research was conducted in the Institute of Chemistry at the University of Potsdam, under the supervision of Prof. Dr. Helmut Schlaad between January 2018 and December 2021. This thesis has not been submitted for any other qualifications at this or any other institution. This dissertation is the original work of the author and does not include any research that is the outcome of work done in collaboration with others, except where specifically indicated in the text and acknowledgments.

## Eidesstattliche Erklärung

Die vorliegende Arbeit wurde in der Zeit von Januar 2018 bis Dezember 2021 an der Universität Potsdam im Institut für Chemie unter der Leitung von Prof. Dr. Helmut Schlaad angefertigt. Die Arbeit ist bisher an keiner anderen Hochschule eingereicht worden und wurde zudem selbständig und ausschließlich mit den angegebenen Mitteln angefertigt. Hiermit erkläre ich an Eides statt, dass ich die vorliegende Arbeit selbstständig verfasst und nur unter Zuhilfenahme der ausgewiesenen Quellen und Hilfsmittel angefertigt habe. Beiträge von Kooperationspartnern wurden explizit gekennzeichnet.

Potsdam, den 14.12.2021 _____

(Nils Lüdecke

## Acknowledgments

I would like to take the opportunity to thank all those who have helped me to complete this work. This includes, first and foremost, the support that is directly related to this work: Thank you Professor Dr. Helmut Schlaad, for this exciting and challenging topic and the excellent support and advice. I would like to thank Professor Dr. André Laschewsky for taking the second opinion. I would like to thank the entire spectroscopic department for the measurements of all these spectra. I would like to thank Dr. Marek Bekir for advising me on the QCM-D and always helping me out with his knowledge. I would like to thank Dr. Matthias Hartlieb for his scientific input and words of encouragement during the last few years. I would like to thank Steffen Weidner for measuring all the MALDI-MS spectra. I would like to thank Dr. Ina Dambowsky and Dr. Sebastian Noack for lively discussions, funny and challenging conversations, and the proofreading of this work. I would like to thank Sascha Prenzel for his support in the lab and the several conversations about traveling, fishing, and cycling. I would like to thank the entire Schlaad working group for the wonderful, sometimes challenging, time. Finally, I would like to thank the University of Potsdam for funding my work and making it possible for me to write this thesis.

Some people were not directly involved in the thesis but contributed no less to its successful completion: First, many thanks to my entire family without whose good encouragement I could have despaired at times. Many thanks to the "base camp" in Moischt run by my parents Inge and Martin. Many thanks to my sister Marit, who corrected the linguistic escapades. I would also like to thank my brother Jan, who certainly looked over my shoulder critically and with interest. I would like to thank Jolle for the wonderful time in the hut and in the woods, which always gave me strength. I would like to thank Oli, who has always been and still is a great friend to me over the years. I would also like to thank all my other friends who have accompanied me on the way here. I would like to thank Britta and Christian for teaching me so that I was physically able to complete this work. I would like to thank the Open Team of the Goldfingers, with whom I was able to celebrate great successes that gave me strength and self-confidence.

An indescribably big thank you goes to my girlfriend Klara, who has been laughing and singing with me every day on the way to this thesis.

## Abstract

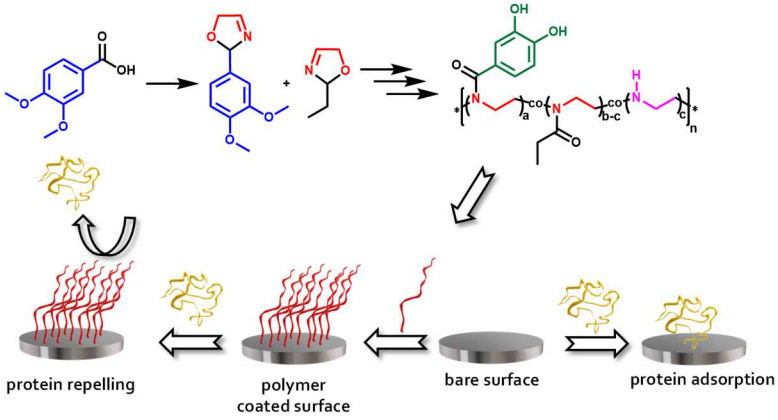


Nature developed countless systems for many applications. In maritime environments, several organisms established extra-ordinary mechanisms to attach to surfaces. Over the past years, the scientific interest to employ those mechanisms for coatings and long-lasting adhering materials gained significant attention.

This work describes the synthesis of bio-inspired adsorbing copoly(2-oxazoline)s for surface coatings with protein repelling effects, mimicking mussel glue proteins. From a set of methoxy substituted phenyl, benzyl, and cinnamyl acids, 2-oxazoline monomers were synthesized. All synthesized 2-oxazolines were analyzed by FT-IR spectroscopy, NMR spectroscopy, and EI mass spectrometry. With those newly synthesized 2-oxazoline monomers and 2-ethyl-2-oxazoline, kinetic studies concerning homo- and copolymerization in a microwave reactor were conducted. The success of the polymerization reactions was demonstrated by FT-IR spectroscopy, NMR spectroscopy, MALDI-TOF mass spectrometry, and size exclusion chromatography (SEC). The copolymerization of 2-ethyl-2-oxazoline with a selection of methoxy-substituted 2-oxazolines resulted in water-soluble copolymers. To release the adsorbing catechol and cationic units, the copoly(2-oxazoline)s were modified. The catechol units were (partially) released by a methyl aryl ether cleavage reaction. A subsequent partial acidic hydrolysis of the ethyl unit resulted in mussel glue protein-inspired catechol and cation-containing copolymers. The modified copolymers were analyzed by NMR spectroscopy, UV-VIS spectroscopy, and SEC. The catechol- and cation-containing copolymers and their precursors were examined by a Quartz Crystal Microbalance with Dissipation (QCM-D), so study the adsorption performance on gold, borosilicate, iron, and polystyrene surfaces. An exemplary study revealed that a catechol and cation-containing copoly(2-oxazoline)-coated gold surface exhibits strong protein repelling properties.

## Kurzzusammenfassung


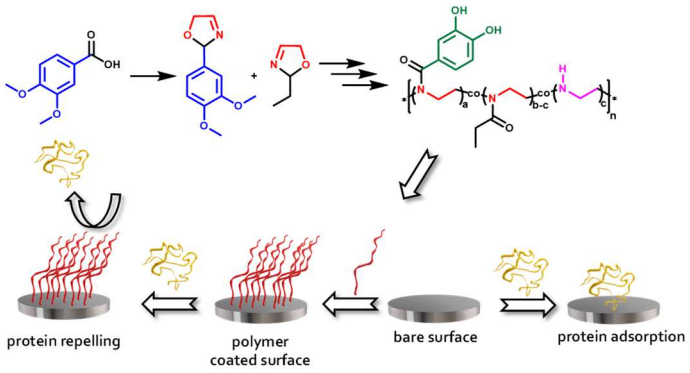


In der Natur entwickelten sich unzählige Anpassungen für ebenso viele Lebensbereiche. In maritimen Umgebungen haben sich beispielsweise bei verschiedenen Organismen außergewöhnliche Strategien entwickelt, um sich an Oberflächen an-zuheften. In den letzten Jahren hat das wissenschaftliche Interesse an der Nutzung dieser Mechanismen für an Oberflächen haftende Materialien stark zugenommen.

Diese Arbeit beschreibt die Synthese von Muschelklebeprotein nachahmenden, bioinspirierten Copoly(2-oxazolinen) für Oberflächen-beschichtungen mit protein-abweisender Wirkung. Aus einer Gruppe von methoxysubstituierten Phenyl-, Benzyl-, und Zimtsäuren wurden 2-Oxazolin-Monomere synthetisiert. Alle synthetisierten 2-Oxazoline wurden mittels FT-IR-Spektroskopie, NMR Spektroskopie und EI-Massenspektrometrie analysiert. Mit diesen neu synthetisierten 2-Oxazolin-Monomeren und 2-Ethyl-2-oxazolin (wasserlösliche Komponente) wurden kinetische Studien zur Homo- und Copolymerisation in einem Mikrowellenreaktor durchgeführt. Der Nachweis der Polymerisationsreaktionen erfolgte durch FT-IR Spektroskopie, NMR Spektroskopie, MALDI-TOF Massenspektrometrie und Gel-Permeations-Chromatographie (GPC). Die Copolymerisation von 2-Ethyl-2-Oxazolin mit Methoxyaryl-substituierten 2-Oxazolinen führte zu wasserlöslichen Copolymeren. Um die adsorbierenden Catechol- und kationischen-Einheiten freizusetzen, wurden die Copolymere modifiziert. Die Catechol-Einheiten wurden durch eine (partielle) Methylarylletherspaltung freigesetzt. Eine anschließende partielle saure Hydrolyse der Ethyleinheit führte zu, von Muschelklebeproteinen inspirierten, catechol- und kationen-haltigen Copolymeren. Die modifizierten Copolymere wurde mittels NMR Spektroskopie, UV-VIS Spektroskopie und SEC analysiert. Die catechol- und kationenhaltigen Copolymere und deren Vorläufercopolymere wurden mittels einer Quarzkristallmikrowaage mit Dissipation (QCM-D) hinsichtlich ihrer Adsorptionsfähigkeit an den Oberflächen Gold, Borosilicat, Eisen und Polystyrol untersucht. Exemplarisch wurde gezeigt, dass eine mit catechol und kationenhaltigem Copoly(2-oxazoline) beschichtete Goldoberfläche, stark proteinabweisende Eigenschaften aufweist.

# Table of Contents

# 1 Introduction

## 1.1 Maritime glue proteins

The potential of long-lasting adhering materials on different surfaces in different environments, like permanently changing maritime surroundings, is an outstanding ability of maritime organisms like mussels or barnacles.[1–3]

Especially the feet of mussels feature outstanding mechanisms of sticking on various surfaces, which excites the scientific interest in using and mimicking it.[4–6] In 1981, Waite et al found polyphenolic proteins in mussel foot and byssus fibers attributing the responsibility for the gluing properties to high amounts of 3,4-dihydroxy-L-phenylalanine (L-Dopa), lysine, and 3-/4-hydroxyproline.[7] These three components are part of a major structure within the byssal plaque that consists of various mussel foot proteins (Mfp's), containing different quantities and sequences of Dopa and lysine (Figure 1).[7–11]

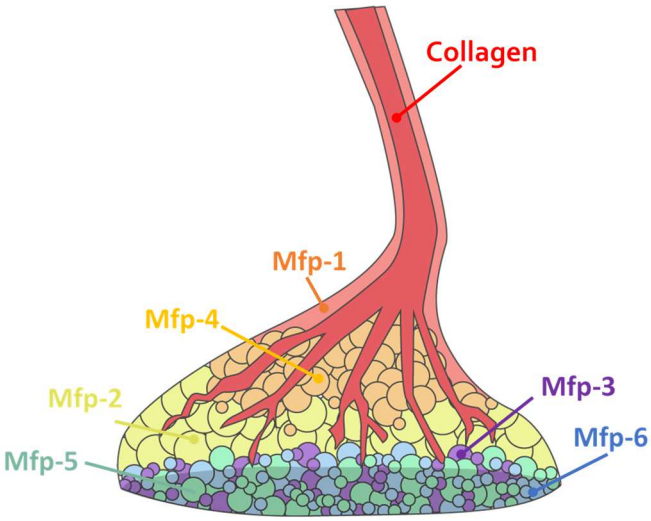


*Figure 1: Schematic depiction of a mussel byssus thread containing different Mfp's in different areas of the foot with discrete properties to crosslink and adhere.*

The amount of Dopa within the Mfp´s has a range of 0.1 to 30 % whereat Mfp´s 1-6 are containing 2-30 % of Dopa.[9,11] Thus, is the quantity of Dopa with its catechol moiety the only reason for adhering on surfaces? Certainly, the discrete environment consists of different Mfp´s, which interact and interconnect via bridging with ions. The different behavior of Mfp-1 and Mfp-3 despite similar amounts of Dopa, the length variation of the Mfp´s, and sequences of amino acids in the peptide suggest Dopa does not have to be the exclusive cause of the adhering mechanism.[11–14] For instance, adjacent lysine is involved in the removal of hydrated cations from surfaces and allows the binding of the Dopa catechol unit on the ground level.[15] The nature of the environment is playing a big role as well. For instance, a pH value above 5.5 could lead to oxidation of the catechol units to quinones which results in less hydrogen bond capacity, thus minor binding on oxide or metal surfaces.[16,17] Those quinones are not inactive since they are capable of coordination and oxidative crosslinking.[18] To further understand the mussel thread adhesion on various surfaces, the catechol moiety needs to be considered individually.

## 1.2 The character of catechol-type surface interactions

Catechol, despite its simple structure, is capable of interacting with various surfaces in different ways. The bonding types can be distinguished in hydrogen bonding, π-π-stacking, cation-π-stacking, and coordination bonding (Figure 2).

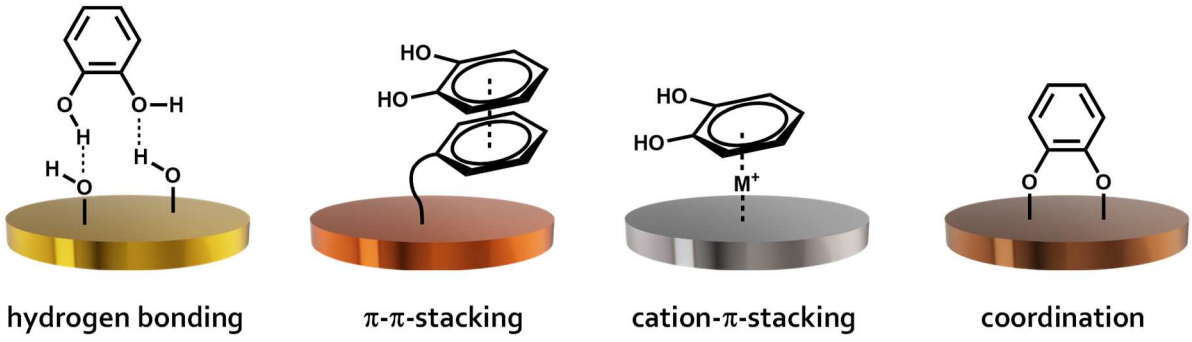


*Figure 2: Bonding types of catechol with various surfaces, thus different resulting bonds.*

The most obvious type of interaction is the adherence on surfaces via hydrogen bonding. But why and how is catechol so effective in forming hydrogen bonds in an aqueous environment in which water and hydrated ions are covering the surface?

Theoretical studies show that the binding energy ($\Delta E$) from catechol to $\alpha$- and $\beta$–cristobalite is much higher (14.15 and 11.65 kcal/mol) than the corresponding $\Delta E$ values from water (1.98 and 0.57 kcal/mol).[19] One reason for the stronger binding is a higher number of hydrogen bonds per molecule formed by the catechol. For a direct surface-catechol interaction and a strong bonding in aqueous environments, the water molecules, attached to the surface, are needed to be removed. This surface-bound water molecule network results by release in an entropic increase and leads to the conclusion of an entropically driven mechanism.[20] Calculations indicate the removal of water by the catechol molecule itself. The displacement of the water molecules allows the perpendicular attachment of catechol to the substrate.[21,22] Apparently, the two vicinal hydroxy groups of the catechol moiety are necessary to displace water from the surface. Consequential, and experimental data confirm, polymers, containing tyrosine instead of Dopa do bind weaker. This is caused due to the incapability of water displacement, hence it seems that catechol, concerning hydrogen bonding in a maritime context, is unavoidable.[4] For that purpose catechol, 3,4-dihydroxy phenylethylamine, and phenol were compared regarding their works of adhesion. The adhesion of catechol and 3,4-dihydroxy phenylethylamine was three magnitudes stronger than that of phenol. This result again shows the importance of the bidental binding mechanism of catechol derivatives. Pyrogallol was considered as well, but the third hydroxy group gave no further benefit in comparison to catechol and 3,4-dihydroxy phenylethylamine.[23]

Yet aromatic interactions as $\pi$-stacking and electrostatic interactions as well as interactions between the aromatic moiety of the catechol itself cannot be ruled out. The catechol units do have an almost perpendicular position in respect to inorganic surfaces suggesting the formation of $\pi$-interactions between the aromatic moieties leading to an increase of the absorption energy.[23]

A coverage of π-system containing surfaces with catechol-containing polymers, via π-stacking, can have advantages as the following report shows: Carbon nanotubes were covered with the π-donor polydopamine which resulted in an increase of biocompatibility and dispersibility in water.[24] Other investigations with sum-frequency generation spectroscopy of catechol-containing polymers (poly[(3,4-dihydroxystyrene)-*co*-styrene]) on polystyrene showed an interface π-π-stacking as the most possible adhesive propulsion.[25]

Considering metal (oxide) surfaces, coordinating interactions should be mentioned due to the capability of those surfaces to form coordination bonds with catechol moieties. Titanium oxide ($TiO_2$) is one of the most in-depth examined surfaces regarding the interaction of catechol derivatives with it. The catechol moiety could bind in basically three possible different types of mechanisms on $TiO_2$: monodentate, bridging bidentate, and chelating.[26] The result of the adsorption of dopamine on $TiO_2$ (Rutile 110) was a bidentate adsorption on the surface due to the high binding energy. However, the authors could not distinguish between the bridging and the chelating binding mechanism. Additionally, they were able to measure an almost perpendicular contact angle ((78 ± 5)°) of dopamine which results in a possible higher coverage of the surface compared to pyrocatechol with a tilt of 20°.[27,28] Not only $TiO_2$ but also other metal oxide surfaces were examined regarding their interactions with catechol moieties. For instance, zinc oxide was coated with ethyl 3,4-dihydroxybenzoate and gave similar results as the coating of Rutile. The contact angle was 75.1° and the binding mechanism was considered as bidental.[29,30] Covering, not only zinc oxide but also other semiconductor surfaces (SiC, GaN, InN, CdS, CdSe) with catechol, results in an identification of optoelectronic properties leading to a band alignment by the presence of surface electronic states.

Thus, the nature of catechol and catechol-containing polymers interacting with surfaces has great diversity, as well as the bonding has a great strength compared to other compounds. These characteristics are making catechol-containing materials interesting for several applications. However, so far only catechol-surface interactions were mentioned in this chapter, and the role of intra molecular interactions and the influence

of the potential polymeric backbone and side groups were not considered. The next chapter will discuss these parameters and their influence on the corresponding properties.

## 1.3 Catechol and cation containing polymers

As mentioned in chapter 1.1, the catechol moiety is not singularly responsible for the extraordinary absorption characteristics of Mfp´s but also the presence of non-polar, polar, cationic, and anionic functional groups.[31,32] Initially the hydrophilicity is important due to enhancing surface interactions. Especially at hydrophilic surfaces, hydrophobic polymers could weaken the binding by reverse hydrophilicity.[33] An inverse effect could occur by introducing ionic groups in the polymer: generally, ionic groups do have more strengthen effects on the surface binding. But as already mentioned in chapter 1.1 concerning the number of catechol units an excess of ionic units can result in charge repulsion.[34] Finding the proper proportion, interval, and the number of specific functional groups could be challenging, yet ionic groups do have an important role in the binding mechanism. Catechol, besides the binding, does have the ability to remove bonded water from surfaces to replace the binding sites.[21,22] Cationic groups for instance are not only able to clean off the surface from water but also from salt generating neat binding sites, thus enabling catechol-surface interactions without interference. Besides, the positively charged groups, whether they are in the backbone or the side chain, are also forming ionic bonds to the surface. Hence, they are not only responsible for cleaning the surface but also directly participating in the binding process as well.[15,35] Recent studies show once more the significance of the collaboration of catechol and ionic groups by spatial proximity. The ability to remove salt and water from surfaces and form bonds enhances by the pairing of these functional groups. However, this effect occurs off an areal distance at most 5 Å.[36]

The removal of the ions is an important mechanism by cationic groups to enable strong surface interactions. Yet, ions are not only disruptive due to the surface binding effects

regarding the catechol bonding mechanism. Certainly, ions are needed to be removed from the surfaces, but also facilitating cross-linking, thus facilitating the formation of plaques and the improvement of mechanical strength of the bond substrate.[37] In the process, marine organisms are concentrating ions, like copper, iron, manganese, and zinc to enable the cross-linking process to construct their plaques. Studies show that besides other ions the iron-(III)-ions play the most important role in cross-linking within maritime glue proteins and plaques.[38,39] The iron-(III)-ion has generally six binding sites and forms octahedral geometries.[40] Hence, due to the two dendric structures of catechol, iron-(III)-ions can bind up to three catechol units as ligands at once. The formation, whether the mono-, bi- or three ligand complexes depends on the iron-(III)-ion concentration. Lower concentrations of iron-(III)-ions (10 µM with Mfp-1) results in the tris complex and ten times higher concentrations in the mono complex (Figure 3).[41] Hence the concentration of iron-(III)-ions within the plaques is crucial for their properties. If the proper concentration is given, for short periods, the chelate complex is strong but also reversible and in consequence self-healing. Over time, the chelate forms, due to the redox potential of the iron-(III)-ions, a longer-lasting, less reversible, and self-healing complex, which enables the potential of a long-term hold.

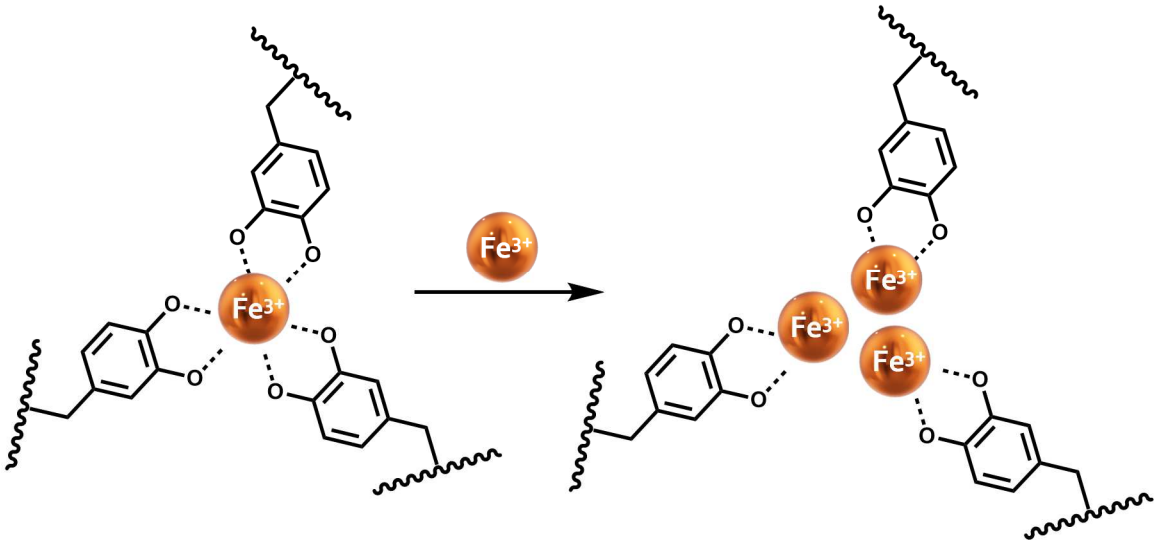


*Figure 3: Catechol-containing polymers forming tris complexes in lower iron-(III)-ion concentrations (left). With an increase of the iron-(III)-ion concentration mono complexes are formed thus less cross-linking emerges (right).*

Accordingly, catechol-containing materials can interact with multiple surfaces in different ways. The contact angle and the nature of the surface are significant. Catechol moieties can remove bound water from surfaces to enable direct binding to the surface. To enhance the surface cleaning and thus the binding, not only water needs to be removed from the surfaces, but also ions. Ionic, especially cationic groups, within a defined area around the catechol are instrumental for the removal of surface-bound ions. Overloading of the material with catechol and ionic functional groups does not enhance the process due to repulsing and intermolecular interaction effects. The presence of (transition) metal ions in solution, furthermore, facilitates the formation of complexes between the catechol moieties and the ions which result in crosslinking and leads to potentially self-healing materials. In this context iron-(III)-ions are giving the best results in complexation, stability, and crosslinking.

## 1.4 Catechol-containing biopolymers

Versatile applications of catechol-containing polymers legitimate the great interest in these materials. The main feature of catechol-containing materials is the potential to adhere on almost every surface, interact with different ions and various materials whether it is nano-, micro-, or macroscopic, and form self-healing adhesive hydrogels.[42]

Besides, antifouling, antimicrobial, and biomedical coatings and materials are part of the key applications for catechol-containing biopolymers. There are more applications, like energy storage, anti-corrosion, and hydrophilic/hydrophobic coatings, coacervated polymers, and micro- /nanoscopic surface functionalization (for further information read [42]). After the remarks, given in the previous chapters, the great scientific interest in mimicking Mfp´s, thus synthesizing catechol-containing polymers is not surprising. As manifold are the natural approaches of building adhesive materials, as versatile are the synthetic approaches of mimicking them. Due to the dimension of this topic, the following will only consider bio-derived or mimick polymers containing catechol units

and no other catechol-containing materials. For further information these reviews are recommendable.[42,43]

Antifouling materials initially mostly consisted of copper and other (heavy) metal-containing materials. They work through killing the fouling organisms, yet caused heavy environmental pollution due to their toxicity. In contrast, polymer-based coating, incorporating properties of natural antifouling compounds, facilitates access to a high variation of biocompatible antifouling materials like poly(ethylene glycol), poly(2-oxazoline)s, polypeptides, polypeptoides, and poly(methyl methacrylate). Long-lasting, durable coating combined with prevention of biofouling and microbial pollution is enabled for instance by polyelectrolytes containing catechol.[44,45]

There are three possibilities to implement catechol groups in a polymer: 1) in the main chain; 2) as a side group; 3) as an end group of the polymer. The synthetic approaches are diverse for each requirement. The most commonly used way to synthesize main-chain catechol-containing polymers is oxidative polymerization.[46] One of the most prominent examples of oxidative polymerization, because of its biocompatibility and its similarity to the natural models, is poly(dopamine).[47]

The major group of catechol-containing biopolymers exhibits the catechol moiety in the side chain. Respectively, the synthetic variability lasts from polypeptide synthesis over ring-opening polymerization of *N*-carboxy anhydride (NCA) to post-synthetic modification and polymerization of catechol containing vinyl monomers (Figure 4).

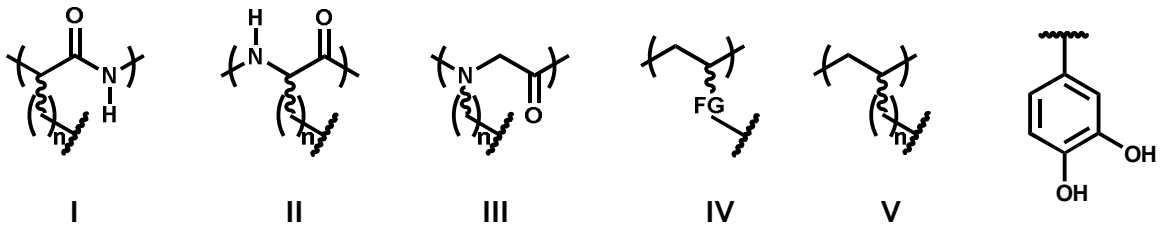


*Figure 4: Illustration of catechol containing polypeptide (**I**), polypeptides (**II**), or peptoides (**III**) synthesized from NCAs, post-synthetic modified polymers (**IV**), and polymers from catechol containing vinyl monomers (**V**).*

The chain end could be functionalized with catechol by using appropriate initiators and agents for atom transfer radical polymerization (ATRP) or reversible-addition-fragmentation chain-transfer polymerization (RAFT). Post synthetic end-capping with catechol-containing reagents is another way of functionalizing the chain ends.[42]

Catechol-containing poly(sarcosine) shows the combination of long-lasting coating with great antifouling and antibacterial properties. The responsibility of the catechol units for adhering is to be complemented with the ability to form Ag nanoparticles by the reduction of $Ag^+$ ions. To facilitate the reduction of the $Ag^+$ ions and adhesion, the number of catechol units needed to be high. The coating enhanced the antibacterial activity and the resistance to protein absorption. Even the biocompatibility with Ag nanoparticles is still given.[45] Yet, this coating still contains and operates with metal (ions).

Though, even biopolymer coatings without using any metal within the polymers, show very promising results concerning antifouling properties. Poly(N-vinyl pyrrolidine) is a biocompatible nontoxic polymer already used in drug delivery but with poor adhesive properties. Post synthetic modification with a catechol-containing unit makes this polymer stick to different surfaces or enhances the adhesion and increases the surface resistance towards proteins. Besides, good biocompatibility was shown by measuring the cytotoxicity of mouse fibroblast cells.[48]

As mentioned above, there are many different biocompatible nontoxic polymers available, with great potentials and each has its right to exist. However, catechol-containing poly(2-oxazoline)s are barely known yet, although poly(2-oxazoline)s are known for their good biocompatibility and diverse chemical and physical properties, like thermosensitivity and their easy synthetic accessibility. There are two reports about poly(2-oxazoline)s containing catechol containing site groups introduced via post-polymerization modification of copoly(2-oxazoline)s.[49,50] Yet, catechol-containing copoly(2-oxazoline)s without post-polymerization modification could shorten the synthesis route and enables a new way to access whether block- or statistical-copoly(2-

oxazoline)s via direct polymerization. Hence, the next chapter will give an overview across poly(2-oxazoline)s, their properties, and synthesis.

## 1.5 Poly(2-oxazoline)s – Chemical and application-drawn properties

Access to well-defined polymers is possible via different polymerization methods like controlled radical and living ionic polymerization. In contrast to the controlled radical polymerization, the living ionic polymerization allows almost quantitative conversion. The addition of different monomers provides access to a wide range of different homo-, co- and block copolymers with a great variety of sequence and architecture.[51]

Poly(2-oxazoline)s (**VII**) are synthesized by cationic ring-opening polymerization (CROP) of 2-oxazolines (**VI**), which was discovered in 1966.[52–54] After the discovery, the scientific interest became quiet concerning poly(2-oxazoline)s. In the early 1990s, attention rose again due to the advantageous properties of poly(2-oxazoline)s, and they were increasingly explored. The CROP of a 2-oxazoline results in an amide-containing polymer, or commonly labeled as pseudo peptide due to their similarity to poly(amino acid)s (**VIII**) (Scheme 1).[55] The variability of the side chain in 2-position allows access to the mentioned wide range of different polymers. The end-capping of the living chain end gives the possibility of introducing more functional groups for further post-polymerization modification.

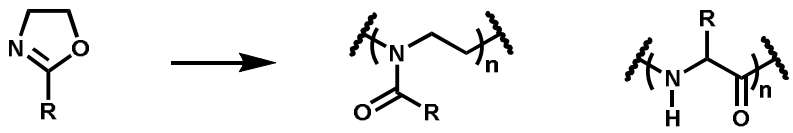


**VI** **VII** **VIII**

*Scheme 1: General illustration of the polymerization of 2-oxazoline (**VI**) and a comparing representation of poly(2-oxazoline)s (**VII**) to polypeptides (**VIII**).*

To understand the synthesis and the nature of poly(2-oxazoline)s, the polymerization mechanism should be considered: The CROP of 2-oxazolines is initiated by an electrophilic compound. This opens a wide field of possible initiators such as sulfonate and sulfate esters, sulfonic anhydrides, triflates alkyl and benzyl halides, protonic acids, Lewis acids, and oxazolinium salts.[56] Functionalized initiators can be used as well, as long as the functionality is not nucleophilic.[57] Thus the polymerization starts with the initiating step by the nucleophilic attack of the free electron pair of the nitrogen, located in the 2-oxazoline ring (**VI**) on the electrophilic center of the initiator (**IX**), forming an oxazolinium cation (**X**) (Scheme 2). During the further nucleophilic attack of 2-oxazolines (**VI**) at the oxazolium cation (**X**) in 5-position, the ring-opening results in forming the backbone (**XI**) and the propagation takes place.

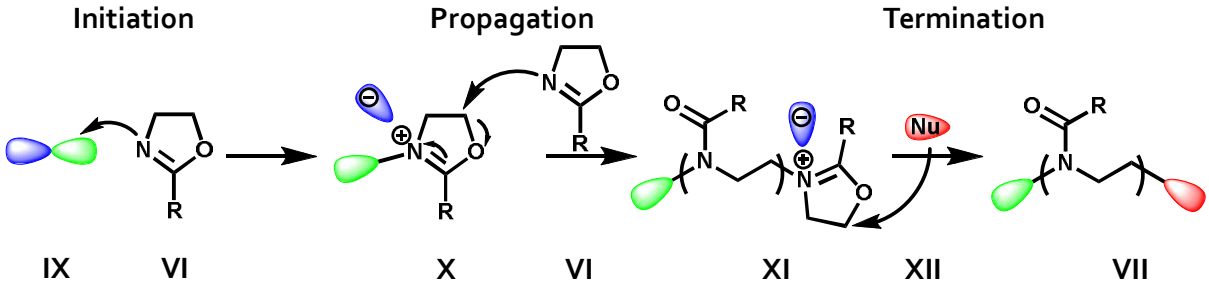


*Scheme 2: Representation of the general three-step mechanism of the 2-oxazoline cationic ring-opening polymerization (CROP) giving the poly(2-oxazoline) (**VII**).*

The termination is carried out by the addition of a nucleophile which attacks the living chain end, resulting in the poly(2-oxazoline) (**VII**). In this chapter, only the cationic mechanism will be considered, although there is also a covalent mechanism proposed. Both mechanisms are taking place, though the character of the mechanism depends on the initiator, the solvent, and the nature of the 2-oxazoline. The mechanism will be discussed in detail later; further information can be found elsewhere.[58]

The cationic nature of the reaction excludes nucleophilic solvents, *i.e.* commonly acetonitrile is used as solvent for the polymerization but there are reports about other solvents like butyronitrile or chlorobenzene. [58,59] Though the solvent supports the ionic

character of the reaction otherwise the reaction rate will drop dramatically.[60] Nucleophilic functional groups within the 2-oxazoline monomer are to be obviously avoided or protected during the polymerization and unprotected or introduced by post-polymerization modification. Certainly, particular attention must be paid is to ensure the absence of any nucleophile, like water, within the polymerization reaction to avoid side or termination reactions.

Considering the kinetics of the polymerization, the reaction rate of 2-oxazolines is comparatively slow. However, some parameters can be used to tune the reaction rate. The influence of the solvent supporting the cationic character of the reaction was already mentioned. The initiator, respectively the counter ion, affects the reaction rate as well. Generally, the reaction rate increases with a decrease of the counter ion´s nucleophilicity.[61] In the referred publication 2-ethyl-2-oxazoline with 2-phenyl-2-oxazoline were compared, using benzyl bromide, benzyl chloride, iodide, and tosylate. The reaction rate increased in that order, and 2-phenyl-2-oxazoline did not react with benzyl chloride at all. This points to the next parameter of the reaction rate: the side group. The polymerization rate of 2-alkyl-2-oxazolines generally increases with a decrease of the inductive effect of the side group. Furthermore, 2-alkyl-2-oxazolines react generally faster than 2-aryl-2-oxazolines.[62]

Due to the comparably low reaction rate, investigations were performed on whether the polymerization rate could be accelerated. Compared to traditional heating, microwave irradiation has the reputation of increasing the reaction rate, conversion, and yield substantially.[63] For instance, comparing the polymerization of 2-phenyl-2-oxazoline traditionally conducted in the oil bath and carried out by microwave irradiation, the polymerization in the microwave is accelerated by the factor of 4.[64] For that reason, polymerizations of 2-oxazolines are nowadays conducted in a microwave reactor.

Thus, poly(2-oxazoline)s can be, due to the CROP, synthesized fast. A well-defined nature and the combination of different monomers to statistical-, gradient- or block-copolymers is possible and accessible. Hence, this allows the control of different properties of poly(2-oxazoline)s depending on several simple tunable characteristics. By

changing the side group "R" (Scheme 1) the hydrophilicity/hydrophobicity can be changed including the synthesis of polymers with thermoresponsive properties. The combination of hydrophilic and hydrophobic monomers, which are easily accessible due to the living character, opens the availability of amphiphilic materials.

Poly(2-methyl-2-oxazoline) and poly(2-ethyl-2-oxazoline) are showing great biocompatibility which makes them interesting for biomedical applications. Yet not only the biocompatibility is promising but also the ability to enable the resistance towards protein absorption. This means poly(2-(m)ethyl-2-oxazoline) coated surfaces result in anti-fouling materials.[65–67] The adhesion properties of poly(2-(m)ethyl-2-oxazoline), though certainly are improvable. Thus, the synthesis of a catechol-containing copoly(2-oxazoline) would increase the adsorption ability to various surfaces and substrates (Chapter 1.3).

The combination of their biological properties of biocompatibility, biodegradability, and the pseudo peptide nature of already known poly(2-oxazoline)s like 2-ethyl-2-oxazoline unlocks the area of adsorbing catechol containing poly(2-oxazoline). Surfaces, coated with such a mussel-protein mimicking polymer would result in biocompatible materials with anti-fouling and protein resistance properties for potential biomedical applications.[68]

# 2 Objectives

Catechol-containing polymers mimicking maritime glue proteins attract more and more interest due to their ability to stick to almost every kind of surface in wet environments (Chapter 1.1). Common synthetic approaches towards catechol-containing polymers are the copolymerization of vinyl catechol derivatives, the functionalization of resins or platform polymers, the step-growth polymerization of methacrylate derivatives, and the ring-opening polymerization of Dopa *N*-thiocarboxyanhydride.[69–73] Catechol-containing poly(2-oxazoline)s are barely known yet. There are only two reports about post-polymerization modification of poly(2-vinyl-2-oxazoline)s published to give catechol-containing poly(2-oxazoline)s.[49,50] Though the copolymerization of 2-ethyl- or 2-methyl-2-oxazoline with catechol containing 2-oxazolines and their subsequent deprotection is not reported yet.

The aim of the work is the synthesis of different bio-derived methoxy-containing phenolic(2-oxazoline)s, their polymerization, and copolymerization with 2-ethyl-2-oxazoline to yield water-soluble catechol-functionalized polymers. The ability of these polymers to adhere to different surfaces in aqueous surroundings shall be tested by measurements with the QCM-D.

The nature of being biocompatible, as well as the variety and accessibility of possible side chains, are diverse. Additionally, the character of water-soluble, peptide-like polymers makes poly(2-oxazolines)s a promising mimic of maritime glue proteins (Chapter 1.5). The chemical proximity of 2-oxazolines to carbonyl compounds suggests the use of naturally occurring carboxylic acids, containing catechol groups such as protocatechuic, 3,4-dihydroxyphenylacetic (DOPAC), caffeic acid, and *L*-tyrosine. Synthetic cationic conditions require the use of protected hydroxy groups (Chapter 1.5) which lead to the corresponding veratric, homoveratric, dimethoxy caffeic acid, and *N*-[(1,1-dimethyl ethoxy)carbonyl]-*O*-methyl-*L*-tyrosine and their higher and lesser substituted derivatives (Scheme 3).

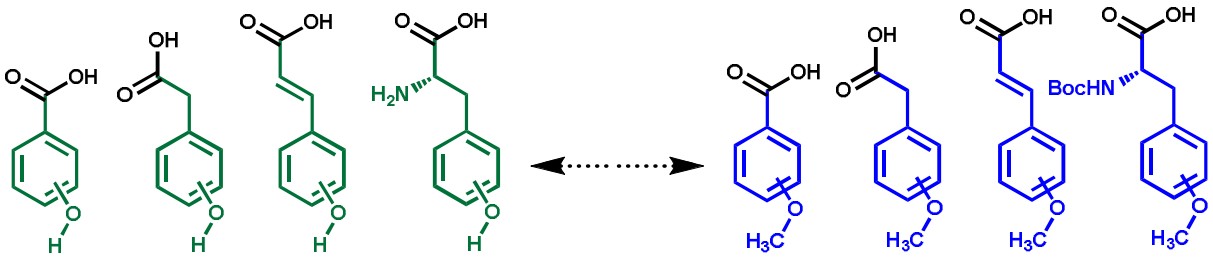

*Scheme 3: Hydroxy-substituted benzoic, benzylic, and cinnamic acid derivatives and L-tyrosine (left) cannot be used for the synthesis of 2-oxazolines, especially for further polymerization. Hence, methoxy and Boc-protected derivatives (right) are used as starting materials for the synthesis.*

The selection of the cinnamic acid and tyrosine derivatives enables the potential for post-polymerization modification at the double bond of the cinnamic acid derivatives and the amino function of the tyrosine upon the release of the catechol moiety. Furthermore, using methoxy-substituted phenolic acids as starting materials for the synthesis of poly(2-oxazoline)s allows numerous synthetic approaches of building the corresponding methoxy-substituted 2-phenolic-2-oxazoline monomers (Scheme 4).[74–77]

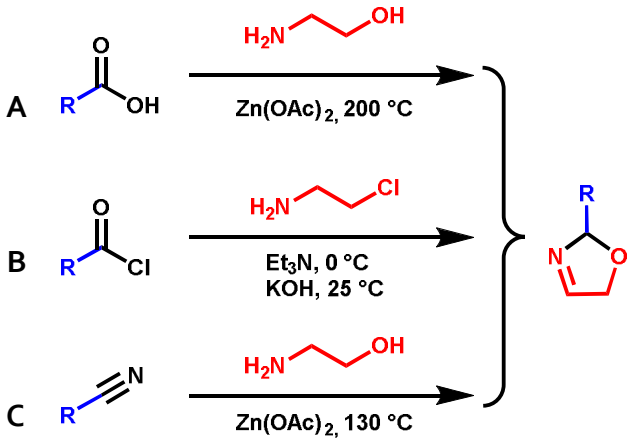


*Scheme 4: Different options of synthesizing a 2-oxazoline: One-step synthesis starting with the acid (A); method, developed by Wenker forming the 2-oxazoline from the acid chloride (B); using nitriles as starting material, established by Witte and Seeliger (C).*

Hence, the first task is the development and the optimization of synthesis routes from the methoxy-substituted phenolic acids to the corresponding 2-oxazolines. Once the methoxy-substituted 2-oxazoline monomers are synthesized, the second task is, to find proper polymerization conditions.

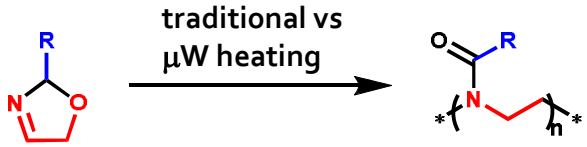


*Scheme 5: The polymerization of 2-oxazolines is conditioned by solvent, temperature, initiator, and method. Kinetic studies needed to be conducted, examining the proper conditions.*

The CROP of 2-oxazolines is strongly controlled by several conditions like method (traditional vs. microwave heating, Scheme 5), solvent, initiator, temperature, and concentration (Chapter 1.5). As most of these mentioned monomers and the polymerization of those were not reported yet, the homo polymerization conditions for those synthesized methoxy-substituted 2-oxazoline monomers needed to be examined by kinetic studies.

To mimic maritime glue proteins, a crucial requirement is the water solubility of the poly(2-oxazoline)s. In addition, the mole fraction of the catechol units within the polymers should be between 2 and 30 % to enable the full potential of the gluing units (Chapter 1.1). These properties are not fulfilled by the mentioned homopolymers. Thus, copolymers with appropriate mole fractions needed to be synthesized. An appropriate comonomer is 2-ethyl-2-oxazoline, which gives a water-soluble and nontoxic/biocompatible polymer.[78,79] The development of the discrete copolymerization conditions concerning the combination of the different synthesized methoxy-substituted phenolic(2-oxazoline)s and 2-ethyl-2-oxazoline needs to be investigated (Scheme 6). For this purpose, copolymerization kinetic studies to find the optimal reaction conditions needed to be conducted.

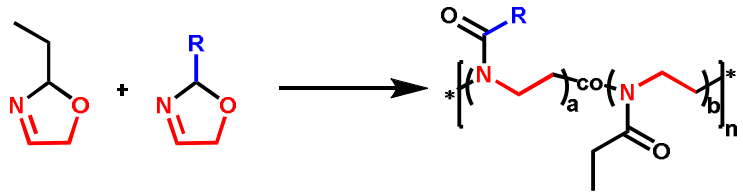

*Scheme 6: Copolymerization of methoxy-substituted phenolic 2-oxazoline derivatives with 2-ethyl-2-oxazoline to produce a water-soluble (protected) catechol-containing polymer.*

For further investigations, concerning surface interactions, the methyl aryl ethers needed to be cleaved to unprotect the catechol units (Scheme 7, A). Subsequently, partial hydrolysis of the copoly(2-ethyl-2-oxazoline) needed to be developed (Scheme 7, B). In consequence, a polycation simultaneously carrying catechol moieties results.

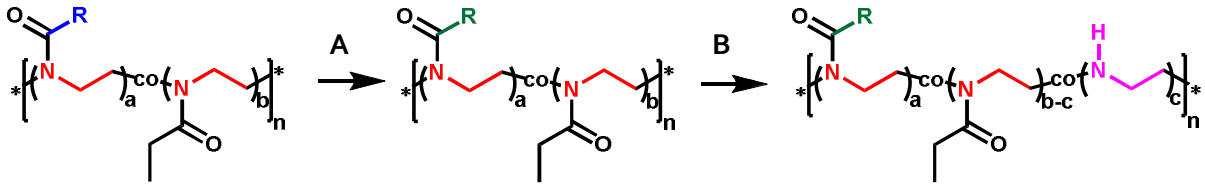

*Scheme 7: Aryl ether cleavage to reactivate the catechol (A) and additional functionalization by partial copoly(2-ethyl-2-oxazoline) hydrolysis to yield a polycation (B).*

The synthesized catechol and cation-functionalized copolymers needed to be examined concerning their adsorption abilities on different surfaces. Information about adsorption kinetics, adsorbed mass, and coating properties such as durability and antifouling abilities were to be investigated by measurements with the Quartz Crystal Micro-balance with Dissipation (QCM-D).

# 3 Methods

## 3.1 Infrared spectroscopy

The absorption of infrared (IR) radiation results in vibrations and rotations of molecules. The measurement of the direct absorption of IR radiation is called IR spectroscopy. Those vibrations (stretching, wagging, twisting) are very unique for organic functional groups, providing information about the nature of functional groups and their bonds. Thus, it can be used for the characterization of molecules. Furthermore, as this technique works with absorbance, consequently it is dependent on the concentration.[80] This fact will be used in this work for kinetic studies, as the area decrease of a signal of certain functional groups was used to determine monomer conversions.

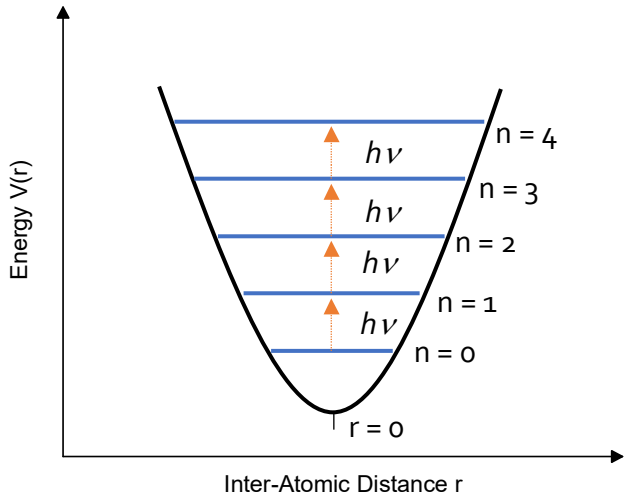


*Figure 5: Hamonic oscillator with discrete vibrational niveous. This is the first approximation towards the description of vibrations between two masses. A two atomic molecule cannot be completely described as yet with this model, as it does not show the dissociation with sufficiently high energy.*

The molecule irradiation is caused by the match between the frequency of the absorbed radiation and the vibrational frequency of the certain bond type mode.

This absorption frequency can be illustrated via the harmonic oscillator (Figure 5). This model describes the vibration of two masses with a mechanic approach using the following equation:

$$\upsilon_{OSC} = \frac{1}{2\pi}\sqrt{\frac{k}{\mu}} \qquad 1$$

with $\nu_{OSC}$ = vibration frequency of the oscillator, $k$ = force constant, and $\mu$ = reduced mass. Unfortunately, this model is limited as it does not describe the dissociation of a molecule with increasing (sufficient) energy.[81] A more accurate description is the anharmonic potential. In this case, the potential curve proceeds asymmetric, and the vibrational niveous have decreasing distances (Figure 6).

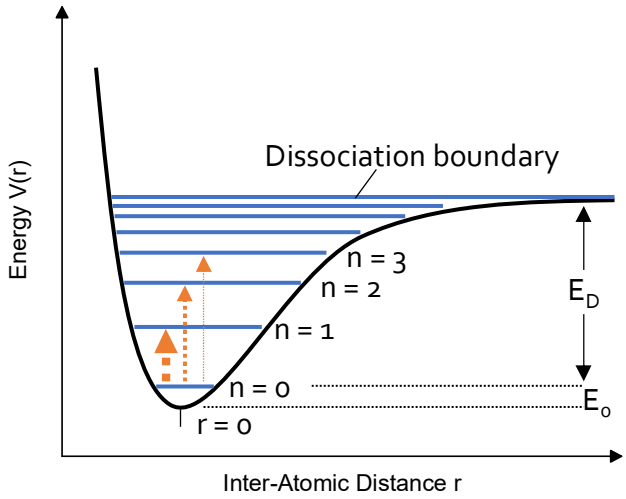


*Figure 6: Anharmonic potential shows the zero-point energy $E_o$ and the dissociation energy $E_D$. The potential niveous have decreasing distances between the quantum number of the vibrational states n. The arrow line thickness models the transition probability.*

The vibrational states are described with the vibrational quantum number *n*. In this regard, radiation absorption takes place in quantum energies. The excitation of vibration thus is the absorption of a light quantum by the vibrational state with the vibrational quantum number *n* and evolves to the next stage *e.g.* n+1, 2, 3(...). The probability of a transition from the zero-point energy to higher states decreases with an increase of *n*. The intensity of the absorbance is conditioned by the probability of transitions. The amount of energy for a vibrational transition $\Delta E_{VIB}$ is the energy difference of two energy values *e.g.* $E_{n=1}$ and $E_n$:

$$\Delta E_{VIB} = E_{n+1} - E_n = h\nu_{OSC} \qquad 2$$

with *h* = Planck constant.

The vibrational energy $E_{VIB}$ is described as follows:

$$E_{VIB} = h\nu_{OSC}\left(n + \frac{1}{2}\right) = \frac{h}{2\pi}\sqrt{\frac{k}{\mu}}\left(n + \frac{1}{2}\right) \qquad 3$$

Besides the quantum conditions, the intensity and the appearance of absorption bands in an IR spectrum are dependent on the dipole moment. IR light can only be absorbed by a molecule if the dipole moment corresponds with the electrical vector of the light. This means that the dipole moment should change for vibration to absorb the IR light. Thus, asymmetric vibrations to the center of symmetry cause a change in the dipole moment and thus are IR-active. Since most of the organic functional groups do not carry a center of symmetry, IR spectroscopy provides much information.

Critical for this work is the ATR-FTIR technique (ATR = attenuated total reflection). This technique allows the direct analysis of liquid or solid samples without any further preparation. It is based on the principle that when light travels through a high refractive index medium (ATR crystal) towards a low refractive index medium (sample) at a certain angle, an evanescent wave occurs. This wave, as it is an oscillating electromagnetic field, interacts with the sample. When the sample is exited within the region of the IR light the

evanescent wave is attenuated. This attenuated energy is sent back to a detector and results in a signal.

The Fourier transform infrared (FTIR) technique allows the detection of all frequencies of the IR light spectrum. This is possible due to the conversion of the poly-frequency IR light with the same intensity by an interferometer. The resulting interferogram is a function of time. The mathematic Fourier transformations convert the interferogram into a frequency-dependent spectrum. This simultaneous measurement of all frequencies (in the IR light spectrum) makes this technique faster than a wavelength-dependent scan.

These two techniques allow a fast and not costly measurement of samples *e.g.* kinetic studies.

## 3.2 Quartz Crystal Micro-Balance with Dissipation

Initially, the Quartz Crystal Micro-Balance with Dissipation (QCM-D) was a device to monitor real-time changes concerning surface interactions. [82,83] Over the years, the method was developed and sophisticated for a broader, more application-drawn field concerning investigations such as ion exchange, swelling, fouling, and sorption.[84–87] A particular feature using the QCM-D is the sensitivity as it even allows the monitoring of mass transport on a molecular scale.[88]

The QCM uses the inverse piezoelectric effect of quartz crystals, which is the application of a voltage to cause mechanical deformation of the quartz crystal.[89,90] An oscillation is caused by an alternating voltage. The basic idea of the QCM-D measurement is that by changing the mass of the sensor, due to coating or even by environmental modification from air to aqueous media, the resonance frequency of this oscillation shifts to lower frequencies. There are various possibilities to conduct QCM measurements, yet the QCM-D method, developed by Rodahl *et al.*, is called the "ring down" method.[91] The applied voltage is switched off periodically thus the oscillation decays. This oscillation decay generates a voltage since the quartz crystal is piezoelectric. The voltage related to the decay is monitored and results in a resonance. This resonance is described by two parameters like frequency, $f$, and bandwidth, $\Gamma$. Subsequently, this results on one hand in the resonance frequency $f_n$ and the other hand in the dissipation, $D_n$, which is calculated from the resonance frequency and the bandwidth:

$$D_n = \frac{2\Gamma_n}{f_n} \qquad 4$$

The change of both these parameters $\Delta f$ and $\Delta D$ are monitored as a function of the time. Thus, by treatment of the crystal whereby adsorption happens on the surface of the crystal, the $\Delta f$, and $\Delta D$ increase, accordingly vice versa while a desorption process. It is noteworthy that for each measurement the "blank" resonance frequency, as well as the dissipation of each distinct crystal in the particular environment, needs to be determined. This is necessary as each individual medium, like different solvents or air, already

influences the resonance frequency and with it $\Delta f$ and $\Delta D$ (Figure 7, B, C). As a consequence, the medium affects the measurement itself by interaction with the adsorbate. An overestimation of the mass due to the high dissipation effect is the result. This effect emerges in particular within very soft coatings with a low density making them more complicated to interpret. From the obtained $\Delta f$ and $\Delta D$ values the respective adsorbed mass can be calculated. Indeed, this calculation includes the potentially bound solvent. The dissipation though allows an estimation of the rigidity thus indicating the respective higher or lower value of the bound solvent.

Continue apriori with the simpler, more rigid type of coating. In this case, the adsorbed mass per area $m_{ads}$ is proportional to the frequency shift $\Delta f$. This correlation is described by the Sauerbrey equation:[92]

$$m_{ads} = -\frac{c}{n} * \Delta f \qquad 5$$

Where $c$ is the crystal constant and $n$ is the overtone number. This equation is limited to thin layers with a very rigid nature. With the density of the coating, $\rho_{coating}$, the respective thickness, $d_{coating}$, can be calculated as follows:

$$d_{coating} = \frac{m_{ads}}{\rho_{coating}} \qquad 6$$

This relation does not consider the change in dissipation $\Delta D$. Including the $\Delta D$ into the considerations, the nature of the coating characterization is more general. Hence, more complex systems can be described more accurately by including fluid effects. For this description, the Sauerbrey equation is modified and considered these fluid effects in the first approaches:[93,94]

$$m_{ads} = -\frac{c}{n} * (\Delta f + \frac{f_n \Delta D}{2}) \qquad 7$$

where $c$ is the crystal constant (in this work $c$ = 17.7 ng/cm²), $n$ the overtone number (in this work $n$ = 5), $f_n$ is the resonance frequency of the crystal ($f_n$ = 4.95 MHz), $\Delta f$ is the frequency and $\Delta D$ the dissipation shift.

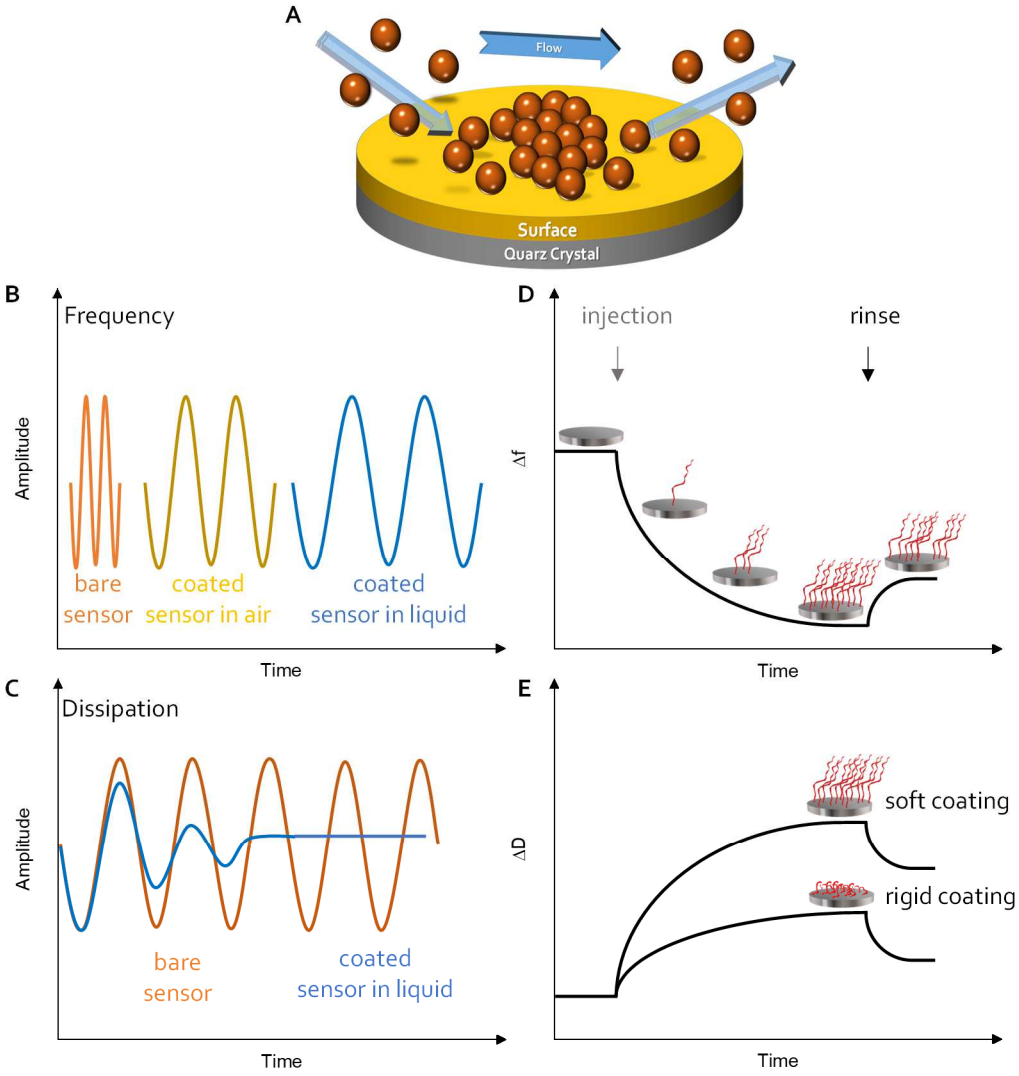


*Figure 7: Schematic depiction of a QCM crystal under treatment of adsorptive by flowing past the surface. A rinsing process can result in a desorption procedure. Environmental variations and the adsorbed mass regarding the sensor, lead to the frequency (B) and the energy dissipation (C) shifts sensor oscillation changes. The frequency (D) indicates the adsorbed mass, whereas the dissipation (E) displays information about the coating's rigidity.*

The QCM-D measures at each overtone (multiplies of the resonance frequency; typically: 1, 3, 5, 7, 9, 11, 13) both, the dissipation and frequency.[95] With an increasing overtone number, a vertical insight into the coating is facilitated as the penetration depth decreases.

If one knows the several parameters like density, $\rho_{coating}$, and viscosity, $\eta_{coating}$, of the coating, the fundamental crystal frequency, $f_o$, and the overtone number $n$, the respective penetration depth, $\delta$, can be calculated as follows:[96]

$$\delta = \sqrt{\frac{\eta_{coating}}{\pi n f_0 \rho_{coating}}} \qquad 8$$

The viscoelastic model uses the density, $\rho_{coating}$, and viscosity, $\eta_{coating}$, of the coating alike. Additionally, the thickness of the coating, $d_{coating}$, and shear modul, $\mu_{coating}$, as well as the medium properties, $\rho_{medium}$, and, $\eta_{medium}$, of air or liquid are included in this model because the frequency and the dissipation are functions of these parameters.[97,98] To determine whether the viscoelastic model should be used, the rule $|\Delta D_n/\Delta f_n| > 1 \times 10^{-8}$ Hz$^{-1}$ was suggested by Cho *et al.*.[99] The viscoelastic model especially is applicable for less rigid polymer films in liquids. Yet, the aforementioned parameters should be known or can be described with the viscoelastic Voigt model (for swollen polymers with solvent above the $T_g$) or the extended Voigt model (including viscosity, shear modules are frequency-dependent).[88] Including three or more overtones within the consideration, the viscoelastic model is a way to describe less rigid coatings, such as polymer films, with high accuracy.[100] Since the viscoelastic model is very complex and requires the knowledge of several coating parameters, the extended Sauerbrey description (equation 7) will be used for the mass calculations in this work.

# 4 Results and discussion

## 4.1 Synthesis of 2-oxazoline monomers

The properties of the polymer are defined by the structure of the monomer. The monomer – in this work the 2-oxazoline molecule – can be diversified by changing the substituents in 2, 4, and 5-position (Scheme 8). The modifications in the 4- and 5-positions are usually less used for monomer synthesis since the reaction rate for the polymerization drops due to steric hindrance.[101] Hence, for most 2-oxazoline monomers the substituent in 2-position is changed to tune the polymer properties. Nucleophilic moieties such as alcohols, amines, or thiols, must be avoided or protected.[102]

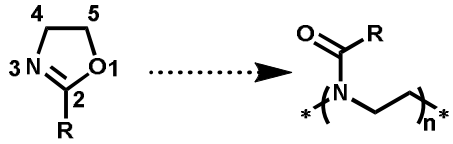


*Scheme 8: The structure and nomenclature of a 2-oxazoline and the corresponding poly(2-oxazoline).*

Several pathways towards 2-substituted 2-oxazolines have been established and described, starting from non-activated carboxylic acids, acid chlorides, aldehydes, or nitriles (Scheme 9).[74,75,77,103–106]

The formation of the 2-oxazoline from a non-activated carboxylic acid (Scheme 9, A) usually needs high temperatures and mostly an activating agent in form of a Lewis acid for the final cyclization into the 2-oxazoline. More moderate conditions require the modified Wenker method (Scheme 9, B). First, the carboxylic acid is transformed into an acid chloride which, is reacted with a $\beta$-halo amine to form a $\beta$-halo amide at milder temperature. Then, the cyclodehydrohalogenation reaction to the 2-oxazoline takes place at 80 °C in presence of a base. The milder conditions in the second step can be explained by the better leaving groups, *i.e.* chloride as compared to the hydroxy group

used in reaction A. Other leaving groups such as tosylates, triflates, and sulfuric acids have been used as well.[107] The preparation of 2-oxazolines from aldehydes is done in one step under milder conditions in presence of a base, iodine, and ethane-1, 2-diamine (Scheme 9, C). The iodine in the reaction is crucial for achieving appropriate to good yields. The simplicity of the reaction, as well as the one-step procedure, makes this an attractive method for the 2-oxazoline synthesis. However, the most prominent procedure is the Witte-Seeliger method (Scheme 9, D). This synthesis starts with a nitrile, which is reacted with 2-aminoethan-1-ol, in presence of zinc(II) acetate or cadmium(II) acetate as a catalyst. This reaction requires higher temperatures than the reaction with aldehydes (C) as starting material.

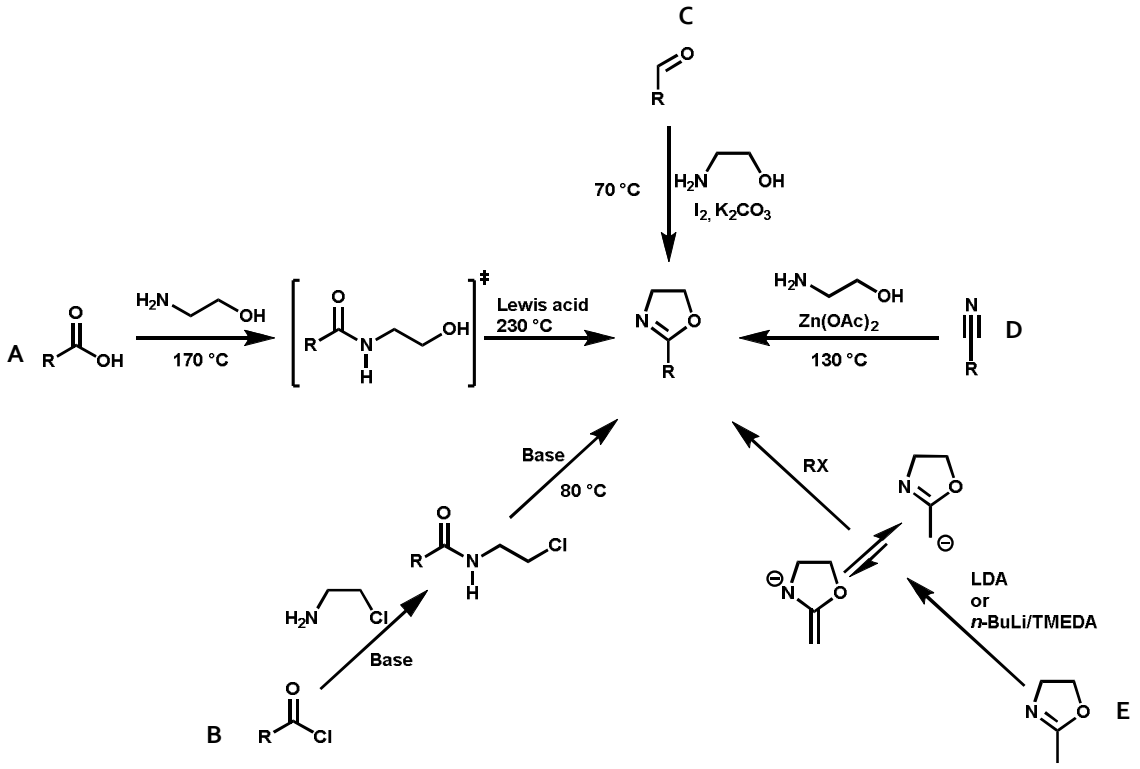


*Scheme 9: Overview across possible methods of synthesizing 2-oxazolines using different starting materials.*

An entirely different approach is the modification of 2-methyl-2-oxazoline by α-deprotonation and reaction with alkyl halogenides to the corresponding modified 2-

oxazoline (Scheme 9, E). This reaction can be a way to synthesize complex 2-oxazolines, though the reaction with lithium diisopropyl amide (LDA) mostly gives a lot of side reactions and poor yields of the modified 2-oxazoline. replacing LDA with a by *n*-butyl lithium *N,N,N´,N´*-tetramethylethane-1,2-diamine (TMEDA) increases the yield. This method should be used when the other methods (A-D) give poor results for more complex 2-oxazolines.

Each method does certainly have its advantages and disadvantages and different starting substrates requiring different conditions and methods. The one-step methods A, C, and D, however, are the most preferred regarding their simplicity and high yields.

### 4.1.1 Development of the 2-oxazoline synthesis based on cinnamic acid

2-Oxazolines can be synthesized from the related carboxylic acid as mentioned in chapter 4.1. Indeed, 2-oxazolines serve as a protection group for carboxylic acids.[108] Thus, the first experiments synthesizing 2-oxazolines follow different approaches going out from carboxylic acids as starting substrates(Figure 8).

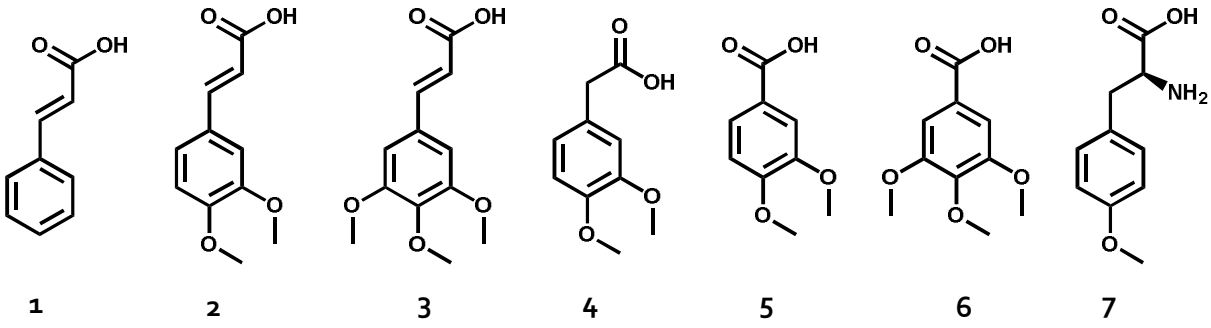


*Figure 8: Overview across the starting substrate carboxylic acids used for the 2-oxazoline synthesis in this work. All acids are naturally occurring and named trivial as follows: Cinnamic acid (**1**); 3,4-Dimethoxycaffeic acid (**2**); 3,4,5-Trimethoxycinnamic acid (**3**); Homoveratric acid (**4**); Veratric acid (**5**); 3,4,5-Trimethoxygallic acid (**6**); O-methyl-L-tyrosine (**7**).*

At this point, the cinnamic acid (**1**) was used as a model compound for the 2-oxazoline synthesis, which should later be applied to more complex acids.

In general, the 2-oxazoline synthesis from the carboxylic acid consists of two condensation reactions with water as a by-product. Ersorb-4 is a zeolite that can adsorb water which is occurring during the reaction. Additionally, there are studies about the potential responsibility of Ersorb-4 for the acylation of amines with carboxylic acids and it was described that Esorb-4 supports the conversion of different carboxylic acids with 2-aminoethan-1-ol in xylene to the corresponding 2-oxazolines.[109,110] Hence, for the synthesis of **1a**, cinnamic acid was treated with 2-aminoethan-1-ol in the presence of Ersorb-4, yet the reaction resulted in no conversion (Scheme 10). This can be explained by the deactivating effects of the cinnamyl unit by hindering the nucleophilic attack of amine alcohol.

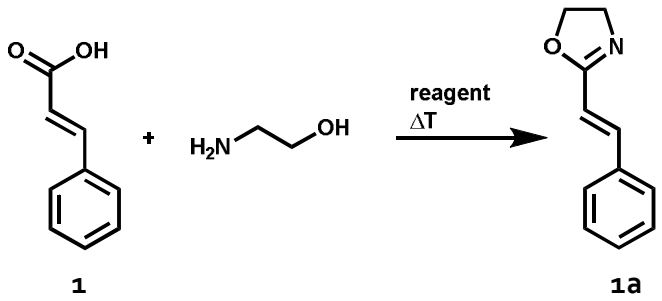


*Scheme 10: General reaction of cinnamic acid (**1**) with 2-aminoethan-1-ol to the 2-cinnamyl-2-oxazoline (**1a**).*

Another promising method is the conversion of carboxylic acids with 2-aminoethan-1-ol in presence of a titanium(IV) alcoholate. The titanium reagent is not only assisting the ring-closing reaction to the 2-oxazoline but also supports the amidation as an intermediate step.[77,111] The reaction of **1** with 2-aminoethan-1-ol in presence of titanium(IV) *i*-propoxide (10 mol%) and molecular sieves (MS, 3 Å) in chlorobenzene (PhCl) at 140 °C gave poor yield (Table 1, entry 1). Increasing the reaction time and the amount of titanium reagent did not lead to a notable increase in the yield (Table 1, entry 2-3). The sequential addition every 24 h over 72 h gave slightly better results but did not

increase the yield of **1a** significantly (Table 1, entry 4). Thus, arising water during the reaction and subsequent decomposition of the titanium reagent can be ruled out. Removing the appearing water, however, can play a role in the reaction equilibrium. The extraction of the appearing water with molecular sieves during the reaction thus can lead to a shift of the reaction equilibrium to the product side. Yet, this approach did not give any increase of the yield of **1a**. Because 2-aminoethan-1-ol (**8**) was already applied in excess a further addition of this reagent was not made.

Thus, the reactivity of the titanium reagent can be a limiting factor for the low conversion. Subsequently, the more reactive Lewis acid boron trifluoride etherate ($Et_2O{\cdot}BF_3$) was considered as an additional reagent. But neither the combination of the titanium and the boron reagents nor the solitary usage of the boron reagent increased the yield (Table 1, entry 5-6).

*Table 1: Overview across the progress of reaction development.*

| Entry | Starting Material | Solvent | Reagent | Amount of reagent | Temp. [°C] | Time [h] | Yield [a] [%] |
|---|---|---|---|---|---|---|---|
| 1 | **1** | PhCl | Ti(O*i*-Pr)4 | 10 mol% | 140 | 24 | 19 |
| 2 | | | | | | 66 | 22 |
| 3 | | | | 1 eq | | 24 | 20 |
| 4 | | | | 4 eq add. sequential | | 72 | 34 – 40 |
| 5 | | | $Ti(O\textit{i}\text{-}Pr)_4$, $Et_2O{\cdot}BF_3$ | 1 eq each | | 24 | 0 |
| 6 | | | $Et_2O{\cdot}BF_3$ | 1 eq | | 24 | 5 |
| 7 | *N*-(2-hydroxyethyl)cinnamyl amide | DCM | MsCl, TEA | 1 eq | 25 | 24 | 0 |
| 8 | *N*-(2-chloroethyl)cinnamyl amide | MeOH | KOH | 1.5 eq | 70 | 18 | 0 |
| 9 | | DMF | $K_2CO_3$ | 1.5 eq | 70 | 18 | 0 |
| 10 | cinnamyl nitrile | PhCl | $Zn(OAc)_2$ | 0.04 eq | 140 | 18 | 73 |

[a] isolated yield

During all these named reactions the intermediate *N*-(2-hydroxyethyl)cinnamyl amide (Scheme 11) can not be isolated. Following this notice, all occurring amide in the reaction proceeded the reaction to the 2-oxazoline (**1a**). Subsequently, the limiting factor can be the amide formation (step 1, *Scheme 11*) and not the ring-closing reaction (step 2, *Scheme 11*). For that reason, the *N*-(2-hydroxyethyl)cinnamyl amide and *N*-(2-chloroethyl)cinnamyl amide was synthesized by purpose and the ring-closing reaction was conducted individually. The chloride derivative was synthesized to introduce a better leaving group compared to the alcohol. Despite similar reactions already published, these reactions did not give any yield of the 2-cinnamyl-2-oxazoline (**1a**) (Table 1, entry 7-9). A reason for the mentioned results cannot be determined.[112,113]

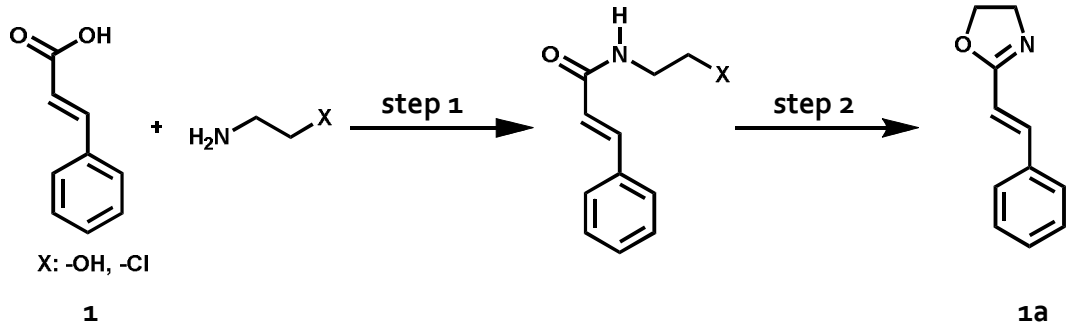


*Scheme 11: The conversion of cinnamic acid (**1**) to the 2-oxazoline **1a** in two steps.*

Due to the discussed poor results, the approach was changed and the procedure, using a nitrile (4.1, Scheme 9, A) was considered further. Since the cinnamyl nitrile is commercially available this nitrile was not synthesized initially. The conversion of carboxylic acids into nitriles will be discussed below.

Cinnamyl nitrile was used as starting material and was converted with catalytic amounts of zinc(II) acetate in chlorobenzene at 140 °C to give the corresponding 2-oxazoline **1a** a yield of 73% (Table 1, entry 10).[104] During the reaction, ammonia is produced as a by-product, which is easily removed from the reaction mixture (Scheme 12). Due to the success of this route, a different method was not considered and most of the other 2-

oxazolines were synthesized via this modified Witte-Seeliger method. Detailed consideration for each 2-oxazoline will follow in the further work.

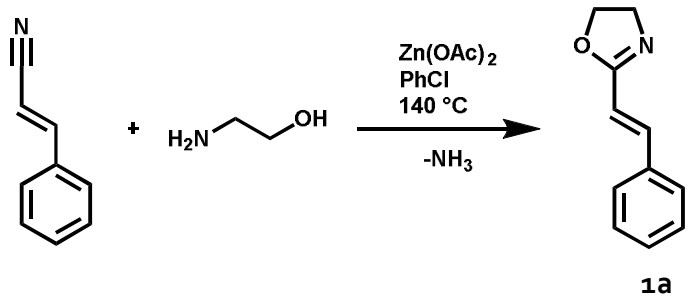


**1a**

*Scheme 12: Successful 2-oxazoline (**1a**) synthesis via the modified Witte-Seeliger method.*

### 4.1.2 Synthesis of nitriles from cinnamic acid derivatives

Since at least the cinnamic acid (**1**) did not give the corresponding 2-oxazoline **1a** in good yields, via the one-pot synthesis, the modified Witte-Seeliger method was used for the 2-oxazoline synthesis. This synthesis requires a nitrile as starting substrate instead of the acid. While the nitriles of cinnamic (**1**), homoveratric (**4**), veratric (**5**), and 3,4,5-trimethoxygallic acid (**6**) are commercially available, the corresponding nitriles of the 3,4-dimethoxycaffeic (**2**) and 3,4,5-trimethoxycaffeic acid (**3**) needed to be synthesized.

A promising method was the direct conversion of carboxylic acids into nitriles by amidation with ethyl carbamate. The reaction is to be completed by dehydration using thionyl chloride.[114] Despite its promising results of high conversions and yield the acids **2** and **3** did not react at all. A second attempt was the conversion of carboxylic acids **2** and **3** into primary amides and a subsequent formation of the nitrile under Swern conditions (Scheme 13).[115]

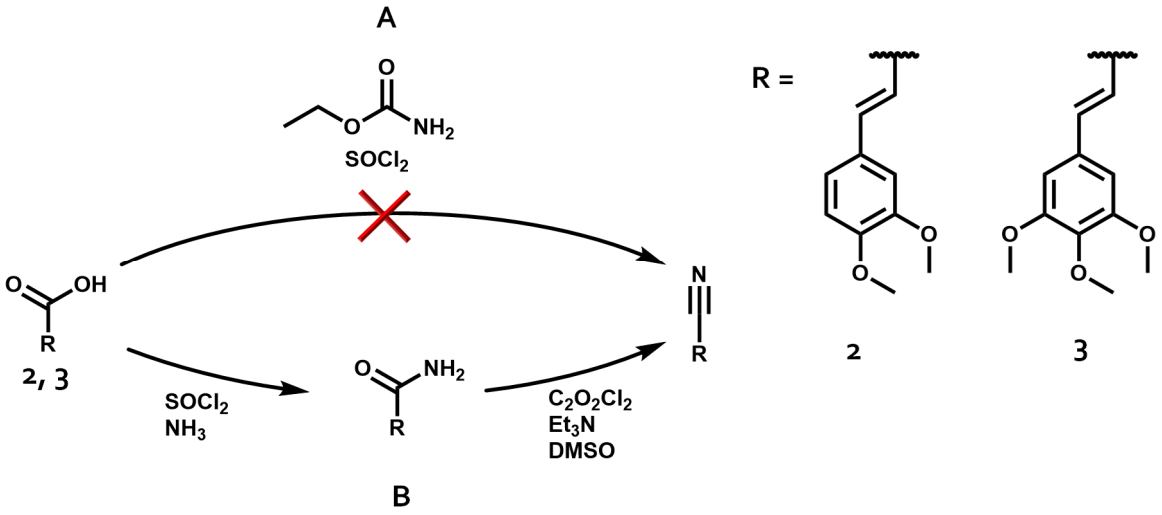


*Scheme 13: Nitrile synthesis starting with the carboxylic acid **2** and **3**. The direct synthesis via amidation and dehydration failed (A), however the conversion of the primary amide, which was synthesized from the acid by treating the acid chloride with ammonia, resulted in the corresponding nitrile in good to very good yield (B).*

Therefore, the carboxylic acids **2** and **3** were converted into acid chlorides with thionyl chloride and subsequently transferred into the primary amide via condensing ammonia into the dry solution containing the acid chloride. The reaction was carried out at -78 °C, since, first, the ammonia gas needed to be condensed into the solution, and second the reaction of ammonia with the acid chloride was keen. The absence of water in this reaction was an important factor as the acid chloride would return to the carboxylic acid. The primary amide may not be separated from the subsequent mixture of acid and amide. Anyhow, by keeping the reaction conditions dry, the conversion of the acid chloride into the primary amide was quantitative. This quantitative reaction allows a quick workup with only using solvent extraction. Any further workup technique as flash chromatography or sublimation was not necessary. Once the primary amides of **2** and **3** were obtained in particularly good yields the synthesis of the corresponding nitriles had to be established.

The already published high yield promising nitrile synthesis under Swern conditions was conducted.[115] Therefore the amides **2** and **3** were treated with oxalyl chloride dimethyl sulfoxide (DMSO) and triethylamine (TEA) under room temperature in acetonitrile (ACN). Compared to the compounds used in the published article, the reaction time, and the temperature during the addition of oxalyl chloride needed to be adjusted. Within short reaction times, the yield was only 55 %. Only extending the reaction time did lead led to a slight increase to 77 % (7 h reaction time) and 60 % (12 h reaction time). During the oxalyl chloride addition, an intense reaction occurred, possibly leading to decomposition or side reactions of reactants. To avoid this, the temperature of the mixture was kept at 0 °C while adding the oxalyl chloride. This change gave a significant increase of the yield to 83 % and 84 %.

### 4.1.3 Monomer synthesis via the Witte-Seeliger method

While the Witte-Seeliger method was established with the cinnamic acid (**1**) as a model compound, the not purchasable nitriles were synthesized, as mentioned in the previous chapter 4.1.2. The other nitriles were not synthesized from the equivalent acids (**1, 4, 5, 6**) since the respective synthesis was already published.[115–118] Generally, the synthesis of the 2-oxazolines **1a**-**6a** was carried out similarly, with only facile modifications of temperature and reaction time. As the catalyst, zinc(II) acetate was used, already mentioned in chapter 4.1.1 (Scheme 14).

Using zinc(II) acetate resulted in good yields of **1a, 2a, 4a**-**6a**. Yet the yield of **3a** was low and following experiments were conducted to increase the yield. First experiments towards **3a** resulted in ~50 % yield. Thus, the 2-aminoethan-1-ol (**8**) ratio was increased to 3 equivalents. However, this led to an increase of side reactions, determined by thin-layer chromatography (TLC). To avoid side reactions, the ratio of ethanolamine was kept at the established 1.5 equivalents. As a change of either reaction temperature, catalyst, and reaction time can raise the yield and reduce the side reactions, initially the catalyst was changed to cadmium(II) acetate. This catalyst was already used besides zinc(II)

acetate, by Witte and Seeliger.[119] Yet using cadmium(II) acetate as the catalyst the yield of **3a** was still 50 %. Thus zinc(II) acetate was used further as the catalyst. The decrease of the reaction temperature from 140 to 100 °C however led to a significant decrease of the side reactions (evidenced by TLC) yet the yield dropped as well. Likewise shortening the reaction time led to a decrease in the yield. Further experiments showed the reaction at 130 °C with zinc(II) acetate within 18 h reaction time were the best conditions to yield **3a** in 55 %.

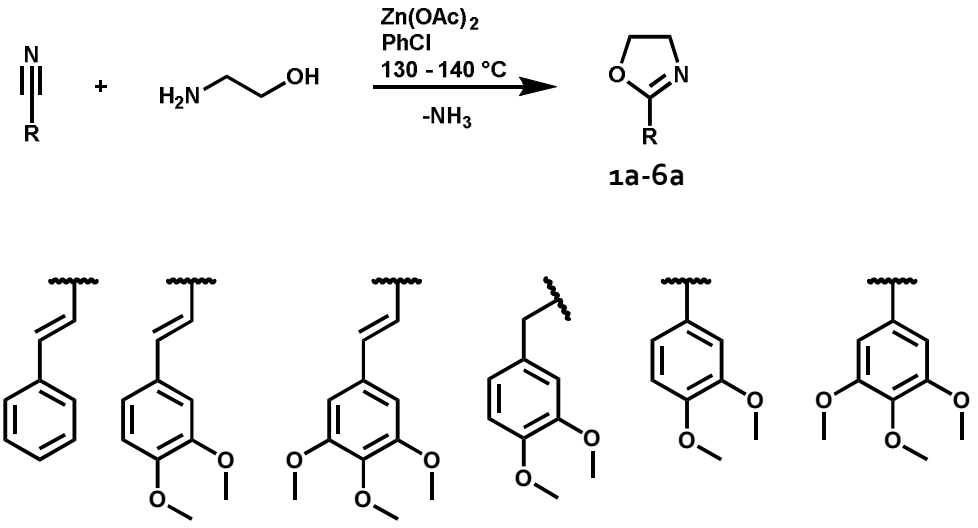


*Scheme 14: Witte-Seeliger method used for the 2-oxazoline synthesis of substances **1a**-**6a**. ([a]Yield refers to 2-oxazolines **1a**-**6a**).*

Hence the 2-oxazoline synthesis was carried out with zinc(II) acetate for all nitriles as the results were best. The reaction time was similar concerning all starting materials, whereas the reaction temperature needed to be slightly adjusted to receive the best results concerning the yield. A general trend concerning the reactivity from the nitrile to the corresponding 2-oxazoline regarding the yield cannot be observed since the yield of **2a** was comparable high as this of **5a** and **6a**.

Altogether six of the seven requested 2-oxazolines were successfully synthesized in good to very good yields with the Witte-Seeliger method. For that method, it was necessary to convert two of the seven carboxylic acids (**2, 3**) into corresponding nitriles. Therefore, two methods were conducted, whereat the direct nitrile synthesis via amidation and dehydration failed. The synthesis of the primary amide and subsequent conversion to the nitrile under Swern conditions was successful. As the other corresponding nitriles (**1, 4, 5, 6**) were purchasable and the synthesis was already published, their synthesis was not conducted. Hereupon the Witte-Seeliger method can be conducted for the corresponding nitriles of **1**-**6** converting them into the 2-oxazolines **1a**-**6a**.

### 4.1.4 Monomer synthesis based on *O*-methyl-*L*-tyrosine

3,4-Dihydroxy-*L*-phenylalanine (*L*-Dopa) provides the catechol unit within the mussel foot proteins giving them the ability to stick to surfaces (Chapter 1.1). Naturally, *L*-Dopa is synthesized by oxidizing *L*-tyrosine with the enzyme tyrosine hydroxylase.[120] Certainly, *L*-Dopa-containing polymers were already synthesized, yet no polymers containing *L*-Dopa or *L*-tyrosine derived from 2-oxazolines are published.[47] Likewise, the 2-oxazolines of *L*-Dopa and *L*-tyrosine are not published yet.

From the *L*-tyrosine, neither the corresponding 2-oxazoline nor the polymer can be synthesized (see Chapter 1.5). Since the nucleophilic amine and hydroxy units would disturb the monomer synthesis and polymerization, they must be protected. As used before the hydroxy group was shielded by a methyl ether. To protect amines the *tert*-butyloxycarbonyl (Boc) group is commonly employed and used. One other popular amine protection group is fluorenylmethyloxycarbonyl (Fmoc). The Fmoc group, however, cleaves under mild basic conditions via proton abstraction. During the monomer synthesis or the polymerization process, this acidic proton can cause undesired side reactions. Hence this group may not be used before the polymerization process. Consequently, the Boc protection group was used as it was assumed to be stable during

the monomer synthesis and polymerization conditions. Thus, the *N*-Boc-*O*-methyl-*L*-tyrosine (**7**) was used as starting material for this synthesis.

Due to less harsh reaction conditions, the two-step reaction via the $\beta$-halo amide (described in chapter 4.1, Scheme 9) is a well-known and established route for the 2-oxazoline synthesis with amino acids.[121] The activation of the carboxyl group of the *O*-methyl-*L*-tyrosine (**7**) for the amid formation was carried out with ethyl chloroformate in presence of TEA in dry *N*,*N*-dimethylformamide (DMF). The reaction was performed at room temperature due to the high reactivity of the active ester. 2-Chlorethylamine hydrochloride and TEA were dissolved in DMF and added to the mixture. The base TEA facilitated the reaction of the 2-chlorethylamine hydrochloride with the active ester. The formation of the $\beta$-halo amide gave a quantitative yield of 97% using the solvent extraction technique (Scheme 17). The product was already pure, as evidenced by $^1$H NMR spectroscopy (Chapter 8, Figure S 14), thus further purification was not necessary.

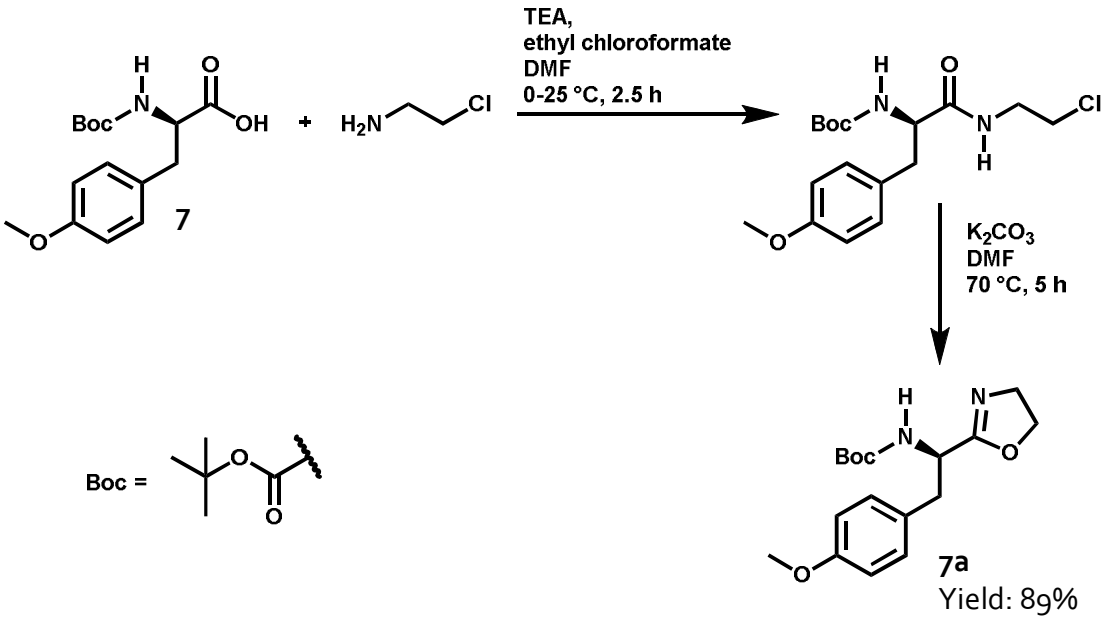


*Scheme 15: Synthesis route of N-tert-Butoxycarbonyl-3-(4-methoxy-L-tyrosin)-2-oxazoline (**7a**) starting via $\beta$-halo amide formation and subsequent ring-closing reaction to yield the 2-oxazoline **7a**.*

*N-tert*-Butoxycarbonyl-3-(4-methoxy-*L*-tyrosin)-2-oxazoline (**7a**) was synthesized via cyclodehydrohalogenation with the corresponding $\beta$-halo amide in dry DMF in presence of potassium carbonate in a yield of 89%.

With that effective synthesis of the 2-oxazoline **7a**, seven desired monomers were successfully produced. Worth mentioning is that the 2-oxazolines **2a**, **3a**, **4a**, and **7a** are not known in the literature yet. Though, we recently published the synthesis of **2a** and **3a**.[122]

The access to the 2-oxazolines **1a**-**7a** enables the path to produce various poly(2-oxazoline)s via CROP. The resulting poly(2-oxazoline)s would contain diverse functional groups like double bonds, protected amines, and protected phenols in different substituent patterns. Since none of these monomers were used to make polymers the reaction conditions for their polymerization are needed to be developed. This will be considered and discussed in the next chapter.

## 4.2 Polymerization of 2-oxazolines

The properties of poly(2-oxazoline)s (POx) were already mentioned in chapter 1.5. Below, the polymerization mechanism and the reaction conditions will be discussed in detail. Poly(2-oxazoline)s are synthesized via a cationic ring-opening polymerization (CROP) to give amide-containing polymers.[55] The thermodynamic more stable amide in the side chain is the result of the ring-opening isomerization of the cyclic 2-oxazoline. This difference between the thermodynamically preferred amide structure and the 2-oxazoline ring is the driving force of polymerization.[56] The living character depends on the purity of the used reagents and solvents: nucleophiles would terminate, and protons (*e.g.* water) can initiate the polymerization. For that reason, it is indispensable to work under absolute water and nucleophile-free conditions, and monomers and solvents should not contain any nucleophiles or acidic protons. The mechanism runs via an ionic and a covalent pathway whereas both are in equilibrium with each other. Whether the equilibrium is on the ionic or covalent side depends on the nucleophilicity of the

monomer, the nature of the counterion, the temperature, and the polarity of the solvent.[123]

The mechanism starts with the initiation by attacking the electrophilic initiator with the free electron pair of the nitrogen within the 2-oxazoline **I** (Scheme 16, A). The resulting oxazolinium cation (**IIa**) is in equilibrium with the covalent species **IIb**. The initiation is a slow reaction and can be accelerated by a temperature increase. At room temperature, the reaction commonly does not take place.[52] The initiation rate is crucial for the resulting polymer mass distribution. Higher dispersity will result from slow or incomplete initiation. Likewise, the reactivity of the initiator plays a role in the initiation process, as bulkier initiators, like PEG-tosylate, are less effective.[124] However, under the proper conditions, even at low temperatures poly(2-oxazoline)s can be synthesized with low dispersity.[125] The most common initiators are alkylating agents like alkyl halides, tosylates, and triflates due to their reactivity, comparably simple handling, availability, and versatility. Various functional groups can be incorporated as end groups by the initiator.

The propagation can be derived into a two-step mechanism (Scheme 16, A). First, the oxazolinium cation (**IIa**), formed during the initiation, gets attacked by a new monomer (**I**) in 5-position and results in the addition of **I**. If the initiation was complete, this addition is the rate-determining step.[126] After this first attack, the reaction rate increases vigorously due to the shift of the equilibrium to the more reactive cationic species **IIIa**. This increase is caused by intermolecular dipole-ion polarization effect **IIc** which favors the formation of **IIIa**.[123] Hence, despite the mechanism of the propagation being similar to the first attack of a monomer on the initiated oxazolinium cation, this can be assessed as the second propagation step. Under certain circumstances, even in the absence of nucleophiles or water, chain-transfer reactions can occur during the propagation. It is commonly accepted that 2-alkyl-2-oxazolines undergo $\alpha$-elimination reactions which result in a ketene *N*, *O*-acetal (**IV**), formerly labeled as enamine (Scheme 16, B).[127] This reaction not only results in a terminated polymer chain **IV** but also in a release of a proton, which can re-initiate a polymer chain **IId**. In consequence, the mass distribution will

become broader. At higher conversions (>75 %) chain coupling reactions were caused by the ketene *N, O*-acetal increase since it provides a reactive center.[127]

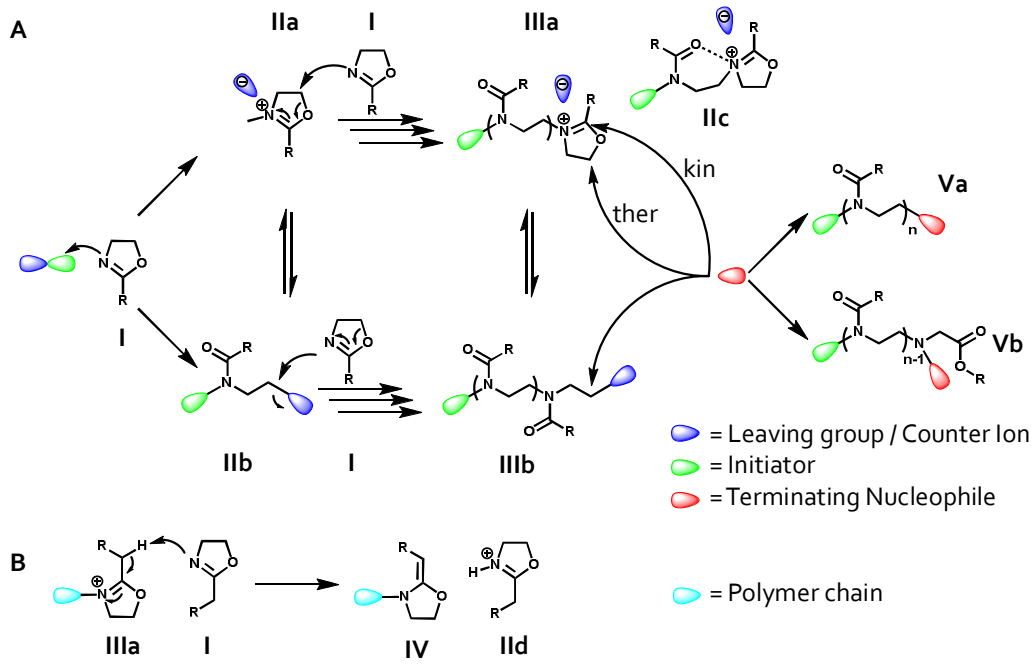


*Scheme 16: A) Detailed 2-oxazoline cationic ring-opening polymerization mechanism depiction. B) Chain-transfer reaction by α-elimination resulting in a ketene N, O-acetal (**IV**), and a proton-initiated monomer (**IId**).*

The termination of a cationic living polymerization is simply carried out by the addition of a nucleophile. The versatility of nucleophiles that can be used is wide and gives an equally wide range of possibilities to introduce functional end groups. Certainly, attention shall be paid to the purity of the reagents since other nucleophiles would terminate also, which results in an end-group mixture. Moreover, two termination mechanisms can occur, which are the thermodynamically and kinetically driven reaction (Scheme 16, A; **Va**, **Vb**). Generally, softer terminating reagents (HSAB-theory) like water undergo the kinetically driven process, whereas harder terminating reagents like piperidine tend to terminate thermodynamically driven. During the kinetically driven reaction, the terminating reagent (*e.g.* water) attacks not in 5-position as the monomers do, but attacks at 2-position, which results in a secondary amine and ester-containing

end group **Vb**.[128] Mostly used is a water/methanolic potassium hydroxide solution giving hydroxyl end groups (**Va**).

The CROP highly depends on the monomer nature, as already mentioned in chapter 1.5. The reaction rate is influenced by the structure of the side chain, as the reaction rate with 2-alky 2-oxazolines decreases by the decrease of the inductive effect. Hence, 2-alky 2-oxazolines, in general, have a higher reaction rate than 2-aryl-2-oxazolines.[62] Unfortunately, the side chain is not always tunable, thus the temperature becomes an important factor. It is common to conduct a 2-oxazoline polymerization at 140 °C, but the usually used solvent acetonitrile has a boiling point of 82 °C. Hence, this superheating can not be conducted with traditional heating without using a pressure reactor. Superheating can also be realized using microwave irradiation with a closed vessel. Comparing the kinetics, the same results were given whether the reaction was conducted in a pressure reactor with traditional heating, or by microwave irradiation in a closed vessel. Thus no difference between these two methods was determined, a microwave effect consequently can be excluded.[63,129] This detailed consideration of the mechanism and the related effects of reagent, solvent, and temperature is important to understand the experimental decisions and observations.

Hereafter, a study about the polymerization of the synthesized monomers (**1**-**7**) will be discussed.

### 4.2.1 Conditions and parameters towards homopolymer synthesis

To establish the proper reaction conditions, concerning the method (traditional vs. microwave heating), solvent, initiator, concentration, temperature, and reaction time needed to be examined. Yet another crucial question was how to determine the monomer conversion for kinetic studies. The most common methods are nuclear magnetic resonance (NMR) spectroscopy and Fourier-transform infrared (FT-IR) spectroscopy.

Acetonitrile (ACN) is the most prevalent solvent for 2-oxazoline polymerizations. The properties of the solvent are supporting both polar and nonpolar compounds. Moreover, the chain-transfer reaction, discussed in the previous chapter 4.2, is not supported by this solvent, yet not suppressed.[102] Thus, due to its overall promising properties, ACN was chosen as a solvent for polymerization.

The options of initiators are versatile, but under closer consideration, the range narrows: First, macroinitiators can be ruled out, because it would change the properties of the polymers dramatically. Thus, an individual investigation of the homopolymers would be impossible. Due to their lower reactivity, benzyl halides are not a proper first option as the 2-benzoic-2-oxazolines **5a** and **6a** most likely have a low reactivity considering the previously mentioned order of reactivity (Chapter 4.2). Hence, the initiator group of triflates and tosylates are the best option. The initiating groups are small alkyl chains to methyl group and their reactivity is high. Thus, methyl tosylate (MeOTos) and methyl triflate (MeOTf) were chosen as initiators.

The monomer concentration within the reaction mixture can range from bulk to low concentrated solutions.[53,130] Since all monomers **1a**-**7a** were solids, a reaction in bulk was discarded. Therefore, a monomer concentration range from 4 M to 1 M was tested for polymerization.

2-Oxazoline polymerization reactions usually require temperatures from 80 to 140 °C. Since ACN was chosen as solvent (bp: 82 °C), superheating becomes an issue. The microwave device is capable to keep overpressure up to 17 bars, thus a reaction above the boiling point with ACN is possible. Consequently, the proper reaction temperature can be set even above the boiling point (range: 80 to 140 °C).

The possibility of conducting two different methods, namely traditional heating, and microwave irradiated heating, has already been discussed (Chapter 1.5 and Chapter 4.2). Both methods were tested during the work. The advantage of traditional heating is the possibility of using higher amounts of starting material. However, with a slow reaction due to low temperature, this advantage indeed is suspended.

The batch size is one of the main disadvantages of the microwave method as the microwave vessels have a limited size of 10 mL. This implies for a reaction in a sealed vessel with super-heated solvent, that the amount of reaction mixture is restricted to 5 mL at best. At a temperature of 140 °C, the maximum amount of solution should not be higher than 1 mL (this was tested during the work as the pressure during the reaction rose to 12 bar). However, the possibility to accelerate the reaction, thus shortening the reaction time by elevating the temperature to 140 °C is the main advantage of microwave irradiation. Hence, the parameter variation with microwave irradiation is broader, compared to traditional heating under the condition of limited batch size.

The verification concerning the accurate determination of the conversion is a crucial part of developing the reaction conditions. As mentioned above, NMR and FT-IR spectroscopy are two commonly approved methods to determine the conversion. Either the decrease of the starting material signal or the increase of the product signal can be used to determine the conversion. 2-Oxazoline monomers usually give two very distinct, individual triplet signals in the $^{1}$H-NMR spectrum between $\delta$4.5 and $\delta$3.5 ppm. These signals rely on the four methylene protons in 4 and 5 positions of the 2-oxazoline ring. The observation of the 2-oxazoline monomer decrease via integration of these signals, related to an internal standard, would be a convenient method to determine the monomer conversion.

FT-IR spectroscopy is likewise convenient to determine the conversion. The 2-oxazoline ring usually shows a distinct signal in the FT-IR spectrum, declared as "ring-breathing" in the literature. In FT-IR spectra, these signals are usually located between ~900-1000 cm$^{-1}$.[52,131,132] Thus, if the "ring-breathing" signal occurs in the FT-IR spectrum independently, the decrease of the monomer concentration can be measured directly in the reaction mixture and determined by integration. Both methods were tested and used during this work, though dependent on the discrete requirements concerning the experiments and the signal nature.

### 4.2.2 Development of the polymerization conditions to yield homopolymers

The parameters and their variations concerning the CROP of 2-oxazolines were discussed in the previous chapter. In the context of the aforementioned reactivity order of 2-oxazolines (Chapter 1.5 and 4.2), **1a** or **4a** were expected to be the most reactive compounds. Accordingly, as the first starting material, 2-cinnamyl-2-oxazoline (**1a**) was chosen exemplarily. Since MeOTf is more reactive as compared to MeOTos, MeOTf was prioritized as the initiator in the first place. Initially, the amount of initiator aimed for a degree of polymerization (DP) of 25, and a comparably high monomer concentration of 4 M in ACN was used. The polymerization was first attempted via the traditional heating method at 80 °C. Even after 6 days of reaction time, no conversion was determined via $^1$H NMR (Figure 9, A). The presence of the two 2-oxazoline triplets at $\delta$4.34 and $\delta$ 3.99 ppm showed the remaining monomer. Moreover, no poly(2-oxazoline) signal (~3.5 ppm, Figure 9, A) belonging to the backbone was monitored.

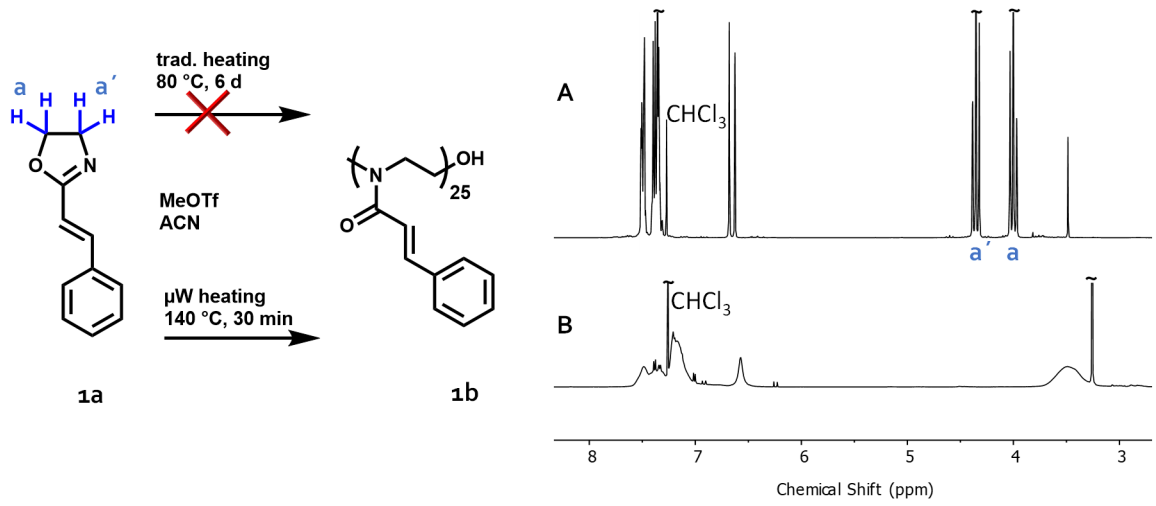


*Figure 9: Polymerization of **1a** via traditional heating at 80 °C (A) and microwave irradiation at 140 °C (B). The $^1$H NMR spectrum (A) showed even after 6 days reaction time only signals related to the monomer **1a**, thus no conversion was monitored. B) For the microwave experiment, no signals related to the monomer were monitored and the specific proton signals of the POx-backbone at $\delta$3.5 ppm are visible.*

Since no conversion was observed with traditional heating, a reaction via microwave irradiation was conducted. The parameters concerning the concentration, initiator, and DP persisted regarding the above-mentioned polymerization reaction. The temperature was elevated to 140 °C and the reaction time was decreased to 30 min. During the reaction, the internal pressure increased to 9 bar with a respective reaction mixture volume of 1 mL in a 10 mL sealed reaction vessel. Thus, an upscaling of the reaction size was limited by the maximum internal pressure of 17 bar. After the reaction was completed, the mixture was cloudy thus precipitation was assumed. The $^{1}$H NMR spectrum (crude mixture) clearly showed depletion of the monomer as determined by the absence of the particular monomer triplets of **1a** at $\delta$ 4.34 and $\delta$ 3.99 ppm (Figure 9, B).

These experiments resulted in the following conclusions. First, traditional heating can be discarded in the very beginning, because even for the expected most reactive monomer in the group of **1a**-**7a** with the more reactive initiator, no conversion was monitored. Second, the microwave irradiated reaction at 140 °C with a sealed vessel showed conversion, thus this method will be used further in this work. Third, the monomer concentration of 4 M was too high due to the observed precipitation of the formed polymer, therefore the concentration needed to be decreased. Fourth, the initiator was changed to MeOTos as it was less expensive and gave similar results during microwave irradiated reactions.

To determine the proper monomer concentration, three experiments with a monomer concentration of 3, 2, 1 M were conducted and checked visually for precipitation. For the concentration values of 3 and 2 M, precipitation of polymer **1b** was observed, yet not for the experiment with 1 M monomer concentration. Subsequently, due to comparability, all further polymerization experiments were conducted with a monomer concentration of 1 M. Consequently, the reaction parameters for the polymerization of the monomers **1a**-**7a** were set as follows: All reactions were conducted in a microwave reactor in ACN at 140 °C, with initial monomer concentration of 1 M and with MeOTos as initiator.

### 4.2.3 First homopolymer kinetic studies

Kinetic studies were performed to estimate the reactivity of newly synthesized monomers. The reaction parameters concerning method, solvent, temperature, and concentration were discussed above. Since NMR spectroscopy is more complex in sample preparation, the focus to determine the conversion was put on FT-IR spectroscopy. The IR spectrum can be recorded directly from the reaction mixture without the need for further sample preparation (see chapter 3.1).

The polymerization reaction mixture contains solvent, initiator, and monomer. To receive an individual monomer/polymer IR spectrum, the IR-background spectrum must include the chamber atmosphere, solvent (ACN), and the initiator. After subtracting this background spectrum, the FT-IR spectrum exclusively showed the monomer/polymer mixture without disturbing signals. This method is highly concentration sensitive, thus the same amount of reaction mixture was placed on the ATR-crystal to ensure comparability. The zero-time value was taken after reaching the desired reaction temperature. This was necessary as the polymerization might have been started during the heating procedure (ramping time). The ramping time varies between 90 and 105 s to reach the desired reaction temperature of 140 °C. It is worth mentioning that each sample came from an individual experiment, as each vessel could only be loaded with a 1 mL reaction mixture, was sealed by a septum, and kept closed during the reaction by an overpressure device. This makes it impossible to take a sample for monomer conversion analysis. Finally, the conversion for **1a** was determined by integrating the normalized IR-band at 911 $cm^{-1}$ (Figure 10), which was assigned to the 2-oxazoline ring breathing vibration.

For $[\mathbf{1a}]_0/[MeOTos]_0 = 25$, in ACN at 140 °C almost quantitative conversion was reached within 1 min reaction time (Figure 10). The SEC traces showed polymer with an apparent number-average molar mass ($M_n^{app}$) of 3.3 kDa for a reaction time of 1 min and 3.6 kDa for 2 mins. This value differs slightly from the targeted value of $M_n^{calc}$ = 4360 kDa, which was attributed to the calibration with polystyrene standards. The dispersity index (Đ), as determined by SEC, increased from 1.19 (1 min) to 1.21 (2 min).

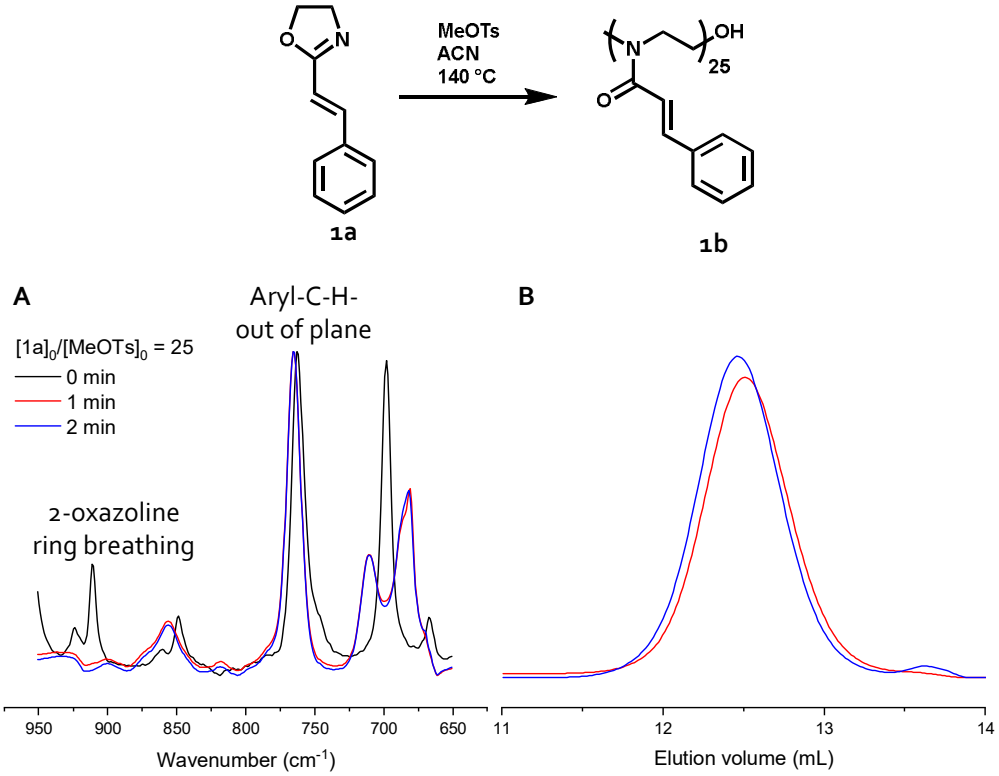


*Figure 10: A) IR-spectra to determine the monomer conversion of **1a** via the decrease of the ring breathing vibration of the monomer **1a**. B) SEC traces of polymer **1b** were obtained after 1 and 2 min.*

The reaction with monomer **1a** showed almost quantitative conversion after 1 min. These reaction conditions were maintained regardless that **1a** was assumed to be the most reactive monomer in the matrix. These established methods were used in this work further for polymerization and analytics.

### 4.2.4 Homopolymer kinetic studies at high temperatures

**1a** was successfully used as a model to set up the reaction parameters and the method for the determination of the monomer conversion. Amongst **1a,** the other cinnamyl monomers **2a** and **3a,** as well as **5a** and **6a,** were examined (Scheme 17). Since **1a** was the non-substituted 2-oxazoline within the cinnamyl-2-oxazoline monomer matrix (**1a**-**3a**), 2-phenyl-2-oxazoline (**8a**) was added to the 2-phenyl-2-oxazoline monomer matrix consisting of the di- and tri-methoxy substituted 2-phenyl-2-oxazolines **5a** and **6a**. It is worth noticing that **1a**-**3a, 5a,** and **6a** have not been used previously to synthesize polymers, except a long alkyl chain derivative of **5a**.[133]

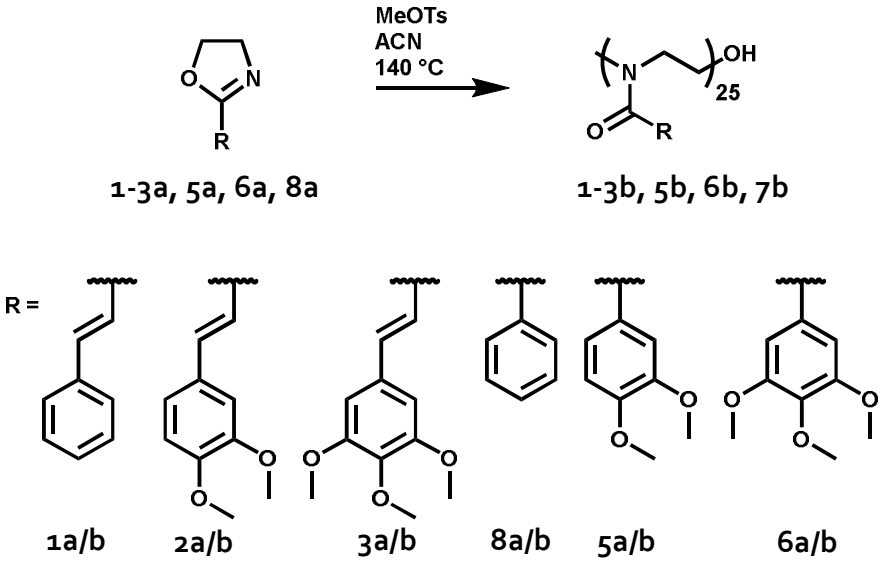


*Scheme 17: Microwave-assisted CROP at 140 °C, in ACN of the monomers **1a**-**3a**, **5a**, **6a**, and **8a**.*

Despite the reaction rate at 140 °C for **1a** was fast, the experimental conditions were maintained at 140 °C since the reaction rate of **5a, 6a,** and **8a** was expected lower (see chapter 1.5). The monomer to initiator ratio was 25 and the initial monomer concentration was 1 M. The conversion was determined via integrating the decreasing value of the normalized 2-oxazoline ring breathing band located between 900-1000 $cm^{-1}$

of the respective FT-IR spectra. Exemplary the relevant FT-IR spectrum section of **5a** and the decrease of the corresponding signals with proceeding time is shown in Figure 11. FT-IR spectra for the homopolymerizations of **1a**-**3a**, **6a**, and **8a** are shown in chapter 8, Figure S 17 - Figure S 19, Figure S 22, and Figure S 24.

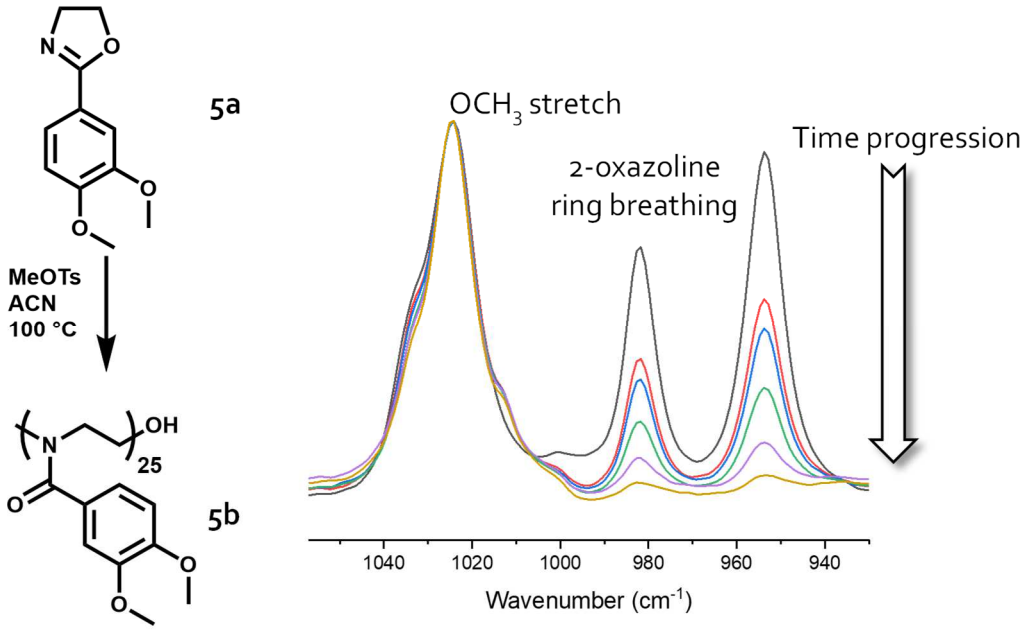


*Figure 11: Exemplary IR-spectra of **5a**, with focus to the relevant section, show the 2-oxazoline ring breathing bands at 980/950 cm$^{-1}$. These spectra were recorded by measuring the crude reaction mixtures at specific reaction times (0-16 min).*

The kinetic study revealed for **1a** 98% of conversion after 1 min, **2a** reached 98% of conversion after 2 min, and **3a** 92% of conversion after 4 min. In contrast, the 2-phenyl-2-oxazolines **5a**, **6a**, and **8a** all have reached 90% of conversion after a longer reaction time. A similar trend is discernible since **8a** did reach a conversion of 97% after 8 min and a comparable value for the methoxy derivatives **5a** (98%) and **6a** (97%) was recorded after 16 min (Figure 12, A). It is noteworthy that the reaction rates from **1a** to **3a** dropped by an approximate factor of 0.5. For **5a**, **6a** and **8a**, a similar behavior was only partly notable: There is a factor 2 only between the substituted (**5a**, **6a**) and the unsubstituted (**8a**) species. This showed a similar reaction rate of the di- and trimethoxy-2-phenyl-2-oxazolines **5a** and **6a**.

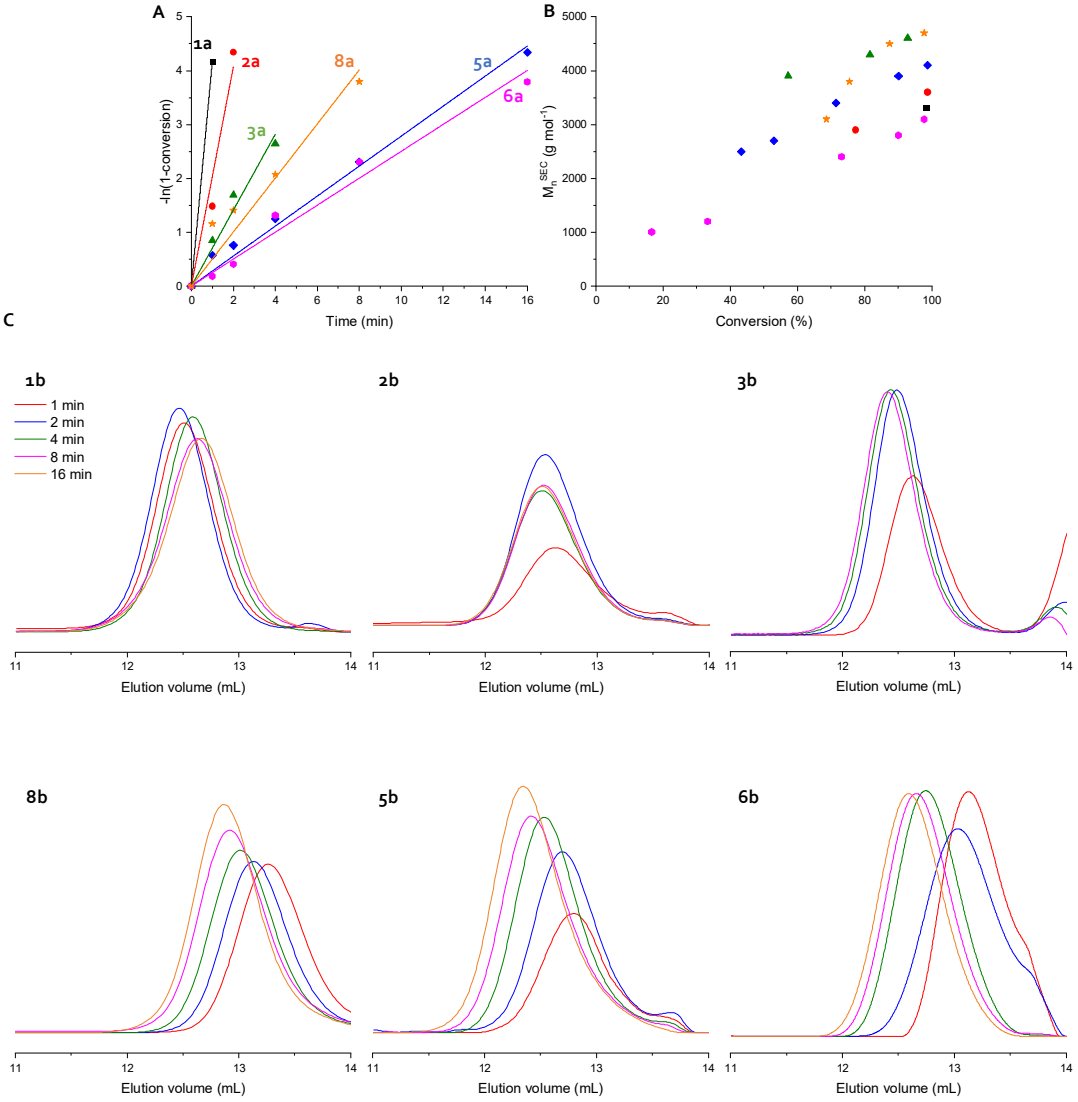


*Figure 12: Kinetic study of (di-/trimethoxy)-2-cinnamyl-2-oxazolines* ***1a-3a*** *and (di-/trimethoxy)-2-phenyl-2-oxazolines* ***5a***, ***6a***, ***8a*** *in 1 M ACN solution, at 140 °C, [Monomer]o/[MeOTos]o = 25. A) First-order time-conversion plots of the microwave-assisted CROP. B) Evolution of the apparent molar mass ($M_n^{SEC}$) with monomer conversion. C) SEC traces of the crude reaction mixtures after specific reaction times.*

This lower rate of polymerization might be referred to the mesomeric effect (+M) of the methoxy substituents at the phenyl moiety. The +M effect seemed to increase the nucleophilicity of the monomer, but it might decrease the electrophilicity of the active oxazolinium chain end. The polymerization rate difference between the 2-cinnamyl- (**1a**-

**3a**) and 2-phenyl-2-oxazolines (**5a, 6a, 8a**) seemed to be attributed to the more aliphatic character of the cinnamyl compounds (**1a**-**3a**), despite the aromatic π-system is connected via conjugation to the 2-oxazoline ring. The polymerization rate of **1a** was eight times faster than that of **8a** with due to the alkene spacer within the 2-cinnamyl-2-oxazoline unit. This shift to aliphatic properties (considering the proposed reaction rate of 2-oxazolines, chapter 4.2), seemed to be the major reason for the accelerated polymerization rate of the 2-cinnamyl-2-oxazolines (**1a**-**3a**) compared to the 2-phenyl-2-oxazolines (**5a, 6a, 8a**). The reaction rate gradient among the matrices themselves was related to the methoxy substituents and their +M effects. However, the similarity of the reaction rates of **5a** and **6a** cannot be rationalized yet.

The monitored first-order kinetics implied a constant concentration of active chain ends with no termination reaction. The linear increase of the molar mass with increasing conversion excludes transfer reactions (Figure 12 B).

All SEC traces of the polymers **1b**-**3b, 5b, 6b,** and **8b** showed monomodal and narrow molar mass distributions with Đ of 1.2-1.3 (Figure 12 C), indicating that no side reactions during the polymerization process occurred.

The mass, determined by SEC ($M_n^{SEC}$), was supplemented by MALDI-TOF measurements ($M_n^{MS}$) (Figure 13 A, exemplarily shown for **1b** and **6b**; for spectra of **2b**, **3b**, **5b**, and **8b** see chapter 8, Figure S 26 - Figure S 29). The corresponding data were summarized in table 2. The MALDI-TOF spectra showed the homologous series of polymers **1b**-**3b, 5b, 6b,** and **8b** attributable to potassium adducts $[M+K]^+$. The homologous series showed the expected mass of the repeating unit and the additional end group mass, related to methyl and hydroxyl groups (Scheme 17). Beside a major homologous series, the spectra showed one or more minor homologous series. One series that all spectra intrinsically showed, was related to the proton-initiated species $[M+K]^+$-14 Da. This proton-initiated series originated from traces of water or chain transfer reactions (discussed in chapter 4.2). The proton-initiated chains resulted in 14 Da lighter polymer chains compared to the methyl-initiated species.

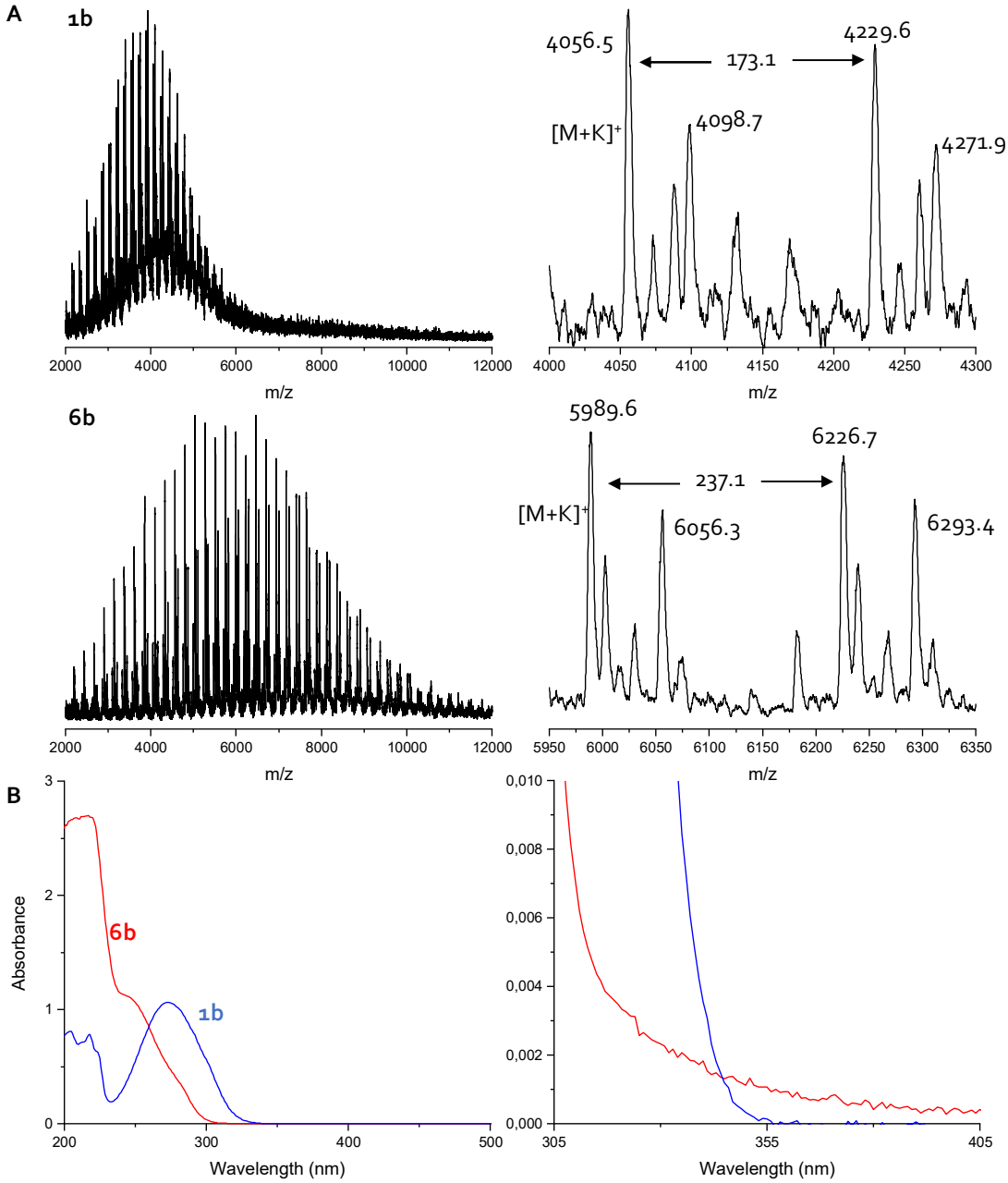


*Figure 13: A) MALDI-TOF mass spectra of polymers **1b** and **6b** showing the homologous series of the corresponding repeating unit as potassium adduct $[M+K]^+$. More homologous series occur in the spectra since the fragmentation of the polymers caused by the laser UV-light (355 nm) happened. B) UV-spectra of the polymers **1b** and **6b** showed absorbance at the laser wavelength of 355 nm.*

**1b** and **6b** showed an additional homologous series that can be related to a polymer fragment, lacking a single side chain (Figure 13). Previously, it was hypothesized that during the microwave-assisted polymerization process at 140 °C, an unidentified side reaction occurred.[122] However, it was found that the observed lack of a side chain was potentially caused during the MALDI-TOF MS measurement as the laser UV-light (λ = 355 nm) was directly absorbed by the polymers. This was proven by recorded UV-spectra (Figure 13, B) of **1b** and **6b**, which showed absorbance at 355 nm for both the polymers.

Table 2: Summarized results of microwave-assisted CROP in a 1 M ACN solution, at 140 °C with a DP of $[Monomer]_0/[MeOTos]_0 = 25$ with the monomers **1a-3a, 5a, 6a, 8a**.

| | Time (min) | Conversion (%)[a] | $M_n^{calc}$ (kg mol$^{-1}$)[b] | $M_n^{app}$ (kg mol$^{-1}$)[c] | $M_n^{MS}$ (kg mol$^{-1}$)[d] | Đ[e] |
|---|---|---|---|---|---|---|
| **1a → 1b** | 32 | >99 | 4.3 | 3.7 | 4.6 | 1.2 |
| **2a → 2b** | 32 | >99 | 5.8 | 4.8 | 5.0 | 1.2 |
| **3a → 3b** | 32 | >99 | 6.5 | 4.4 | 5.0 | 1.2 |
| **5a → 5b** | 32 | >99 | 4.8 | 5.0 | 6.5 | 1.3 |
| **6a → 6b** | 32 | 97 | 5.9 | 4.2 | 5.7 | 1.3 |
| **8a → 8b** | 16 | >99 | 3.7 | 4.3 | 4.9 | 1.3 |

[a] Conversion was determined by IR-spectroscopy. [b] Calculated molar mass for a DP of 25 with the addition of 32 kg mol$^{-1}$ for end group mass. [c] Apparent number-average molar mass determined by SEC. [d] Number-average molar mass, determined by MALDI-TOF MS. [e] Dispersity index, determined by SEC.

Thus, with the above-mentioned polymerization conditions, the monomers **1a**-**3a**, **5a**, **6a**, and **8a** were successfully polymerized and analyzed via SEC, MALDI-TOF-MS, and $^1$H NMR spectroscopy (see Chapter 8, Figure S 17 - Figure S 22, Figure S 24, Figure S 26 - Figure S 29). The kinetics study revealed that the 2-cinnamyl-2-oxazolines **1a**-**3a** had higher polymerization rates (>90% conversion after up to 4 min) than the 2-phenyl-2-oxazolines **5a**, **6a**, and **8a** (>90% conversion after up to 16 min). This difference was attributed to the more aliphatic character of **1a**-**3a** compared to **5a**, **6a**, and **8a**. However, the polymerization rate might be slowed down by decreasing the temperature to acquire more control over the polymerization. Therefore, the reaction temperature was decreased to 100 °C and the reaction rates were examined under these changed conditions.

### 4.2.5 Homopolymer kinetic studies at lower temperatures

In the previous chapter, the polymerization kinetics of the monomers **1a**-**3a**, **5a**, **6a**, and **8a** at 140 °C were examined. Since the polymerization rates were fast (98% conversion after 1 min for **1a**), the reaction temperature was lowered to gain more control about the behavior of the reaction, while all other parameters remained equal (Scheme 18). The subsequent increase of the reaction time decreases the effect of the mentioned ramping time, as the time taken to reach the desired temperature of 100 °C lowered to about 1 min. The zero-point for the kinetic study was set yet again after reaching the desired reaction temperature. Besides the already mentioned monomers, the 2-oxazolines **4a** and **7a** will be considered under these conditions as well. **8a** was not examined as its polymerization is well known.[62]

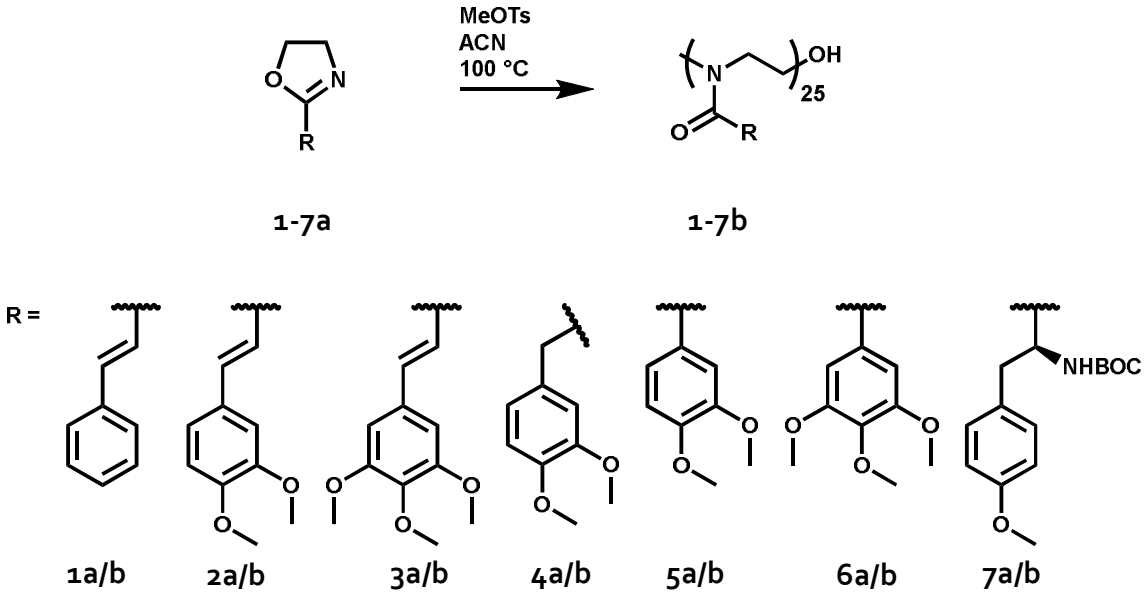


*Scheme 18: Microwave-assisted CROP at 100 °C, in ACN of the monomers **1a**-**7a**.*

The time-conversion plot for the polymerization at 100 °C showed a drastic reaction rate decrease (Figure 14, A). The linear increase of the molar mass with increasing conversion excludes transfer reactions (Figure 14, B). At 140 °C, **1a** showed 98% of conversion after 1 min, yet at 100 °C just after 64 min, **1a** reached a conversion of 98%. The reaction rate

decreases within the polymer matrix followed the same order at 100 °C as at 140 °C. The unsubstituted monomer **1a** still reacted faster than the substituted monomers **2a** and **3a**. **3a** showed an even slower reaction rate following the formerly discussed influence of the +M effect caused by the methoxy substituents. The phenyl monomers **5a** and **6a** acted in the same manner since the reaction rate of **6a** was slower than that of **5a**.

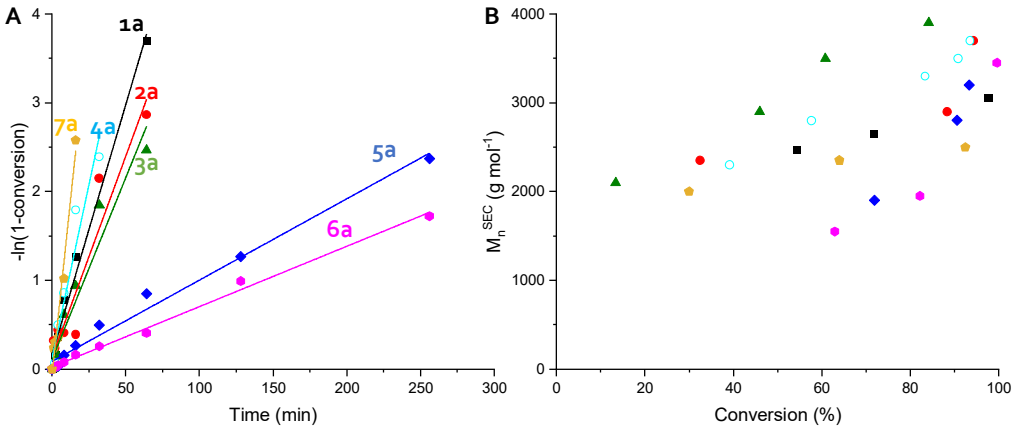


*Figure 14: Kinetic study of monomers **1a**-**7a**. A) First-order time-conversion plots revealed the reaction rates and the living character of the microwave-assisted CROP. B) Evolution of the apparent molar mass ($M_n^{SEC}$) while conversion progressed.*

Noteworthy the reaction rate of **4a** was similar or even slightly faster than that of **1a-3a**. Comparing **2a** and **4a**, which have the same substitution pattern of methoxy moieties, **4a** was faster than **2a**. It seems that the methylene spacer between the aromatic moiety and the 2-oxazoline ring of **4a** shields the 2-oxazoline ring, respectively the active oxazolinium species, to some extent against the +M effect.

Yet, **7a** appeared to polymerize even faster than **4a**. The BOC-protected amine might be influenced by an -I (inductive) effect, increasing the electrophilicity of the active oxazolinium chain end slightly, leading to a reaction rate increase. However, the $M_n^{SEC}$ was unexpected low ($M_n^{SEC}$ = 2.5 kDa vs $M_n^{calc}$ = 8.0 kDa). Although $M_n^{SEC}$ can not be seen as an absolute value, this deviation seems to be too high.

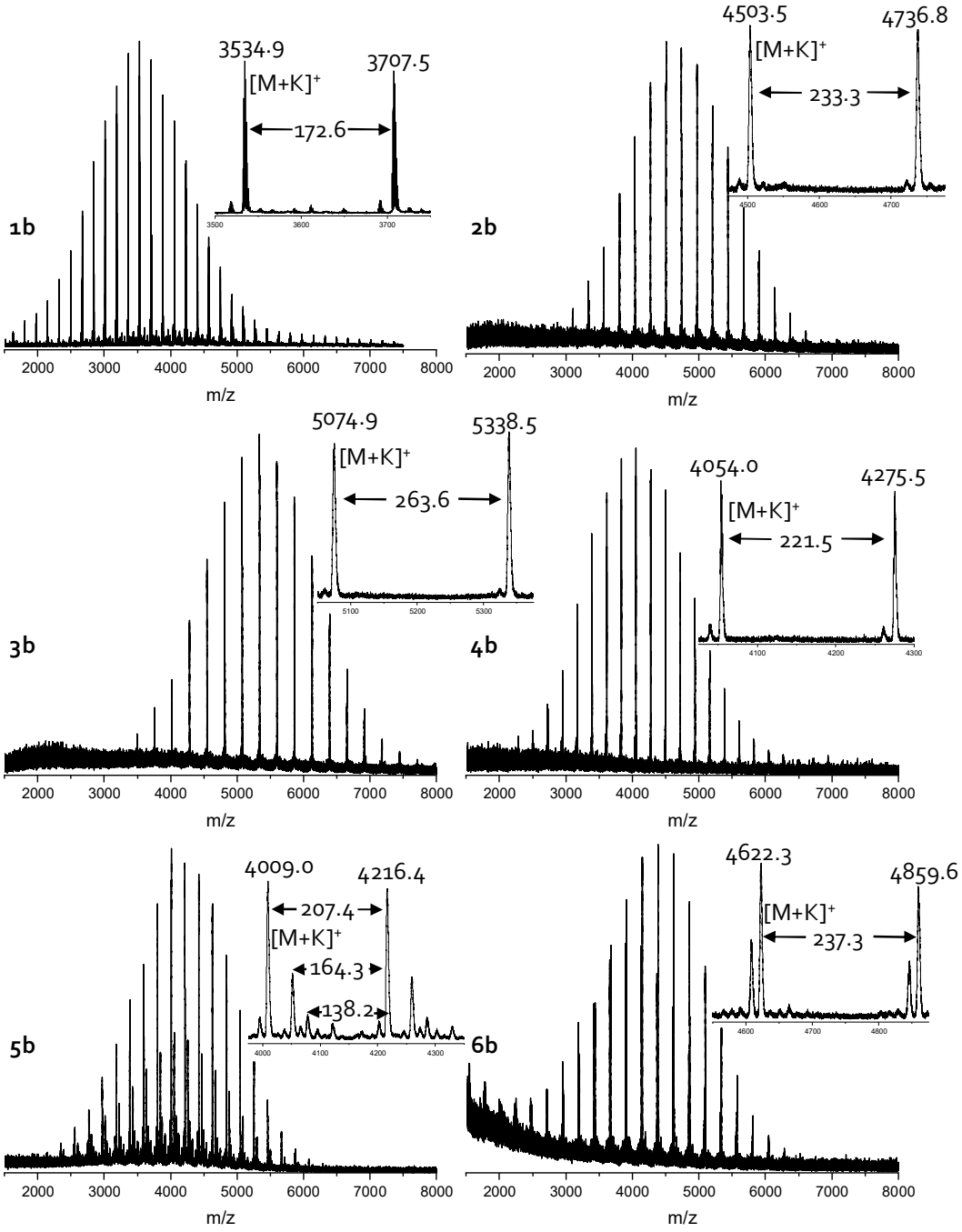


*Figure 15: MALDI-TOF MS spectra of the homopolymers **1b**-**6b** show the homologous series respectively. Every spectrum show at least traces of proton-initiated polymers by minor series related to $[M+K]^+$-14. Additional minor series within the spectrum related to **5b** show a decomposition by lacking a side chain due to laser irradiation during the ionization process by the MALDI-TOF measurement.*

MALDI-TOF MS measurements could have provided data for potential proton initiation or chain transfer reactions as already mentioned and seen in other spectra (Chapter 4.2.4). Unfortunately, no MALDI-TOF spectrum could be recorded. As mentioned previously (Chapter 4.2.4), the polymers can decompose during the MALDI-TOF ionization process by the UV-laser ($\lambda$ = 355 nm). This could have been a reason for the not quantifiable MALDI-TOF MS spectrum of **7b**. The recorded UV spectrum, however, did not show absorbance in the region of 355 nm (see Chapter 8, Figure S 30). Yet, the unexpected low SEC measured mass of **7a** ($M_n^{SEC}$ = 2.5) can not be verified by MALDI-TOF MS and a reason for that was not found yet. The polymers **1b**-**6b s**howed monomodal mass distributions with low dispersity of Đ = 1.2-1.3 (Chapter 8, Figure S 17 - Figure S 23). The mass determined by SEC ($M_n^{SEC}$) was supplemented by MALDI-TOF MS measurements ($M_n^{MS}$). The corresponding data were summarized in Table 3.

The MALDI-TOF mass spectra (Figure 15) showed the corresponding homologous series of the polymers **1b**-**6b** attributable to the potassium adducts $[M+K]^+$. The series showed the expected repeating unit and additionally the methyl/hydroxy end groups.

The homologous series of **1b**-**6b** again showed, one or more minor series beside the major series. All polymers showed the minor series $[M+K]^+$-14 Da, related to the proton-initiated polymers. This proton initiation was presumably caused by traces of moisture within the reaction mixture or by chain transfer reactions already mentioned in chapter 4.2.4 and discussed in chapter 4.2.

The primarily somewhat lower than targeted molar masses can be explained by this additional initiation of either moisture or chain transfer reactions (Table 3). Also, an instrumentation issue can be the reason for the lower measured masses, due to sample preparation and instrumental issues can have a significant impact on the measured $M_n^{MS}$.[134,135]

Moreover, **5b** showed a minor series, lacking the mass of a side chain caused by direct absorption of the laser UV light ($\lambda$ = 355 nm) as discussed previously (chapter 4.2.4).

Finally, the polymerization of monomers **1a**-**7a** at 100 °C was successfully conducted. Yet, a similar reaction rate trend at 100 °C and 140 °C was observed. **4a** though reacted

even faster than **1a** despite its methoxy substitution pattern comparable with **2a**. Thus, the accelerated reaction rate of **4a** seems to originate from a more alkyl character due to the methylene spacer between the aromatic and the 2-oxazoline moiety. Besides, the methylene spacer may increase the shielding of the 2-oxazoline/oxazolinium species from the +M effect related to the methoxy groups, and thus lead to a higher reaction rate. Yet, **7a** was the monomer with the fastest reaction rate, presumably increased by the +I effect originating from the BOC-protected amine group. However, the SEC measured apparent molar masses were very low. Unfortunately, the molar masses cannot be confirmed via MALDI-TOF MS measurements. Hence, it can be concluded that the monomers **1a**-**7a** are polymerizable under different conditions. Generally, the polymerization showed a living character, so that no transfer reaction was observable. The MALDI-TOF MS spectra however revealed proton initiation reactions; whether they result from traces of water or chain transfer reaction were not clarified yet. Additionally, it was demonstrated that all monomers can be polymerized at either 100 °C or 140 °C with low dispersity and mainly to the aimed molar mass. The related SEC traces, MALDI-TOF MS, and $^{1}$H NMR spectra can be consulted in chapter 8, Figure S 17 - Figure S 23.

*Table 3: Summarized results of microwave-assisted CROP in 1 M ACN solution, at 100 °C with a DP of $[Monomer]_0/[MeOTos]_0$ = 25 of the monomers **1a**-**7a**.*

| | Time (min) | Conversion (%)[a] | $M_n^{calc}$ (kg mol$^{-1}$)[b] | $M_n^{SEC}$ (kg mol$^{-1}$)[c] | $M_n^{MS}$ (kg mol$^{-1}$)[d] | Đ[e] |
|---|---|---|---|---|---|---|
| **1a** → **1b** | 64 | 98 | 4.3 | 3.0 | 4.0 | 1.2 |
| **2a** → **2b** | 128 | 99 | 5.8 | 3.5 | 4.7 | 1.2 |
| **3a** → **3b** | 128 | 97 | 6.5 | 4.1 | 5.4 | 1.2 |
| **4a** → **4b** | 64 | 94 | 5.3 | 3.7 | 4.1 | 1.2 |
| **5a** → **5b** | 480 | 93 | 4.8 | 3.2 | 4.2 | 1.3 |
| **6a** → **6b** | 480 | 99 | 5.9 | 3.5 | 4.3 | 1.2 |
| **7a** → **7b** | 16 | 95 | 8.0 | 2.5 | - | 1.2 |

[a] Conversion was determined by IR-spectroscopy. [b] Calculated molar mass for a DP of 25 with the addition of 32 kg mol$^{-1}$ for end group mass. [c] Apparent number-average molar distribution determined by SEC. [d] Number-average molar mass, determined by MALDI-TOF MS. [e] Dispersity index, determined by SEC.

This cumulative data about the new monomers opens the path towards more application-drawn polymers: As mentioned above, this work aimed to mimic mussel proteins by synthesizing adsorbing polymers to functionalize surfaces and examine their properties. These adsorbing polymers certainly cannot originate from the synthesized homopolymers **1b**-**8b** since they were simply not water-soluble. A further reason was the mole fraction of catechol-carrying units within the polymer. In chapter 1.3 was outlined, that the adsorption performance does not increase with the number of catechols. Mussels use 2-30% catechol units within their glue proteins. Yet the surface interacting proteins usually carry 10-30 mol% gluing units.[136] However, even if not the above-synthesized homopolymers, but copolymers can comply to this requirement. As 2-oxazolines usually are co-polymerizable, the amount of comonomers is limited by the properties and not by the method. 2-ethyl-2-oxazoline (**9a**) was, as mentioned in chapter 2, a proper comonomer. The following chapter thus will discuss the copolymerization of different new monomers with 2-ethyl-2-oxazoline (**9a**).

## 4.3 Copolymerization to yield water-soluble glue protein mimicking precursors

Considering maritime glue proteins, several properties are in common: They are water-soluble, carry catechol, and usually cationic units. Most of the above newly synthesized monomers, discussed in chapters 4.1.3 and 4.1.4, carry protected catechol or pyrogallol moieties. The corresponding homopolymers however were not water-soluble at all. Additionally, within the homopolymers, the number of catechol-containing units would be too high, regarding the investigations of naturally occurring glue proteins which usually carry 2-30% catechol units (Chapter 1.1). These issues can be avoided by copolymers, whereby the second comonomer should give water-soluble polymers. 2-Ethyl-2-oxazoline (**9a**) was a proper option as it is a well-known monomer, used for several applications with appropriate properties: Poly(2-ethyl-2-oxazoline) (PEtOx, **9b**) is soluble in water and polar organic solvents, has high thermal stability, and enhances the adsorption on organic and inorganic surfaces.[137] Furthermore, PEtOx (**9b**) has

moderate cytotoxicity, comparable to poly(ethylene glycol) (PEG), which is already used and well-proven in a medical context.[138] Advantageously, PEtOx (**9b**) is highly stable which is important for physicochemical applications.

The copolymerization of EtOx (**9a**) with the different comonomers **1a**-**8a** will be examined. The composition of maritime glue proteins is more or less statistical.[136] This allowed the simultaneous addition of both comonomers as no block-like polymer structure was required. Due to different comonomer reactivities, kinetic studies were conducted to determine the respective copolymer composition. The established homopolymerization reaction conditions were used in the following copolymerization reactions. Initially, a brief examination of 2-ethyl-2-oxazoline (**9a**) as a monomer was necessary. After that, the copolymerization of **9a** with different monomers from the matrix, **1a**-**8a** will be discussed.

### 4.3.1 2-Ethyl-2-oxazoline as comonomer

A kinetic study of the homopolymerization of 2-ethyl-2-oxazoline (**9a**) to PEtOx (**9b**) was conducted under the previously established reaction conditions.

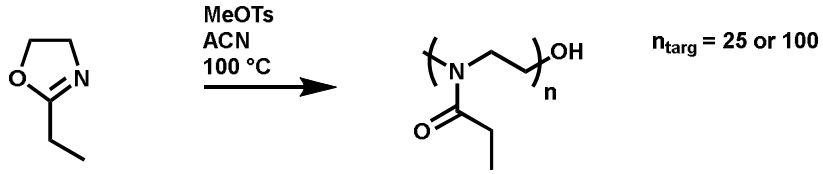


**9a** **9b**

*Scheme 19: Microwave-assisted CROP of 2-ethyl-2-oxazoline (**9a**) to yield PEtOx (**9b**).*

Initially, **9a** was polymerized in the same way as the monomers **1a**-**7a** previously (Chapter 4.2.5). Thus, the microwave-assisted CROP was conducted at 100 °C with a 1 M ACN solution with a targeted DP of $[\mathbf{9a}]_0/[MeOTos]_0$ = 25 or 100 (Scheme 19). The conversion was determined FT-IR-spectroscopy using the characteristic 2-oxazoline ring breathing vibration of **9a** between 890 and 918 $cm^{-1}$ (Chapter 8, Figure S 25).

The kinetic study revealed that the polymerization rate of EtOx (**9a**) with a DP of 25 under the mentioned conditions was comparable to the rate of **2a** (Figure 16). **5a** though had a dramatically lower reaction rate than **9a**. However, such a fast reaction rate of **9a** was expected. The DP = 25 of **9a** was used only for a comparing view to gain knowledge about the reaction rate with the same DP as monomers **1a**-**8a** were examined. However, later in this work, the DP of the copolymers will aim at a value of approximately 100. For that reason, a homopolymerization kinetics study of **9a** with a DP of $[\mathbf{9a}]_0/[MeOTos]_0$ = 100 was conducted. This higher DP was reasoned to keep the water solubility of PEtOx (**9b**) even for the prospective copolymers. Thus, the ratio of the two comonomers was shifted to the side of EtOx (**9a**), considering the mentioned mussels catechol group ratio of 2-30%.

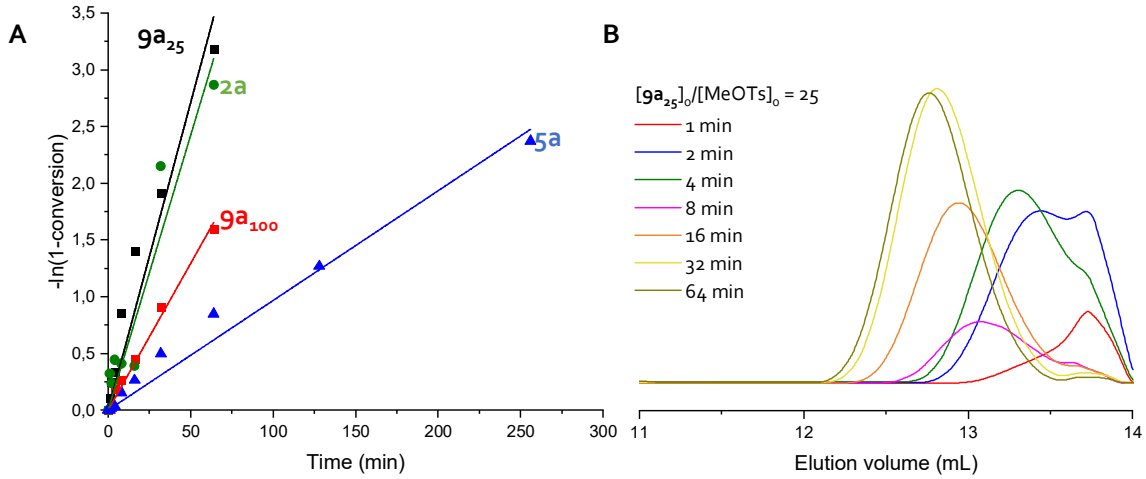


*Figure 16: A) Kinetic study of **9a** with DPs of $[\mathbf{9a}]_0/[MeOTos]_0$ = 25 or 100 at 100 °C in 1 M ACN solution. B) The SEC traces showed the hydrodynamic radius increase of $\mathbf{9a}_{25}$ within progressing reaction time.*

These results finally led to the following conclusions: The copolymerization of **9a** with the monomers with higher reaction rates like **1a**-**4a** and **7a** would presumably give more uniform copolymers. However, the monomers **5a**, **6a**, and **8a** would give more gradient-like copolymers. After all, it was indispensable to conduct individual copolymerization kinetic studies of **9a** with different desired monomers to clarify and confirm the prior assumption.

### 4.3.2 Copolymerization of methoxy containing 2-oxazolines and 2-ethyl-2-oxazoline

The chosen methoxy-containing monomers were **2a, 4a, 5a,** and **7a**. The comonomer mole fraction was first targeted to 10 mol% of methoxy-containing components **2a, 4a, 5a,** and **7a,** and to 90 mol% of **9a**. The microwave-assisted copolymerization was conducted under the established conditions with an overall monomer concentration of 1 M at 100 °C, with a targeted DP of $[\mathbf{9a}_{90}+(\mathbf{2a, 4a, 5a, 7a})_{10}]_0/[MeOTos]_0 = 100$ (Scheme 20).

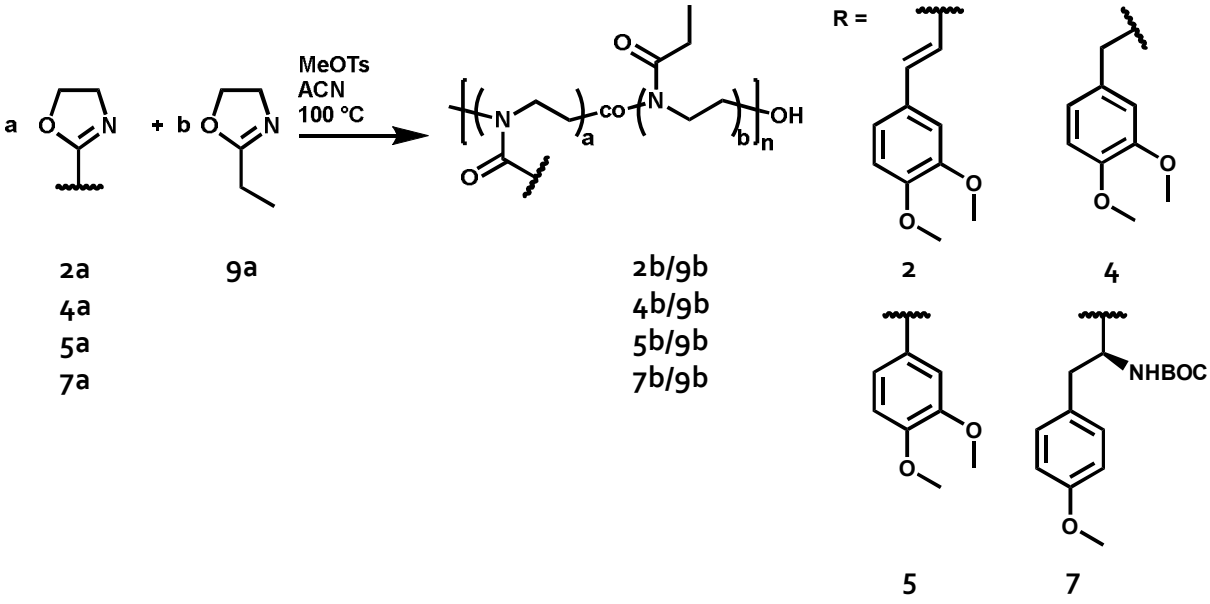


*Scheme 20: Microwave-assisted CROP of **9a** with the particular comonomers **2a**, **4a**, **5a**, and **7a**. **9a** was used with a mole fraction of 90 mol%. The aimed DP was $[\mathbf{9a}_{90}+(\mathbf{2a, 4a, 5a, 7a})_{10}]_0/[MeOTos]_0 = 100$.*

For the kinetics study, samples were taken at reaction times of 2-256 min, the ramping time (time to reach the desired reaction temperature) was set as zero. It is worth to remind, that each data point was one individual experiment, hence individual stock

solutions in proper concentrations of each monomer (**2a, 4a, 5a, 7a, 9a**) were prepared in advance to ensure comparability. The observation of the conversion during the homopolymerization was conducted by FT-IR spectroscopy due to the individual consideration of the respective 2-oxazoline ring breathing band located between 900 and 1000 $cm^{-1}$ (Chapter 4.2.3). Unfortunately, the ring breathing bands of the monomers **2a, 4a, 5a,** and **7a** were partly overlapping with those of **9a**, this made an appropriate independent observation impossible. Hence, FT-IR spectroscopy could not be used to determine the conversion during the copolymerization process. $^1$H NMR spectroscopy was used instead. In chapter 4.2.3, it was already mentioned that 2-oxazolines have two characteristic triplet signals between $\delta$4.5 and $\delta$3.5 ppm related to the methylene protons in 4 and 5 positions. Since these signals can be integrated individually, they can be used for the determination of the individual comonomer conversion. Unfortunately, **4a** did not give independent 2-oxazoline $^1$H NMR signals related to the methylene protons in 4 and 5 positions. The $\alpha$-methylene protons singlet signal at $\delta$3.49 ppm was shifted after the polymerization, thus it was used instead for **4a**. For the other monomers **2a, 4a,** and **7a,** the 2-oxazoline ring proton signals were used.

Since the crude reaction mixtures were used to determine the conversion, the termination of the reaction became an issue: Using the termination reagent (2 M KOH/$H_2O$/MeOH solution) the massive signals of $H_2O$ at $\delta$3.33 and MeOH at $\delta$3.16 would disturb the spectrum and proper integration would not be possible.[139] Thus, samples of the reaction mixture were quenched with wet deuterated dimethyl sulfoxide (DMSO-$d_6$), and the ACN signal at $\delta$ 2.07 ppm was used as the internal standard. This signal can be applied since the signal was independent and the comparability was kept due to the usage of stock solutions.

Figure 17 presents an exemplary kinetics study of the copolymerization of **2a** with **9a**. The $^1$H NMR spectra were recorded at specified reaction times as mentioned above. The additional $^1$H NMR spectra concerning the kinetic study of **4a**/**9a**, **5a**/**9a**, and **7a**/**9a** are shown in chapter 8, Figure S 35 - Figure S 38. The mole fraction of the value of the integral of the protons "a" and "a´" at 0 min reaction time amounted to 13% of **2a** and 87% of **9a**.

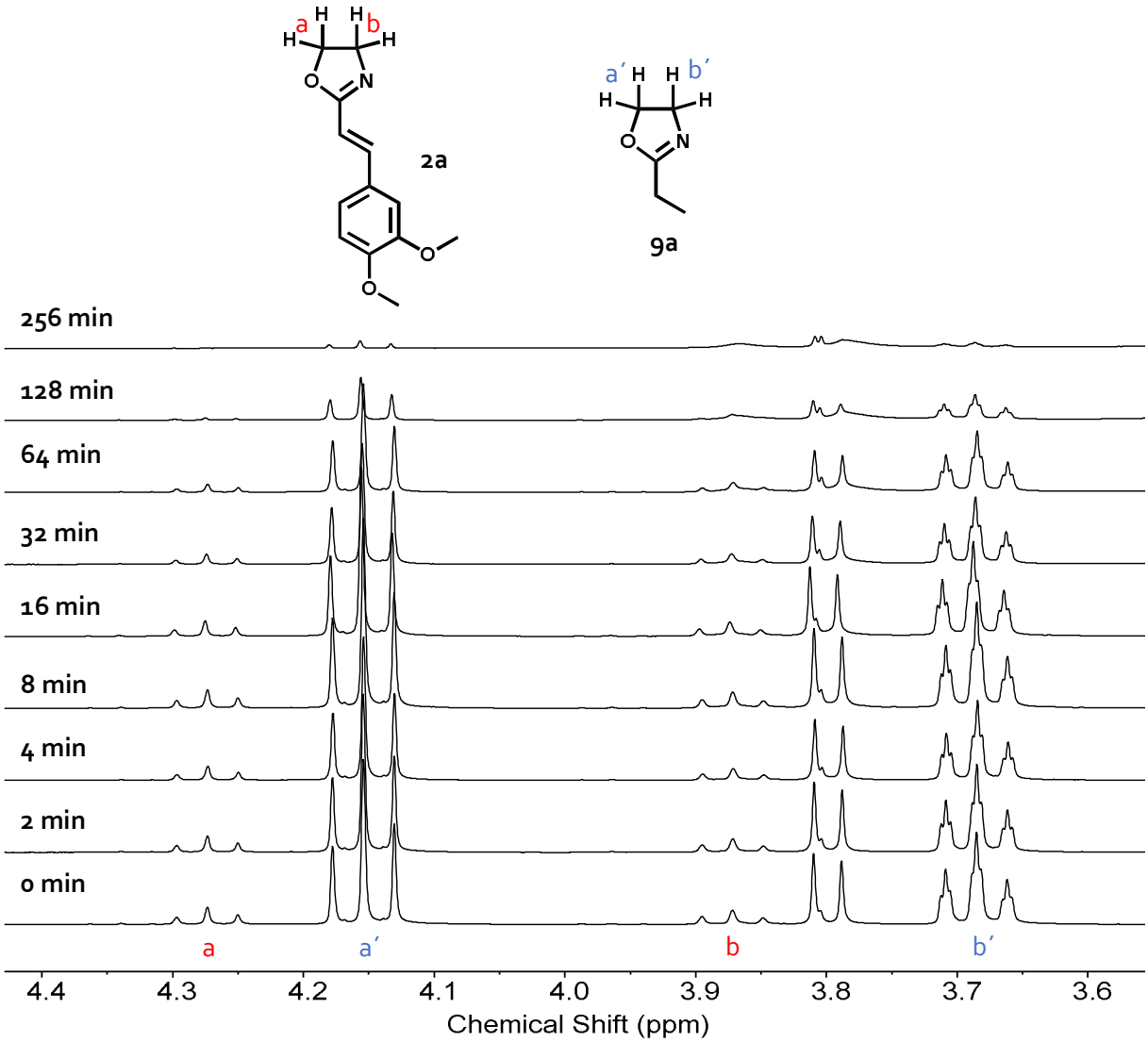


*Figure 17: $^1$H-NMR (300 MHz) spectrum zoomed into the specific 2-oxazoline ring proton area between δ3.5 and δ4.5 ppm. The spectra show the different starting concentrations at 0 min of **2a** and **9a**, and the decrease of the respective 2-oxazoline ring signals (**2a**: a, b; **9a**, a´, b´) during time progression.*

The slight deviation of the targeted 10% (**2a**) and 90% (**9a**) can be reasoned by the ramping time because the reaction might already have started. The reaction between the initiator (MeOTos) and **9a** was more probable due to the higher concentration of **9a**. Concerning different monomer concentrations, the addition of a new monomer **9a** to a copolymer chain end was more likely than the addition of **2a**. With the reaction

progressing the addition of **2a** became more likely. The conversion was calculated by this integral value of the 2-oxazoline ring proton signals "a" and "b" (**2a**) and "a´" and "b´" (**9a**). The integrals were normalized to the ACN signal (not shown in the zoom) at $\delta$2.07 ppm. Figure 18 A shows the corresponding plot of the respective conversions of **2a**/**9a** and the other monomer combinations **4a**/**9a**, **5a**/**9a**, and **7a**/**9a**. This presentation was chosen to point out that the consumptions of the respective monomers were different. The dotted line in Figure 18 A shows the hypothesized ideal azeotropic copolymerization behavior.

Certainly, none of the copolymerizations followed this ideal model. However, **2a**/**9a** seemed to follow an almost ideal azeotropic copolymerization, since the monomer consumptions of **2a** and **9a** were nearly the same over the reaction time. As the consumptions of **2a** and **9a** followed almost the ideal azeotropic reaction and no compositional drift was observed, it can be assumed that the copolymer composition **2b**/**9b** virtually resulted in a random copolymer.

Considering the combination of **4a**/**9a** and **7a**/**9a** the reaction was expected to be similar to that of **2a**/**9a** regarding the homopolymerization behavior. **4a**/**9a** showed, compared to **2a**/**9a** and **7a**/**9a**, a drift concerning the monomer composition. The consumption of **9a** was faster in early reaction stages compared to **4a**; over time progression the consumption of **4a** increased. This was supposedly reasoned by the slower cross-step from the oxazolinium chain end of **9b** to the monomer **4a**. For that reason, the copolymer **4a**/**9a** exhibits a gradient-like structure. **7a**/**9a** in total did not follow the ideal azeotropic behavior as **9a** was consumed faster than **7a**. Thus a gradient-like structure of **7b**/**9b** can be reasonably assumed. For **5a**/**9a**, a slower reaction of **5a** than **9a** was observed. This type of reactivity though was expected since the homopolymerization rate of **5a** was much slower than that of **9a** (see Chapter 4.3.1). During the copolymerization of **5a**/**9a**, the conversion of **9a** at 256 min reaction time was >95% and **5a** just reached 40%. Hence, the copolymer **5b**/**9b** seemed to result in a gradient-like structure at full monomer conversion.

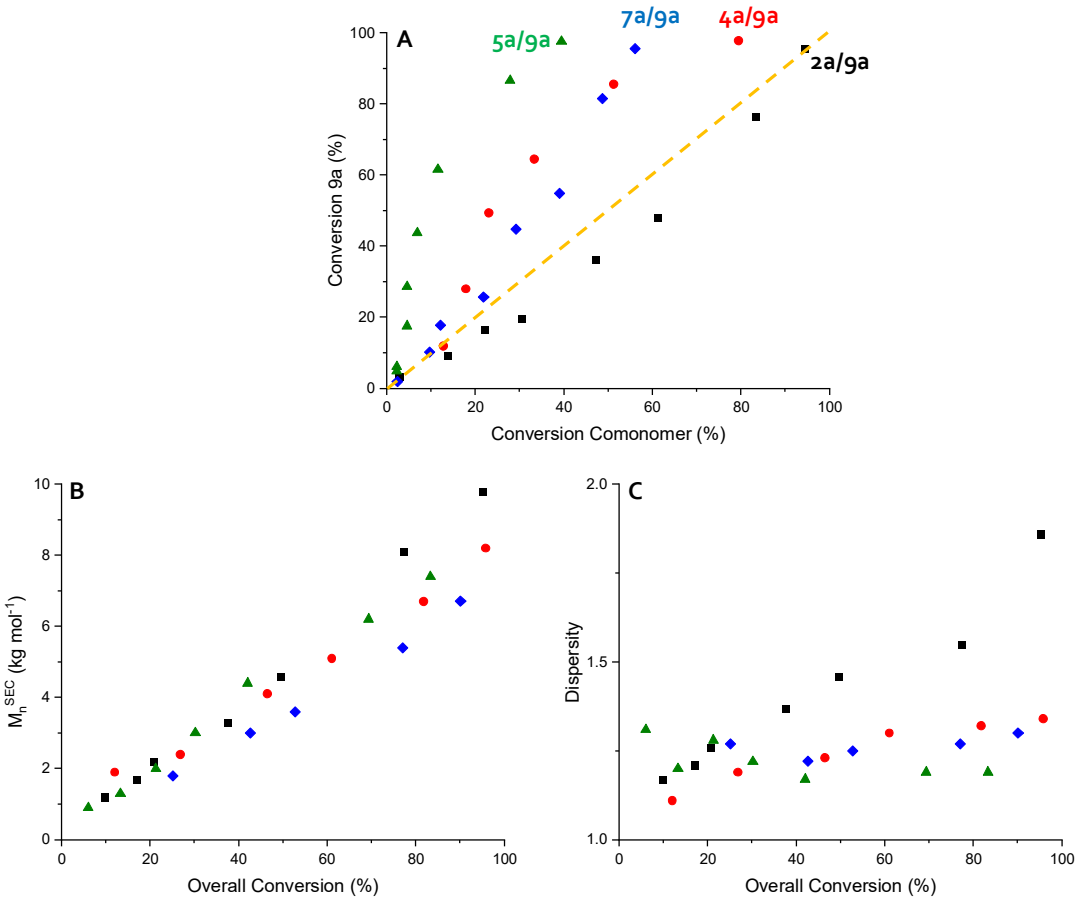


*Figure 18: Copolymerization study of the microwave-assisted CROcoP of **2a**, **4a**, **5a**, and **7a** with **9a** at 100 °C in ACN with a targeted DP of 100. A) Plot of the conversion of **9a** (y-axis) vs. the conversion of the comonomers **2a**, **4a**, **5a**, and **7a** (x-axis), determined by $^1$H-NMR spectroscopy. Plots of the $M_n^{SEC}$ (B) and Dispersity (C) of the copolymers **2b/9b**, **4b/9b**, **5b/9b**, and **7b/9b** vs. the overall conversion of both monomers.*

Considering the SEC data, $M_n^{app}$ (Figure 18, B) and the dispersity (Figure 18, C) of the copolymers during conversion progression needed to be discussed. $M_n^{app}$ increased linearly with monomer conversion for all monomer combinations except **2a/9a**. The $M_n^{app}$ for **2b/9b** at conversions above 50% shift to higher molar masses. The dispersity values of **4b/9b**, **5b/9b**, and **7b/9b** were between 1.1 and 1.3 and showed monomodal distributions (Figure 18, C; Figure 19). The dispersity of **2b/9b** though shifted from 1.2 (20% conversion) to 1.6 (77% conversion) and 1.9 (95% conversion) respectively. Besides,

the SEC traces did not show a monomodal, but a bimodal distribution at least at a conversion over 40% for **2b/9b** (Figure 19).

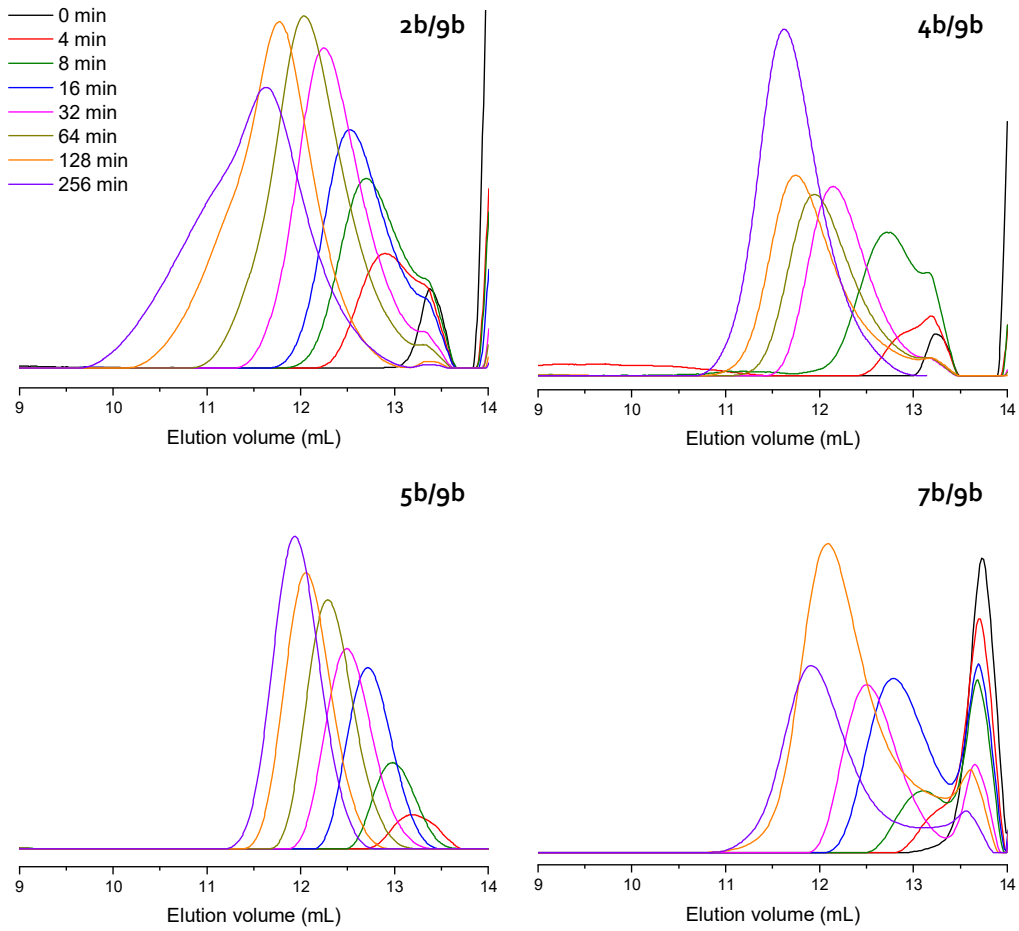


*Figure 19: SEC-traces of the copolymers **2b/9b**, **4b/9b**, **5b/9b** and **7b/9b** with a targeted DP and ratio of [**9a**$_{90}$/(**2a, 4a, 5a, 7a**)$_{10}$]$_0$/[MeOTos]$_0$ = 100. For three of the four copolymers the traces show consistently a monomodal distribution. For **2b/9b** above 40% conversion, the distribution showed up bimodal.*

This bimodal distribution for **2b/9b** indicated a side reaction during the polymerization process. The increasing dispersity showed that the side reaction occurred at conversions of 40% and higher. Since the three other combinations **4a/9a, 5a/9a,** and **7a/9a** did not result in any visible side reaction, it was assumed that the exocyclic double bond of the cinnamyl side chain was the reactive center for the side reaction. However, the

homopolymers **1b**-**3b** did not show any side reaction at all (confirmed by SEC, see Chapter 4.2.4 and 4.2.5) although they all carry the exocyclic cinnamyl double bond. To confirm the responsibility of the double bond for the side reaction during the copolymerization, copolymers **1b**/**9b** and **3b**/**9b** were produced under the same conditions as **2b**/**9b**. The respective SEC traces of **1b**/**9b** and **3b**/**9b** showed bimodal distributions (Figure 20, A), consequently, the exocyclic double bond most likely was responsible for this side reaction.

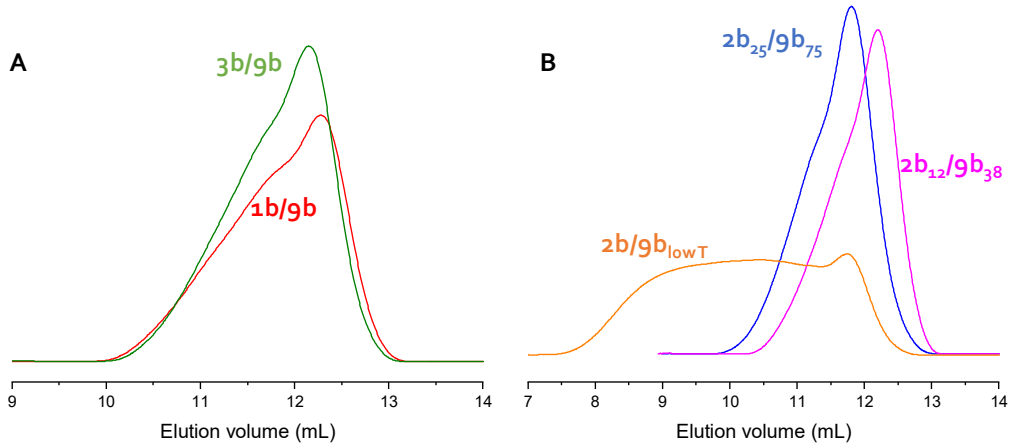


*Figure 20: SEC-traces showed bimodal distributions for the copolymerization of **9a** with different cinnamyl-2-oxazolines **1a**-**3a**. A) Copolymers **1b**/**9b** and **3b**/**9b** showed bimodal distributions as **2b**/**9b** did. This indicated that the exocyclic cinnamyl double bond was responsible for a side rection. B) Different approaches to avoid the side reaction via lowering the reaction temperature to 80 °C (orange), changing the targeted mole fraction of the comonomers (blue), and lowering the targeted DP from 100 to 50 (purple) resulted in similar bimodal distributions.*

To avoid the side reaction, several parameters were changed: the comonomer mole fraction was changed by increasing the number of cinnamyl units **2a**, the targeted DP was decreased from 100 to 50, and the reaction temperature was lowered to 80 °C (Figure 20, B). Still, the results were largely the same, at least each reaction resulted in bimodal SEC-traces. Furthermore, the presence of double bonds could make light-induced

reactions possible, however, this was unlikely since the reaction in the microwave was carried out in the dark anyway. To ensure any light-induced reaction, the quenching and SEC measurement were carried out in the dark, the result though was the same as in all experiments mentioned before.

By these results, the double bond of the cinnamyl unit was indirectly confirmed as one part of the side reaction. Yet, the homopolymerization did not show any side reaction (Chapter 4.2.4 and 4.2.5). Thus, comonomer **9a** had to be the responsible counterpart of this reaction. It is commonly accepted that 2-ethyl-2-oxazoline (**9a**) undergoes a side reaction, as a $\beta$-proton of an oxazolinium chain end initiates a new monomer which results in a ketene *N*, *O*-acetal (Chapter 4.2).[127] The side reaction during the copolymerization of **1a**-**3a** with **9a** presumably was caused by a reaction between this terminal ketene *N*, *O*-acetal, and the exocyclic cinnamyl double bond. To verify this assumption, instead of 2-ethyl-2-oxazoline (**9a**), 2-phenyl-2-oxazoline (**8a**) was used for the copolymerization since **8a** is not capable to form the ketene *N*, *O*-acetal (Scheme 21).

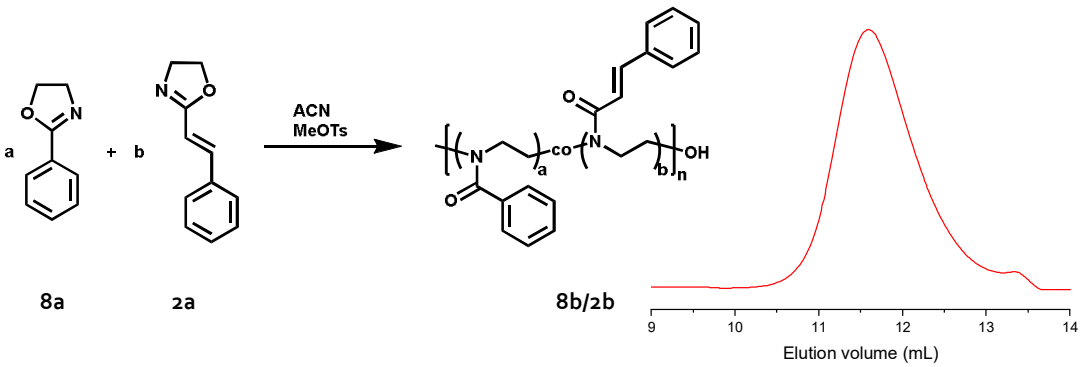


*Scheme 21: SEC-trace of the copolymer* ***2b₁₀/8b₉₀****. The monomer* ***8a*** *lacks a $\beta$-proton, hence the chain coupling effect can not occur and the possible formation of the ketene N, O-acetal was avoided. The SEC trace of this reaction showed monomodal distribution for the copolymer* ***2b₁₀/8b₉₀*** *providing indirect evidence for the responsibility of the ketene N, O-acetal concerning side reaction.*

The respective SEC trace showed monomodal distribution thus the side reaction did not take place and showed indirect evidence that the ketene *N*, *O*-acetal (of **9b**), and the exocyclic double bond undergo any side reaction. Since a [2+2] photocycloaddition can be ruled out, a Michael-type addition reaction was supposed to happen, supported by recent investigations of cinnamyl derivatives and their facility to perform Michael-type reactions.[140] A Michael-type addition with a cinnamyl side-chain carrying (co)polymer **III** (Scheme 22), with a ketene *N*, *O*-acetal (**II**) thus can be assumed. The ketene *N*, *O*-acetal potentially reacts as a nucleophile with the cinnamyl side-chain carrying (co)polymer **III** to give a chain coupling product **IV** and then **V**.

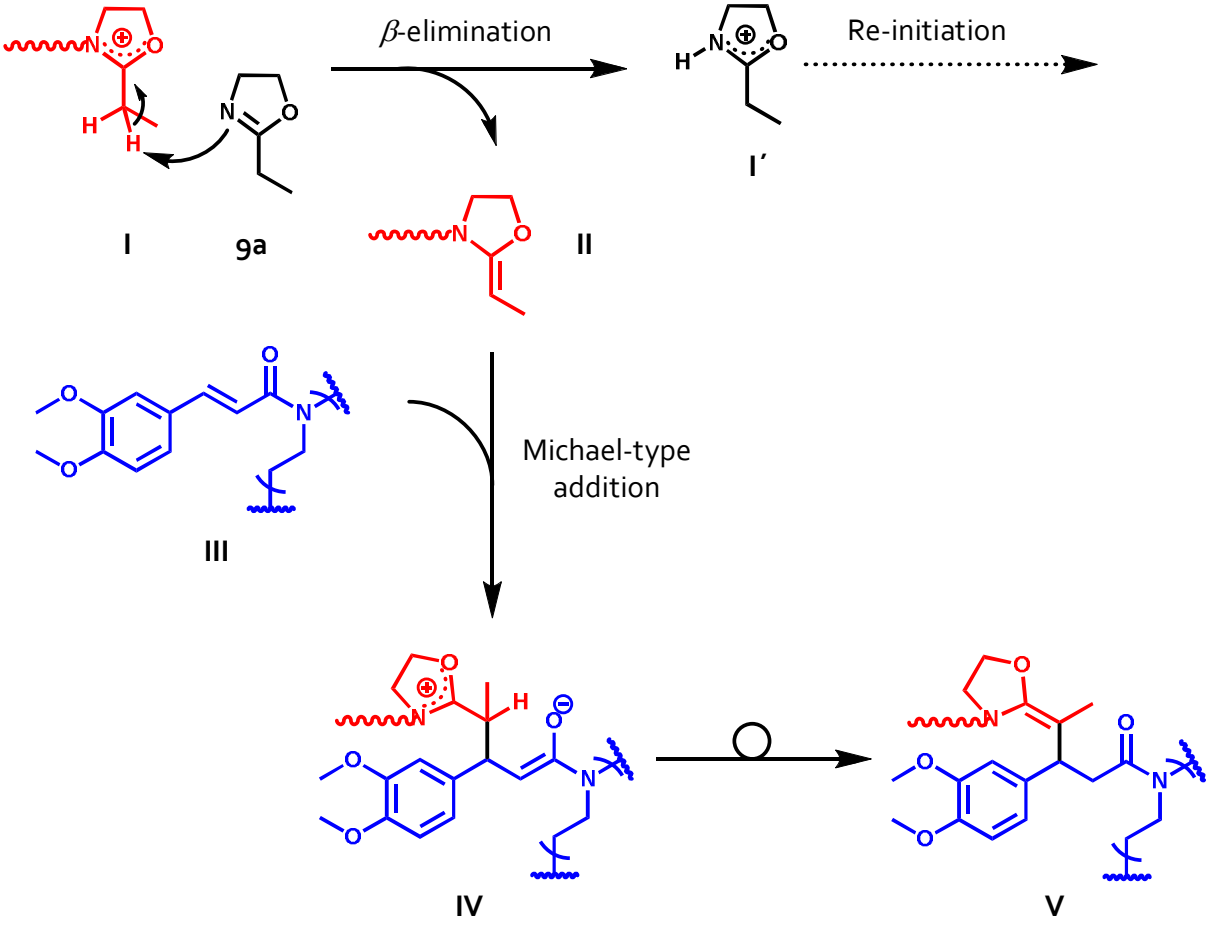


*Scheme 22: Chain transfer reaction via β-elimination, resulting in a ketene N, O-acetal (**II**). The ketene N, O-acetal (**II**) was supposed to undergo a Michael-type addition with the exocyclic double bond of the polymeric cinnamyl side-chain **III** to give a polymeric coupling product **IV** and **V** respectively.*

The coupling product **V** however could not be identified by $^{13}C$-, $^{1}H$ NMR or FT-IR spectroscopy. Hence, only indirect evidence supported this Michael-type addition reaction. However, all experimental indications pointed towards that proposal. Further experiments to enhance the indirect evidence were made: **9a** was homo-polymerized in the presence of cinnamyl nitrile which provided the Michael acceptor double bond. If any addition would have taken place, the respective polymer should bear aromatic units, visible in the UV signal of the SEC trace. The UV SEC trace though did not show any signal at all.

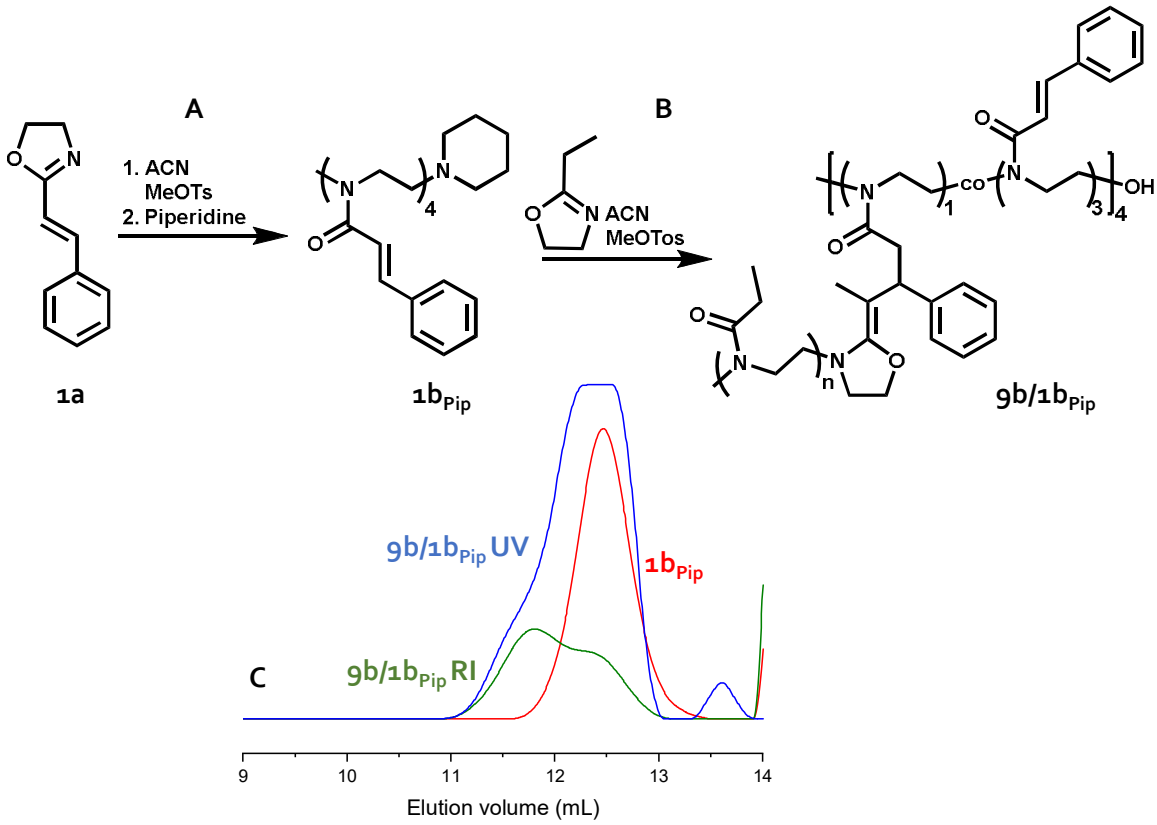


*Scheme 23: Attempt to confirm the Michael-type side reaction by polymerizing **9a** in presence of **1b$_{Pip}$** (A, B). **9b** showed a UV signal in the SEC after the reaction, indicating incorporation of **1b$_{Pip}$** with **9b**, the Michael-type reaction however was confirmed by neither NMR spectroscopy nor MALDI-TOF MS spectrometry.*

To simulate the reaction conditions and the Michael acceptor behavior better than with the above-considered nitrile, an oligomer **1b**$_{Pip}$ was produced (Scheme 23, A). The termination was conducted with dry pyridine to avoid the hydroxyl end group. Subsequently, **9a** was polymerized in presence of **1b**$_{pip}$ (Scheme 23, B). For that reason, the hydroxyl end group was substituted with piperidine, to prevent any reaction with the end group, without the participation of the **1b**$_{pip}$ double bond. If the product was **9b** no UV traces should be recorded by SEC. Yet, a UV signal appeared, which demonstrated incorporation of **1b**$_{Pip}$ in **9b** (Scheme 23, C). Unfortunately, the structure of the coupling product was not proven with either NMR spectroscopy or MALDI-TOF MS.

However, the occurring side reaction provides further indirect confirmation of the ketene *N, O*-acetal formation which was not proven yet. Moreover, the potential of the Michael addition at the cinnamyl double bond certainly opens the possibility of conducting various polymer modifications. The addition of an amine for instance would introduce a positive group in direct proximity to the catechol moiety. However, the prevention of the side reaction would be the condition for using the 2-cinnamyl-2-oxazolines **1a**-**3a** as monomers. The crucial issue remains as $\beta$-elimination is hardly avoidable. There are attempts to suppress the chain transfer reaction for instance by lowering the temperature to 40 °C and spending effort to increase the purity of the monomers to perfection.[141] The authors showed a ten times lower chain transfer coefficient, yet, the chain transfer reaction was not entirely prevented, thus the Michael addition can occur at that low temperatures as well. As a result, the presence of the $\beta$-proton keeps being the relevant factor. Sterically hindrance within the 2-isopropyl-2-oxazoline showed promising results concerning chain coupling prevention which makes it a promising comonomer to replace **9a**.[142] Besides, poly(2-isopropyl-2-oxazoline) still is a water-soluble substance keeping the requirements for the maritime glue protein mimics in mind. This work though will keep 2-ethyl-2-oxazoline (**9a**) as a comonomer. The possibilities and options of changing the comonomer and the possible advantages of the Michael addition at a double bond will be mentioned in Chapter 5.

Despite the side reaction of **1a**-**3a** with **9a,** the other comonomers **4a**, **5a**, and **7a** were successfully copolymerized in narrow distributions and without any identified side

reaction. The corresponding copolymerizations were controlled and gave well-defined copolymers. Kinetic studies revealed that the comonomers **2a**/**9a** followed an almost azeotropic behavior which presumably gave the virtually random statistical copolymer **2b**/**9b**. Although, due to the observed side reaction, **2b**/**9b** was not used in this work further. **5b**/**9b** exhibits a gradient structure since the consumption of **9a** was much faster than that of **5a**. **4b**/**9b** and **7b**/**9b** both exhibit gradient-like structures as well. Due to faster consumption of either **4a** and **7a**, the gradient was less strong compared with that of **5b**/**9b**. However, the architectural different copolymers made them independently interesting for further investigations concerning their performance on surfaces after releasing the catechol units.

Since the copolymers **4b**/**9b**, **5b**/**9b**, and **7b**/**9b** were successfully produced, in the next section the post-polymerization modification of these copolymers, including the deprotection of the catechol units and the following introduction of positive groups by partial hydrolysis, will be discussed.

## 4.4 Post-polymerization modifications

The copolymers **4b**/**9b**, **5b**/**9b**, and **7b**/**9b** create a promising platform to obtain various possible catechol-containing copolymers. These (co)polymers were examined considering their copolymerization behavior in the previous chapter 4.3.2. Previously it was described that the catechol and cation units are responsible for the adhesive properties of the mussel proteins (Chapter 1.1-1.3). The first aim thus was to release the catechol units of the copolymers by post-polymerization modification via aryl methyl ether cleavage. Usually, Lewis acid reagents like boron or aluminum halides were used for the methyl ether cleavage.[143,144] Sang *et al.* developed a method for the aryl methyl ether cleavage using aluminum triiodide ($AlI_3$) in presence of *N*, *N´*-diisopropyl carbodiimide (DIC).[145,146] They reported even for compounds containing carboxylic acids and amides up to quantitative yields. The tolerance of the reaction concerning the presence of amides was crucial as each repeating unit within poly(2-oxazoline)s contains

an amide group. Besides, the used solvent was ACN, which already showed the solvency capacity towards (co)poly(2-oxazoline)s during the polymerization reactions. For those reasons, this method was chosen. Initially, the method was tested with the homopolymer **5b**, which is discussed in the following chapter.

### 4.4.1 Methyl aryl ether cleavage of poly(2-dimethoxy phenyl-2-oxazoline)

Methyl aryl ethers can be cleaved with $AlI_3$ in presence of DIC in ACN. The homopolymer **5b** was used (Figure 21, A) to test this particular reaction with poly(2-oxazoline)s.

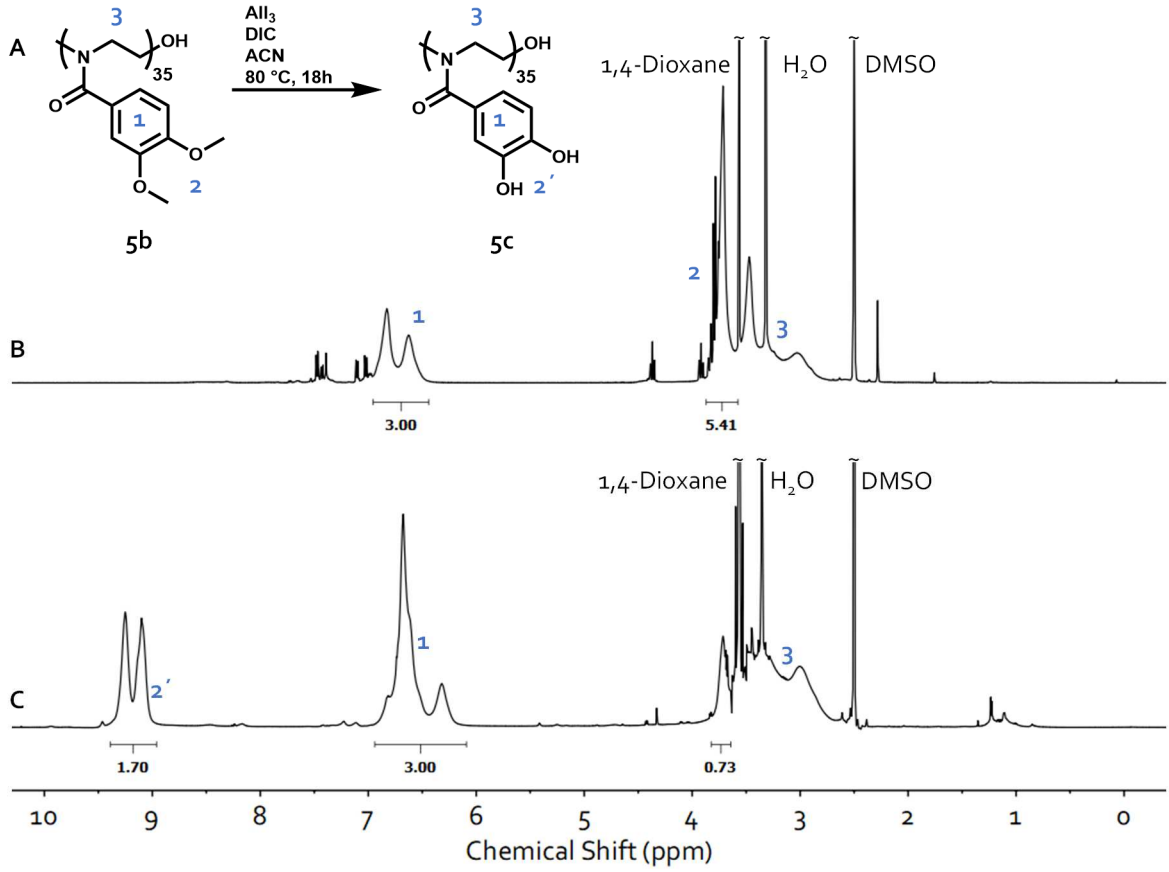


*Figure 21: A) Methyl aryl ether cleavage with homopolymer **5b** using $AlI_3$ as Lewis acid in presence of DIC to yield the catechol-containing polymer **5c**. $^1$H-NMR spectra of **5b** (B) and **5c** (C) in comparison. Visible the relative decrease of the methyl groups "2" and the appearance of the hydroxy groups "2´" in the spectrum of **5c**.*

Initially, the $AlI_3$ was suspended in hot ACN to which a solution of **5b** in ACN and DIC was added. After the addition of the solution containing **5b**, immediate precipitation was observed. Potentially the Lewis acid coordinated to the amide groups of **5b** and caused the precipitation by multi-dental coordination. Despite the heterogeneous reaction mixture, the reaction was carried out at 80 °C for 18 h. Since a work-up process by extraction was not possible, a dialysis procedure was conducted to substitute the extraction process. Initially, the dialysis was conducted with sodium thiosulphate to remove the iodine from the mixture. To prevent the formation of sulfur, the mixture was subsequently dialyzed against water and only then with 2 M hydrochloric acid to remove the aluminum species. The consecutive mixture was dialyzed multiple times against water to give the polymer **5c** with a yield of 81 %. The $^1$H NMR spectra of **5b** and **5c** (Figure 21, B, and C) revealed that the aryl ether cleavage was performed with 89% conversion. For this calculation, the integrals were normalized to aryl protons (1) and the conversion of 89% was calculated from the remaining methyl ether protons (2) in the NMR spectra (Figure 21, B, and C). This value can be confirmed by a calculated conversion value of 85% using the hydroxy group signal (2′). Thus the reaction was successful despite its heterogeneous nature. Unfortunately, neither MALDI-TOF MS nor SEC can be used for further analysis of **5c**. Hence, whether or not **5c** was damaged during the reaction, cannot be judged. This reaction was chosen for the methyl aryl ether cleavage of copoly(2-oxazoline)s to yield catechol functionalized water-soluble copolymers.

### 4.4.2 Methyl aryl ether cleavage of catechol-containing copolymers

Initially, the copolymer **5b**/**9b** was selected for post-polymerization modifications since this copolymer was edging the most gradient-like structure and the methyl aryl ether cleavage was already conducted with the respective homopolymer **5b**.

It was already mentioned that the mussel glue proteins carry between 2 and 30% catechol units, whereby the adhesive proteins carry 10-30% (Chapter 1.1).[136] Thus the targeted comonomer ratio **5a** : **9a** was correspondingly modeled as follows: $[\mathbf{5a}_x]_0/[\mathbf{9a}_y]_0 = 100$,

with x: 10, 8, 5, 3 and y: 90, 92, 95, 97. The reactions were carried out at 140 °C to shorten the reaction time from 512 min at 100 °C to 64 min (Figure 22, A). All other parameters remained as mentioned in chapter 4.3.2. Each reaction regarding the appropriate ratio was carried out 20 times to produce larger amounts of the copolymers **5b**$_x$/**9b**$_y$. The same stock solutions of the monomers **5a** and **9a** and of the initiator (MeOTos) were used to produce comparable copolymers. In this regard, the microwave-assisted CROP appeared to show the major disadvantage as each microwave vial only can be equipped with a limited amount of reaction mixture (1 mL per reaction).

The SEC traces (Figure 22, C) showed the four different copolymers with comparable chain lengths ($M_n^{SEC}$ between 6.6 kDa and 7.4 kDa; see Chapter 8, Figure S 40) and dispersity between 1.2 and 1.3. The absolute chain length could not be determined by $^1$H NMR spectroscopy, as the end group signals were hidden in the backbone signals (Figure 22, B, signals 3, 4) from $\delta$3.76-2.95 ppm. The comonomer ratio was determined by $^1$H NMR spectroscopy via setting the integrals of the aryl signal "1" and the methyl groups signal "6" of the poly(2-ethyl-2-oxazoline)-part in proportion (Figure 22, B). With the targeted number x = 3, 5, 8, 10 for the comonomer **5a** the copolymer composition was: **5b**$_3$/**9b**$_{121}$, **5b**$_5$/**9b**$_{78}$, **5b**$_8$/**9b**$_{110}$, and **5b**$_{10}$/**9b**$_{94}$. Yet indeed these numbers and chain length were not absolute. Nonetheless, for lack of methods to determine the absolute composition and chain length of those copolymers, these numbers and the resulting nomenclature will be used in further work. The four copolymers **5b**$_x$/**9b**$_y$ were used as starting material for the catechol release via the established methyl aryl ether cleavage reaction. The demethylation reaction was set for each produced copolymer **5b**$_x$/**9b**$_y$ individually, considering the respective number of methylated catechol units within the copolymer (Figure 23, A). Due to solvency issues, the copolymer concentration within the aryl ether cleavage reaction mixture was lowered to 0.08 M compared to the previously used concentration of 0.125 M (**5b** → **5c**). During the addition of the copolymer solution **5b**$_x$/**9b**$_y$ in ACN to the reaction mixture consisting of suspended $AlI_3$ in ACN, precipitation occurred, as earlier observed for the homopolymer reaction **5b** → **5c**. Thus, homogeneity was not given during the reaction process.

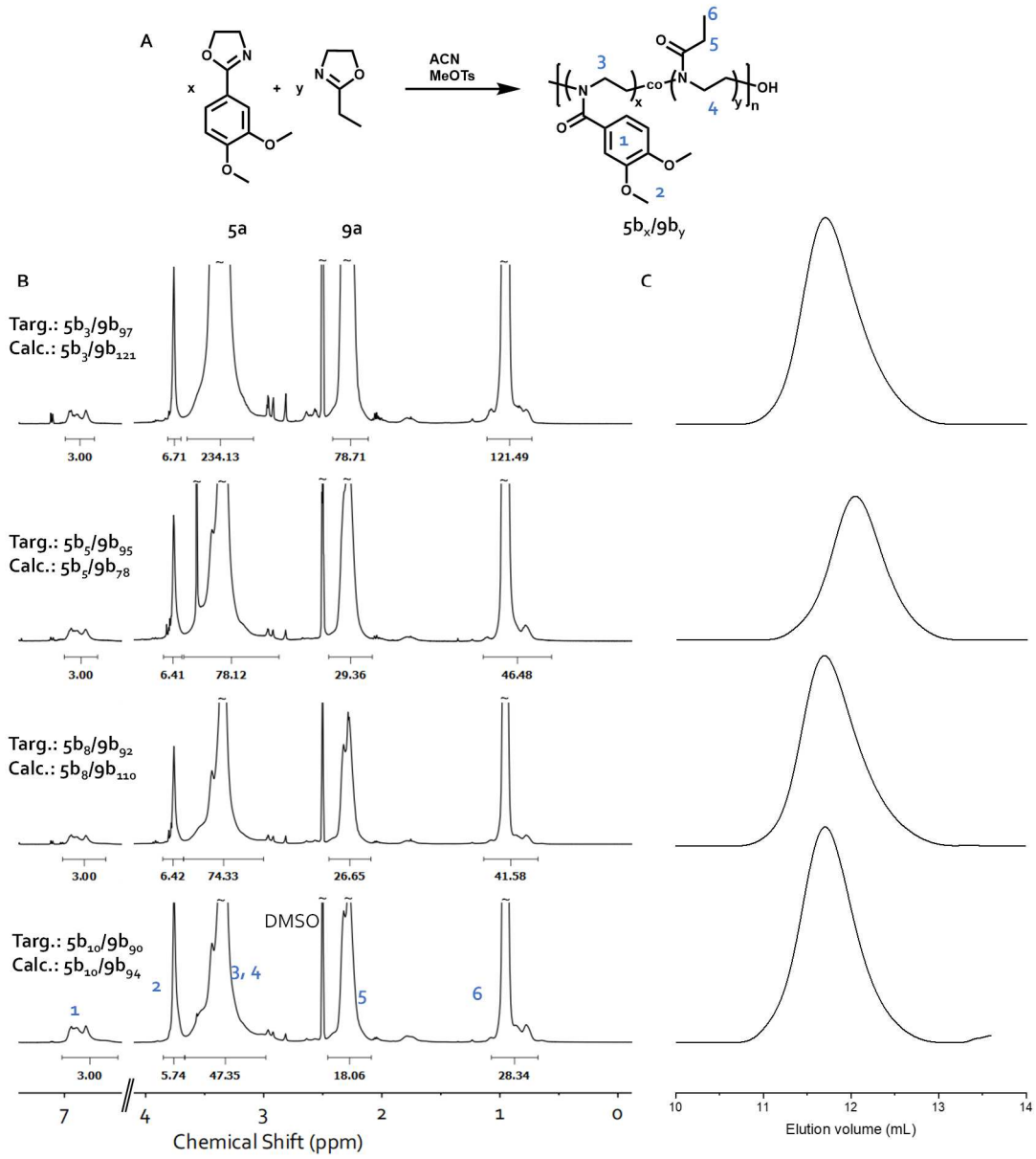


*Figure 22: A) Production of larger amounts of the copolymers* ***5b****$_x$/****9b****$_y$ with different comonomer mole fractions. B) $^1$H NMR spectra showed the individual comonomer mole fraction by comparison of the aryl protons (1) and methyl protons (6) integrals. C) SEC traces of the copolymers after combining the individual experiments.*

This precipitation was potentially caused by multi-dental coordination of the $Al^{3+}$ ion to the amide groups of the poly(2-oxazoline)s.[147] The ability of $Al^{3+}$ Ions to create more than one coordination bond most likely caused cross-linking and led to network structures and

thus to precipitation. The methyl aryl ether cleavage with the copolymers **5b**$_x$/**9b**$_y$ yet was less successful as the demethylation with the homopolymer **5b**. The conversion within the copolymer matrix **5b**$_x$/**9b**$_y$ was between 30 and 37%, determined by the comparison of the aryl proton integrals "1" at $\delta$7.0-6.6 ppm and the integrals of the remaining methyl ether protons "2" at $\delta$3.77 ppm (Figure 23, B). This conversion resulted in the following copolymer composition **5b**$_{x\text{-}z}$/**5c**$_z$/**9b**$_y$: **5b**$_2$/**5c**$_1$/**9b**$_{115}$, **5b**$_3$/**5c**$_2$/**9b**$_{78}$, **5b**$_5$/**5c**$_3$/**9b**$_{112}$, **5b**$_6$/**5c**$_4$/**9b**$_{94}$ (these compositions pertain only under the above-made assumption that the number of targeted **5b** corresponds to the number of used **5b**).

Since during the reaction from **5b** to **5c** precipitation was observed as well, the low conversion with the copolymers **5b**$_x$/**9b**$_y$ can not only be attributed to the precipitation effect. The 1.5 times lower concentration during the reaction to **5b**$_{x\text{-}z}$/**5c**$_z$/**9b**$_y$ probably was a further reason. Unfortunately, the copolymer concentration during the aryl ether cleavage could not be increased due to prior reaction solvency issues of the precursors **5b**$_x$/**9b**$_y$. Considering the degree of demethylation there was the issue of whether both or only one hydroxyl group was released. The $^1$H NMR spectra in Figure 23, B demonstrated that if demethylation took place then highly likely both ethers were cleaved. This can be seen in the bottom spectrum, since the two signals at $\delta$9.30 and $\delta$ 9.14 ppm, related to the released hydroxy groups, indicated a "symmetric" cleavage with similar integrals of both signals. SEC traces of the starting copolymers **5b**$_x$/**9b**$_y$ and the modified copolymers **5b**$_{x\text{-}z}$/**5c**$_z$/**9b**$_y$ were similar indicating that no decomposition during the cleavage occurred (Figure 23, C).

Certainly, as mentioned above, the demethylation reaction can be realized not only by the conducted method. With the copolymer **4b**$_x$/**9b**$_y$, a study concerning two different methyl aryl cleavage methods was carried out.[148] The used methods were on the one hand the previously described method, developed by Sang *et al.* using $AlI_3$ as Lewis acid. On the other hand, $BBr_3$ was employed as Lewis acid following the report from Albrecht *et al.*.[149] The results regarding both methods with the copolymer **4b**$_x$/**9b**$_y$ were similar as the deprotection with both methods resulted in a conversion of ~30%. Precipitation was observed with both Lewis acids. Accordingly, the $BBr_3$ Lewis acid led to precipitation as well. Consequently, neither the change of the Lewis acid nor the slight chemical variation

of the copolymers (**4b**$_x$/**9b**$_y$ vs **5b**$_x$/**9b**$_y$) had any impact on the conversion. Yet, the reaction conditions with $BBr_3$ were milder, hence, this reaction can advance in that concern.

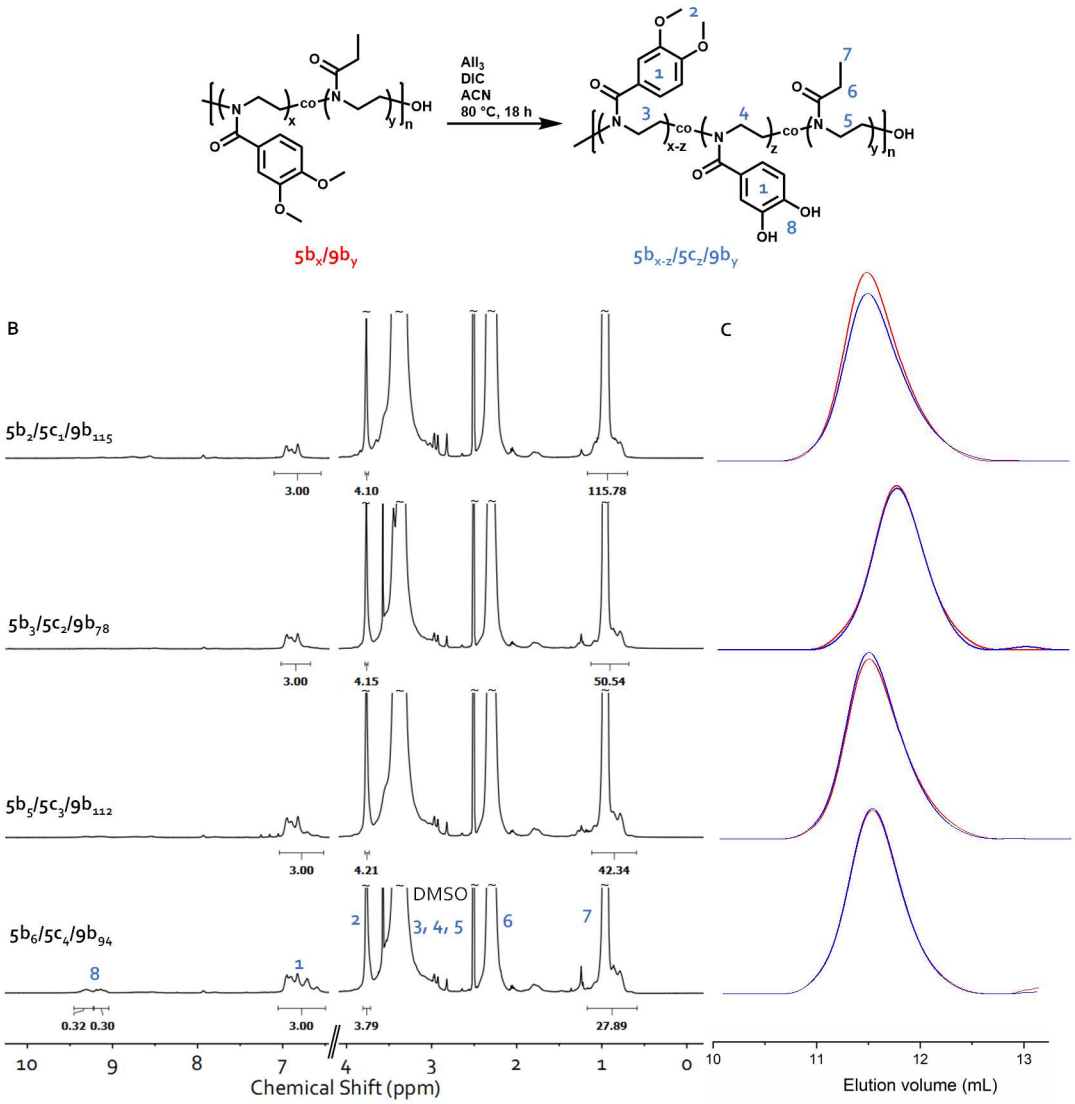


*Figure 23: A) Demethylation reaction to yield* ***5b***$_{x\text{-}z}$/***5c***$_z$/***9b***$_y$*. B) $^1$H-NMR spectra show the copolymers* ***5b***$_{x\text{-}z}$/***5c***$_z$/***9b***$_y$ *with their different ratio of the catechol containing unit* ***5b/c****. The integral of the aryl proton from δ7.0-6.6 ppm compared with the integral of the singlet at δ3.77 ppm indicating a degree of methylation of only 30-37%. C) SEC traces of* ***5b***$_x$/***9b***$_y$ *(red) and the corresponding demethylated copolymers* ***5b***$_{x\text{-}z}$/***5c***$_z$/***9b***$_y$ *(blue) show no difference. Thus, no decomposition of the copolymers during the demethylation process was monitored.*

The demethylation of the copolymers thus still was a crucial concern to increase the conversion. Since the most promising methods gave comparable results even with different copolymers, potentially the approach needs to be changed. Most demethylation reactions use Lewis acids as cleaving reagents.[150] Yet a worthwhile approach would be the decrease of the possible coordination sites of the Lewis acid to prevent the mentioned cross-linking and consequent precipitation. For instance, *tris*-(pentafluorphenyl)-borane ($B(C_6F_5)_3$ would be such a Lewis acid and would possibly not lead to precipitation.[151] Still, this reaction was not conducted with the copolymers **4b**/**9b** and **5b**/**9b** nevertheless promising for future work.

This work though was not considering further optimization of the methyl aryl ether cleavage as the catechol partially was released, as proven by $^1$H-NMR spectroscopy. The degree of demethylation was between 30 and 37%, indicating that on average at least every copolymer, even at the lowest synthesized ratio, carries one free catechol unit. The SEC traces showed the intact copolymers after the post-polymerization modification. Thus, the copolymer matrix **5b**$_{x\text{-}z}$/**5c**$_z$/**9b**$_y$ was used for further modification by the partial hydrolysis of the component **9b** in the copolymers **5b**$_{x\text{-}z}$/**5c**$_z$/**9b**$_y$ to create cationic groups.

### 4.4.3 Partial acidic hydrolysis of the copolymers to introduce cationic groups

Mussel glue proteins use cationic groups for several purposes. Besides the ability to remove bound water and ions from surfaces, cationic groups facilitate the binding since they can interact with surfaces as well. The influence of cationic groups was already discussed more in detail in chapter 1.3.

To release cationic groups, the produced copolymers **5b**$_{x\text{-}z}$/**5c**$_z$/**9b**$_y$ were used for further post-polymerization modification. It is well known that linear poly(ethyleneimine) (PEI) can be produced from poly(2-ethyl-2-oxazoline)s (**9b**) by basic or acidic hydrolysis.[152–154] This was a simple and promising approach to introduce cationic groups into the catechol-containing copolymers. Published kinetic studies on the acidic hydrolysis of poly(2-alkyl-2-oxazoline)s revealed, that the rate of hydrolysis was faster the smaller the side-chain

substituent is.[155] Thus it was assumed that the aryl side chain would not be removed as the ethyl side chain within the copolymers **5b**$_{x\text{-}z}$/**5c**$_z$/**9b**$_y$ reacts much faster. Additionally, the study revealed that the hydrolysis of poly(2-ethyl-2-oxazoline) (**9b**) can be simply controlled by the reaction time. Thus, this study was used as the template for the partial hydrolysis of the copolymers **5b**$_{x\text{-}z}$/**5c**$_z$/**9b**$_y$. Therefore, the microwave-assisted hydrolysis was performed at 100 °C for 5 min with an aqueous 2 M hydrochloric acid solution as solvent and reagent and the copolymers **5b**$_{x\text{-}z}$/**5c**$_z$/**9b**$_y$ as starting materials (Figure 24, A). According to the extrapolation, published in the above-mentioned kinetic study, the degree of hydrolysis was aimed towards less than 10% with a 5 min reaction time.

The degree of hydrolyzed units was determined by $^1$H NMR spectroscopy. The $^1$H NMR spectra of the hydrolyzed and the precursor copolymer were considered concerning the integral value of the respective aryl signal (1) at $\delta$7.03-6.41 ppm and the methyl signal (7) $\delta$0.95 ppm (Figure 24, B). These integral values were put into relation to give a conversion of ~9%. Certainly, this calculation was only possible under the assumption that the aryl side group was not cleaved during the reaction process.

Above it was already assumed that the aryl-containing 2-oxazoline unit would be not hydrolyzed due to lower reactivity. The $^1$H NMR spectrum was not reliable for that purpose, as the backbone signal at $\delta$3.7.-2.7 ppm did not give an independent signal due to possible water traces. Since the aryl content within the copolymer needed to be verified before and after the reaction, UV-VIS spectroscopy would be a reasonable method. The UV-VIS absorbance would be equal for the hydrolyzed (**5b**$_{x\text{-}z}$/**5c**$_z$/**9b**$_{y\text{-}h}$**9c**$_h$) and the precursor (**5b**$_{x\text{-}z}$/**5c**$_z$/**9b**$_y$) copolymer if no aryl unit was cleaved and the aryl unit concentration was the same. The Lambert-Beer Law made this possible since it describes a direct coherence between the concentration and the extinction coefficient.[156] Exemplary the copolymers **5b**$_6$/**5c**$_4$/**9b**$_{94}$ and **5b**$_6$/**5c4**/**9b**$_{86}$**9c**$_8$ were used since the number of aryl units was the highest. UV-VIS spectra of both the copolymers revealed, that there was no difference between them in terms of absorbance (concentration 0.125 mg/mL aqueous solution; Figure 24, C).

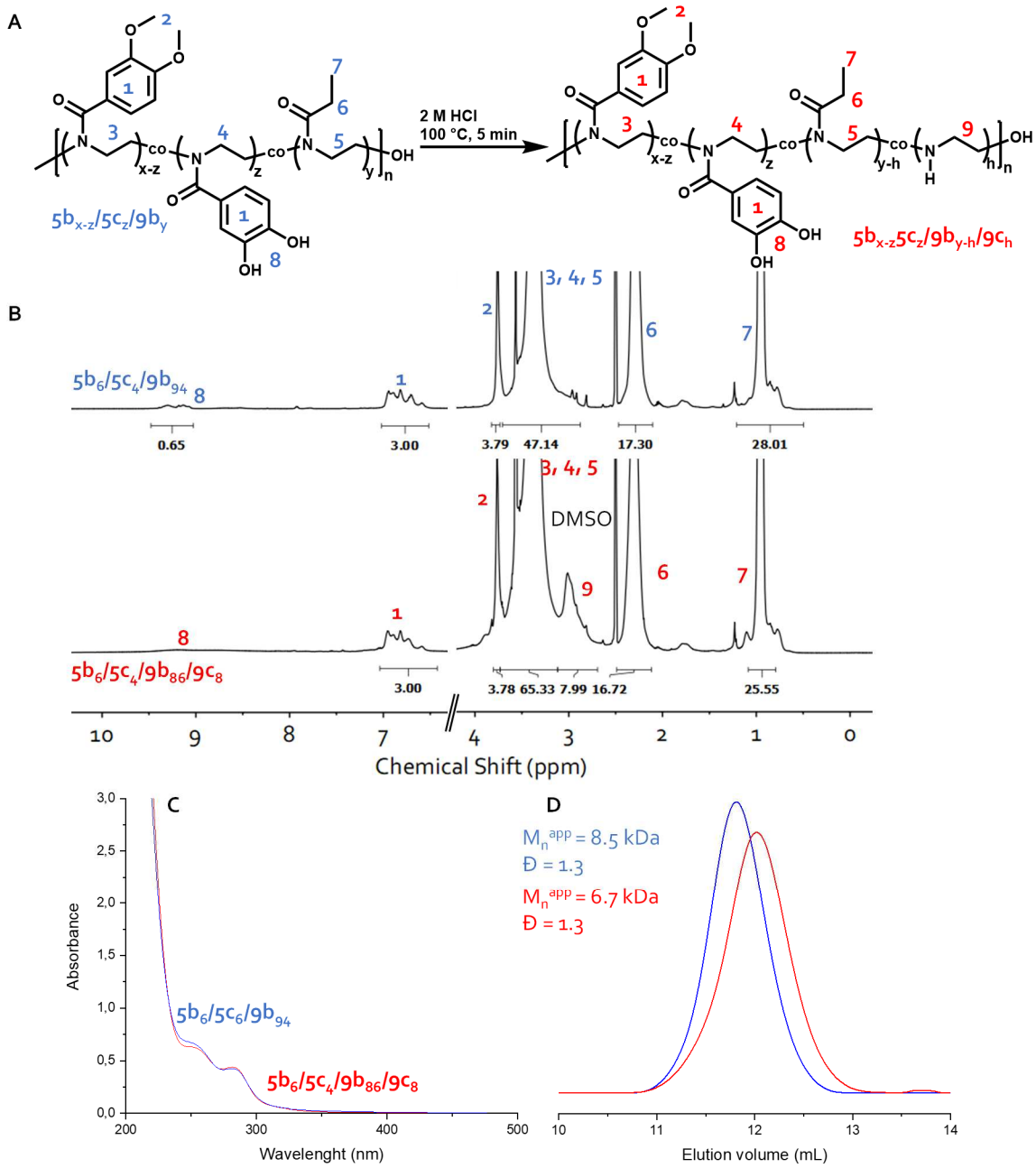


*Figure 24: A) Hydrolysis reaction to yield cation and catechol-containing copolymers. B) $^1$H NMR spectra show the precursor and the modified copolymers. C) UV-VIS spectra show an equal absorbance for both copolymers* **$5b_6/5c_4/9b_{94}$** *and* **$5b_6/5c_4/9b_{86}9c_8$**, *thus no aryl containing unit was hydrolyzed. D) Monomodal SEC traces indicated no decomposition of the copolymer itself.*

This proved the assumption that only the ethyl units of the **9b** copolymer unit were hydrolyzed. Thus the calculated degree of hydrolyzed units via $^1$H NMR spectroscopy was validated.

The monomodal SEC traces (Figure 24, D) additionally showed that the copolymer did not suffer from any decomposition reaction during the hydrolysis process. The respective slightly higher elution time of the SEC traces could be caused by the significant change of the hydrodynamic behavior of the copolymers as they became a polycation instead of a "neutral" polymer. Yet, a different behavior was not only monitored by the SEC measurements but also visible in the $^1$H NMR spectra (Figure 24, B). It was proven by UV-VIS spectroscopy that no aryl side-chain was removed during the partial hydrolysis. The catechol proton signals (8) at $\delta$9.30 and $\delta$ 9.14 ppm, related to the unhydrolyzed copolymer **5b**$_6$/**5c**$_4$/**9b**$_{94}$ though, seemed to disappear in the **5b**$_6$/**5c**$_4$/**9b**$_{86}$**9c**$_8$ related $^1$H NMR spectrum. Yet the signals broadened in the spectrum of **5b**$_6$/**5c**$_4$/**9b**$_{86}$**9c**$_8$ since the cations within the copolymer provided possibilities for hydrogen bonding. This resulted in longer relaxation times regarding the catechol protons which were expressed by broader signals. Water as a hydrogen bond participant can be excluded since the solvent (DMSO-$d_6$) especially was dried for that purpose.

$\zeta$-Potential measurements provided further proof of the presence of cationic groups within the copolymer **5b**$_6$/**5c**$_4$/**9b**$_{86}$**9c**$_8$. The measurement was conducted in a 0.1 wt% aqueous solution of both the presumably non-ionic (**5b**$_6$/**5c**$_4$/**9b**$_{94}$) and ionic copolymer (**5b**$_6$/**5c**$_4$/**9b**$_{86}$**9c**$_8$). They revealed a positive value of +15 mV for the cationic species **5b**$_6$/**5c**$_4$/**9b**$_{86}$**9c**$_8$ and a negative value for the non-ionic species **5b**$_6$/**5c**$_4$/**9b**$_{94}$ of -14. This additionally shows the presence of cationic groups within the copolymer **5b**$_6$/**5c**$_4$/**9b**$_{86}$/**9c**$_8$.

All four copolymers with their different catechol unit mole fraction were thus partially hydrolyzed in the same fashion. The copolymers **5b**$_3$/**5c**$_2$/**9b**$_{78}$, **5b**$_5$/**5c**$_3$/**9b**$_{112}$, and **5b**$_6$/**5c**$_4$/**9b**$_{94}$ all had a degree of hydrolysis of 7-9%. For whatever reason the hydrolysis degree of the copolymer **5b**$_2$/**5c**$_1$/**9b**$_{115}$ though was 30% (data shown in chapter 8, Figure S 41 - Figure S 43). The reaction was repeated with the same outcome.

Furthermore, the copolymer **5b**$_{10}$/**9b**$_{94}$ was partially hydrolyzed under the established conditions to yield the copolymer **5b**$_{10}$/**9b**$_{84}$**9c**$_{10}$ (data shown in chapter 8, Figure S 44). This non-catechol cation-containing copolymer was produced to provide a compound to compare with the catechol carrying copolymers **5b**$_{x-z}$/**5c**$_z$/**9b**$_{y-h}$**9c**$_h$ in future experiments concerning surface interactions. For the same reason, **9b** and **9c** (linear PEI) were produced in bigger amounts to give polymers without any aryl side chain within (Scheme 24).

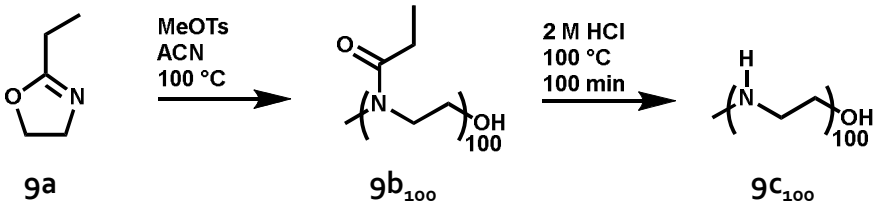


*Scheme 24: Microwave-assisted CROP of **9a** to yield **9b**$_{100}$ as starting material for the acidic hydrolyzation towards linear PEI (**9c**$_{100}$). These polymers did not carry any catechol or aryl group to compare the surface interaction abilities with the matrix **5b**$_{x-z}$/**5c**$_z$/**9b**$_{y-h}$**9c**$_h$.*

The synthesis of **9b** was already described in chapter 4.3.1. The DP of **9b** was aimed at [**9a**]$_0$/[MeOTos]$_0$ = 100. **9c** was synthesized starting from **9b** and conducting full hydrolysis with a reaction time of 100 min at 100 °C in aqueous 2 M hydrochloric acid solution. $^1$H NMR spectra analysis showed that the polymers **9b** and **9c**, were obtained in the desired chain length (DP = 100) utilizing the methyl end group for the calculation (Chapter 8, Figure S 31, Figure S 32). The $M_n^{App}$ of **9c** could not be determined via SEC since it was not soluble in NMP.

Overall, a matrix of water-soluble copolymers was produced considering all degrees of functionalization: Pure poly(2-ethyl-2-oxazoline) (**9b**) and linear PEI (**9c**) were produced to compare with the aryl, catechol, and cation carrying copolymers in future experiments. Four different copolymers **5b**$_x$/**9b**$_y$ with different mole fractions of dimethoxy aryl side chains were produced and subsequently functionalized by the (partially) release of the catechol side group to yield another four different copolymers **5b**$_x$/**5c**$_y$/**9b**$_z$. To complete the matrix not only to consider catechol but also cationic

copolymers **5b**$_x$/**5c**$_y$/**9b**$_z$ and **5b**$_{10}$/**9b**$_{94}$ were partially hydrolyzed to yield five different polyelectrolytes **5b**$_{x-z}$/**5c**$_z$/**9b**$_{y-h}$**9c**$_h$ and **5b**$_{10}$/**9b**$_{84}$**9c**$_{10}$. The respective degree of functionalization was successfully determined by $^1$H NMR spectroscopy supported by UV-VIS spectroscopy. All (co)polymers showed monomodal SEC traces and narrow distributions. This set of 15 different (co)polymers, inspired by mussel glue proteins, further will be examined towards their ability to adsorb on different surfaces.

Indeed, more monomers and copolymers were already synthesized, yet to be examined by post polymerization modification. Especially the copolymer **7b**$_x$/**9b**$_y$ containing *N*-BOC-*L*-tyrosine would be a captivating option for mussel glue protein mimics. In particular, the mussel uses *L*-DOPA as catechol containing unit which is made by oxidation of *L*-tyrosine with the enzyme tyrosine oxygenase.[157] Attempts to modify the copolymer **7b**$_x$/**9b**$_y$ were made, yet not successful. The BOC protection group, stable during the (co)polymerization, was not stable during the aryl ether cleavage reaction. Further, the cleaning of the modified copolymer **7b**$_{x-z}$/**7b**$_z$/**9b**$_y$ after this cleavage reaction turned out to be impossible. It was assumed that the Lewis acid coordinated on the (partially) deprotected amine moiety. Attempts to change the protection group from BOC to the fluorenylmehyloxycarbonyl protecting group (Fmoc) within the copolymer were not successful. Introducing the Fmoc group before the copolymerization was conducted since the Fmoc group could cause problems due to its acidic proton. This proton can lead to undesired initiation or side reactions and the subsequent products could cause termination and crosslinking reactions by their reactive decomposition species. For that reason, the post-polymerization modification of **7b**$_x$/**9b**$_y$ was not pursued anymore although it was an interesting and option to mimic mussel glue proteins.

The copolymers (**1b**$_x$,**2b**$_x$,**3b**$_x$/**9b**$_y$) were excluded since they all underwent chain transfer reactions, discussed in chapter 4.3.2. However, there are still possibilities of making water-soluble polymers with **1a**, **2a**, and **3a**, not using 2-ethyl-2-oxazoline (**9a**) but for instance 2-isopropyl-2-oxazoline. The bulkier side group of 2-isopropyl-2-oxazoline could prevent an $\beta$-elimination reaction and subsequently prohibit the chain coupling

reaction with the cinnamyl double bond unit. As poly(2-isopropyl-2-oxazoline) is water-it would be a proper option as comonomer the cinnamyl-2-oxazolines **1a, 2a,** and **3a**.

Finally, **4b**$_x$/**9b**$_y$ and **6b**$_x$/**9b**$_y$ remain interesting to compare with **5b**$_x$/**9b**$_y$. Initially, the copolymer **6b**$_x$/**9b**$_y$, carrying (methylated) pyrogallol units, may have different properties regarding the adsorption abilities. Studies showed, that under certain circumstances pyrogallol-carrying polymers have great abilities to adsorb on surfaces and act as an antioxidant.[158] For that reason, it would be sublime to compare **5b**$_x$/**9b**$_y$ and **6b**$_x$/**9b**$_y$ and their catechol and cationic-containing successors. However, this will not be part of this work as the focus of this work lies in mimicking mussel glue proteins that carry catechol but not pyrogallol units. The above-mentioned study with **4b**$_x$/**9b**$_y$ showed the demethylation with different methods. Interestingly, there was no difference regarding the degree of demethylation degree of **4b**$_x$/**9b**$_y$ and **5b**$_x$/**9b**$_y$ (Chapter 4.4.2).[148] This can make the copolymer matrices, from **4b**$_x$/**9b**$_y$ and **5b**$_x$/**9b**$_y$, an interesting pair to compare in future work.

The synthesized matrix around the copolymer **5b**$_x$/**9b**$_y$ finally was a promising prospect to mimic mussel glue proteins with 2-oxazolines. The combination of a catechol carrying unit with 2-ethyl-2-oxazoline (**9a**) resulted in a water-soluble set of copolymers **5b**$_x$/**9b**$_y$, **5b**$_x$/**5c**$_y$/**9b**$_z$, and **5b**$_{x\text{-}z}$/**5c**$_z$/**9b**$_{y\text{-}h}$**9c**$_h$. Thus the (co)polymer matrix **9b, 9c, 5b**$_x$/**9b**$_y$, **5b**$_x$/**5c**$_y$/**9b**$_z$, and **5b**$_{x\text{-}z}$/**5c**$_z$/**9b**$_{y\text{-}h}$**9c**$_h$ will be examined concerning surface interactions via QCM-D adsorption studies.

## 4.5 QCM-D adsorption studies

The Quartz Crystal Microbalance with Dissipation QCM-D (Chapter 3.2) certainly is a substantial method for investigations of surface/polymer interference in aqueous surroundings. Accordingly, the QCM-D was the key method in this work to examine the interaction between the synthesized (co)polymers (Figure 25) and different surfaces (gold (Au), borosilicate (BS), iron (Fe), and polystyrene (PS)). The set of synthesized (co)polymers was extended by the commercially available polymers polyethylene glycol (PEG) and polyacrylic acid (PAA). These polymers were chosen to provide data to compare them with the synthesized (co)polymers.

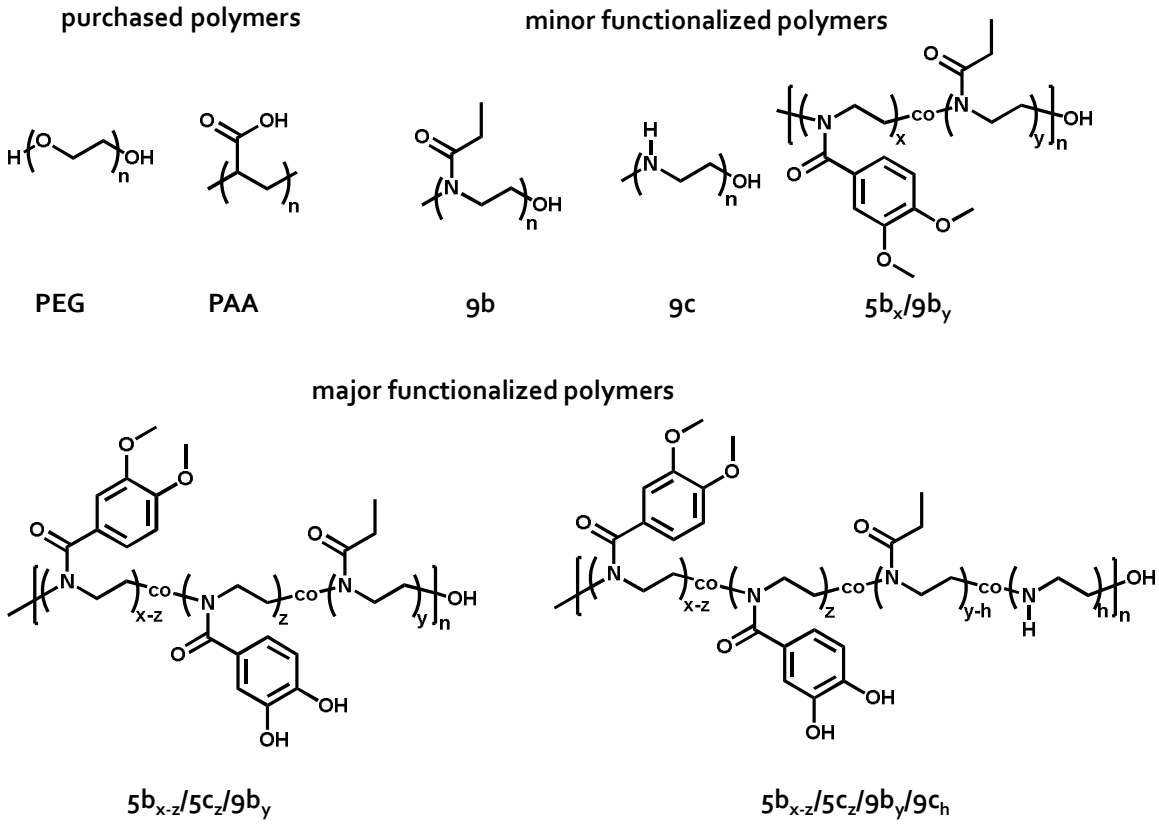


*Figure 25: The set of (co)polymers to consider and examine on their adsorption ability on the surfaces Au, BS, Fe, and PS by QCM-D measurements.*

The initial aim was to identify whether the produced - potentially gluing - mussel mimicking (co)polymers interact with the mentioned surfaces. For that purpose, the mass value of adsorbed (co)polymer the respective kinetics were determined and will be discussed in the following section

The method QCM-D was introduced in detail in chapter 3.2, thus only a brief explanation follows. The QCM-D is a device to monitor (*i.a.*) mass values at or near surfaces with peculiar high resolution (ng/cm²) in real-time. In particular, it measures the changes in frequency and energy dissipation, which are caused by the interference of substrates with surfaces on a piezoelectric quartz crystal sensor due to environmental changes or substrate deposition.[94] In consequence, this technique is indicative of the consideration of solid/liquid interfaces in the process. Dissolved substrates, respectively the deposition on surfaces during flow-through treatment can be monitored and quantified. Accordingly, the QCM-D fits perfectly for the examination of adsorption effects in aqueous surroundings with mussel mimicking adsorbing (co)polymers. The QCM-D technique allows, besides the quantification of deposed mass values per area, a further examination of the coated surface in situ. The treatment of coated surfaces with different solvents and solutions gives essential evidence and information regarding the sustainability, durability, and (in)activity of those functionalized surfaces. The dissipation shift ($\Delta D$) measurement can provide data about the layer rigidity during and after the coating process. The QCM-D thus is not only a valid method to gain fundamental information about surface coatings but permits a more profound consideration regarding the behavior of the substrate on a major variety of different surfaces.

Thus, the QCM-D technique was used to examine the synthesized (co)polymers concerning their adsorption ability on different surface types. The aim of these measurements was the production of an overview through the adsorption performance of the synthesized (co)polymers. In most instances, the discussion concerning the QCM-D data was referred and reduced to quantitative specifications and placements. A particular classification of kinetic models and mechanistic theories about (co)polymer adsorption onto solid surfaces was to some extend not possible due to insufficient data.[159–161]

A quantitative classification regarding QCM-D data, concerning published maritime glue protein mimicking (co)polymers, was complex. The respective compounds differed highly in composition and size as they ranged from branched and functionalized (dendric) poly(glycerol ether)s over poly(methacryl amide)s to poly(vinyl catechol/gallol)s.[158,162–165] Until now, cation and catechol functionalized poly(2-oxazoline)s were not examined by QCM-D measurements, which made this investigation highly valuable, yet complex to classify. For this reason, the measurement with the QCM-D needed to be established ab initio.

### 4.5.1 Parameter determination and general measurement technique

The adsorption ability was examined in an aqueous environment. For that purpose, a flow-through technique was used. All (co)polymers were dissolved in extra pure water with a (co)polymer concentration of 0.1 mg/mL 2 h before the measurement started. The flow rate was determined manually, with a value of 126 µL/min. This value was determined frequently, and the rate did not change notably. The temperature and pressure were kept constant at room condition, as environmentally possible. For the mass calculation, the extended Sauerbrey equation (Eq 7, Chapter 3.2) was used. Furthermore, only the overtone 5 was used for the mass calculation. It should be noted that the (in this work) sensed mass includes besides the adsorptive, the hydrodynamically coupled water within the adsorbate, since the specified masses were all determined in aqueous environments. The adsorption constants $k_A$ were determined by exponential (Chapter 6.1.1, Eq. 39, 41), respectively linear (Chapter 6.1.1, Eq. 14, 17) fitting. The derivation one can look up in chapter 6.1.1.

Additionally, it must be mentioned that the reverse driving forces during the adsorption processes, the entropy loss, and the osmotic pressure, were assumed as the general restricting potency for each coating. In some cases, these forces were consulted, evidenced by $\Delta D$ values.

All QCM-D adsorption measurements were conducted as follows: The QCM-D sensors were carefully placed into the respective chambers. Subsequently, all chambers and surfaces were rinsed with extra pure water until no baseline shift was observed anymore. Then the (co)polymer solution was injected, and the surfaces were treated until a frequency equilibrium was monitored. Afterward, the coated surfaces were rinsed with extra pure water or Phosphate-buffered saline (PBS) buffer solution.

To ensure reproducibility, cleaning was an essential part, to generate reliable data over multiple attempts (for cleaning protocols, see chapter 6.1.1). To prove the reproducibility, one Au sensor was cleaned and treated with the same copolymer solution (**5b**$_6$/**5c**$_4$/**9b**$_{94}$) multiple times. The respective adsorption graphs of all four experiments showed similar results which demonstrated the reproducibility (Figure 26).

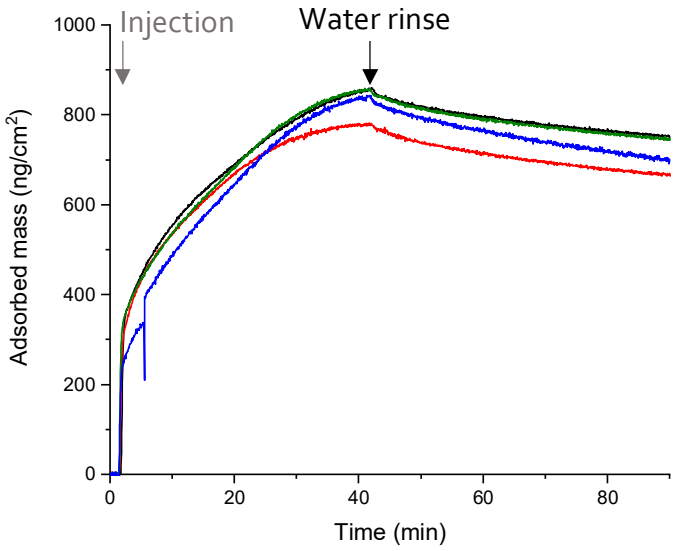


*Figure 26: QCM-D measurements of a 0.1 mg/mL aqueous* ***5b***$_6$/***5c***$_4$/***9b***$_{94}$ *solution. The reproducibility was successfully demonstrated as the individual adsorption graphs did not differ significantly.*

Certainly, this measurement was already conducted with the synthesized copolymer **5b**$_6$/**5c**$_4$/**9b**$_{94}$. This measurement was only meant to test the general measurement parameters. The discussion concerning the data follows in the next chapters. However,

the promising result considering the adsorption performance of the copolymer **5b**$_6$/**5c**$_4$/**9b**$_{94}$ though can be highlighted here already. The setup concerning concentration, flowrate, and cleaning protocol seemed to provide reliable data thus were used further.

### 4.5.2 First QCM-D measurements with gold surfaces

The synthesized different (co)polymers provided different degrees of functionalization (Figure 25). Initially, the purchasable polymers PEG and PAA and the synthesized polymers **9b** and **9c** (synthesis in chapter 4.4.3)were examined to provide basic comparative data.

Poly(2-ethyl-2-oxazoline) (**9b**) ($M_n^{App}$ ≈ 2.6 kDa, DP ≈ 100), represents the main copolymer component, solely lacking the aryl, catechol, and ethylene imine units.

Polyethylene glycol (PEG, $M_n$ = 5.0 kDa, DP ≈ 110), represents a purchasable and medicinal well-known counterpart to PEtOx.[68]

Polyethyleneimine (**9c**) ($M_n^{App}$, not det., DP ≈ 100; det. by $^1$H-NMR), represents a polycation, to compare with the partially hydrolyzed (co)polymers.

Polyacrylic acid (PAA, $M_n$ = 5.0 kDa, DP ≈ 70), represents a gluing polymer with a carboxylic acid moiety.

Subsequently, Au surfaces were treated with the four polymers (**9b**, **9c**, PEG, PAA) until saturation occurred (Figure 27, A). It is generally to mention, that a (first) stage of saturation with polymers took place within seconds, visible in the zoomed plot. However, besides that similar first adsorption velocity, the adsorption graphs differed strongly: Considering PEtOx (**9b**) and PEG both the polymers reached a full equilibrium saturation within seconds, whereby the adsorbed mass was twice as much for **9b** than for PEG (with PEG ≈ 100 ng/cm², **9b** ≈ 200 ng/cm²).

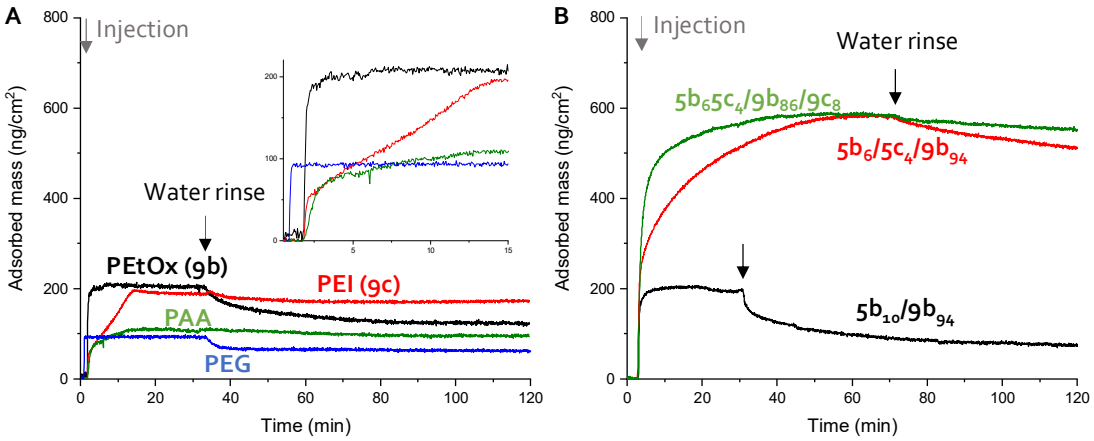


*Figure 27: QCM-D pots of the adsorbed mass of purchasable polymers PAA and PEG and low functionalized synthesized polymers **9b** and **9c** (A) and the first set of copolymers (B) on gold surfaces.*

PAA reached an equilibrium saturation within 10 min, which was slower than **9b** and PEG. However, the adsorbed mass value was comparable to the adsorbed mass of PEG (with PAA and PEG ≈ 100 ng/cm²). For the adsorption process of PEI, two different kinetic stages were monitored. The first stage was determined within seconds at a mass value of 50 ng/cm², the second stage was reached just after 15 min with an adsorbed mass value of about 200 ng/cm². Presumably, the change of the adsorption kinetic of **9c** was caused by a different adsorption mechanism after the surface was covered with the polymer initially. The other three polymers did not show two kinetic stages. It seemed that at least two adsorption mechanisms were monitored. However, no mechanistic proposal can be made reasoned by this data. After reaching a saturation equilibrium, the coated surfaces were treated with highly pure water. **9c** and PAA interestingly were not washed off at all, whereby an approximately adsorbed mass loss of 30-40% of **9b** and PEG was determined during the rinsing process. This can lead to the assumption, that the (partially) charged polymers can result in more durable coatings. Further, it can be concluded that a certain amount of any polymer, yet measured, was bound on Au surfaces. Further, a certain amount of bound polymer stuck to the surface after water rinsing. The amount of bound

polymer and the adsorption velocity though differed highly. Solely these observed characteristics, concerning the adsorption kinetics and layer nature were worth an investigation, but these polymers were only meant to provide data to compare. Thus, this work will not examine these four polymers entirely.

Afterward, the (co)polymers **5b**$_{10}$/**9b**$_{94}$, and **5b**$_{6}$/**5c**$_{4}$/**9b**$_{94}$, and **5b**$_{6}$/**5c**$_{4}$/**9b**$_{86}$/**9c**$_{8}$ were used to treat Au surfaces (Figure 27, B). Comparing the graphs of **9b** and **5b**$_{10}$/**9b**$_{94}$, it seemed that the methoxy aryl moiety did not have a significant influence on the adsorption velocity or adsorption value on Au surfaces. However, the coating durability seemed to be influenced by the aryl units. The coating of **5b**$_{10}$/**9b**$_{94}$ lost 65% of its mass and the coating of **9b** only 40%. This suggested that the copolymer **5b**$_{10}$/**9b**$_{94}$ did not bind as tight as **9b**. The dissipation shift ($\Delta$D) of **5b**$_{10}$/**9b**$_{94}$ ($\Delta D = 1 \times 10^{-6}$) showed a value twice as much as that of **9b** ($\Delta D = 0.5 \times 10^{-6}$) (see Chapter 8, Figure S 45). Thus **5b**$_{10}$/**9b**$_{94}$ formed a less rigid layer than **9b**, indicating a bigger hydrodynamic radius and a spatial more demanding polymer coil which potentially was bound less tight, consequently washed off in higher amounts.

The adsorption graphs of **5b**$_{6}$/**5c**$_{4}$/**9b**$_{94}$ and **5b**$_{6}$/**5c**$_{4}$/**9b**$_{86}$/**9c**$_{8}$ demonstrated the significant impact of the catechol units on the adsorption performance. Comparing **9b** and **5b**$_{10}$/**9b**$_{94}$ with **5b**$_{6}$/**5c**$_{4}$/**9b**$_{94}$ and **5b**$_{6}$/**5c**$_{4}$/**9b**$_{86}$/**9c**$_{8}$ the amount of adsorbed mass was three times higher (~600 ng/cm²) for the catechol-containing copolymers. The portion of coating washed off the surfaces during the rinsing process was ~28% for **5b**$_{6}$/**5c**$_{4}$/**9b**$_{94}$ and ~12% for **5b**$_{6}$/**5c**$_{4}$/**9b**$_{86}$/**9c**$_{8}$. Consequently, it can be assumed that the catechol moieties support better adsorption performances. Further, the cationic groups may promote the durability of the coating against water rinsing processes.

### 4.5.3 Quantitative and kinetic examination of the (co)polymer matrix with QCM-D

#### 4.5.3.1 Adsorption of minor functionalized (co)polymers on gold surfaces

The initial measurements showed a large impact of the catechol units, as the adsorbed mass was three to six times higher for the catechol-functionalized copolymers (**5b**$_6$/**5c**$_4$/**9b**$_{94}$, **5b**$_6$/**5c**$_4$/**9b**$_{86}$/**9c**$_8$) than for **9b**, **9c**, PAA, and PEG. However, before the catechol-containing copolymers can be discussed, the respective minor functionalized precursors **5b**$_5$/**9b**$_{78}$ and **5b**$_{10}$/**9b**$_{94}$ shall be considered on Au surfaces briefly:

**9b** and **5b**$_{10}$/**9b**$_{94}$, showed comparable amounts of adsorbed mass of 200 ng/cm², for **5b**$_5$/**9b**$_{78}$ in contrast ~150 ng/cm² was monitored ((Figure 28, A). The minor adsorbed mass of **5b**$_5$/**9b**$_{78}$ can be caused by its shorter chains, yet, only under the assumption that the degree of occupation was the same for all three (co)polymers. These data indicated a limitation of the adsorbed mass at ~200 ng/cm² for the considered minor functionalized (co)polymers with the established measurement parameters.

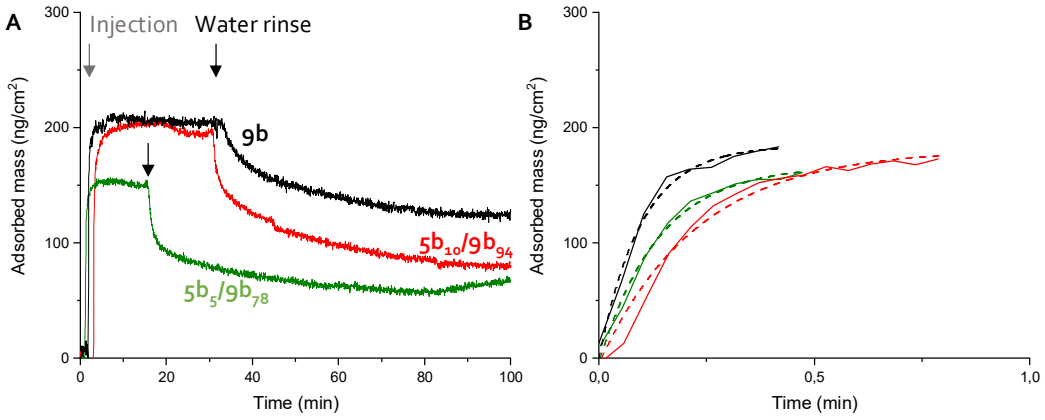


*Figure 28: A) Adsorption graphs of* ***9b*** *and* ***5b***$_{10}$/***9b***$_{94}$ *and* ***5b***$_5$/***9b***$_{78}$ *on Au surfaces. B) Exponential fitting of the initial adsorption graph to determine the respective adsorption constants* $k_A$. *The* $k_A$ *indicated a dependence of the adsorption velocity of the aryl unit content.*

Further, the adsorption constants ($k_A$) of each (co)polymer were determined by an exponential fitting: $1.89*10^{-2}$ mg/ml s (**9b**); $1.22*10^{-2}$ mL/mg s (**5b**$_5$/**9b**$_{78}$); $0.80*10^{-2}$ mg/ml s (**5b**$_{10}$/**9b**$_{94}$) (Figure 28, B). These $k_A$´s indicated slower adsorption, the more methoxy aryl moieties the (co)polymers contained. This might be caused by the gradient-like structure of the copolymers **5b**$_5$/**9b**$_{78}$ and **5b**$_{10}$/**9b**$_{94}$ (Chapter 4.3.2).

Since these copolymers showed a predominance of aryl units at one chain-end, it can be assumed that they are amphiphilic. In aqueous surroundings, these amphiphilic copolymers might form micelles, which accordingly had lower diffusion velocity in comparison to the dissolved polymer chains of **9b**. DLS measurements revealed that no intermolecular micellization occurred (Chapter 8, Figure S 47). Regardless, due to the amphiphilic character with an accumulation of hydrophobic domains still can be assumed reasoned by intramolecular micellization (coiling). Thus, the $k_A$ decrease can potentially be traced back to the lower diffusion velocity by coiling.

#### 4.5.3.2 Influence of catechol units on gold surface adsorption

Further, the examination of the catechol functionalized copolymers **5b**$_6$/**5c**$_4$/**9b**$_{94}$, **5b**$_5$/**5c**$_3$/**9b**$_{112}$, **5b**$_3$/**5c**$_2$/**9b**$_{78}$, and **5b**$_2$/**5c**$_1$/**9b**$_{115}$ on Au surfaces was conducted. In chapter 4.5.2, the advantages of the adsorption performance of the major functionalized copolymers compared to the minor functionalized (co)polymers were already demonstrated. The adsorption graphs of **5b**$_6$/**5c**$_4$/**9b**$_{94}$, **5b**$_5$/**5c**$_3$/**9b**$_{112}$, **5b**$_3$/**5c**$_2$/**9b**$_{78}$, and **5b**$_2$/**5c**$_1$/**9b**$_{115}$ on Au showed a similar trend in the very beginning but with time progression the adsorption behavior differs for the copolymer **5b**$_3$/**5c**$_2$/**9b**$_{78}$ enormously (Figure 29, A). The copolymers **5b**$_6$/**5c**$_4$/**9b**$_{94}$ and **5b**$_5$/**5c**$_3$/**9b**$_{112}$ showed an overall similar trend with comparable maximum adsorbed masses of ~600 ng/cm². For **5b**$_2$/**5c**$_1$/**9b**$_{115}$ only ~400 ng/cm² maximum adsorbed mass was monitored. It is noteworthy that a copolymer averaging only one catechol unit (**5b**$_2$/**5c**$_1$/**9b**$_{115}$) led to a doubling of the adsorbed mass compared to the non-catechol-containing (co)polymers **9b**, **5b**$_5$/**9b**$_{78}$, and **5b**$_{10}$/**9b**$_{94}$. This showed the effectiveness of the catechol binding.

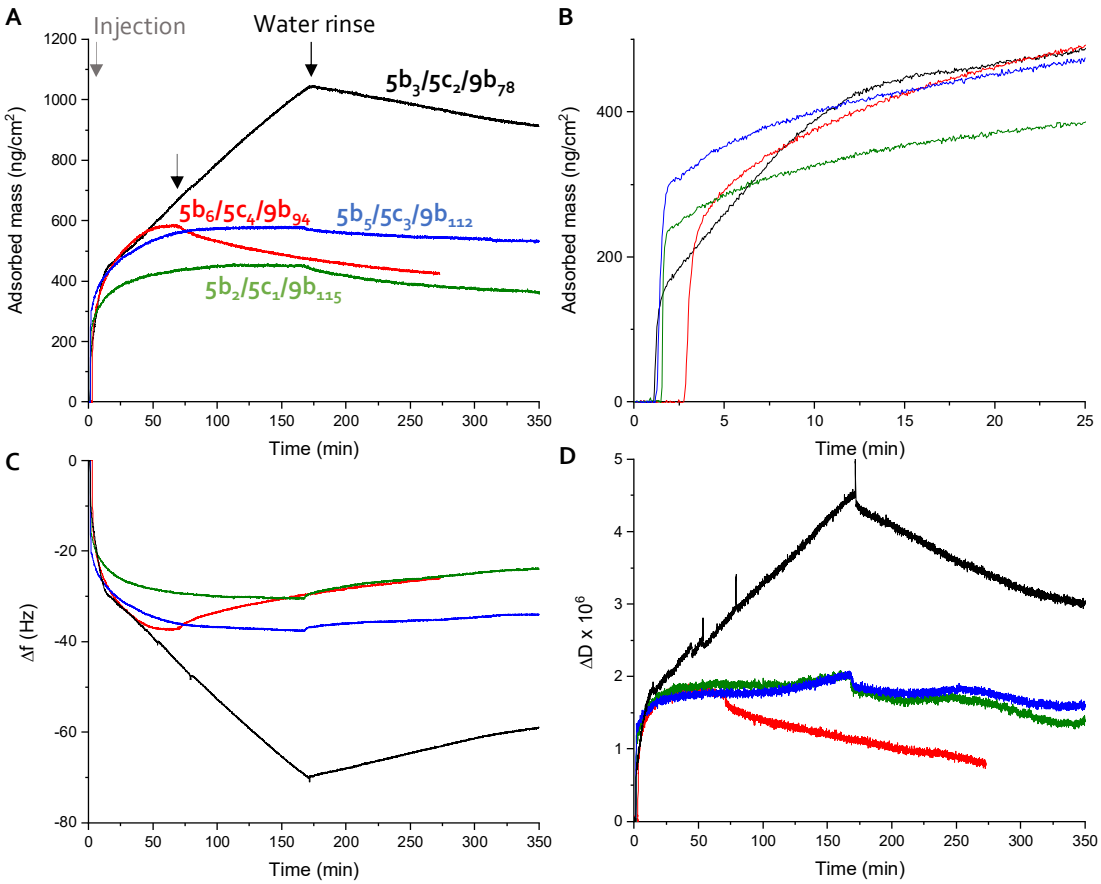


*Figure 29: A) QCM-D measurements on Au surfaces of the catechol-containing copolymers. B) After reaching a certain state of saturation the copolymer* ***5b3/5c2/9b78*** *differs highly regarding the adsorption behavior compared to the other three copolymers* ***5b6/5c4/9b94***, ***5b5/5c3/9b112***, ***5b2/5c1/9b115***. *It was noteworthy, that for the copolymer* ***5b3/5c2/9b78*** *no saturation was monitored, as after 172 min the coated surface was rinsed with water without reaching a state of saturation. The plot of the respective frequency (C) and dissipation shifts (D) during the measurement.*

The dissipation shift showed similar values of ~$1.8*10^{-6}$ for **5b6/5c4/9b94**, **5b5/5c3/9b112**, and **5b2/5c1/9b115** (Figure 29, D). However, for **5b2/5c1/9b115** less adsorbed mass was monitored compared to the copolymers **5b6/5c4/9b94** and **5b5/5c3/9b112**. Thus, less polymer interacted with the surface while ΔD values were equal. Consequently, it can be

assumed that the coating of **5b$_2$/5c$_1$/9b$_{115}$** was less rigid and dense than that of **5b$_6$/5c$_4$/9b$_{94}$** and **5b$_5$/5c$_3$/9b$_{112}$**.

Including the copolymer **5b$_3$/5c$_2$/9b$_{78}$** in the discussion, a significantly different behavior was observed. After the initial fast adsorption (0.3 min, ~170 ng/cm²), a second slower adsorption process happened (12 min, ~430 ng/cm²) until the behavior changed again, and a once slower third adsorption process was monitored. Interestingly, the third adsorption process did not reach any state of saturation but proceeded linearly for another 160 min. After that 160 min, the copolymer solution emptied, and the rinsing process was started. During the adsorption process, the ΔD values continuously increased up to ~$4.5*10^{-6}$. Subsequently, a long-time experiment was conducted to check whether any saturation can be reached. Even after treating the Au surface for 24 h with copolymer **5b$_3$/5c$_2$/9b$_{78}$**, neither a slowing down nor a stoppage of the adsorption process was monitored (Chapter 8, Figure S 48). Thus, considering the discussed data of all copolymers **5b$_6$/5c$_4$/9b$_{94}$**, **5b$_5$/5c$_3$/9b$_{112}$**, **5b$_3$/5c$_2$/9b$_{78}$**, and **5b$_2$/5c$_1$/9b$_{115}$**, it indicated, that a higher number of catechol units did not necessarily result in higher adsorbed mass values.

The initial kinetic from the copolymers **5b$_6$/5c$_4$/9b$_{94}$**, **5b$_5$/5c$_3$/9b$_{112}$**, **5b$_3$/5c$_2$/9b$_{78}$**, and **5b$_2$/5c$_1$/9b$_{115}$** did not differ significantly, hence the initial adsorption process seemed to be similar. The mentioned adsorption process of **5b$_3$/5c$_2$/9b$_{78}$** however seemed to be extraordinary, thus initially, the adsorption constants of the three stages ($k_{A1\text{-}3}$) were determined. The first stage was analyzed with the exponential term and the second and third stages linearly (Figure 30) to give the adsorption constants $k_{A1}$ = $6.51*10^{-3}$ mL/mg s, $k_{A2}$ = $2.55*10^{-4}$ mL/mg s and $k_{A3}$ = $3.96*10^{-5}$ mL/mg s. The $k_{A1\text{-}3}$ values decreased by ~$10^{-1}$ with progression to the next stage, finally approaching a constant value in stage 3. The linear progression and the virtually infinite adsorption indicated zero-order kinetic. For a zero-order kinetic adsorption process, the number of binding sites is the crucial concentration, that needs to remain constant as the adsorption constant ($k_A$) is proportional to the number of binding sites ($N_B$) multiplied by the diffusion ($D_{Dif}$) ($k_A \sim N_B * D_{Dif}$). A decrease of $N_B$ in stage 1 and 2 can be concluded, as a (partial) saturation and a kinetic change was observed. In consequence, the number of binding sites did not change

anymore in stage 3 because no saturation was observed. While the adsorbed mass in stage 3 increased linearly (virtually infinite), in consequence, it can be reasonably assumed that the bound copolymers created the new binding sites.

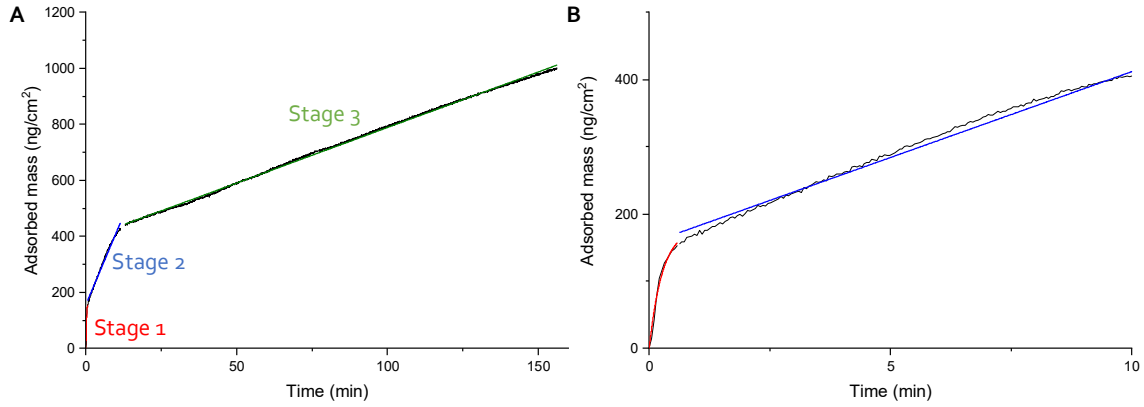


*Figure 30: A) Adsorption behavior of* ***5b***$_3$*/****5c***$_2$*/****9b***$_{78}$ *on Au surfaces with the respective fitting of the three kinetic stages. B) Zoom to the first two kinetic stages showed the initial exponential kinetic process into the second slower linear one. The third adsorption process was linear and did not reach any state of saturation, thus it can be assumed that a zero-order kinetic was observed.*

It is noteworthy to keep in mind, that the numbers of the functional groups within the copolymers are not absolute. Due to readability, the argumentation will not always name that in particular, yet respect the average functional number count within all copolymers. Under these conditions, the following (assumed) picture can be drawn (Figure 31):

As discussed above, for **5b**$_2$**/5c**$_1$**/9b**$_{115}$ a less dense layer and minor adsorbed mass were recorded in comparison to **5b**$_6$**/5c**$_4$**/9b**$_{94}$ and **5b**$_5$**/5c**$_3$**/9b**$_{112}$. Because **5b**$_2$**/5c**$_1$**/9b**$_{115}$ provided only one catechol unit on average, the copolymer was bound beside the **9b** units with one catechol on the Au surface (Figure 31, A; see chapter 4.5.3.1 for data of **9b**). The possibility of the interaction between two catechol units thus was very low since only via **9b** units bound (co)polymer could provide its catechol unit for the linkage. The fact that only the catechol units were held responsible for the main sustainable surface-polymer/polymer linkage will be discussed below.

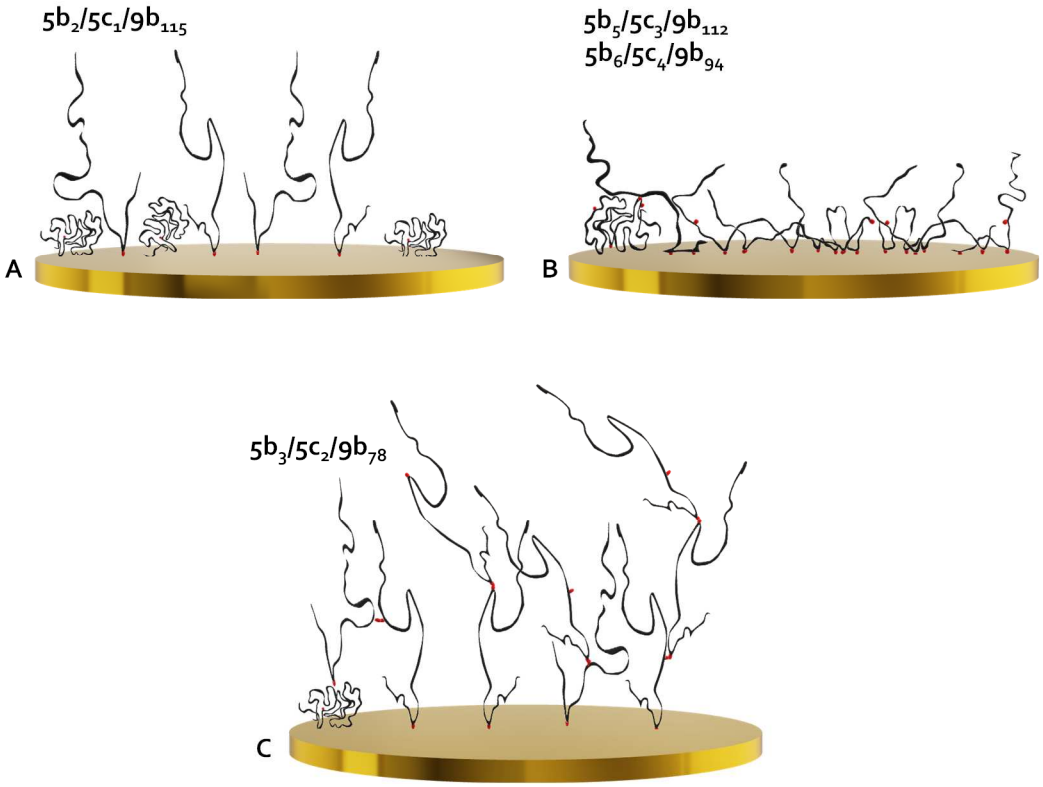


*Figure 31: Schematic depiction of the four catechol-containing copolymers* ***5b*** $_6$***/5c*** $_4$***/9b*** $_{94}$, ***5b*** $_5$***/5c*** $_3$***/9b*** $_{112}$, ***5b*** $_3$***/5c*** $_2$***/9b*** $_{78}$, *and* ***5b*** $_2$***/5c*** $_1$***/9b*** $_{115}$ *and their assumed binding behavior. A)* ***5b*** $_2$***/5c*** $_1$***/9b*** $_{115}$ *bound by one catechol or* ***9b****-units resulting in a less dense layer. B)* ***5b*** $_6$***/5c*** $_4$***/9b*** $_{94}$, ***5b*** $_5$***/5c*** $_3$***/9b*** $_{112}$ *bound by more catechol units resulting in a denser layer with higher adsorbed mass. Here, the catechol units were not only bound to the surface but assumably were linked with each other. C)* ***5b*** $_3$***/5c*** $_2$***/9b*** $_{78}$ *carrying two catechol units on average, anchoring with one unit on Au surface and enabling the formation of multi-layers by linking further copolymers onto bound copolymers with catechol-catechol interaction. (Comment: It was not verified that (co)polymers, bound via* ***9b****-units existing in coil-like structures. This depiction was used to show the more rigid manner of the layer and the harder accessibility of the catechol moiety within the bound polymer.)*

In contrast, the copolymers **5b** $_5$**/5c** $_3$**/9b** $_{94}$ and **5b** $_6$**/5c** $_4$**/9b** $_{112}$ contained three, respectively four catechol units on average. This higher number of catechol units enabled the

interaction of one copolymer with multiple binding sites. Additionally, a surface-bound copolymer can provide catechol units for interactions with other copolymers (Figure 31, B). The depicted higher rigidity of the coatings of **5b**$_5$**/5c**$_3$**/9b**$_{94}$ and **5b**$_6$**/5c**$_4$**/9b**$_{112}$ compared to the coating of **5b**$_2$**/5c**$_1$**/9b**$_{115}$, was reasoned by the monitored $\Delta$D values (Figure 29, D).

Copolymer **5b**$_3$**/5c**$_2$**/9b**$_{78}$ provided two catechol units on average, hence seemingly having the perfect architecture for surface and intermolecular binding interactions. Thus, it was assumed that this copolymer interacted, besides the **9b** units, with either one or two catechol units with the surface. The fact that one copolymer can provide two catechol moieties, enabled the possibility of binding on the surface and simultaneously facilitated an intermolecular polymer/polymer linkage. Though this happened without forming a flat layer on the surface like **5b**$_5$**/5c**$_3$**/9b**$_{94}$ and **5b**$_6$**/5c**$_4$**/9b**$_{112}$ did (Figure 31, C). Subsequently, an equilibrium between single and double-bound copolymer was set during the first two adsorption stages of **5b**$_3$**/5c**$_2$**/9b**$_{78}$ (Figure 30). The zero-order kinetic in stage 3, with its equilibrium between the occupated binding sites, and the formation of new binding sites, can be reasoned by this proposed mechanism. This mechanism was facilitated by carrying two catechol units on average within copolymer **5b**$_3$**/5c**$_2$**/9b**$_{78}$. Moreover, an equilibrium seemed to be built up between the free adsorption energy as an attractive force, and the osmotic pressure and the entropy as repelling forces. The osmotic pressure might be comparatively low due to the low density of the coating of **5b**$_3$**/5c**$_2$**/9b**$_{78}$.

But how and why can only the catechol-catechol intermolecular interaction be made responsible for this proposed mechanism? There were certainly existing catechol-amide/polymer backbone interactions potentially resulting in linked polymer chains. But certainly, this would happen for every shown copolymer in the same manner as the four copolymers had equal structures. The only difference was the number of catechol units within the copolymers. Though, if a general polymer-catechol interaction was responsible for the linkage behavior, especially **5b**$_3$**/5c**$_2$**/9b**$_{78}$ showed, every examined copolymer should have shown similar behavior, or the linkage should have increased by the number of catechol units. Hence, this performance was reasoned by catechol-

catechol linkage as seemingly **5b**$_3$/**5c**$_2$/**9b**$_{78}$, fortunately, hit the overall composition of catechol units to facilitate this mechanism.

Considering the previously observed data it was not surprising that an overall good adsorption of all four copolymers on Au surfaces was monitored. Even only one catechol unit on average was sufficient to double the amount of adsorbed copolymer (**5b**$_2$/**5c**$_1$/**9b**$_{115}$) in comparison to the non-functionalized (co)polymers (**9b**, **5b**$_{10}$/**9b**$_{94}$, and **5b**$_5$/**9b**$_{78}$). This showed the efficiency of the catechol moiety concerning adsorption processes on surfaces. The copolymers containing three and four catechol units (**5b**$_5$/**5c**$_3$/**9b**$_{94}$, **5b**$_6$/**5c**$_4$/**9b**$_{112}$), gave another 200 ng/cm² heavier coatings with an overall adsorbed mass value of ~600 ng/cm². The most outstanding observation was made with the copolymer **5b**$_3$/**5c**$_2$/**9b**$_{78}$, as a zero-order kinetic was observed, while even after 24 h of surface treatment no saturation was observed. The respective adsorption constants were determined and based on the present data, an adsorption mechanism and coating architectures were proposed and justified. As a result, it seemed that a higher number of catechol units was not decisive for good or bad adsorption, but the proper number was. After a short discussion about the surface coverage of the coating in the next chapter, the examination of the cation and catechol-containing copolymers will follow.

#### 4.5.3.2.1 Occupation approximation within copolymer coatings

Not only the adsorbed mass but also the degree of occupation and the number of polymers per area provide information. To this date, there is no method existing to determine the absolute number of adsorbed polymers concerning the produced coatings. However, via indirect methods, the number of adsorbed polymers can be estimated. One way would be a coating thickness determination via Atomic Force Microscopy (AFM) and with the approximated polymer size, the number of polymers can be approximately calculated. Unfortunately, it could not be excluded that the sensor was damaged due to sample preparation processes. Thus, the evaluation was only conducted for a **5b**$_3$/**5c**$_2$/**9b**$_{78}$ coated sensor.

For the approximation of the polymer number ($N_P$) within the coating, some hypotheses have been put forward:

It was assumed that the dissolved polymer had the same size as the bound. This allowed an approximation of the polymer sized via the radius of gyration ($R_G$):[166]

$$R_G = \sqrt{\frac{1}{6} * N_M * L^2} \qquad 9$$

With $N_M \approx 83$, the number of monomer units, and $L$, the segment length of the poly(2-oxazoline) repeat unit.

$L$ was calculated by dividing the poly(2-oxazoline) structure into triangles. The bond length equates the edge length ($l_{C\text{-}N}$ = 1,47 Å and $l_{C\text{-}C}$ = 1.54 Å), and the bond angles (120° for C-N-C and 109.5° for C-C-N) equates the angles between the respective triangular thighs (Figure 32). The edge length for the triangles then is:

$$x_1 = 2 * a * \sin\left(\frac{120°}{2}\right) = 2.55 \text{ Å}$$

$$x_2 = \sqrt{a^2 * b^2 + 2ab * \cos(109.5°)} = 2.46 \text{ Å}$$

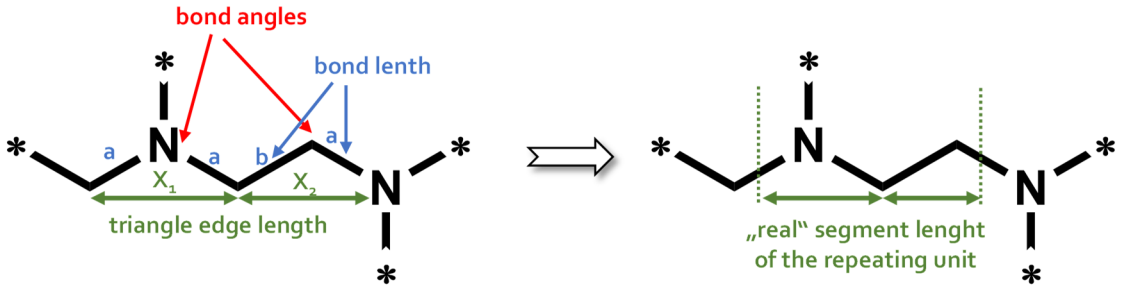


*Figure 32: Schematic explanation of the segment length calculation.*

The "real" segment length of the repeating unit one can say is approximately ¾ of the respectively calculated triangle edge length:

$$L = \frac{3}{4} * 2.55\ \text{Å} + \frac{3}{4} * 2.46\text{Å} = 3.76\ \text{Å}$$

the radius of gyration then would be:

$$R_G \approx \sqrt{\frac{1}{6} * 83 * 3.76\ \text{Å}^2} = 13.98\ \text{Å}$$

As the polymer was not one but three-dimensional, it was assumed that a sphere-like structure was present. Consequently, the spherical volume $V_{Sphere}$ was determined:

$$V_{Sphere} = \frac{4}{3} * \pi * {R_G}^3 \qquad 10$$

$$V_{Sphere} = \frac{4}{3} * \pi * 13.98\ \text{Å}^3 = 11445\ \text{Å}^3$$

To determine the coating thickness with AFM (Figure 33)., the coated sensor was removed from the QCM-D device and dried under argon since the AFM measurement was not feasible in situ. Thus, utilizing the hydrodynamic radius for the calculation would give a too high value, compared to the real value. The $R_G$ was indeed not the ideal description of the polymer size since it describes dissolved macromolecules. However, the $R_G$ does not include any solvent effects within the calculation, thus this method was chosen. Still, this is a rough approximation due to uncertain parameters like structural differences between surface-bound and dissolved polymer.

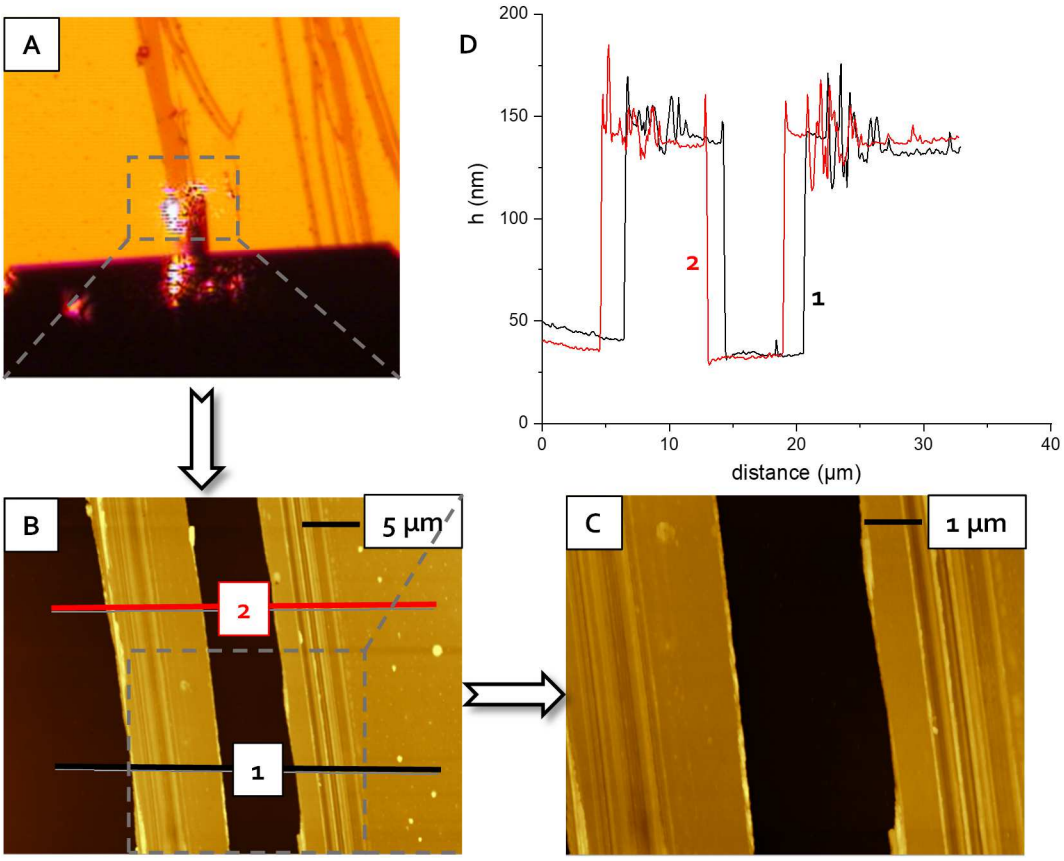


*Figure 33: The* ***5b***$_3$***/5c***$_2$***/9b***$_{78}$ *coating was scratched to determine the thickness via AFM. A) A smooth and even coating covered the sensor surface, and no intermediate spaces were visible beside the scratches. B, C) Pictured zoomed into the scratch area. D) The coating showed at two different sections a thickness of 100 nm.*

With the AFM determined coating thickness of 100 nm (1000 Å), and $V_{Sphere}$ = 10895 Å$^3$, $N_P$ can be calculated as follows:

$$N_P = \frac{1000\ \text{Å} * \ 1 * 10^{14}\ \text{Å}^2}{V_{Sphere}} = 8.74 * 10^{12}\ polymers/cm^2$$

An approximate number of polymers (**5b**$_3$/**5c**$_2$/**9b**$_{78}$) of $8.74*10^{12}$ within an area of 1 cm² with a coating's height of 1000 Å was calculated.

Regardless, this calculation was only a rough approximation of the absolute number of polymers within the coating. As the height measurement would have been made in aqueous surroundings, the general picture of spherical architectures would have been less accurate, as three different adsorption mechanisms were observed. In all probability at least three different general architectures can be assumed since three different adsorption kinetics were observed. Hence the architectural mixture was summarized under the term "sphere" to allow a simplified description of the polymers.

For comparison, another rough calculation, utilizing the $M_n^{App}$ of the respective polymer and the adsorbed mass was conducted as follows.

The $M_n^{App}$ of **5b**$_3$/**5c**$_2$/**9b**$_{78}$ was 7700 g/mol ($7.7*10^{11}$ ng/mol) and the measured adsorbed mass was 2160 ng/cm².

With $N_A$ = $6.022*10^{23}$ mol$^{-1}$ followed

$$\frac{7.7 * 10^{11}\ ng/mol}{N_A} = 1.28 * 10^{-12}\ ng/polymer$$

and with the adsorbed mass of 2160 ng/cm² followed

$$N_P = \frac{2160\ ng/cm^2}{1.28 * 10^{-12}\ ng/polymer} = 1.69 * 10^{15}\ polymers/cm^2$$

Comparing the values of both calculations, the evaluation using the adsorbed mass was $10^3$ orders of magnitude bigger than that of the evaluation using the height of the coating. This higher number can be reasoned by the different surroundings of the coating. Since the adsorbed mass included a substantial part of water within the coating, it certainly affected the value towards higher masses. The AFM height measurement

though was conducted after drying the coating, subsequently, the coating shrank. Thus, the lower number was explainable by the absence of water during the measurement. In this context, the calculated numbers $N_{P(dry)}$ = $8.74*10^{12}$ polymers/cm² and $N_{P(wet)}$ = $1.96*10^{15}$ polymers/cm² were located in a similar range and can be used – with certain caution concerning the made assumptions – as an approximation of the polymer number, adsorbed on the surface.

### 4.5.3.3 Influence of cationic units on the surface binding of catechol-containing copolymers

Finally, Au surfaces were treated with cation and catechol-containing copolymers **5b**$_2$/**5c**$_1$/**9b**$_{80}$/**9c**$_{35}$, **5b**$_3$/**5c**$_2$/**9b**$_{71}$/**9c**$_7$, **5b**$_5$/**5c**$_3$/**9b**$_{102}$/**9c**$_{10}$ and **5b**$_6$/**5c**$_4$/**9b**$_{86}$/**9c**$_8$. These copolymers were expected to build the most sustainable and durable coating, regarding the entire (co)polymer matrix, as these copolymers were closest to the models. First measurements (Chapter 4.5.2), already indicated a faster absorption process and a more durable coating.

Considering the adsorption graphs in Figure 34 A, the cation and catechol-containing copolymers showed a different behavior compared to their precursors. The absolute adsorbed mass for the copolymers **5b**$_2$/**5c**$_1$/**9b**$_{80}$/**9c**$_{35}$ and **5b**$_5$/**5c**$_3$/**9b**$_{102}$/**9c**$_{10}$ in contrast to the non-cationic precursors **5b**$_2$/**5c**$_1$/**9b**$_{115}$ and **5b**$_5$/**5c**$_3$/**9b**$_{112}$ halved. For the copolymer **5b**$_3$/**5c**$_2$/**9b**$_{71}$/**9c**$_7$ a comparison was difficult since the precursor **5b**$_3$/**5c**$_2$/**9b**$_{78}$ did not reach a state of saturation. Yet taking a certain point at 50 min treatment (**5b**$_3$/**5c**$_2$/**9b**$_{71}$/**9c**$_7$ reached at 50 min a state of saturation), the adsorbed amount of the cationic species **5b**$_3$/**5c**$_2$/**9b**$_{71}$/**9c**$_7$ valued only 2/3 of the adsorbed amount of the precursor **5b**$_3$/**5c**$_2$/**9b**$_{78}$. The copolymer **5b**$_6$/**5c**$_4$/**9b**$_{86}$/**9c**$_8$ though showed an equal amount of adsorbed mass compared to the relating non-cationic precursor **5b**$_6$/**5c**$_4$/**9b**$_{94}$. The data of **5b**$_2$/**5c**$_1$/**9b**$_{80}$/**9c**$_{35}$ however should be integrated with caution, since the number of cationic groups was much higher than that of the other copolymers (Chapter 4.4.3).

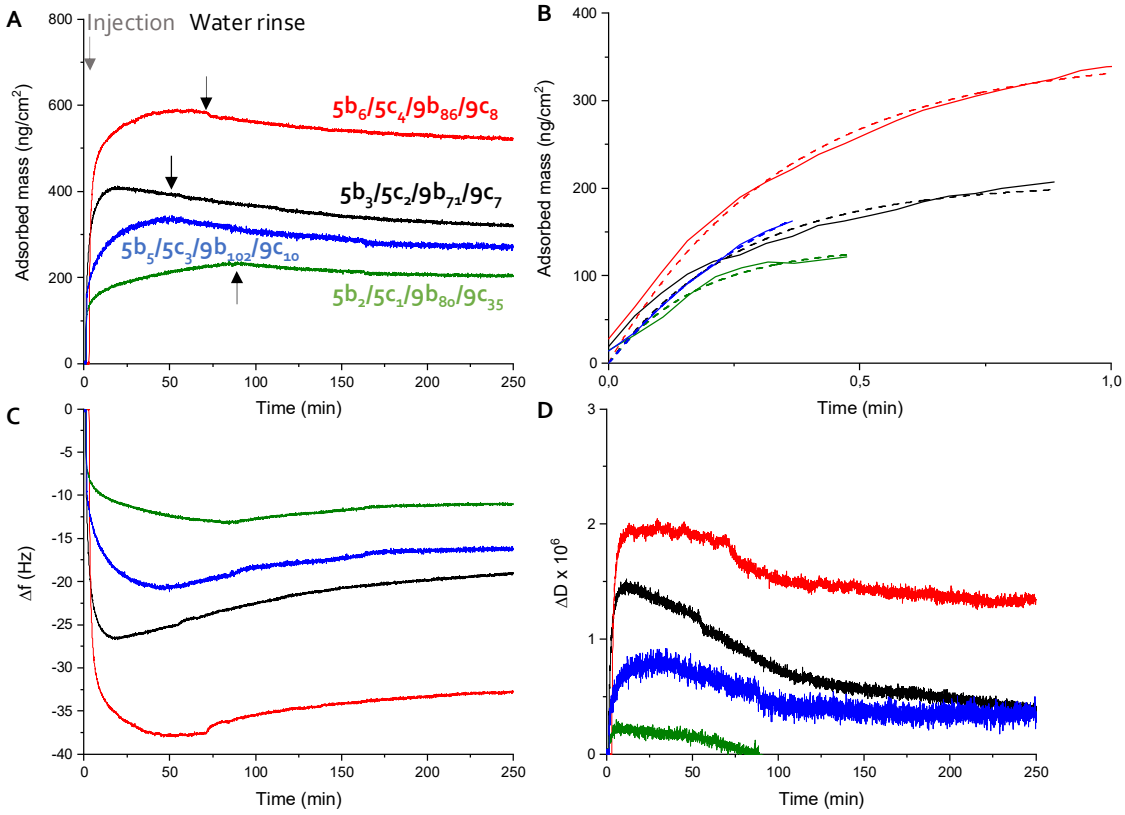


*Figure 34: A) Adsorption graphs of cation and catechol-containing copolymers* ***5b2/5c1/9b80/9c35***, ***5b3/5c2/9b71/9c7***, ***5b5/5c3/9b102/9c10***, ***5b6/5c4/9b86/9c8***. *B) Exponential fitting of the initial adsorption curve over 1 min. C, D) Graphic depiction of the related frequency and dissipation shifts.*

The data of **5b**$_2$**/5c**$_1$**/9b**$_{80}$**/9c**$_{35}$ however allowed the conclusion, that the number of cations had a large effect on the adsorption performance. With a high number of cationic units, rivalry by charge repulsion can occur (Chapter 1.3). This could have caused the observed low mass adsorption of **5b**$_2$**/5c**$_1$**/9b**$_{80}$**/9c**$_{35}$ with only ~200 ng/cm². This charge repulsion effect seemed to be not stronger with more than the 35 ethyleneimine units of **5b**$_2$**/5c**$_1$**/9b**$_{80}$**/9c**$_{35}$ because PEI (**9c**) showed similar adsorbed mass values. Consequently, the mass adsorption did not appear to suffer from more cationic units than 35. Apparently, at ~200 ng/cm² a limitation of the mass adsorption for particular (co)polymers **9b**, **9c**, and **5b**$_2$**/5c**$_1$**/9b**$_{80}$**/9c**$_{35}$ was observed. This limitation may originate

from a hydration layer above the high concentrated (co)polymer coatings, facilitating osmotic pressure with a subsequent repulsion. For the cation-containing (co)polymers, the mechanism of charge repulsion and osmotic repulsion certainly acted together. For **9b** however, the repulsion may originate only from the increased osmotic pressure.

The three catechol-containing copolymers **5b**$_3$/**5c**$_2$/**9b**$_{71}$/**9c**$_7$, **5b**$_5$/**5c**$_3$/**9b**$_{102}$/**9c**$_{10}$, and **5b**$_6$/**5c**$_4$/**9b**$_{86}$/**9c**$_8$ did not form such rigid coatings (see $\Delta$D values in Figure 34 D), subsequently, the osmotic pressure was lower and more copolymer was adsorbed.

The adsorption velocity of the cation and catechol-containing copolymers ($k_A^{Cation}$(7.2∗10$^{-3}$ - 1.0∗10$^{-2}$ mL/mg s)) showed overall the same values as their precursors ($k_A^{Precursor}$(5.6∗10$^{-3}$ - 1.1∗10$^{-2}$ mL/mg s)). Thus no general influence of the cation unit towards the adsorption velocity can be concluded.

After the rinsing process for the **5b**$_6$/**5c**$_4$/**9b**$_{86}$/**9c**$_8$ and **5b**$_2$/**5c**$_1$/**9b**$_{80}$/**9c**$_{35}$ coating ~10% and for **5b**$_5$/**5c**$_3$/**9b**$_{102}$/**9c**$_{10}$ and **5b**$_3$/**5c**$_2$/**9b**$_{71}$/**9c**$_7$ ~20% mass loss was monitored. The durability of the cation and catechol-containing copolymer coatings was partially improved compared to their precursors. An absolute trend however was not identified. Yet, even with a mass loss of 20%, the durability was still great. Besides, for applications (*e.g.* anti-fouling), the durability of the coatings needed to be tested with more environmentally surroundings like buffer solution which will be discussed later.

Considering all things, no clean proof for a general advantage of the coatings of cation and catechol-containing copolymers, compared to the precursor coatings on Au surfaces can be concluded as of yet. In the next section, a discussion of the adsorption behavior of the (co)polymer matrix towards different surface types follows.

#### 4.5.3.4 Adsorption of minor functionalized (co)polymers on various surfaces

The investigation concerning adsorption on Au surfaces of the (co)polymer matrix was further extended by the surface types borosilicate (BS), iron (Fe), and polystyrene (PS). These surface types were chosen to create a more general profile through the adsorption

behavior on metallic, inorganic polar, and organic-non-polar surfaces. Initially, the minor functionalized (co)polymers **9b**, **5b**$_5$/**9b**$_{78}$, and **5b**$_{10}$/**9b**$_{94}$ will be discussed and the major functionalized polymers will be included successively with raising functionalization.

For all the minor functionalized (co)polymers **9b**, **5b**$_5$/**9b**$_{78}$, and **5b**$_{10}$/**9b**$_{94}$ adsorption on Au, BS, and PS was observed (Figure 35, A, B, D), yet almost no adsorption on Fe surfaces was monitored (Figure 35, C). Further, a special observation, of the adsorption graphs of **5b**$_5$/**9b**$_{78}$ and **5b**$_{10}$/**9b**$_{94}$ on BS and Fe and **9b** on PS surfaces was made. For the initial adsorbed mass, a high mass shift was monitored, which decreased fast with time progression. This behavior was caused by fast (co)polymer adsorption with a high value of hydrodynamically coupled water. This ephemeral configuration collapsed by leaving bound water, enabling more rigid bound (co)polymer. The high mass value thus was an overestimation. Indeed, the adsorption constants in this regard were not comparable, thus, the $k_A$ numbers, in this case, were not comparable. In a general sense considering the absolute adsorbed mass, BS and PS surfaces showed most with about ~330 ng/cm² and 320 ng/cm² respectively (Figure 35, B, D). The least adsorbed mass was monitored on Fe surfaces with a maximum of ~20 ng/cm² (Figure 35, C).

Noteworthy are the results considering the adsorption on PS surfaces. On PS surfaces the highest amount of adsorbed mass did not show the copolymer with the highest aryl proportion (**5b**$_{10}$/**9b**$_{94}$) but the copolymer with fewer (**5b**$_5$/**9b**$_{78}$) (Figure 35, D). Even for **9b**, higher adsorption values on PS surfaces were monitored, compared to **5b**$_{10}$/**9b**$_{94}$. These results were antithetical to an expectable outcome, as the influence of π-stacking with more aryl units was anticipated to be more impactful with higher adsorbed mass values. The previously discussed coiling effect of the amphiphilic copolymers **5b**$_5$/**9b**$_{78}$ and **5b**$_{10}$/**9b**$_{94}$ can be consulted here also (Chapter 4.5.3.2). The assumed coil-like structure would keep the aryl units inside, shielded from water and surface interactions. This effect would increase – to some extent – with the aryl unit number which can explain the observed trend. The $k_A$ values may support this observed trend, as the $k_A$(**5b**$_{10}$/**9b**$_{94}$) = 1,91*10$^{-2}$ mL/mg s was significantly lower compared to the $k_A$(**5b**$_5$/**9b**$_{78}$) = 3,38*10$^{-2}$ mL/mg s. This suggested a lower diffusion velocity due to coiling. The overall higher adsorbed mass on PS and BS surfaces seemed to be caused by less coating density

(verified by higher ΔD values, Chapter 8, Figure S 46) and consequential lower osmotic pressure within the adsorbate. Considering the Fe surfaces, virtually no adsorbed mass was monitored, which cannot be explained yet.

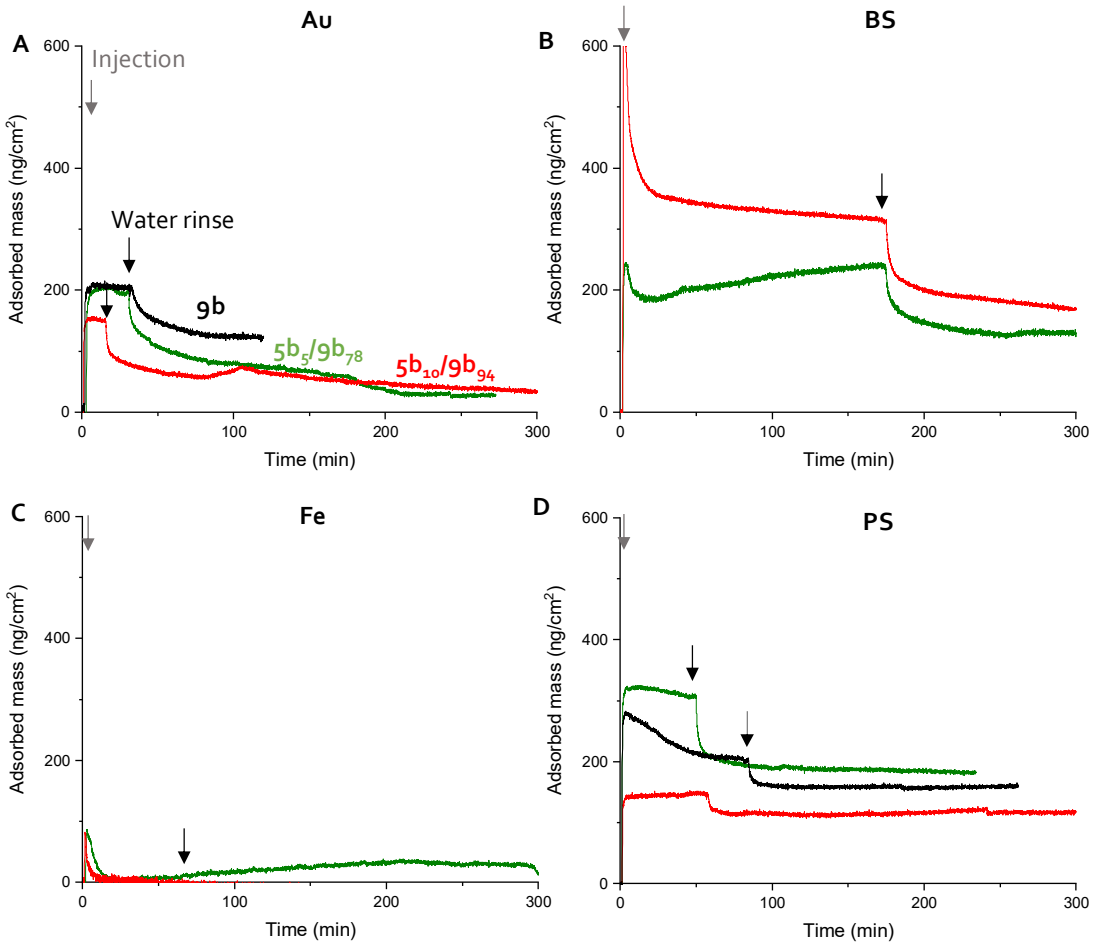


*Figure 35: Adsorption graphs of the minor functionalized (co)polymers with gold (A), borosilicate (B), iron (C), and polystyrene surfaces (D) surfaces.*

Considering the durability of the coatings in comparison, it can be concluded that the coatings of **5b**$_5$/**9b**$_{78}$ and **5b**$_{10}$/**9b**$_{94}$ did not show a significant difference in the mass loss for Au (**5b**$_5$/**9b**$_{78}$ ~61%, **5b**$_{10}$/**9b**$_{94}$ ~60%) and for BS (**5b**$_5$/**9b**$_{78}$ ~46%, **5b**$_{10}$/**9b**$_{94}$ ~48%). Whereat the coating on PS surfaces **5b**$_{10}$/**9b**$_{94}$ only lost ~20% and **5b**$_5$/**9b**$_{78}$ lost ~42% of the adsorbed mass. Among these copolymers, the number of aryl units seemed to have an impact on the coating's sustainability on PS surfaces by potential π-stacking.

However, this can not be the explanation for the comparable low mass loss of **9b** on PS surfaces of ~23%. Still, there was no evidence or reason found for that high adsorption value and the low mass loss concerning **9b**, especially on PS surfaces.

It can be concluded that even the minor functionalized (co)polymers adsorb and stick to various surface types whether metallic, anionic, or hydrophobic. However, almost no adsorbed mass was monitored for the copolymers on Fe surfaces. Further investigations will show if the catechol-containing copolymers are capable to improve the adsorption performance.

### 4.5.3.5 Influence of catechol units on the binding on various surfaces

Further on, the catechol-containing copolymers **5b$_6$/5c$_4$/9b$_{94}$**, **5b$_5$/5c$_3$/9b$_{112}$**, **5b$_3$/5c$_2$/9b$_{78}$** and **5b$_2$/5c$_1$/9b$_{115}$** were considered concerning the surface types Au, BS, Fe and PS (Figure 36). Initially recognizable was that all copolymers showed attractive interactions with all surfaces types. Further, the overall similarity, concerning the adsorption behavior on Au and BS surfaces of the catechol-containing copolymers (Figure 36, A, and B) was noteworthy. For **5b$_3$/5c$_2$/9b$_{78}$**, the same zero-order adsorption kinetic was monitored for both surfaces. The $k_A$´s showed similar values with $k_{A3}^{Au}$ = 3,96∗10$^{-5}$ mL/mg s and $k_{A3}^{BS}$ = 4,46∗10$^{-5}$ mL/mg s. However, not three but two kinetic stages were identifiable on BS surfaces, as the initial adsorption transitioned straight into the zero-order kinetic stage ($k_{A3}$). The initial stage showed almost twice the value of adsorption velocity on BS than on Au ($k_{A1}^{Au}$ = 6,51∗10$^{-3}$ mL/mg s; $k_{A1}^{BS}$ = 1,12∗10$^{-2}$ mL/mg s). This was reasoned by the fact that the first stage on BS already reached the amount of adsorbed mass, which was first reached on Au in the second stage (Figure 37, A and B). Except for the differing initial adsorption behavior, the copolymer behaved similarly on Au and BS. It must therefore be assumed that a similar zero-order adsorption mechanism (proposed and discussed in chapter 4.5.3.2) can be applied for both Au and BS surfaces. Considering **5b$_6$/5c$_4$/9b$_{94}$**, the behavior differed in the adsorption performance on Au and BS not strongly (Figure 36, A, B).

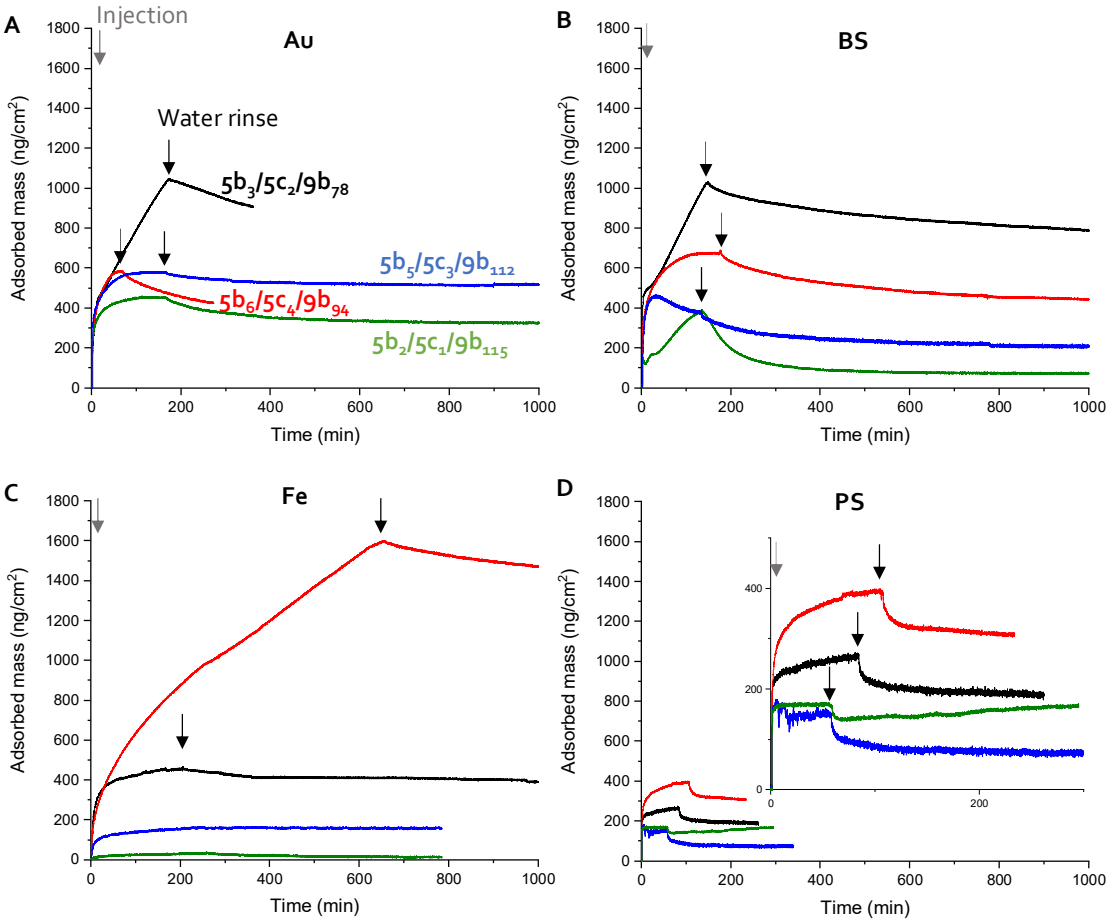


*Figure 36: Catechol functionalized copolymers* ***5b$_6$/5c$_4$/9b$_{94}$***, ***5b$_5$/5c$_3$/9b$_{112}$***, ***5b$_3$/5c$_2$/9b$_{78}$*** *and* ***5b$_2$/5c$_1$/9b$_{115}$*** *examined on various surfaces. The copolymer* ***5b$_3$/5c$_2$/9b$_{78}$*** *did show a zero-order kinetic behavior on Au (A) and BS (B) surfaces; yet, on Fe (C) for* ***5b$_6$/5c$_4$/9b$_{94}$*** *this kinetic behavior was monitored instead. On PS (D) surfaces, the copolymers* ***5b$_6$/5c$_4$/9b$_{94}$*** *and* ***5b$_3$/5c$_2$/9b$_{78}$*** *acted vice versa to their precursors* ***5b$_{10}$/9b$_{94}$*** *and* ***5b$_5$/9b$_{78}$****. The catechol moiety presumably prevented the coiling effects caused by amphiphilic properties.*

The adsorption maximum on Au was ~600 ng/cm² and on BS 680 ng/cm². The mass loss on Au was slightly bigger with 28% compared to BS with 24%. The performance of **5b$_5$/5c$_3$/9b$_{112}$** differed more, as the adsorbed mass equilibrium on BS was with ~400 ng/cm² at about 1/3 lower than that on Au. For **5b$_2$/5c$_1$/9b$_{115}$** the adsorbed mass value on BS and Au surfaces was similar with ~400 ng/cm², even if the kinetic differed. Only **5b$_5$/5c$_3$/9b$_{112}$** differed with its adsorption performance, which can not be explained by the present data.

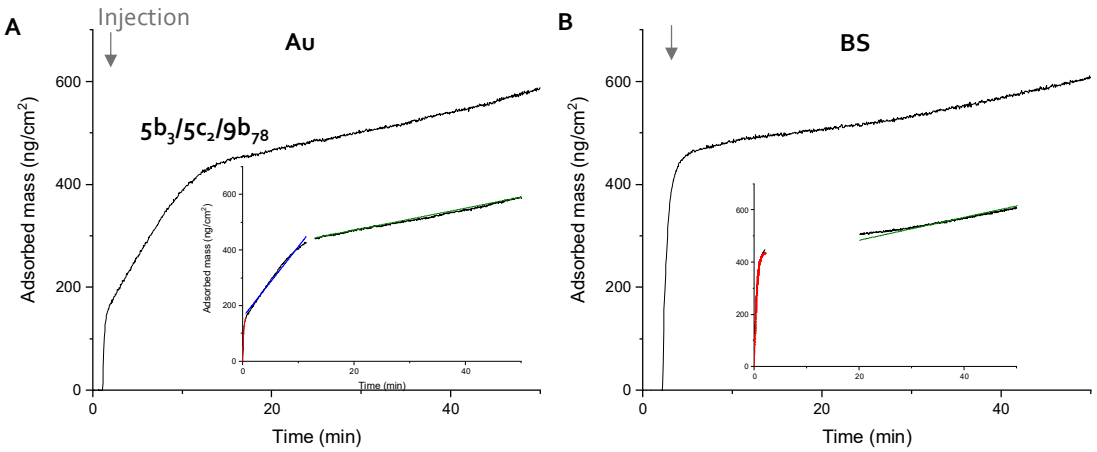


*Figure 37: Zoom of the primary adsorption graphs of* ***5b₃/5c₂/9b₇₈*** *and the respective exponential and linear fits for the* $k_{A1\text{-}3}$ *determination to illustrate the three-step adsorption kinetics on Au (A) and the two-step kinetics on BS (B).*

The adsorption of **5b₂/5c₁/9b₁₁₅** on BS surfaces should be discussed at this point. Initially, it seemed, that **5b₂/5c₁/9b₁₁₅** showed also a zero-order kinetic behavior on BS surfaces, as **5b₃/5c₂/9b₇₈** did. However, under closer inspection, the adsorption graph showed a very slow approximation to a state of saturation (Figure 38, A, and B). The ΔD values though did not indicate any density change within the adsorbate of **5b₂/5c₁/9b₁₁₅** since the value remained equal from min ~45 to ~135. Thus, the additional adsorbed mass which was almost ¾ of the overall adsorbed mass resulted in a very rigid adsorbate. Hence, it can be assumed that the first kinetic stage produced a less dense coating with an additional, very rigid coating during the second stage. Considering the desorption during the rinsing, this additional mass was removed entirely, as the adsorbed mass value dropped at ~70%. This showed a big difference between Au and BS surfaces as the mass loss at Au surfaces was only ~20%. This indicated for **5b₂/5c₁/9b₁₁₅** a different adsorption mechanism on BS compared to Au. Since the other three copolymers **5b₆/5c₄/9b₉₄**, **5b₅/5c₃/9b₁₁₂** and **5b₃/5c₂/9b₇₈** did not show a difference in the kinetics, a trend or a reasonable mechanistic proposal for the adsorption process of **5b₂/5c₁/9b₁₁₅**, could not be

made.

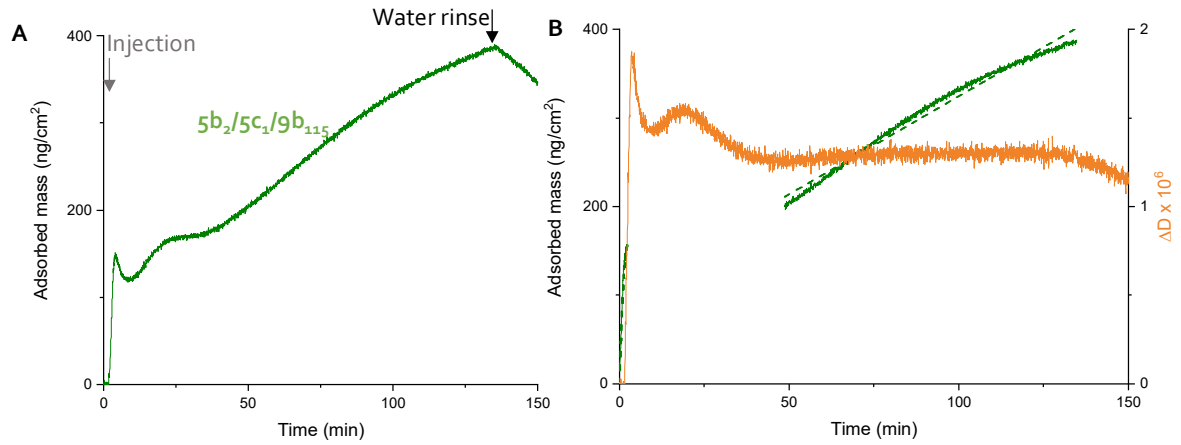


*Figure 38: Adsorption graph of* ***5b₂/5c₁/9b₁₁₅*** *on BS surfaces (A) and the respective exponential and linear fit paired with the dissipation shifts (B).*

Considering the remaining mass on BS, after equal adsorption and rinsing time progression, the remaining mass was approximately doubled simultaneously by number increase of catechol units: **5b₂/5c₁/9b₁₁₅** ~80 ng/cm²; **5b₅/5c₃/9b₁₁₂** ~200 ng/cm²; **5b₆/5c₄/9b₉₄** ~450 ng/cm²; (**5b₃/5c₂/9b₇₈** ~790 ng/cm²). In this context, **5b₃/5c₂/9b₇₈** was excluded due to its zero-order behavior. In this regard, a trend was recognizable concerning the connection between catechol number and durability on BS surfaces.

On Fe surfaces, an outstanding observation was made. The copolymer **5b₆/5c₄/9b₉₄,** not **5b₃/5c₂/9b₇₈** showed a zero-order kinetic behavior (Figure 36, A, B, C; Figure 39, A). This outcome was confirmed by remeasuring the copolymer **5b₃/5c₂/9b₇₈** with the same result. This behavior change and the comparably low overall adsorbed mass of the copolymers **5b₅/5c₃/9b₁₁₂**, **5b₃/5c₂/9b₇₈**, and **5b₂/5c₁/9b₁₁₅** indicated a high impact of the catechol unit number on Fe surfaces. **5b₂/5c₁/9b₁₁₅** did almost not adsorb on Fe surfaces ($m_{max}$ ~ 35 ng/cm²) averaging only one catechol unit. In that context, primarily unexpected was the performance of **5b₅/5c₃/9b₁₁₂** and **5b₃/5c₂/9b₇₈** in comparison, as for **5b₅/5c₃/9b₁₁₂** ~160 ng/cm² and for **5b₃/5c₂/9b₇₈** ~ 450 ng/cm² was monitored. Consulting the dissipation shifts (Figure 39, B), **5b₅/5c₃/9b₁₁₂** showed a highly rigid coating. This

indicated that **5b**$_5$**/5c**$_3$**/9b**$_{112}$ adsorbed flatter on the surface, and presumably was not able to provide a catechol unit for a linkage between the copolymers like **5b**$_6$**/5c**$_4$**/9b**$_{94}$ was capable. **5b**$_3$**/5c**$_2$**/9b**$_{78}$, averaging two catechol units, was assembled less dense (see ΔD values Figure 39, B). Hence, following this argumentation, the impact on the adsorption performance on Fe surfaces depended particularly on the number of catechol units. This is supported additionally as the unfunctionalized copolymers **5b**$_5$**/9b**$_{78}$ and **5b**$_{10}$**/9b**$_{94}$ did not adsorb on Fe surfaces at all (Figure 35, C). Thus, finally, it can be assumed that adsorption on Fe surfaces thus required more free catechol units than on Au and BS surfaces.

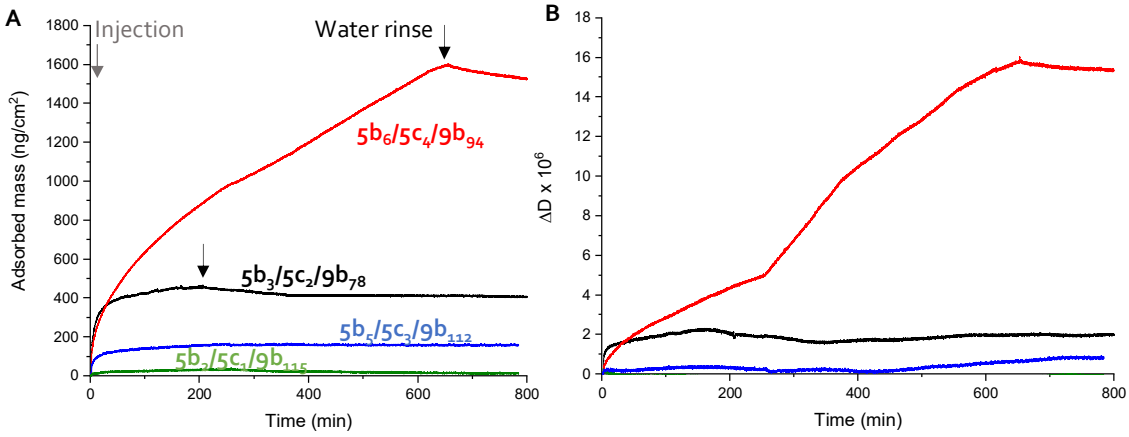


*Figure 39: A) Adsorption graphs of the catechol-containing copolymers on Fe surfaces with the respective ΔD graphs (B). Noteworthy was, that not* ***5b***$_3$***/5c***$_2$***/9b***$_{78}$ *but* ***5b***$_6$***/5c***$_4$***/9b***$_{94}$ *showed a zero-order kinetic behavior on Fe surfaces.*

Generally, the initial adsorption velocity on Fe surfaces was slower than on BS and Au surfaces for all the copolymers **5b**$_6$**/5c**$_4$**/9b**$_{94}$, **5b**$_5$**/5c**$_3$**/9b**$_{112}$, **5b**$_3$**/5c**$_2$**/9b**$_{78}$, and **5b**$_2$**/5c**$_1$**/9b**$_{115}$. Considering the zero-order kinetic behavior of **5b**$_3$**/5c**$_2$**/9b**$_{78}$ on Au and BS and of **5b**$_6$**/5c**$_4$**/9b**$_{94}$ on Fe surfaces in comparison, the difference was significant (Figure 40). The initial adsorption constants already showed some difference ($k_{A1}^{Au}$(**5b**$_3$**/5c**$_2$**/9b**$_{78}$) = 6.51∗10$^{-3}$ mL/mg s; $k_{A1}^{BS}$(**5b**$_3$**/5c**$_2$**/9b**$_{78}$) = 1.12∗10$^{-2}$ mL/mg s; $k_{A1}^{Fe}$(**5b**$_6$**/5c**$_4$**/9b**$_{94}$) = 1.37∗10$^{-3}$ mL/mg s; Figure 40, C). Yet the third, linear kinetic stage showed less than half the

adsorption velocity for $k_{A_3}^{Fe}$(**5b**$_6$/**5c**$_4$/**9b**$_{94}$) = 1.64*10$^{-5}$ mL/mg s compared to $k_{A_3}^{Au}$(**5b**$_3$/**5c**$_2$/**9b**$_{78}$) = 3.96*10$^{-5}$ mL/mg s and $k_{A_3}^{BS}$(**5b**$_3$/**5c**$_2$/**9b**$_{78}$) = 4.46*10$^{-5}$ mL/mg s (Figure 40, D).

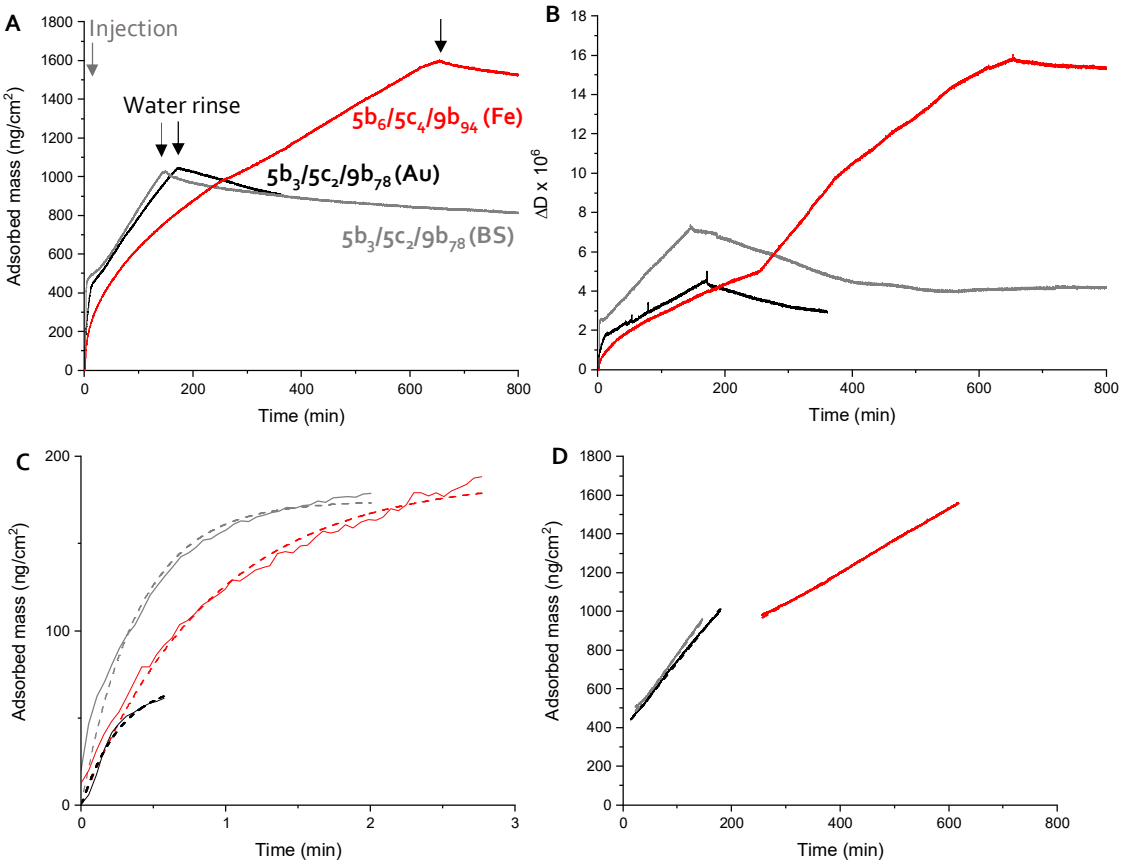


*Figure 40: Adsorption graphs of* ***5b***$_6$/***5c***$_4$/***9b***$_{94}$ *on Au and BS and* ***5b***$_3$/***5c***$_2$/***9b***$_{78}$ *on Fe surfaces (A) with the respective dissipation shifts (B). C, D) Kinetical comparison between the two polymers regarding the three different surfaces.*

The initial slower adsorption on Fe surfaces indicated an inhibited adsorption mechanism. A primary inhibition caused by Fe ions, as Fe is highly sensitive for oxidation, initially was obvious. A potential cleaning of the surface from the occurring Fe ions by binding on catechol units would presumably cause a linkage between the copolymers as mentioned previously (Chapter 1.3). A linkage of **5b**$_5$/**5c**$_3$/**9b**$_{112}$ (providing three catechol units on average) with a simultaneously surface binding, though would be more likely

than with **5b**$_3$**/5c**$_2$**/9b**$_{78}$ (providing two catechol units on average). But the adsorption performance of **5b**$_5$**/5c**$_3$**/9b**$_{112}$ and **5b**$_3$**/5c**$_2$**/9b**$_{78}$ proceeded contrarily (Figure 39, A). A possible assumption would be, that the higher density of the **5b**$_5$**/5c**$_3$**/9b**$_{112}$ coating can be caused by crosslinking with Fe ions. However, the data of the copolymer **5b**$_6$**/5c**$_4$**/9b**$_{94}$ did not fit that assumption since the observed zero-order kinetic then would not happen. At least for the adsorption behavior of **5b**$_6$**/5c**$_4$**/9b**$_{94}$, the following can be concluded. Once the adsorption of **5b**$_6$**/5c**$_4$**/9b**$_{94}$ on the Fe surface reached a certain stage (~255 min; ~970 ng/cm$^2$), the binding mechanism changed, visible in the $\Delta$D graph (Figure 40, B). Interestingly, the velocity of mass adsorption decreased while the dissipation shift increased. Accordingly, the coating beyond that mark was comparably soft. This suggested fewer binding sites for the zero-order kinetic procedure of **5b**$_6$**/5c**$_4$**/9b**$_{94}$ than for the previously observed zero-order kinetic on Au and BS with **5b**$_3$**/5c**$_2$**/9b**$_{78}$. Less binding sides during the zero-order kinetic process for the copolymer **5b**$_6$**/5c**$_4$**/9b**$_{94}$, although providing overall twice as many catechol units as its counterpart **5b**$_3$**/5c**$_2$**/9b**$_{78}$, indicated an inhibition by an occupation of catechol units within the adsorbate on the Fe surfaces. That applies under the assumption that the zero-order behavior was facilitated by a catechol-catechol interaction as discussed in chapter 4.5.3.2. Inhibition of the zero-order kinetic by Fe ions can be ruled out since the Fe surface was already coated and a constant supply of Fe ions via oxidation thus was not likely. The overall durability of the catechol-containing copolymer coatings on Fe surfaces seemed to be good against water rinsing processes. Excluding **5b**$_2$**/5c**$_1$**/9b**$_{115}$, the mass loss during the rinsing process was in a range of ~2 and ~13%. Especially for **5b**$_6$**/5c**$_4$**/9b**$_{94}$ lower osmotic pressure can be reasoned for that observation, as the low density of the coating indicated a high amount of hydrodynamically bound water.

After all, no definitive reasons for the slower kinetic performance and the differing adsorption behavior on Fe surfaces were found. However, it can be concluded that the physicochemical properties of Fe surfaces influenced the adsorption performance in particular. Whether Fe ions due to oxidation during the adsorption process were responsible for this outcome could not be verified yet. For a determination, a combination of QCM-D and FT-IR spectroscopy can potentially be appropriate.[167]

Overall, it seemed that adsorption on Fe surfaces needed a higher catechol unit count, yet once copolymer bound to the surface, the durability of the coating against water rinsing processes was good.

Finally, PS surfaces were taken into consideration as an example for non-polar surfaces (Figure 36, D; Figure 41, A). As above mentioned, the amphiphilic character of the minor functionalized copolymers **5b**$_5$/**9b**$_{78}$ and **5b**$_{10}$/**9b**$_{94}$ was reasoned for the recognized trend on PS surfaces (Figure 35, D). The free catechol units within the copolymers **5b**$_6$/**5c**$_4$/**9b**$_{94}$, **5b**$_5$/**5c**$_3$/**9b**$_{112}$, **5b**$_3$/**5c**$_2$/**9b**$_{78}$, and **5b**$_2$/**5c**$_1$/**9b**$_{115}$ could be held responsible for repealing the hydrophobicity, to facilitate a π-interaction between copolymer and PS surface. Indeed, **5b**$_6$/**5c**$_4$/**9b**$_{94}$ showed an adsorbed mass duplication compared to the coating of the precursor **5b**$_{10}$/**9b**$_{94}$. For **5b**$_3$/**5c**$_2$/**9b**$_{78}$ a similar adsorbed mass maximum was recorded compared to its precursor **5b**$_5$/**9b**$_{78}$.

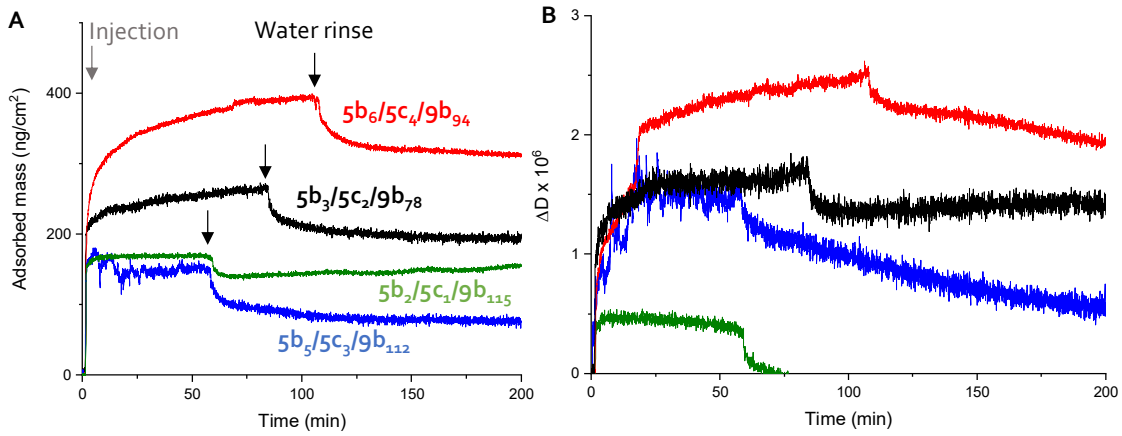


*Figure 41: Adsorption graphs of catechol-containing polymers on PS surfaces (A) with the related dissipation shifts (B).*

Low interaction was monitored with **5b**$_5$/**5c**$_3$/**9b**$_{112}$ and **5b**$_2$/**5c**$_1$/**9b**$_{115}$, yet their precursors were not considered on PS surfaces. The low adsorbed mass for **5b**$_2$/**5c**$_1$/**9b**$_{115}$ was explainable with the low content of aryl groups, as **9b** showed similar results (Chapter 4.5.3.4). Due to the number of aryl units, the copolymer **5b**$_5$/**5c**$_3$/**9b**$_{112}$ though certainly was expected to show a mass value between the copolymers **5b**$_6$/**5c**$_4$/**9b**$_{94}$ and

**5b**$_3$**/5c**$_2$**/9b**$_{78}$. Consulting the related dissipation shifts (Figure 41, B) the ΔD values of **5b**$_5$**/5c**$_3$**/9b**$_{112}$ distinguished substantial from the one of **5b**$_2$**/5c**$_1$**/9b**$_{115}$, despite, both showed a similar adsorbed mass value. This implied various binding mechanisms as the layer showed massive different properties. Still, with the present data, a potential mechanism cannot be proposed. One can only assume that the **5b**$_5$**/5c**$_3$**/9b**$_{112}$ coating was highly soft while carrying a great amount of hydrodynamically coupled water. The durability of the coatings towards the water rinsing process overall was good. The coatings showed mass losses between ~14 and 28% for **5b**$_6$**/5c**$_4$**/9b**$_{94}$, **5b**$_3$**/5c**$_2$**/9b**$_{78}$, and **5b**$_2$**/5c**$_1$**/9b**$_{115}$. The copolymer **5b**$_5$**/5c**$_3$**/9b**$_{112}$ though was washed off the surfaces at ~50%. Due to the low rigidity of the **5b**$_5$**/5c**$_3$**/9b**$_{112}$ coating, the osmotic pressure can be excluded as the main driving force for its desorption process. More likely was mechanically desorption by shear forces due to less tight binding.

The adsorption velocity of the catechol-containing copolymers was slower compared to the rapid adsorption of the precursors ($k_a$(**5b**$_6$**/5c**$_4$**/9b**$_{94}$) = $7.67*10^{-3}$ mL/mg s; $k_a$(**5b**$_5$**/5c**$_3$**/9b**$_{112}$) = $1.12*10^{-2}$ mL/mg s; $k_a$(**5b**$_3$**/5c**$_2$**/9b**$_{78}$) = $1.60*10^{-2}$ mL/mg s; $k_a$(**5b**$_2$**/5c**$_1$**/9b**$_{115}$) = $7.46*10^{-3}$ mL/mg s; $k_a$(**5b**$_5$**/9b**$_{78}$) = $3,38*10^{-2}$ mL/mg s; $k_a$(**5b**$_{10}$**/9b**$_{94}$) = $1,91*10^{-2}$ mL/mg s). Catechol seemingly did not accelerate, but rather enabled the adsorption process on PS surfaces for the copolymer with the highest aryl content due to countering the amphiphilicity. This feature facilitates the possibility to coat (π-system-containing) hydrophobic surfaces by π-π-interactions in aqueous environments. This demonstrated the big influence of the catechols, not only to act as a binding unit but also as an assistant to enable unconventional performance.

Overall, it was demonstrated that catechol had a big impact on the adsorption performance of the copolymers regarding the considered surface gold, borosilicate, iron, and polystyrene. Yet it can be concluded that even one catechol unit (on average) was enough to build up an appreciable coating on Au and BS surfaces. A slightly higher number of catechol units within the copolymers caused a thicker and more durable coating. However, not the highest catechol unit count facilitated the thickest or most durable coating on Au or Bs surfaces. Furthermore, a zero-order adsorption kinetic was discovered, monitored for **5b**$_3$**/5c**$_2$**/9b**$_{78}$ on Au and BS and **5b**$_6$**/5c**$_4$**/9b**$_{94}$ on Fe surfaces. On

Fe surfaces, overall more catechol units were required to build up an appreciable coating. The treatment of the PS surfaces demonstrated the influence of the catechol unit to facilitate π-π-interactions with hydrophobic surfaces in aqueous environments. Regardless of which surface, the catechol-containing copolymers bound, and most coatings were highly durable.

Maritime organisms use alongside the catechol units cation units within their glue proteins to promote the binding (Chapter 1.3). In the next section, the adsorption behavior on Au, BS, Fe, and PS surfaces of the catechol and cation-containing copolymers (**5b**$_2$/**5c**$_1$/**9b**$_{80}$/**9c**$_{35}$, **5b**$_3$/**5c**$_2$/**9b**$_{71}$/**9c**$_7$, **5b**$_5$/**5c**$_3$/**9b**$_{102}$/**9c**$_{10}$, **5b**$_6$/**5c**$_4$/**9b**$_{86}$/**9c**$_8$) will be discussed.

### 4.5.3.6 Influence of cationic units on the binding on various surfaces

Below, the influence of the cationic units within the catechol-containing copolymers on the adsorption performance on the surfaces gold, borosilicate, iron, and polystyrene will be discussed. The copolymer matrix **5b**$_2$/**5c**$_1$/**9b**$_{80}$/**9c**$_{35}$, **5b**$_3$/**5c**$_2$/**9b**$_{71}$/**9c**$_7$, **5b**$_5$/**5c**$_3$/**9b**$_{102}$/**9c**$_{10}$ and **5b**$_6$/**5c**$_4$/**9b**$_{86}$/**9c**$_8$ was extended by the copolymer **5b**$_{10}$/**9b**$_{84}$/**9c**$_{10}$. This copolymer carried methoxy-protected catechol and ethyleneimine units to verify the influence of the catechol unit on the adsorption performance. The influence of cations on the binding on Au surfaces was discussed in chapter 4.5.3.3, thus only a brief placement of the copolymer **5b**$_{10}$/**9b**$_{84}$/**9c**$_{10}$ will follow.

Generally, the five mentioned copolymers all showed attractive interactions with all surfaces, and the rinsing process indicated overall good durability (Figure 42). However, the overall adsorbed mass maximum was lower compared to the adsorbed mass of the precursor copolymers (**5b**$_6$/**5c**$_4$/**9b**$_{94}$, **5b**$_5$/**5c**$_3$/**9b**$_{112}$, **5b**$_3$/**5c**$_2$/**9b**$_{78}$, **5b**$_2$/**5c**$_1$/**9b**$_{115}$). Noteworthy was the adsorption performance of **5b**$_{10}$/**9b**$_{84}$/**9c**$_{10}$ on Au surfaces, as it showed similar or better results, regarding its maximum adsorbed mass, compared to the other cation-containing copolymers, except **5b**$_6$/**5c**$_4$/**9b**$_{94}$ (Figure 42, A). It seemed, that on Au surfaces, catechol units were not desperately necessary for an appreciable

coating. Yet the (co)polymers **5b**$_2$**/5c**$_1$**/9b**$_{115}$ and **9c** (Chapter 4.5.2) both showed lower adsorbed masses than **5b**$_{10}$**/9b**$_{84}$**/9c**$_{10}$. Thus the charge repulsion effects did not seem to be an issue with the cation unit count of **5b**$_{10}$**/9b**$_{84}$**/9c**$_{10}$. Accordingly, the mass adsorption of the catechol and cation-containing copolymers may be suffered from occupated catechol and cation units by attractive interactions between those.

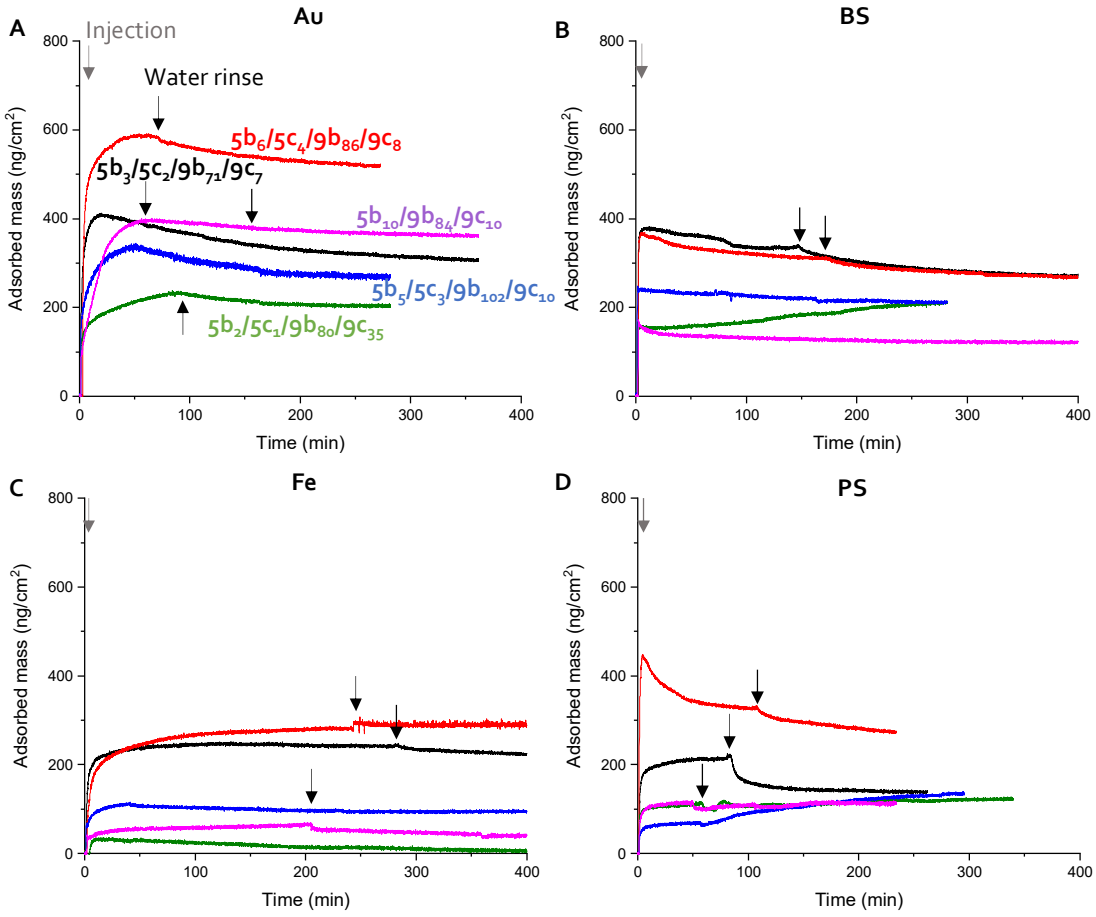


*Figure 42: Adsorption graphs of the cation and catechol-containing copolymers on various surfaces. Overall, the copolymers showed attractive interactions with all the different surfaces and the coating showed high durability during the water rinsing process.*

Thus at least on Au surfaces a higher content of catechol units was necessary to substantially enhance the adsorption performance of cation-containing copolymers. A certain cation count seemed to improve the durability of the coating; however, once the

cation content was above ~10% an improvement was not monitored. It seemed that the ratio of cation and catechol units played a role in the durability. The copolymer **5b**$_{10}$/**9b**$_{84}$/**9c**$_{10}$ showed higher durability than all the catechol-containing copolymers. Even the lowest durability, the coating of **5b**$_{6}$/**5c**$_{4}$/**9b**$_{86}$/**9c**$_{8}$ showed, which was the copolymer with the lowest catechol-cation ratio with 1:2. Thus, one can say, to improve the maximum adsorbed mass on Au surfaces a higher catechol content was necessary, to improve the durability, a higher cation count was required.

The adsorption velocity did not show any clear trend. The adsorption constants were all in a range of $k_A$(**5b**$_5$/**5c**$_3$/**9b**$_{112}$) = $7.21*10^{-3}$ mL/mg s (slowest) to $k_A$(**5b**$_6$/**5c**$_4$/**9b**$_{86}$/**9c**$_8$) = $1.00*10^{-3}$ mL/mg s (fastest). The copolymer **5b**$_{10}$/**9b**$_{84}$/**9c**$_{10}$ showed two stages of adsorption with $k_{A1}$(**5b**$_{10}$/**9b**$_{84}$/**9c**$_{10}$) = $5.11*10^{-3}$ mL/mg s and $k_{A2}$(**5b**$_{10}$/**9b**$_{84}$/**9c**$_{10}$) = $1.05*10^{-4}$ mL/mg s. These two stages were also monitored for PEI (Chapter 4.5.2). That indicated a mechanistic change during the adsorption, which was not observed for the catechol-containing copolymers.

Considering all things, one can conclude that to some extent, the durability of the coatings of the catechol and cation-containing copolymers on Au surfaces seemed to suffer from a higher catechol count, yet the highest recorded mass loss still was only 20%. The maximum adsorbed mass potentially can be improved with a higher catechol count or at least with a low catechol-cation ratio which may be examined in future works.

Comparing the cationic catechol-containing and non-cationic catechol-containing copolymers on BS Surfaces, the overall maximum adsorbed mass was lower. Further, **5b**$_3$/**5c**$_2$/**9b**$_{71}$/**9c**$_7$ did not show the zero-order kinetic behavior as the precursor **5b**$_3$/**5c**$_2$/**9b**$_{78}$ did (Figure 43, A, B). The adsorbed mass seemed to be limited at ~400 ng/cm$^2$. This was significantly lower than that of the non-cationic precursors. Yet, the coating of the cationic catechol-containing copolymers, obviously thinner, showed substantially major durability. While the non-cationic catechol-containing copolymers came up with a mass loss of minimum at ~23% (**5b**$_3$/**5c**$_2$/**9b**$_{78}$) and a maximum at ~81% (**5b**$_2$/**5c**$_1$/**9b**$_{115}$), all the cation and catechol-containing copolymers appeared to remain without getting washed off the BS surface (**5b**$_2$/**5c**$_1$/**9b**$_{115}$) or showed a maximum mass

loss of 19% (**5b$_3$/5c$_2$/9b$_{78}$**). **5b$_{10}$/9b$_{84}$/9c$_{10}$** showed no mass loss at all, resulting in the lowest amount of adsorbed mass regardless.

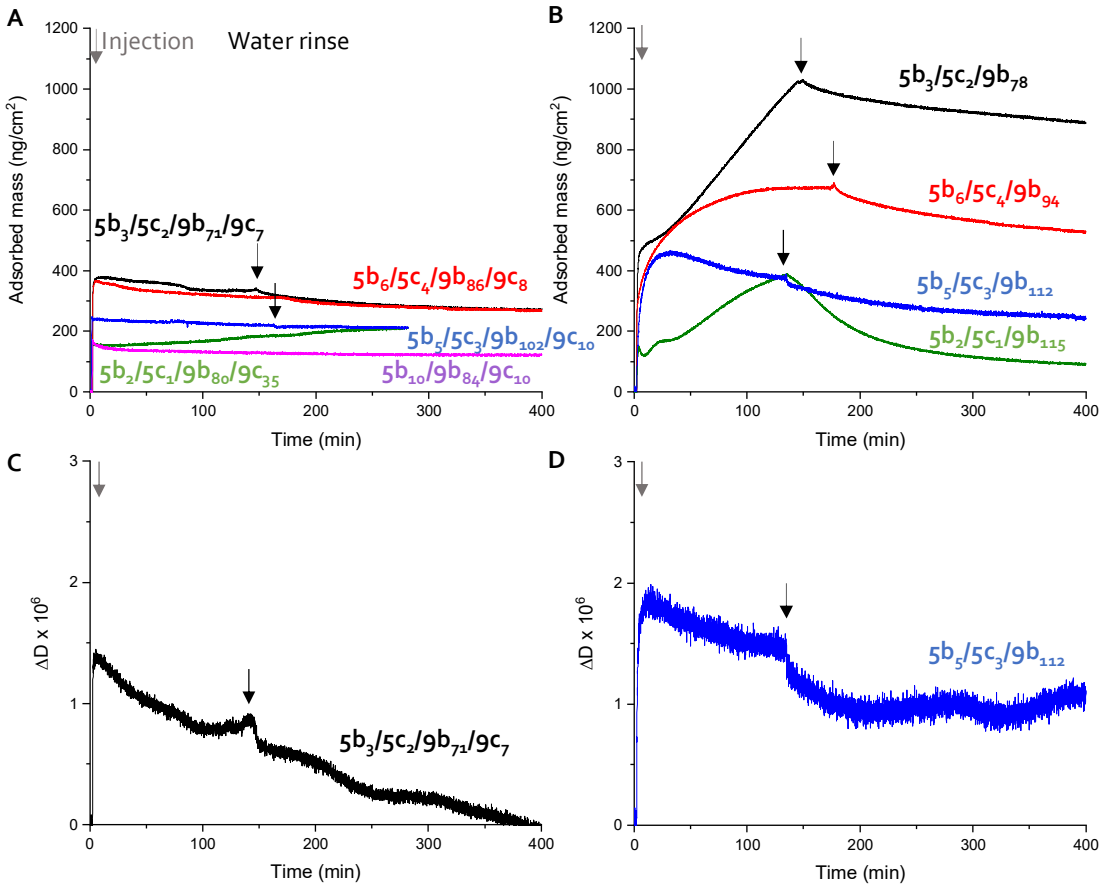


*Figure 43: Adsorption graphs of the cation and catechol-containing (A) and non-cationic catechol-containing copolymers (B) monitored on BS surfaces. ΔD values in comparison, showed a denser coating of the cation and catechol-containing copolymer **5b$_5$/5c$_3$/9b$_{102}$/9c$_{10}$** (C) than for the non-cationic catechol-containing copolymer **5b$_5$/5c$_3$/9b$_{112}$** (D).*

The density of the coating of **5b$_5$/5c$_3$/9b$_{102}$/9c$_{10}$** appeared to be higher with the cations than without, as the ΔD values showed lower amounts with similar adsorbed masses (Figure 43, C, D, **5b$_5$/5c$_3$/9b$_{102}$/9c$_{10}$** was chosen exemplarily). The high oxygen content of the BS surfaces, presumably, provided additional binding sides not only for the catechol but also for the cations. The broader distribution and the additional availability of attractive copolymer-surface interactions by cation units led to the higher density of the

coatings. The higher density of the coatings generated a higher osmotic pressure which explains the early limitation of mass adsorbance.

The adsorption velocity on BS surfaces seemed to benefit from the cations. The highest acceleration was monitored with a factor of ~8 for $k_A^{BS}$(**5b**$_2$/**5c**$_1$/**9b**$_{80}$/**9c**$_{35}$) = 1.28∗10$^{-2}$ mL/mg s in comparison to $k_A^{BS}$(**5b2/5c**$_1$/**9b**$_{115}$) = 1.52∗10$^{-3}$ mL/mg s for the non-cationic precursor. **5b**$_5$/**5c**$_3$/**9b**$_{102}$/**9c**$_{10}$ on BS still showed an adsorption velocity of **5b**$_5$/**5c**$_3$/**9b**$_{112}$ ($k_A^{BS}$(**5b**$_5$/**5c**$_3$/**9b**$_{102}$/**9c**$_{10}$) = 1.04∗10$^{-2}$ mL/mg s by the factor of ~6 accelerated to the precursor with $k_A^{BS}$(**5b**$_5$/**5c**$_3$/**9b**$_{112}$) = 1.73∗10$^{-3}$ mL/mg s. Further, the adsorption velocity difference narrowed as the catechol number increased: ($k_A^{BS}$(**5b**$_3$/**5c**$_2$/**9b**$_{71}$/**9c**$_7$) = 3.11∗10$^{-2}$ mL/mg s, $k_A^{BS}$(**5b**$_3$/**5c**$_2$/**9b**$_{78}$) = 1.12∗10$^{-2}$ mL/mg s; $k_A^{BS}$(**5b**$_6$/**5c**$_4$/**9b**$_{86}$/**9c**$_8$) = 1.04∗10$^{-2}$ mL/mg s, $k_A^{BS}$(**5b**$_6$/**5c**$_4$/**9b**$_{94}$) = 1.76∗10$^{-2}$ mL/mg s. A high amount of cation accordingly seemed to support a fast adsorption process on BS surfaces, potentially caused by the above-mentioned supplementary cation-oxygen interaction. At a certain point, however, the adsorption acceleration, driven by the cation number, worked at the expense of the adsorbed mass value.

Generally, the overall adsorbed mass was lower on BS surfaces compared with Au surfaces. Yet the adsorption velocity was faster and the durability of the coatings was higher on BS than on Au surfaces. Due to the BS surface oxygen content, it can be assumed that the cation units had a larger impact on the overall adsorption performance on BS than on Au surfaces. Yet, the subsequent higher density of the coatings on BS seemed, that the osmotic pressure limited adsorption already at ~400 ng/cm² whereat on Au surfaces a higher amount of copolymer can be adsorbed.

Further the cationic copolymer matrix **5b**$_2$/**5c**$_1$/**9b**$_{80}$/**9c**$_{35}$, **5b**$_3$/**5c**$_2$/**9b**$_{71}$/**9c**$_7$, **5b**$_5$/**5c**$_3$/**9b**$_{102}$/**9c**$_{10}$, **5b**$_6$/**5c**$_4$/**9b**$_{86}$/**9c**$_8$ and **5b**$_{10}$/**9b**$_{84}$/**9c**$_{10}$ was compared with the non-cationic catechol-containing matrix **5b**$_6$/**5c**$_4$/**9b**$_{94}$, **5b**$_5$/**5c**$_3$/**9b**$_{112}$, **5b**$_3$/**5c**$_2$/**9b**$_{78}$ and **5b**$_2$/**5c**$_1$/**9b**$_{115}$ on Fe surfaces.

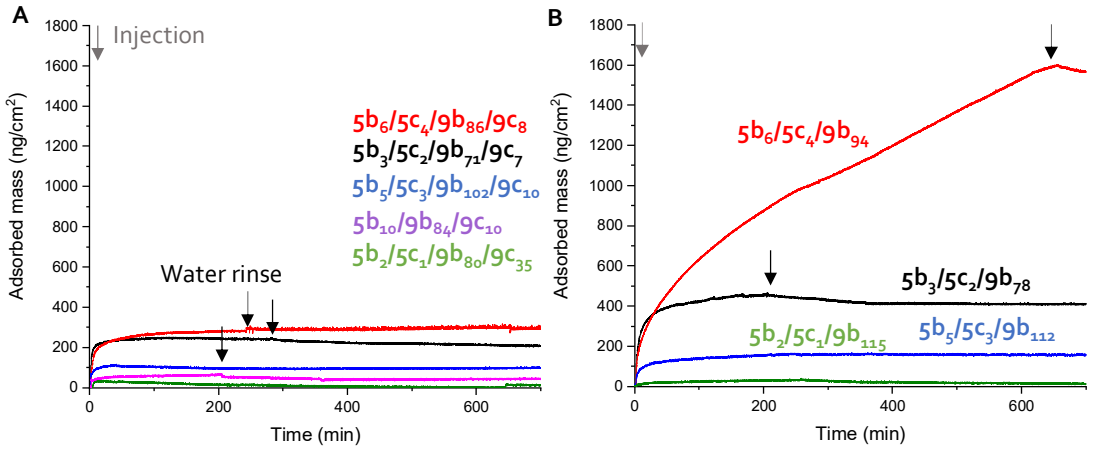


*Figure 44: Fe surfaces, treated with the cation-containing (A) and with the catechol-containing copolymer matrix (B). The adsorption performance suffered from the introduction of the cationic units. The durability of the coating towards the water rinsing process increased or remained equal.*

For the cation and catechol-containing copolymer matrix, a substantially lower adsorbed mass maximum was monitored (Figure 44, A and B). Comparing the maximum adsorbed mass of both the matrices, a decrease of up to ~70% (**5b$_6$/5c$_4$/9b$_{94}$** vs **5b$_6$/5c$_4$/9b$_{86}$/9c$_8$**) was monitored. The copolymers with a low catechol or a high cation number showed very low adsorbed mass maxima. However, this data indicated the necessity of a higher catechol or a lower cation unit count within the copolymers concerning the adsorption on Fe surfaces. This supported the assumption, that a higher catechol content was necessary to adsorb on Fe surfaces (Chapter 4.5.3.5).

The catechol units presumably were occupied by interaction with cation units, thus not enough free catechol units were available to bind properly. This attractive force between the functional groups is not only associated with Fe surfaces. The impact of this interaction though was higher as on the one hand the cations seemingly did not interact attractively with the Fe surfaces (Figure 44, A, **5b$_{10}$/9b$_{84}$/9c$_{10}$**) and on the other hand, more catechol was required for the interaction.

Further, with an increasing amount of catechol units, the amount of copolymer washed off the surfaces decreased. While the **5b**$_{10}$/**9b**$_{84}$/**9c**$_{10}$ coating was removed at ~37% during the water rinsing process, the **5b**$_{2}$/**5c**$_{1}$/**9b**$_{80}$/**9c**$_{35}$ coating only lost ~7%. The copolymer with the highest catechol content **5b**$_{6}$/**5c**$_{4}$/**9b**$_{86}$/**9c**$_{8}$ was not washed off the surfaces by water at all. This interestingly occurred contrarily to the observed trends as a higher catechol content led mostly to less durable coatings. The adsorption and durability thus seemed to be highly dependent on the catechol number and not on the cation number. A higher amount of catechol or a lower amount of cation units within the copolymers could give a thicker coating. However, if the coating of *e.g.* **5b**$_{6}$/**5c**$_{4}$/**9b**$_{86}$/**9c**$_{8}$ was thin and highly durable, a thicker coating would not be necessary for antifouling application experiments.

Finally, PS surfaces were treated with the copolymers **5b**$_{2}$/**5c**$_{1}$/**9b**$_{80}$/**9c**$_{35}$, **5b**$_{3}$/**5c**$_{2}$/**9b**$_{71}$/**9c**$_{7}$, **5b**$_{5}$/**5c**$_{3}$/**9b**$_{102}$/**9c**$_{10}$, **5b**$_{6}$/**5c**$_{4}$/**9b**$_{86}$/**9c**$_{8}$ and **5b**$_{10}$/**9b**$_{84}$/**9c**$_{10}$. Overall, all copolymers showed attractive interactions with the PS surfaces (Figure 45, A). The overall durability of the coatings with the cation copolymers was higher than with the respective precursors. Above, it was noticed that the aryl content had a big impact on the adsorption performance as, presumably, the main attractive force was the π-π-interaction. The monitored adsorption progression thus largely was as expected (Figure 45, A). The adsorbed mass though was minimum at 17% lower for **5b**$_{6}$/**5c**$_{4}$/**9b**$_{86}$/**9c**$_{8}$ and maximum at 55% lower for **5b**$_{5}$/**5c**$_{3}$/**9b**$_{102}$/**9c**$_{10}$ compared to the respective precursors **5b**$_{6}$/**5c**$_{4}$/**9b**$_{94}$ and **5b**$_{5}$/**5c**$_{3}$/**9b**$_{112}$. Further, a generally lower adsorption velocity was monitored. This may be caused as the cationic copolymers were potentially energetic more attracted to stay dissolved in water, instead of being bound via cation-π-interactions. This effect potentially can be controlled by solvent polarity.

The copolymer **5b**$_{10}$/**9b**$_{84}$/**9c**$_{10}$ showed comparable results to its precursor **5b**$_{10}$/**9b**$_{94}$ on Ps surfaces (Chapter 4.5.3.4). The mentioned coiling effect and shielding of the aryl units from water and surface interactions was not prevented by the cation units. It can even reasonably be assumed that the copolymer **5b**$_{10}$/**9b**$_{84}$/**9c**$_{10}$ formed micelles as the DLS measurement indicated (Chapter 8, Figure S 47). A certain catechol content for these gradient copolymers seemed to be necessary to enable aryl interactions with the PS

surfaces by preventing micellization or coiling. One can say that the cations overall decreased the adsorbed masses and lowered the adsorption velocities, yet increased coating durability compared to the precursor copolymer data.

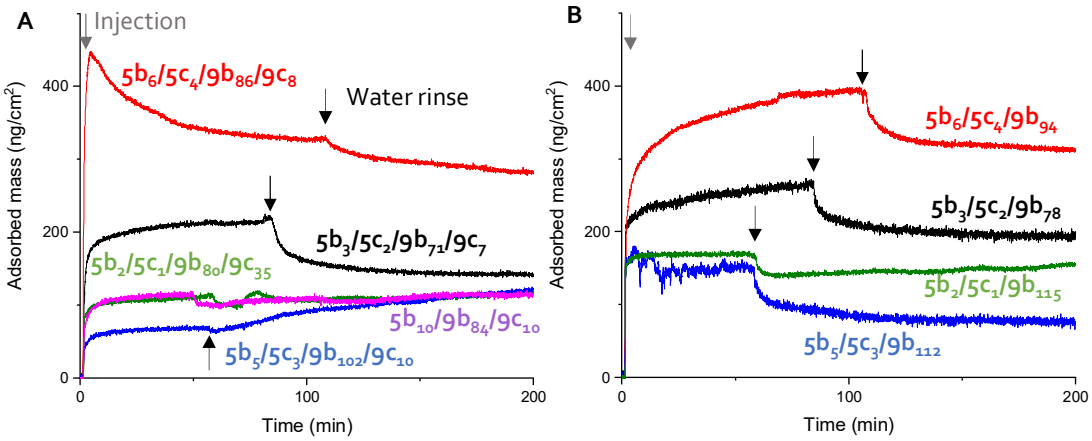


*Figure 45: The cation catechol-containing copolymers (A) showed slightly lower adsorbed mass values on PS than the non-cation catechol-containing matrix (B). Still, the copolymers adsorbed on the hydrophobic surface.*

All things considered, screening four different surfaces with a (co)polymer matrix containing minor and major functionalized (co)polymers resulted in some great discoveries. Indeed, the discussion was more quantitative than qualitative, yet at certain stages, some reasonable assumptions concerning mechanisms and adsorption- and durability-behavior were made. It was demonstrated that already poly(2-ethyl-2-oxazoline)s (**9b**) and aryl containing copoly(2-oxazoline)s (**$5b_5/9b_{78}$**, **$5b_{10}/9b_{94}$**) can adsorb on various surfaces. The catechol-containing copolymers **$5b_6/5c_4/9b_{94}$**, **$5b_5/5c_3/9b_{112}$**, **$5b_3/5c_2/9b_{78}$**, and **$5b_2/5c_1/9b_{115}$**, showed a significant improvement of the adsorption performance by an overall higher adsorbed mass and durability on all used surface types. Besides, some copolymers showed a zero-order kinetic behavior dependent on the number of catechol units and the surface type. The cation and catechol-containing copolymers **$5b_2/5c_1/9b_{80}/9c_{35}$**, **$5b_3/5c_2/9b_{71}/9c_7$**, **$5b_5/5c_3/9b_{102}/9c_{10}$**, and **$5b_6/5c_4/9b_{86}/9c_8$** showed an overall lower adsorbed mass than the precursor copolymers, yet the durability

of the coatings overall increased on all used surface types, as in some cases, virtually the entire coating remained on the surface during the water rinsing process. This makes this copolymer matrix a prosperous platform for further investigations concerning application-drawn coatings.

## 4.6 Influence of (co)polymer coatings on protein repelling properties

The great progression from successful monomer and (co)polymer synthesis, followed up by the post-polymerization modification to release the catechol and cationic units, which were evidenced being substantial for adsorption processes, was meant to be completed by an examination of whether the (co)polymer coatings were promising towards anti-fouling properties.

To prevent surface fouling processes, bacterial interaction on the surfaces was inhibited by obviating biomacromolecule (protein) attachment.[168] Surface protection by prohibiting bio-fouling is a major issue as the respective applications range from packaging over biomedical devices to marine equipment.[169] Coatings, consisting of PEG but as well as poly(2-oxazoline)s, showed efficient anti-fouling properties.[170,171] Yet, an anti-fouling coating requires the attachment of the desired adsorptive to facilitate the anti-fouling properties. On this occasion, catechol functionalized copolymers were catching the concern. The combination of the catechol-cation-supported adsorption qualities with the already indicated anti-fouling properties of poly(2-oxazoline)s made the above-mentioned and examined (co)polymer matrix promising for those applications.

To test those anti-fouling properties, the available (co)polymer matrix, consisting of minor, catechol, and cation-catechol functionalized (co)polymers, was narrowed using exemplarily three different (co)polymers. Poly(2-ethyl-2-oxazoline) (**9b**) was chosen as a comparative compound of minor functionalized (co)polymers. Additionally, the major functionalized copolymers **5b**$_3$/**5c**$_2$/**9b**$_{78}$ and **5b**$_3$/**5c**$_2$/**9b**$_{71}$/**9c**$_7$ were selected as they had the most consistent results on all various surfaces. The anti-fouling experiments all were

conducted using Au surfaces, as it is the most commonly used surface. The surfaces were treated with the named (co)polymers to produce coatings, yet for comparison issues, one Au surface was left bare without (co)polymer treatment (Figure 46, A). After the coating process, all surfaces were treated with a 1x PBS (phosphate-buffered saline) solution to create a physiological surrounding at pH 7.4. The (coated) surfaces were rinsed until the adsorption graphs showed an equilibrium. Subsequently, a bovine serum albumin (BSA) solution (1 mg/mL in 1x PBS) was injected. BSA was used for that experiment as this protein is used commonly for anti-fouling experiments.[172]

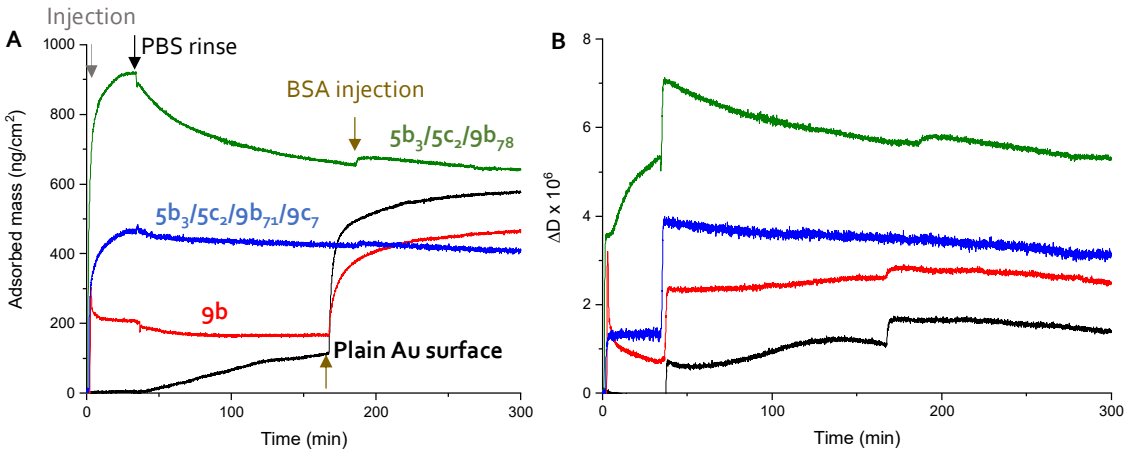


*Figure 46: Testing anti-fouling properties (co)polymer-coated Au surfaces. A) The surfaces were coated with (co)polymers, rinsed with PBS buffer solution, and then were treated with a BSA solution (1 mg/mL in 1x PBS). The bare Au and* ***9b*** *coated surfaces interacted attractively with BSA. Whereas the* ***5b₃/5c₂/9b₇₈*** *coated surface showed minor attractive interactions with BSA and for the* ***5b₃/5c₂/9b₇₁/9c₇*** *functionalized surface almost no interaction was monitored. B) Depiction of the respective dissipation values during the coating, PBS, and BSA treatment process.*

Initially, the resistance of the coating against the PBS solution was considered by associated numbers. The offset, visible in the dissipation values (Figure 46, B) were caused by environmental changes due to the PBS injection. The **9b** coating showed surprisingly high durability against the PBS rinsing process as only a mass loss of 19% was

recorded. Interestingly, this **9b** coating was more stable against a PBS solution than water (38% mass loss during water rinsing).

The catechol-containing copolymer **5b**$_3$/**5c**$_2$/**9b**$_{78}$ showed the less durable coating against the PBS rinsing process as a mass loss of 29% was recorded. The highest durability within the physiological environment showed the **5b**$_3$/**5c**$_2$/**9b**$_{71}$/**9c**$_7$ coating with a mass loss of 10%. Worth mentioning was the interaction and deposit of PBS salts (~111 ng/cm²) on the plane Au surfaces which was inhibited by all (co)polymer coatings. Once, an equilibrium was set during the rinsing process and the coating was stable in this environment, the (coated) surfaces were treated with a BSA solution. The adsorption graphs showed a clear correlation concerning the adsorbed protein and the functionality degree of the coatings. While the non-coated, bare Au surface adsorbed ~470 ng/cm² BSA, already the **9b** coated surface only adsorbed 295 ng/cm² BSA. Still, this was a significant amount of protein bound to the coated surface. However, the catechol-containing copolymer **5b**$_3$/**5c**$_2$/**9b**$_{78}$ only adsorbed 21 ng/cm². Almost no adsorbed BSA was recorded for the **5b**$_3$/**5c**$_2$/**9b**$_{71}$/**9c**$_7$ coated surface (3 ng/cm²). This demonstrated that the additional functional groups were not only necessary, to build sustainable coatings, but also to increase protein repelling effects. The higher functionality with the catechol units, on the one hand, resulted in a thicker coating, on the other hand, an even higher functionality with the cationic units gave more dense coatings. A thicker coating facilitates a high osmotic pressure than a thinner or no coating. This was, presumably, the driving force for the more repelling properties of the thick **5b**$_3$/**5c**$_2$/**9b**$_{78}$ coating, compared to the thin **9b** coating. Even more, repelling effects showed the **5b**$_3$/**5c**$_2$/**9b**$_{71}$/**9c**$_7$ coating, as the density was significantly higher, compared with the **5b**$_3$/**5c**$_2$/**9b**$_{78}$ coating (dissipation values Figure 46, B). The higher density correlated with an even higher osmotic pressure and with a stronger repelling effect. A direct correlation between the protein resistance and the coating was shown by De Gennes *et al.*.[173] This explained the coating repelling forces. However, attractive forces can occur between the coatings and proteins such as electrostatic attraction. For instance, an anionic protein can interact with the cation-containing copolymer **5b**$_3$/**5c**$_2$/**9b**$_{71}$/**9c**$_7$. Yet in that context, two indications were of certainty: First, at a pH of 7.42, the specific charge of BSA is -0.27 mmol/g in PDDA

(poly(dimethyl diallyl ammonium chloride).[174] Thus, in this context, for the protein resistance measurements, BSA can be assumed as a neutral compound as the experiment was conducted in PBS with a pH value of 7.4. Second, still, the real charge was arguably slightly negative. The cation units within the coating though participated in the binding and linkage effects. Thus, the availability of the cation units at the interface between the coating and the protein solution can be assumed as extremely low. At least apparently, the repelling forces like the osmotic pressure were of stronger propulsion than the mentioned potential occurring attractive forces.

This narrowed (co)polymer matrix was selected to create an intersectional overview of the potential of the above-produced wide (co)polymer matrix. This exemplary experiment demonstrated the high potential of the cation-catechol-containing copoly(2-oxazoline) coatings for various applications. The copolymers **5b**$_3$/**5c**$_2$/**9b**$_{78}$ and **5b**$_3$/**5c**$_2$/**9b**$_{71}$/**9c**$_7$ were capable to adsorb and stick on Au surfaces, even during PBS treatment. Both coatings showed high protein (BSA) repelling properties, which were assumably originated from a high density caused by osmotic pressure. These outcomes open up a path to new bioderived catechol and cation-containing copoly(2-oxazoline)s with the ability to create anti-fouling coatings on various surfaces.

# 5 Conclusion and outlook

The aim of this work was the development of adsorbing mussel glue protein mimicking poly(2-oxazoline)s for anti-fouling coatings. This task was accomplished within four stages: **a)** 2-oxazoline monomer synthesis development; **b)** homo- and copolymerization studies to yield water-soluble copolymers; **c)** post-polymerization modifications to release the catechol and cation units; **d)** surface adsorption and anti-fouling studies via QCM-D.

### a) 2-oxazoline Synthesis

Starting materials for the monomer synthesis were the naturally occurring carboxylic acids veratric, homoveratric, dimethoxy caffeic acid, and *N*-Boc-*O*-methyl-*L*-tyrosine and their higher and lesser substituted derivatives. The associated hydroxy and amine functionalities were used in the methyl- and BOC-protected form.

2-Oxazolines can be synthesized by various methods. Initially, several direct 2-oxazoline synthesis approaches from the cinnamic acid were attempted, which all resulted in poor yields. Thus, the synthesis route was changed to the Witte-Seeliger method, with nitriles as starting materials (Scheme 25). The corresponding nitriles were either synthesized or purchased and 2-oxazolines **1a**-**6a** were successfully synthesized in yields of 55-93%. The *N*-Boc-*O*-methyl-*L*- tyrosine **7** was successfully converted via $\beta$-chloroethyl amide to the 2-oxazoline **7a** in a yield of 89%.

Due to those excellent results, the modified Witte-Seeliger method can be confirmed as a highly efficient method for the 2-oxazoline synthesis. In consequence, different 2-oxazolines were synthesized, whereat **2a**-**4a** and **7a** were not yet known.

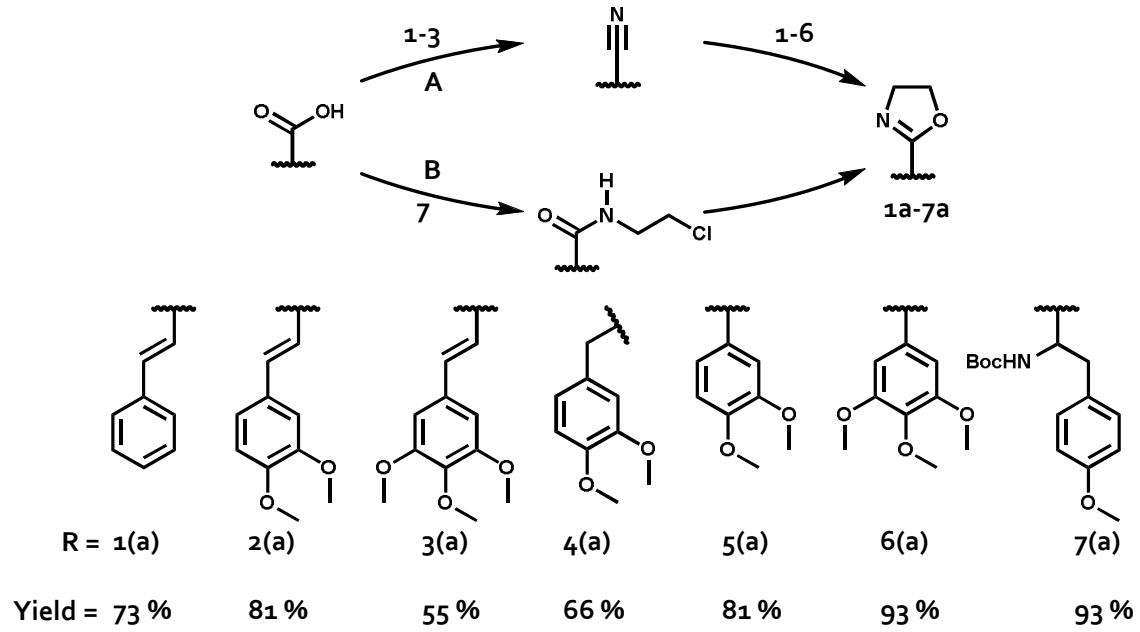


*Scheme 25: Review of the developed and conducted 2-oxazoline monomer synthesis.*

### b) Homo- and copolymerization studies to yield water-soluble copolymers

There are two ways to polymerize 2-oxazolines: First via traditional heating, utilizing an oil bath, or second via microwave irradiation. It rapidly turned out that the 2-oxazolines **1a**-**7a** were not polymerizable via traditional heating as the model compound **1a** showed no conversion. The polymerization of **1a** in a microwave reactor however showed promising results. Subsequently, microwave irradiation was used for further (co)polymerization reactions. Since the polymerization of **1a**-**7a** was not reported before, homopolymerization kinetic studies at 100 and 140 °C were conducted in the microwave reactor (Scheme 26, A). The kinetic studies revealed that, with a targeted DP of ~25 at 140 °C, the conversion reached >90% within 4 min for **1a**-**3a** and within 16 min for **5a** and **6a**. At 100 °C though, the conversion reached >90% within 60 min for **1a** (fastest) and within 480 min for **5a** (slowest). The monomer conversion was determined via FT-IR spectroscopy. All homopolymers **1b**-**7b** were characterized by SEC, FT-IR, and $^{1}$H NMR spectroscopy; additionally, **1b**-**6b** were analyzed by MALDI-TOF MS. These results facilitated the subsequent copolymerization studies.

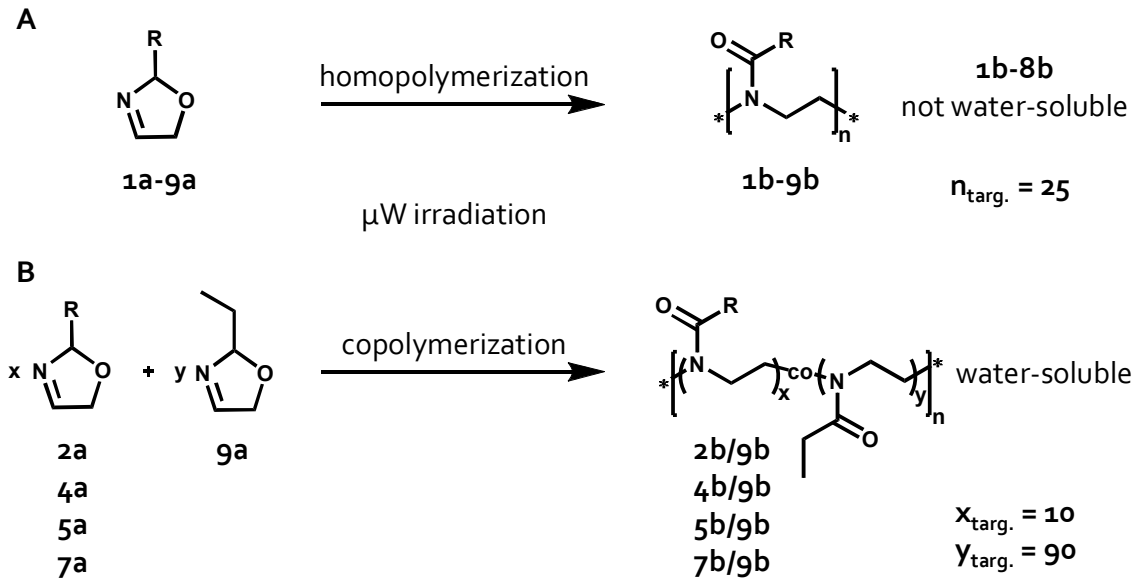


*Scheme 26: The microwave-irradiation enabled the (co)polymerization of the 2-oxazolines **1a**-**9a**. A) Kinetic studies were conducted at 100 and 140 °C of the monomers **1a**-**9a**. B) The 2-oxazolines **2a**, **4a**, **5a**, and **7a** were copolymerized with **9a** to yield the water-soluble copolymers **2b**/**9b**, **4b**/**9b**, **5b**/**9b**, and **7b**/**9b**.*

Copolymerization kinetic studies were conducted with the established polymerization conditions. The monomer conversion was determined with $^{1}$H NMR spectroscopy. The monomers **2a, 4a, 5a,** and **7a** were copolymerized with -ethyl-2-oxazoline (**9a**) with a targeted number of 10 of **2a, 4a, 5a,** and **7a** and 90 of **9a** (Scheme 26, B). This low amount of the (protected) catechol-containing comonomer unit was reasoned by the catechol content of 2-30% in maritime glue proteins (Chapter 1.1). Kinetic studies revealed a virtually azeotropic copolymerization character for the conversion of **2a**/**9a** and **7a**/**9a** to the copolymers **2b**/**9b** and **7b**/**9b**. Additionally, the study provided evidence for the slight gradient-like character of **4b**/**9b** and an even stronger gradient-like copolymer **5b**/**9b**.

For **2b**/**9b** a side reaction during the copolymerization process was monitored. Indirect evidence strongly suggested a Michael-type addition, facilitated by a $\beta$-proton elimination of an active **9b** chain end. It was assumed that a nucleophilic attack of the formed ketene *N, O*-acetal on the exocyclic cinnamyl double bond resulted in a Michael-

type-addition chain coupling product. Yet, neither the ketene *N, O*-acetal nor the coupling product was proven by spectroscopic methods. The assumption was indirectly evidenced by several experiments *i.a.* excluding an acidic $\beta$-proton and the cinnamyl double bond.

The side reaction inhibited the further use of **2b**/**9b** for post-polymerization modification. The Michael-type reaction potential, however, can be used for post-polymerization reactions in future works, if the side reaction can be suppressed. Since the cinnamyl double bond is required for the desired Michael addition, the comonomer must be changed. As the ketene *N, O*-acetal caused the side reaction, the formation of this compound must be avoided. Sterically hindrance can be one way to avoid the $\beta$-elimination and the subsequent formation of the ketene *N, O*-acetal. 2-*i*-Propyl-2-oxazoline presumably can be one promising compound as the reactive proton is more shielded (Scheme 27, A). A copolymerization of **2a** and 2-*i*-propyl-2-oxazoline would probably result in a water-soluble, thermoresponsive copolymer with the potential of post-polymerization modification at the cinnamyl double bond.[175] The ways to modify the cinnamyl exocyclic double bond are various.[176] The Michael addition though apparently is a proper choice, since it already (presumably) occurred. A particular type of Michael addition namely the aza-Michael reaction though would be promising, regarding mussel glue protein mimicking copolymers.[177,178] Establishing this reaction with Dopamine (Scheme 27, B) would yield a catechol-containing cationic copolymer within one step and without protection group chemistry. This copolymer would carry the catechol and the cationic unit nearby which is significant as mentioned in chapter 1.3. Thus, the discovered side reaction opens a new direction to elaborate the system. The copoly(2-oxazoline)s **4b**/**9b**, **5b**/**9b,** and **7b**/**9b** however were successfully synthesized, analyzed by SEC, FT-IR, and $^1$H NMR spectroscopy. All these copolymers are promising candidates to mimic mussel glue proteins, yet in this work, **5b**/**9b** was considered further for post-polymerization modifications.

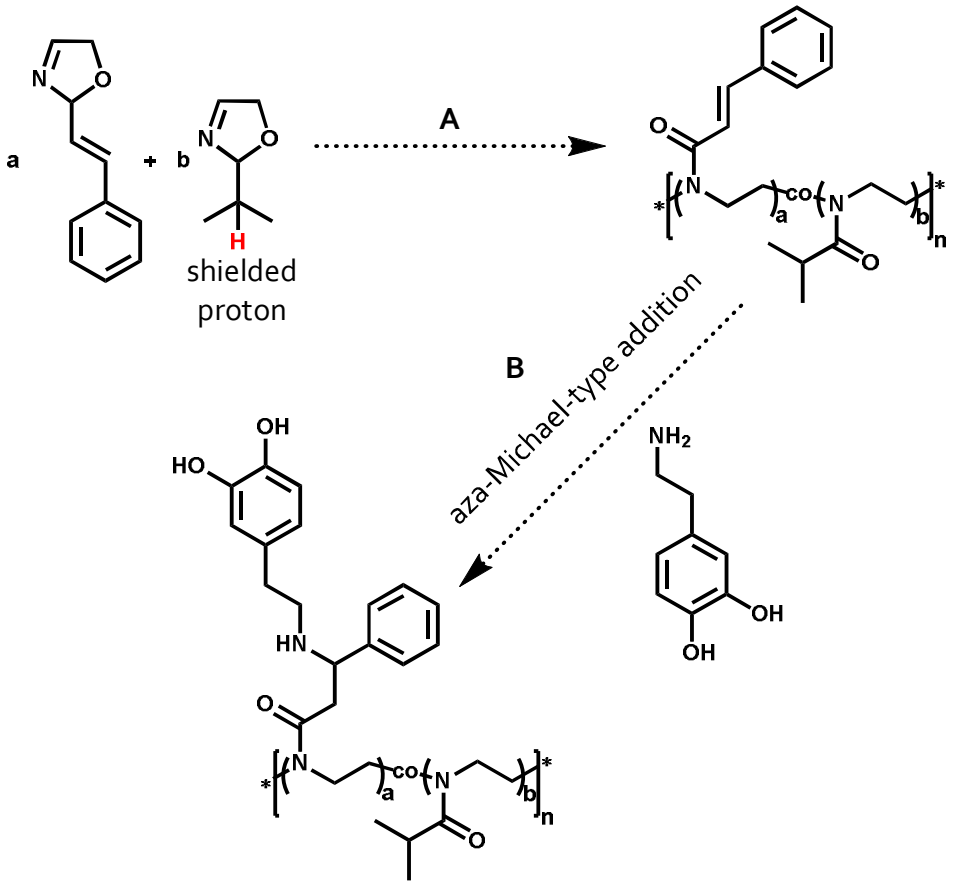


*Scheme 27: A) 2-iPr-2-oxazoline potentially would inhibit the chain transfer reaction by shielding the reactive proton. This would give a water-soluble thermoresponsive copolymer with the potential aza-Michael-reactions with Dopamine (B) to yield catechol and cation-containing copolymers with an even ratio and proximity of the cation and the catechol.*

### c) Post-polymerization modifications to release the catechol and cation units

In general, the adsorption properties concerning gluing maritime proteins are attributed to the catechol and the cationic unit (Chapter 1.1). To release the catechol units a methyl aryl ether cleavage was conducted with either the homopolymer **5b** and a matrix of copolymers $\mathbf{5b}_3/\mathbf{9b}_{121}$, $\mathbf{5b}_5/\mathbf{9b}_{78}$, $\mathbf{5b}_8/\mathbf{9b}_{110}$, and $\mathbf{5b}_{10}/\mathbf{9b}_{94}$ (Scheme 28). Despite the promising results of the cleaving reaction with **5b**, the conversion to the catechol-containing copolymers $\mathbf{5b}_x/\mathbf{9b}_y \rightarrow \mathbf{5b}_{x\text{-}z}\mathbf{5c}_z/\mathbf{9b}_y$ was only 30-37%, determined by $^1$H NMR analysis.

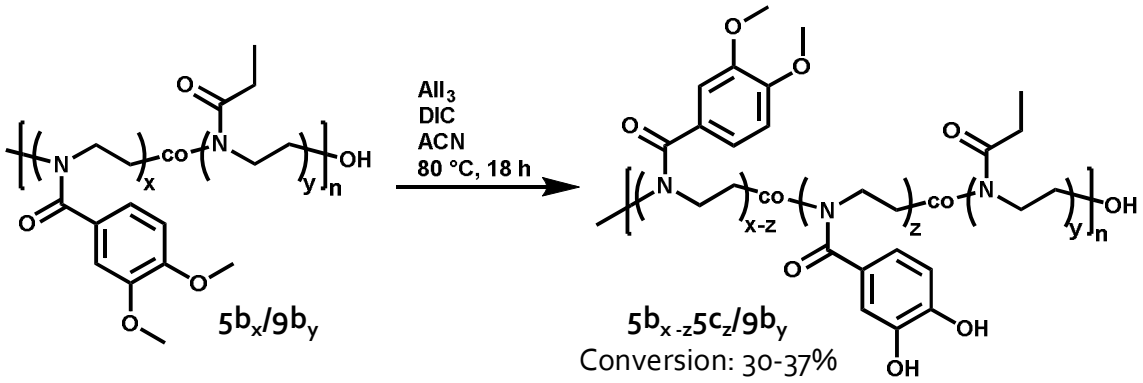


*Scheme 28: Post-polymerization modification by methyl aryl ether cleavage had a conversion of 30-37%.*

The minor conversion was assumed to be caused by a precipitation effect due to coordination from the Lewis acid reactant with the amide moiety within the copoly(2-oxazoline)s. As a supervised side project revealed, that a different Lewis acid (changed from $AlI_3$ to $BBr_3$) and a different copoly(2-oxazoline) (**4b**/**9b** instead of **5b**/**9b**) did not lead to higher conversions (Chapter 4.4.2).[148]

To improve the deprotection reaction, Lewis acids, carrying sterically demanding groups like $B(C_6F_5)_3$ can potentially avoid the precipitation effect and enable higher conversions.[151] This approach is promising for future works as with higher conversions the full potential of the introduced protected catechol groups would be enabled. To circumvent the protection group chemistry, the aza-Michael addition approach would be highly valuable again. However, the first task to release the adsorbing units thus was partially accomplished and the copolymers were characterized via NMR spectroscopy and SEC.

To release the cationic units, partial acidic hydrolysis of the **9b** unit within the catechol-containing copolymer was conducted (Scheme 29). The hydrolysis resulted in cation- and catechol-containing copolymers with a cation content of ~9% ethyleneimine units (**9c**). The cation number within the copolymers was desired to be small since high amounts of cationic units can cause undesired repelling effects during adsorption experiments.

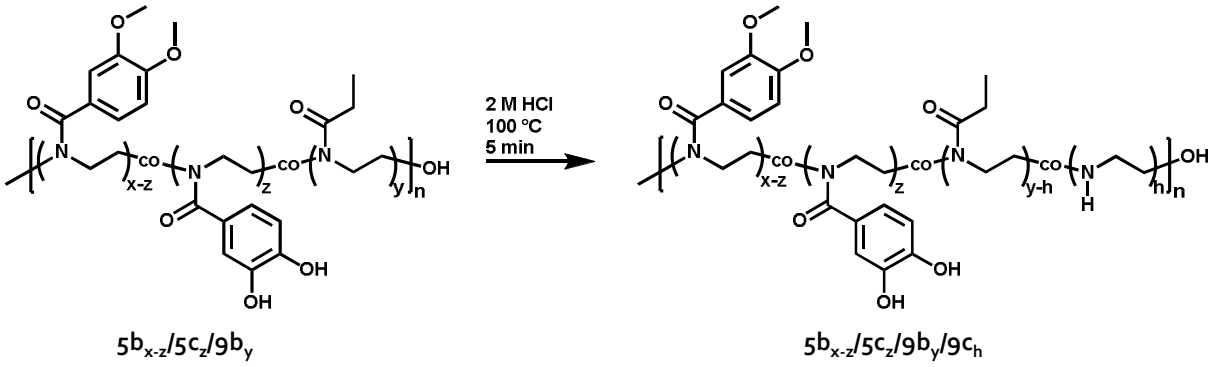


*Scheme 29: Partial hydrolysis of the catechol-containing copolymers to yield catechol and cation-containing polymers.*

The exclusive hydrolysis of the **9b** unit was proven by UV-VIS spectroscopy, as the absorbance remained equal for both the hydrolyzed and the non-hydrolyzed copolymer.

Maritime glue proteins use both, catechol, and cation units in proximity to support each other. Within the synthesized cation and catechol-containing copolymers, the cations and catechols are randomly distributed. This certain infirmity can be circumvented by using the aforementioned approach concerning the aza-Michael addition as the amine unit would be located close to the catechol moiety.

Regardless, a large matrix of (co)polymers with minor and major functionalities was successfully synthesized. The catechol units were (partially) released and the partial hydrolysis allowed access to major functionalized copolymers, mimicking maritime gluing proteins.

### d) Surface adsorption and antifouling studies via QCM-D on various surfaces

Finally, the (co)polymer matrix (Figure 47) was tested concerning adsorbing abilities on various surfaces (Au, BS, Fe, PS) via QCM-D measurements. It was demonstrated that the catechol moieties were substantial for the adsorption performance on all types of surfaces as better adsorption performances were evidenced by comparing **5b**$_{x-z}$/**5c**$_z$/**9b**$_y$ with **9b, 9c, 5b**$_x$/**9b**$_y$. Even only one free catechol unit (in average) within a copolymer was

sufficient to double the adsorbed mass on Au surfaces to the respective non-catechol-containing precursor. This showed the effectiveness and significance of catechol units concerning adsorbing compounds. Yet, not only the surface binding but also the durability of the coatings was fortified by the catechol units. Examinations with the catechol and cation-containing copolymers **5b**$_{x\text{-}z}$/**5c**$_z$/**9b**$_{y\text{-}h}$/**9c**$_h$ demonstrated that the cationic units further reinforce the durability of the coatings, yet the overall adsorbed mass decreased, compared to the non-cationic precursors.

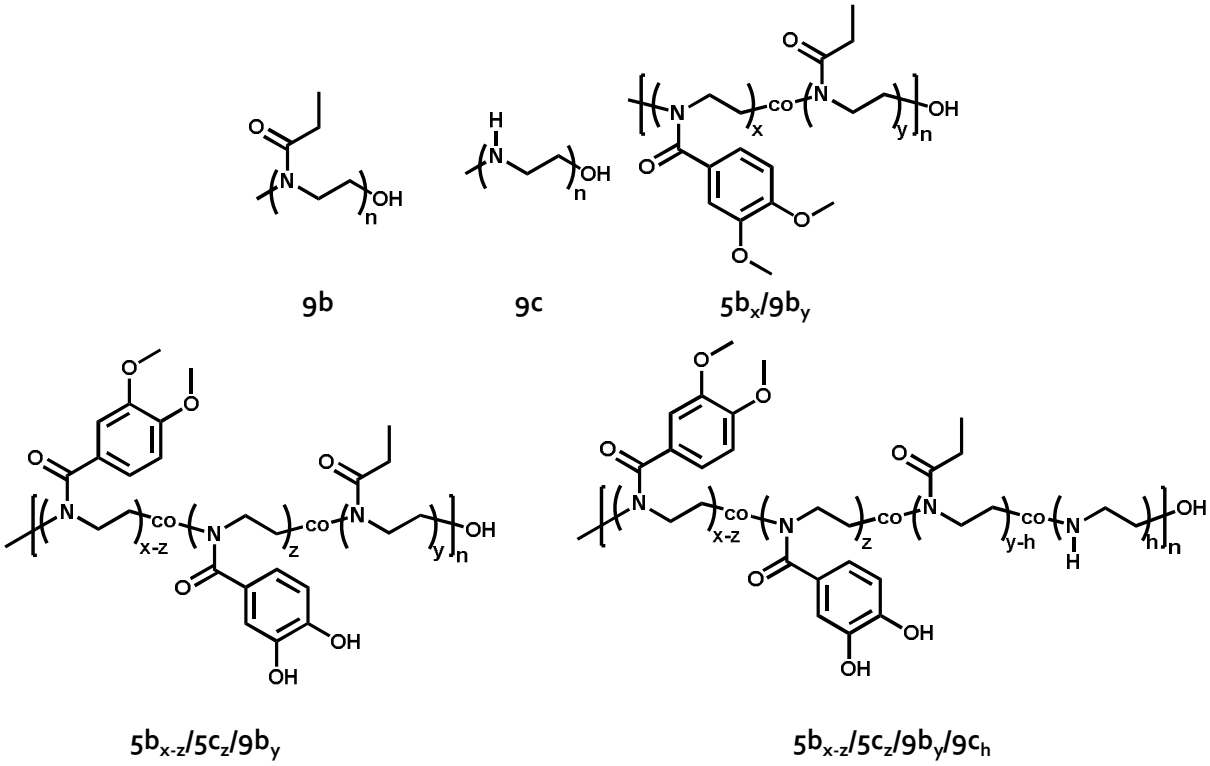


*Figure 47: The certain polymer matrix considered and examined concerning their adsorption performance on various surfaces by QCM-D measurements.*

Considering all things, even a small number of catechol (min <1%, max ~4% regarding the respective polymer) and cation (min ~9%, max ~30%) units showed a significant improvement concerning coating amount and durability on all examined surfaces.

For future work, the observations concerning the coherence of the catechol-cation ratio and the adsorption performance can potentially be investigated, by QCM-D

measurements as a function of the catechol-cation ratio. Further, very intriguing would be a comparing study between the examined (co)polymer matrix with an aza-Michael addition synthesized set of copolymers.

To test the anti-fouling properties of the (co)polymer matrix, Au surfaces were exemplarily coated with **9b**, **5b**$_3$/**5c**$_2$/**9b**$_{78}$, and **5b**$_3$/**5c**$_2$/**9b**$_{71}$/**9c**$_7$ and subsequently treated with a BSA solution.

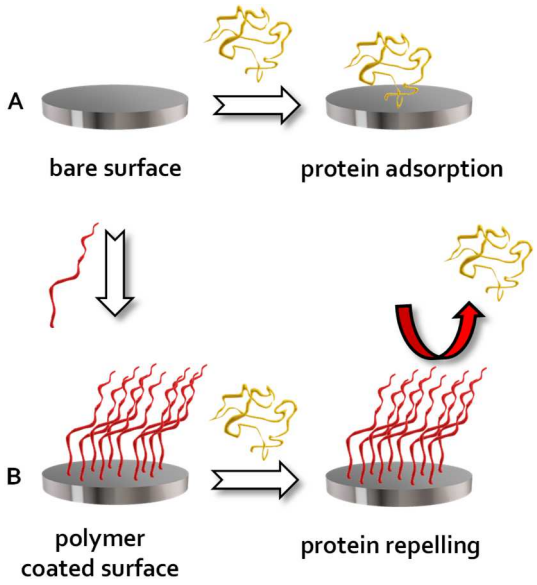


*Figure 48: It was demonstrated that bare Au surfaces, treated with BSA, adsorbed the protein in large amounts allowing biofouling processes. After coating Au surfaces with synthesized copolymers, a strong protein repelling effect was monitored.*

The measurements revealed that the bare and **9b** coated Au surface interacted attractively with BSA (Figure 48, A). Au surfaces, coated with **5b**$_3$/**5c**$_2$/**9b**$_{78}$ and **5b**$_3$/**5c**$_2$/**9b**$_{71}$/**9c**$_7$ showed strong protein repelling effects as no BSA adsorption was monitored (Figure 48, B). It was additionally shown that the coatings were not only stable against water but also buffer solution rinsing processes.

Future work can investigate the influence of the catechol and cation units and the surface type concerting the repelling effect.

With these summarized results, this work opens a great possibility for research options in various directions. As mentioned, one route can be a variation of the synthetic route by the aza-Michael approach. Still, the established system offers numerous options as follows: one can examine more deeply the binding mechanisms on surfaces of the established system. An investigation of a networking behavior in ionic solutions via light scattering methods with the subsequent effect for the adsorbing processes can be another promising project. Finally, more experiments concerning the application-drawn properties to consolidate the above shown anti-fouling performance can be an additional route for future research.

This work demonstrated the successful synthesis of maritime glue protein mimicking copolymers, which started with 2-oxazoline monomer synthesis and was followed by homo and copolymer kinetic studies. Copolymers were successfully synthesized and modified to release the adsorbing units. The adsorption ability and anti-fouling properties of these modified copolymers were successfully demonstrated by QCM-D measurements.

# 6 Experimental section

## 6.1 General methods and materials

### 6.1.1 Analytical instrumentation and methods

Nuclear magnetic resonance (NMR) spectra were recorded at room temperature on Bruker Avance 300 MHz or Bruker Avance III 600 MHz spectrometers. Samples were prepared in $CDCl_3$ or DMSO-$d_6$. Signals were referenced to the respective solvent peaks; $CDCl_3$ $\delta(^1H)$ 7.26 ppm, $\delta(^{13}C)$ 77.16 ppm or DMSO-$d_6$ $\delta(^1H)$ 2.50 ppm, $\delta(^{13}C)$ 39.52 ppm.

Electron ionization (EI) mass spectrometry was performed on a GC/MS instrument with a time-of-flight (TOF) mass analyzer (micromass/Waters Inc.); energy of ionizing electrons: 70 eV. Samples were dissolved in chloroform.

Melting points were obtained by a MEL-TEMP II device (Laboratory Devices Inc., USA); measurements were conducted in open capillaries.

The Atomic force microscopy (AFM) height measurements were carried out using an NTEGRA AFM (NT-MDT) operating in intermittent contact mode. Commercial tips (Nanoworld-Point probe) with a resonance frequency of 320 kHz, and a spring constant of 42 N/m were used.

FT-IR spectra were recorded on a Bruker Vertex 70 fitted with a PLATINUM ATR. Samples were placed directly on the ATR diamond under an argon flow. Spectra were acquired and processed with the OPUS 7.0 software; the number of scans was 32. For liquid

samples (kinetics), the background was generated using the same solvent as the one used for the sample; for solid samples, the built-in atmospheric correction function was turned on and the background was automatically subtracted.

Size exclusion chromatography (SEC) with simultaneous UV and RI (differential refractive index) detection was performed with *N*-methyl-2-pyrrolidone (NMP) + 0.5 wt% LiBr as the eluent (flow rate: 0.5 mL·min$^{-1}$) at room temperature. The stationary phase was a 300 x 8 mm$^2$ PSS-GRAM analytical linear column (particle size 7 µm, separation range $10^2$-$10^6$ Da). Solutions containing ~0.15 wt% polymer were filtered through 0.45 µm filters; the injected volume was 100 µL. Polystyrene standards (PSS, Mainz, Germany) were used for calibration.

MALDI-TOF mass spectrometry was performed with an Autoflex III Smartbeam (Bruker Daltonik, Bremen, Germany) mass spectrometer equipped with a Nd-YAG laser ($\lambda$ = 355 nm) running at 200 Hz. Spectra were recorded in linear mode. Pre-mixed solutions consisting of 5 µL of potassium trifluoroacetate (2 mg·ml$^{-1}$), 50 µL matrix solution (*trans*-2-[3-(4-tert-butyl phenyl)-2-methyl-2-propenylidene]- malononitrile (DCTB), 20 mg·mL$^{-1}$), and 20 µL of dissolved polymer samples (3-5 mg·mL$^{-1}$, $CHCl_3$)) were prepared. Finally, 1 µL of the mixed solution was deposited on a stainless-steel target. Typically, 2000 single spectra recorded on different positions were accumulated for one spectrum. Recording and evaluation of spectra was performed using the manufactures software (FlexControl and FlexAnalysis).

UV-VIS spectra of polymer solutions (0.05 or 0.01 mg mL$^{-1}$, acetonitrile) were measured with a PerkinElmer Lambda 2 spectrometer at room temperature.

Zeta-potentials of 0.1 wt% polymer dissolved in ultrapure water were measured with a Malvern Zetasizer Nano ZS at room temperature.

Dynamic light scattering (DLS) of 0.1 wt% polymer dissolved in ultrapure water were measured with a Malvern Zetasizer Nano ZS at room temperature.

The quartz crystal microbalance with dissipation (QCM-D) instrument was a Q-Sense E4 System from Biolin Scientific (Gothenburg, Sweden). All substrates were tested at room temperature using sensors from Quantum Design GmbH (Darmstadt, Germany). Gold and borosilicate sensors were cleaned by multiple sonications for 10 min (2% SDS solution; 2% Hellmanex® solution; acetone; methanol; water)–rinsing (water; water; acetone; methanol; water)–drying (nitrogen flow) cycles. Sensors were finally treated with oxygen plasma for 10 min. Iron sensors were cleaned by immersing in 1% Hellmanex II solution at room temperature for 3 h; sonicated in absolute ethanol for 10 min; Between and after the cycles the sensor was rinsed with water and dried under nitrogen flow. Polystyrene sensors were cleaned by immersing in 1% Deconex 11 solution for 30 min at 30 °C. Rinsed and kept in water for 3 h and rinsed with absolute ethanol and dried under nitrogen flow. Measurements were performed with 0.01 wt% polymer solutions in Milli-Q water and a (measured) cell flow of ~100 µL $min^{-1}$. The baseline was set with Milli-Q water. The adsorbed mass of polymer was calculated using a modified Sauerbrey equation (Chapter 3.2).

Linear determination of $k_A$:

For zero-order kinetic counts:

$$\frac{dN}{dt} = 0 \qquad 11$$

With $N$ = binding sites

$$\frac{dN}{dt} = k_A * c * N \qquad 12$$

$$dN = k_A * c * N * dt \quad (13)$$

With $c*N = c_{eff}$

$$m = k_A * c_{eff} * t \quad (14)$$

with $m$ = adsorbed mass (det. By QCM-D measurement ng∗cm$^{-2}$), $c_{eff}$ = concentration of the solution (0.1 mg∗mL$^{-1}$) , $t$ = time (s).

With

$$slope = \frac{m}{t} \quad (15)$$

is

$$slope = k_A * c_{eff} \quad (16)$$

$$k_A = \frac{slope}{c_{eff}} \quad (17)$$

Exponential determination of $k_A$:

$$\frac{dm}{dt} = k_A * c * (m_{max} - m) - k_D * m \quad (18)$$

with $k_A$ = adsoprtions constant, $k_D$ = desorption constant, $m$ = adsorbed mass (det. By QCM-D measurement ng∗cm$^{-2}$), $c$ = concentration of the solution (0.1 mg∗mL$^{-1}$) , $m_{max}$ = maximum mass adsorption (not det.)

with $A = k_{\mathrm{A}} * c$ and $B = k_{\mathrm{D}}$ it follows

$$\frac{dm}{dt} = A * (m_{max} - m) - B * m \qquad 19$$

$$\frac{dm}{dt} = A * m_{max} - A * m - B * m \qquad 20$$

$$\frac{dm}{dt} = A * m_{max} - (A + B) * m \qquad 21$$

with $A * m_{\max} = C$ it follows:

$$\frac{dm}{dt} = C - (A + B) * m \qquad 22$$

$$\int_0^m \frac{1}{C-(A+B)*m}\, dm = \int_0^t dt \qquad 23$$

$$\left[\frac{-\ln(C-(A+B)*m)}{A+B}\right]_0^m = t \quad (24)$$

$$\frac{1}{A+B} * [-\ln(C-(A+B)*m) + \ln(C-(A+B)*0)] = t \quad (25)$$

$$\frac{1}{A+B} * [-\ln(C-(A+B)*m) + \ln(C)] = t \quad (26)$$

$$-\ln(C-(A+B)*m) + \ln(C) = (A+B)*t \quad (27)$$

$$\ln(C-(A+B)*m) - \ln(C) = -(A+B)*t \quad (28)$$

$$\ln\left(\frac{C-(A+B)*m}{C}\right) = -(A+B)*t \quad (29)$$

$$\frac{C-(A+B)*m}{C} = exp[-(A+B)*t] \quad (30)$$

$$-(A+B)*m = C*exp[-(A+B)*t] - C \quad (31)$$

$$(A+B)*m = -C*exp[-(A+B)*t] + C \quad (32)$$

$$(A+B)*m = C - C*exp[-(A+B)*t] \quad (33)$$

$$m = \frac{C-C*exp[-(A+B)*t]}{(A+B)} \quad (34)$$

$$m = \frac{C}{A+B}*(1-exp[-(A+B)*t]) \quad (35)$$

$$m = \frac{k_A*c*m_{max}}{k_A*c+k_D}*(1-exp[-(k_A*c+k_D)*t]) \quad (36)$$

$$m = m_{max}\frac{k_A*c}{k_A*c+k_D}*(1-exp[-(k_A*c+k_D)*t]) \quad (37)$$

With $\Delta m = m_{max}\frac{k_A*c}{k_A*c+k_D}$

$$m = \Delta m * (1 - exp[-(k_A * c + k_D) * t]) \quad 38$$

$$m = \Delta m * \left(1 - exp\left[-\frac{t}{\tau}\right]\right) \quad 39$$

From an experimental point of view only matters the ratio between adsorption and desorption. Thus, the factor $m_{max}$ was set 1. This results in the following conclusion:

$$\Delta m \sim \frac{k_A * c}{(k_A * c + k_D)} = k_A * c * \tau \quad 40$$

With $\tau = \frac{1}{(k_A * c + k_D)}$

$$k_A = \frac{\Delta m}{c} * \tau \quad 41$$

$$k_D = \frac{1}{\tau} - k_A * c \quad 42$$

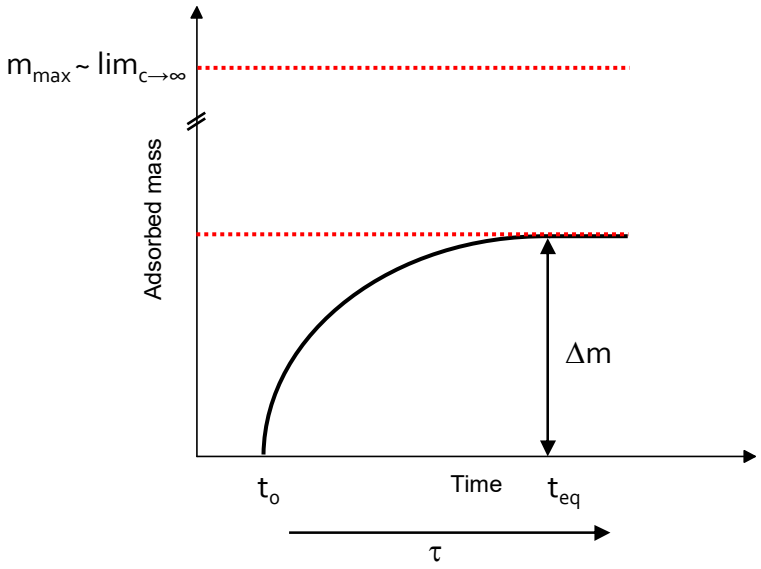


*Figure 49: Schematic representation of the experimental data of the QCM-D measurements.*

Consideration of the units:

$$\frac{dm}{dt} = k_A * c * (m_{max} - m) - k_D * m \qquad 43$$

Into units:

$$\left[\frac{ng}{cm^2} * \frac{1}{s}\right] = \left[\frac{mL}{mg} * \frac{1}{s}\right] * \left[\frac{mg}{mL}\right] * \left(\left[\frac{ng}{cm^2}\right]\right) - \left[\frac{1}{s}\right] * \left[\frac{ng}{cm^2}\right] \qquad 44$$

$$k_A = \left[\frac{mL}{mg} * \frac{1}{s}\right] \qquad 45$$

$$k_D = \left[\frac{1}{s}\right] \qquad 46$$

$$m = m_{max}\frac{k_A \cdot c}{k_A \cdot c + k_D} \cdot \left(1 - exp\left[-\frac{t}{\tau}\right]\right) \quad 47$$

Into units:

$$\left[\frac{ng}{cm^2}\right] = \left[\frac{ng}{cm^2}\right] \cdot \frac{\left[\frac{mL}{mg}\frac{1}{s}\right] \cdot \left[\frac{mg}{mL}\right]}{\left[\frac{mL}{mg}\frac{1}{s}\right] \cdot \left[\frac{mg}{mL}\right] + \left[\frac{1}{s}\right]} \cdot \left(1 - exp\left[-\frac{[s]}{[s]}\right]\right) \quad 48$$

$$\left[\frac{ng}{cm^2}\right] = \left[\frac{ng}{cm^2}\right] \cdot \frac{\left[\frac{1}{s}\right]}{\left[\frac{1}{s}\right] + \left[\frac{1}{s}\right]} \cdot \left(1 - exp\left[-\frac{[s]}{[s]}\right]\right) \quad 49$$

$$\left[\frac{ng}{cm^2}\right] = \left[\frac{ng}{cm^2}\right] \cdot \frac{\left[\frac{1}{s}\right]}{\left[\frac{1}{s}\right]} \cdot \left(1 - exp\left[-\frac{[s]}{[s]}\right]\right) \quad 50$$

### 6.1.2 Chemical list

| Chemical | Supplier | Purity | Comments |
|---|---|---|---|
| 3,4- dimethoxybenzonitrile | Alfa Aesar | 98% | |
| 1,4-dioxane | VWR | 99% | |
| 2-Chloroethylamine hydrochloride | Merck | 99% | |
| 3,4,5-trimethoxybenzonitrile | Alfa Aesar | 97% | |
| 3,4,5-trimethoxycinnamic acid | Alfa Aesar | 97% | predominately *trans* |
| 3,4-dimethoxycinnamic acid | Alfa Aesar | 99% | predominately *trans* |
| 3,4-dimethoxyphenylacetonitrile | Alfa Aesar | 98% | |
| Acetonitrile | Sigma Aldrich | 99.97% | anhydrous |
| Aluminum oxide, basic | Sigma Aldrich | | 50-200 mm, 60 Å |
| Aluminium iodide | ABCR | 95% | stored under Argon |
| Ammonia | Air Liquide | 99.99% | anhydrous |
| Benzene | Alfa Aesar | 99% | |
| Benzonitrile | Sigma Aldrich | 99.9% | dried over molecular sieves 3 Å |
| Boron trifluoride etherate | Sigma Aldrich | 46.5% $BF_3$ | anhydrous |
| BSA | Merck | 98% | pH 7 |
| Celite | Fluka | | 500 fine |
| Chlorobenzene | Sigma Aldrich | 99.8% | |
| Chloroform-$d_1$ | Deutero GmbH | 99.8% atom D | |
| Cinnamic acid | Alfa Aesar | 99% | predominately *trans* |

| | | | |
|---|---|---|---|
| Dichloromethane | | | Distilled prior use |
| Dimethyl sulfoxide (DMSO) | Sigma Aldrich | 99.9% | |
| DMSO-$d_6$ | Deutero GmbH | 99.9% atom D | |
| Ethanolamine | Acros | 99% | |
| Ethyl acetate | | | Distilled prior use |
| Ethyl chloroformate | Sigma Aldrich | 97% | |
| 2-Ethyl-2-oxazoline | Acros | 99.13% | Distilled from $CaH_2$ |
| Hydrochloric acid (HCl) | Fischer | | analytical grade |
| Magnesium sulfate | VWR | 99.7% | |
| Methanesulfonyl chloride | Merck | 99% | |
| Methanol | | | Distilled prior use |
| Methyl *p*-toluene sulfonate (methyl tosylate, MeOTos) | Sigma Aldrich | 97% | Distilled from $CaH_2$ |
| *N*-(*tert.*-Butoxycarbonyl)-*L*-tyrosin | Sigma Aldrich | 98% | |
| *N,N'*-diisopropylcarbodiimide | Acros | 99% | anhydrous |
| Oxalyl chloride | Acros | 98% | |
| *N,N*-Dimethylformamide | Acros | 99.99% | anhydrous |
| Petrol ether | | | Distilled prior use |
| 2-Phenyl-2-oxazoline | Merck | 99% | Distilled from $CaH_2$ |
| Potassium carbonate | Sigma | 99% | anhydrous |
| Potassium hydroxide | Sigma Aldrich | 86% | |
| Silica | Macherey-Nagel | | 60M, 0.04-0.063 mm |
| Sodium thiosulfate | Sigma Aldrich | 98% | |
| Tetrahydrofuran (THF) | Acros | 99.9% | dried over molecular sieves 3 Å |
| Thionyl chloride | Merck | 99% | |
| Titanium(IV) isopropoxide | Aldrich | 97% | |

| | | |
|---|---|---|
| Triethylamine (TEA) | Sigma Aldrich | 99.9% |
| Zinc(II) acetate | Aldrich | 99.9% |

## 6.2 Synthetic procedures

All reactions were carried out in dried glassware under an argon atmosphere unless otherwise noted.

### 6.2.1 3,4-Dimethoxycinnamyl amide

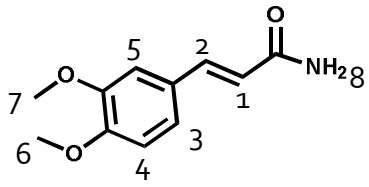


Thionyl chloride (100 mmol, 11.9 g) was added within 5 min to 3,4-dimethoxycinnamic acid (**2**) (50 mmol, 10.4 g) under stirring at room temperature. The mixture was heated to 80 °C and stirred for 5 h, and afterwards, the remaining thionyl chloride was removed under reduced pressure. The crude acid chloride was dissolved in THF (200 mL) cooled to -80 °C and $NH_3$ (g) was condensed into the vessel for 5 min. After finishing the $NH_3$ addition, the mixture was allowed to warm up to 20 °C within 20 h. The reaction was quenched with $H_2O$ (100 mL) and the basic solution was neutralized by adding a 2 M HCl solution (20 mL). The organic phase was separated, and the aqueous layer was extracted with ethyl acetate (3 x 80 mL). The organic extracts were combined and dried over magnesium sulfate. After filtration, the volatiles were removed in vacuum until a colorless solid precipitated. The solid was filtered off and was washed 3 times with cold ethyl acetate (50 mL) and dried in vacuum. Yield 8.95 g (43.2 mmol, 86%), colorless solid.

$^1$H NMR (300 MHz, DMSO-$d_6$): δ (ppm) 7.43 (s, 1H, *H*-8), 7.35 (d, $^3J$ = 15.9 Hz, 1H, *H*-2), 7.15 (d, $^4J$ = 2.0 Hz, 1H, *H*-5), 7.10 (dd, $^4J$ = 2.0 Hz, $^3J$ = 8.3 Hz 1H, *H*-3), 7.00 (s, 1H, *H*-8), 6.97 (d, $^3J$ = 8.2 Hz, 1H, *H*-4), 6.49 (d, $^3J$ = 16.0 Hz, 1H, *H*-1), 3.79 (s, 3H, *H*-6), 3.78 (s, 3H, *H*-7).

### 6.2.2 Cinnamyl amide

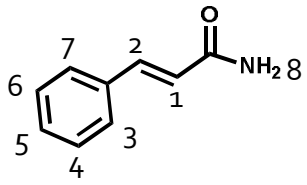


From cinnamic acid (**1**), procedure as above. Yield 4.16 g (28.3 mmol, 95%), colorless solid.

$^1$H NMR (300 MHz, DMSO-$d_6$): δ (ppm) 7.60-7.47 (m, 3H, *H*-2, *H*-3, *H*-7), 7.45-7.35 (m, 4 H, *H*-4, *H*-5, *H*-6, *H*-8), 7.11 (s, 1H, *H*-8), 6.61 (d, $^3J$ = 16.0 Hz, 1H, *H*-1).

### 6.2.3 3,4,5-Trimethoxycinnamyl amide

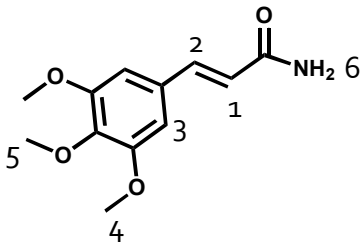


From 3,4,5-trimethoxycinnamic acid (**3**), procedure as above. The crude product was washed with ice-cold ethyl acetate (100 mL) and purified by sublimation (170 °C, 0.002 mbar). Yield 6.12 g (25.8 mmol, 65%), pale yellow solid.

$^1$H NMR (300 MHz, DMSO-$d_6$): δ (ppm) 7.46 (s, 1H, *H*-6), 7.35 (d, $^3J$ = 15.9 Hz, 1H, *H*-2), 7.05 (s, 1H, *H*-6), 6.88 (s, 2H, *H*-3), 6.56 (d, $^3J$ = 16.0 Hz, 1H, *H*-1), 3.81 (s, 6H, *H*-4), 3.68 (s, 3H, *H*-5).

### 6.2.4 Cinnamonitrile

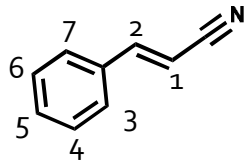


A dry flask was equipped with cinnamyl amide (3.0 mmol, 442 mg) and $SOCl_2$ (4.5 mmol, 535 mg) was added dropwise within 5 min. The mixture was stirred for 5 h at 80 °C and the progress of the reaction was monitored by TLC. After removing the excess of thionyl chloride in vacuum, the reaction was quenched with water (10 mL). The aqueous layer was extracted with dichloromethane (3 x 50 mL), and the combined organic extracts were dried over magnesium sulfate. After filtration, the volatiles were removed in vacuum, and the crude was purified by column chromatography (silica, petrol ether/ethyl acetate 9:1 (v/v), $R_f$ = 0.51). Yield 371 mg (2.8 mmol, 95%), colorless liquid.

$^1$H NMR (300 MHz, $CDCl_3$): $\delta$ (ppm) 7.50-7.35 (m, 6H, *H*-2, *H*-3, *H*-4, *H*-5, *H*-6, *H*-7), 5.88 (d, $^3J$ = 16.6 Hz, 1H, *H*-1).

### 6.2.5 3,4-Dimethoxycinnamonitrile

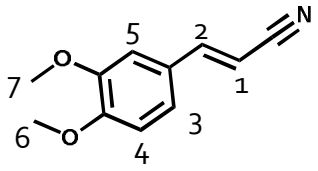


A dry flask was equipped with 3,4-dimethoxycinnamyl amide (3.0 mmol, 622 mg), acetonitrile (10 mL), DMSO (1 drop), and TEA (7.5 mmol, 759 mg), to which a solution of oxalyl chloride (3.6 mmol, 457mg) in acetonitrile (5 mL) was added dropwise within 5 min at 0 °C. The mixture was allowed to warm up to 20 °C and was stirred for 18 h. The progress of the reaction was monitored by TLC. After 18 h, the reaction was quenched with water (10 mL). The aqueous layer was extracted with ethyl acetate (3 x 50 mL) and the combined organic extracts were dried over magnesium sulfate. After filtration, the volatiles were removed in vacuum, and the crude was purified by column chromatography (silica, petrol ether/ethyl acetate 7:3 (v/v), $R_f$ = 0.56). Yield 471 mg (2.5 mmol, 83%), pale yellow solid.

$^1$H NMR (300 MHz, $CDCl_3$): $\delta$ (ppm) 7.31 (d, $^3J$ = 16.3 Hz, 1H, *H*-2), 7.03 (dd, $^3J$ = 8.5 Hz, $^4J$ = 2.4 Hz 1H, *H*-3), 6.93 (d, $^4J$ = 2.3 Hz, 1H, *H*-5), 6.86 (d, $^3J$ = 8.5 Hz, 1H, *H*-4), 5.72 (d, $^3J$ = 16.5 Hz, 1H, *H*-1), 3.92 (s, 3H, *H*-6), 3.91 (s, 3H, *H*-7).

### 6.2.6 3,4,5-Trimethoxycinnamonitrile

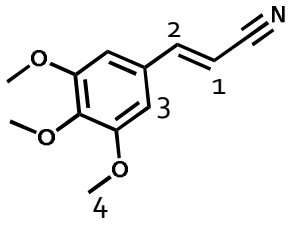


From 3,4,5-trimethoxycinnamyl amide, procedure as above. The crude product was purified by flash chromatography (silica, petrol ether/ethyl acetate 3:7 (v/v), $R_f$ = 0.83). Yield 554 mg (2.3 mmol, 84%), pale yellow solid.

$^1$H NMR (300 MHz, $CDCl_3$): $\delta$ (ppm) 7.30 (d, $^3J$ = 16.5 Hz, 1H, *H*-2), 6.65 (s, 2H, *H*-3), 5.78 (d, $^3J$ = 16.6 Hz, 1H, *H*-1), 3.88 (s, 9H, *H*-4).

### 6.2.7 2-Phenyl-2-oxazoline

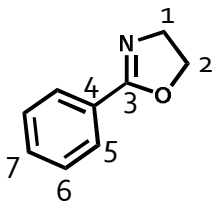


A dry flask was equipped with benzonitrile (25.0 mmol, 2.58 g), chlorobenzene (15 mL), and zinc(II) acetate (0.95 mmol, 174 mg). The mixture was heated to 140 °C and was stirred for 5 min. Then, ethanolamine (33.4 mmol, 2.04 g) was added dropwise within 5 min, and the mixture was stirred at 140 °C for 20 h. After cooling to ambient temperature, the reaction was quenched with water (20 mL). The aqueous phase was extracted with ethyl acetate (3 x 50 mL). The separated organic layer was dried over magnesium sulfate, filtered, and volatiles were removed in vacuum. The crude product was purified by flash chromatography (silica, ethyl acetate, $R_f$ = 0.39). Yield 3.27 g (22.2 mmol, 89%), colorless solid.

$^1$H NMR (600 MHz, $CDCl_3$): δ (ppm) 7.93 (d, $^3J$ = 7.2 Hz, 2H, *H*-5), 7.45 (t, $^3J$ = 7.5 Hz, 1H, *H*-7), 7,39 (t, $^3J$ = 7.9 Hz, 2H, *H*-6), 4.40 (t, $^3J$ = 9.7 Hz, 2H, *H*-1), 4.04 (t, $^3J$ = 9.7 Hz, 2H, *H*-2).

$^{13}$C NMR (150 MHz, $CDCl_3$): δ (ppm) 164.6 (*C*-3), 131.3 (*C*-7), 128.3 (2C, *C*-5), 128.1 (2C, *C*-6), 127.8 (*C*-4), 67.6 (*C*-2), 55.0 (*C*-1).

FT-IR (ATR): 1647 (s), 1357 (m), 1327 (w), 1257 (m), 1078 (m), 1063 (s), 1024 (w), 976 (w), 943 (s), 895 (w), 776 (m), 691 (s), 671 (s) $cm^{-1}$.

### 6.2.8 2-(3,4-Dimethoxyphenyl)-2-oxazoline

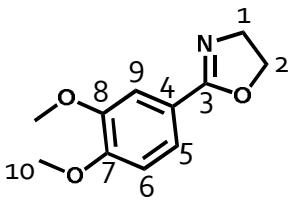


From 3,4-dimethoxybenzonitrile, procedure as above (**8a**). The crude product was purified by flash chromatography (silica, ethyl acetate, $R_f$ = 0.42). Yield 8.46 g (40.8 mmol, 81%), colorless solid.

$^1$H NMR (600 MHz, $CDCl_3$): δ (ppm) 7.50 (dd, $^4J$ = 2.0 Hz, $^3J$ = 8.4 Hz, 1H, *H*-5), 7.47 (d, $^4J$ = 2.0 Hz, 1 H, *H*-9), 6.86 (d, $^3J$ = 8.4 Hz, 1H, *H*-6), 4.40 (t, $^3J$ = 9.6 Hz, 2H, *H*-1), 4.02 (t, $^3J$ = 9.6 Hz, 2H, *H*-2), 3.90 (s, 3H, *H*-10), 3.90 (s, 3H, *H*-10).

$^{13}$C NMR (150 MHz, $CDCl_3$): δ (ppm) 164.5 (*C*-3), 151.6 (*C*-7), 148.6 (*C*-8), 121.5 (*C*-4), 120.4 (*C*-5), 110,6 (*C*-9), 110.4 (*C*-6), 67.6 (*C*-2), 55.9 (2C, *C*-10), 54.9 (*C*-1).

FT-IR (ATR): 1643 (m), 1587 (w), 1511 (s), 1363 (m), 1267 (s), 1249 (s), 1217 (s), 1176 (s), 1131 (s), 1074 (m), 1019 (s), 976 (m), 954 (s), 873 (m), 826 (m), 765 m), 708 (m) $cm^{-1}$.

EI-MS: m/z (%) 207 (100) $[M]^+$, 206 (18) $[M-1]^+$, 177 (19), 162 (11), 121 (10), 77 (5).

Mp: 98 °C.

### 6.2.9 2-(3,4,5-Trimethoxyphenyl)-2-oxazoline

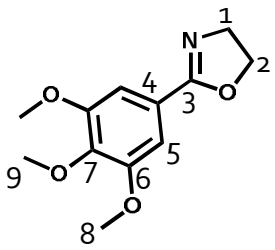


From 3,4,5-trimethoxybenzonitrile, procedure as above (**8a**). The crude product was purified by flash chromatography (silica, ethyl acetate, $R_f$ = 0.41). Yield 5.49 g (23.1 mmol, 93%), colorless solid.

$^{1}$H NMR (600 MHz, $CDCl_3$): δ (ppm) 7.18 (s, 2H, *H*-5), 4.42 (t, $^{3}J$ = 9.6 Hz, 2H, *H*-1), 4.04 (t, $^{3}J$ = 9.5 Hz, 2H, *H*-2), 3.88 (s, 6H, *H*-9), 3.87 (s, 3H, *H*-8).

$^{13}$C NMR (150 MHz, $CDCl_3$): δ (ppm) 164.4 (*C*-3), 153.0 (2C, *C*-6), 140.6 (*C*-7), 123.0 (*C*-4), 105.2 (2C, *C*-5), 67.8 (*C*-2), 60.9 (*C*-9), 56.2 (2C, *C*-8), 54.95 (*C*-1).

FT-IR (ATR): 1647 (w), 1582 (m), 1505 (m), 1462 (w), 1413 (m), 1362 (m), 1229 (m), 1127 (s), 1094 (m), 986 (m), 958 (m), 851 (w), 711 (m) $cm^{-1}$.

EI-MS: m/z (%) 237 (100) $[M]^+$, 236 (7) $[M-1]^+$, 222 (23), 207 (5), 192 (10), 179 (10).

Mp: 68 °C (Lit.: 64-66 °C).[180]

### 6.2.10 2-Cinnamyl-2-oxazoline

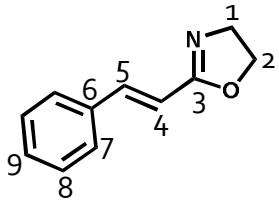


From cinnamonitrile, procedure as above (**8a**). The crude product was purified by flash chromatography (silica, petrol ether/ethyl acetate 1:9 (v/v), $R_f$ = 0.32). Yield 6.30 g (36.4 mmol, 73%), colorless solid.

$^1$H NMR (600 MHz, $CDCl_3$): δ (ppm) 7.5-7.47 (m, 2H, *H*-7), 7.39-7.31 (m, 4H, *H*-5, *H*-8, *H*-9), 6.64 (d, $^3J$ = 16.3 Hz, 1H, *H*-4), 4.34 (t, $^3J$ = 9.5 Hz, 2H, *H*-1), 3.99 (t, $^3J$ = 9.5 Hz, 2H, *H*-2).

$^{13}$C NMR (150 MHz, $CDCl_3$): δ (ppm) 164.4 (*C*-3), 139.8 (*C*-5), 135.3 (*C*-6), 129.4 (*C*-9), 128.8 (2C, *C*-8), 127.5 (2C, *C*-7), 115.2 (*C*-4), 67.3 (*C*-2), 55.0 (*C*-1).

FT-IR (ATR): 1650 (m), 1604 (w), 1360 (m), 1248 (m), 989 (s), 955 (s), 908 (m), 755 (s), 694 (s), 664 (w), 580 (w), 489 (m), 480 (m) $cm^{-1}$.

EI-MS: m/z (%) 173 (22) $[M]^+$, 172 (100) $[M-1]^+$, 128 (18), 115 (42), 102 (8), 77 (7), 51 (5).

Mp: 62 °C (Lit.: 52-54 °C).[181]

### 6.2.10.1 Alternate procedure, from cinnamic acid:

Cinnamic Acid (**1**) (741 mg, 5.0 mmol) and ethanolamine (611 mg, 10.0 mmol) were dissolved in chlorobenzene (10 ml). Then, titanium(IV) isopropoxide (50 mol%, 711 mg, 2.5 mmol) were added, and the mixture was heated to 145 °C and stirred for 96 h (at 24 h, 48h, and 72 h the same amount of catalyst was added to the mixture). The progress of the reaction was monitored by TLC. Afterwards, the reaction was quenched by the addition of ethyl acetate (40 ml) and $H_2O$ (2 ml). Without extraction of the organic layer, the suspension was dried over magnesium sulfate and the solid was filtered off using a glass filter and celite. The solid residue was washed with ethyl acetate (3 x 20 ml). After filtration, the volatiles were removed in vacuum, and the yellow crude product was purified by column chromatography (alox, eluent: ethyl acetate, $R_f$ = 0.90). Yield 346 mg (2.0 mmol, 40%), colorless solid.

### 6.2.11 2-(3,4-Dimethoxycinnamyl)-2-oxazoline

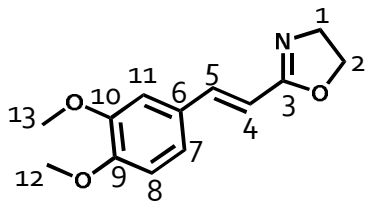


From 3,4-dimethoxycinnamonitrile, procedure as above (**8a**). The crude product was purified by recrystallization from acetonitrile. Yield 4.41 g (18.9 mmol, 73%), colorless solid.

$^{1}$H NMR (600 MHz, $CDCl_3$): δ (ppm) 7.31 (d, $^{3}J$ = 16.2 Hz, 1H, *H*-5), 7.08-7.03 (m, 2H, *H*-7, *H*-8), 6.87 (d, $^{4}J$ = 8.3 Hz, 1H, *H*-11), 6.54 (d, $^{3}J$ = 16.2 Hz, 1H, *H*-4), 4.36 (t, $^{3}J$ = 9.5 Hz, 2H, *H*-1), 4.00 (t, $^{3}J$ = 9.4 Hz, 2H, *H*-2), 3.92 (s, 3H, *H*-12), 3.92 (s, 3H, *H*-13).

$^{13}$C NMR (150 MHz, $CDCl_3$): δ (ppm) 164.5 (*C*-3), 150.4 (*C*-9), 149.2 (*C*-10), 139.5, (*C*-5), 128.3 (*C*-6), 121.6 (*C*-7), 113.1 (*C*-4), 111.0 (*C*-11), 109.1 (*C*-8), 67.2 (*C*-2), 56.0 (*C*-12), 55.9 (*C*-13), 55.8 (*C*-1).

FT-IR (ATR): 1649 (m), 1599 (w), 1510 (m), 1421 (w), 1262 (s), 1249 (m), 1224 (m), 1160 (m), 1143 (s), 1023 (s), 975 (s), 954 (m), 809 (m) $cm^{-1}$.

EI-MS: m/z (%) 233 (21) $[M]^+$, 232 (100) $[M-1]^+$, 216 (12), 188 (6).

Mp: 116-117 °C.

### 6.2.12 2-(3,4,5-Trimethoxycinnamyl)-2-oxazoline

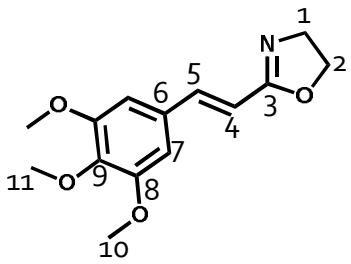


From 3,4,5-trimethoxycinnamonnitrile, procedure as above (**8a**). The crude product was purified by column chromatography (alox, ethyl acetate/petrol ether 2:3 (v/v) with a gradient to pure ethyl acetate, $R_f$ = 0.34). Yield 529 mg (2.0 mmol, 55%), colorless to pale yellow solid.

$^{1}$H NMR (600 MHz, $CDCl_3$): δ (ppm) 7.25 (d, $^{3}J$ = 16.3 Hz, 1H, *H*-5), 6.69 (s, 2H, *H*-7), 6.54 (d, $^{3}J$ = 16.2 Hz, 1H, *H*-4), 4.33 (t, $^{3}J$ = 9.33 Hz, 2H, *H*-1), 3.98 (t, $^{3}J$ = 9.5 Hz, 2H, *H*-2), 3.86 (s, 6H, *H*-10), 3.85 (s, 3H, *H*-11).

$^{13}$C NMR (150 MHz, $CDCl_3$): δ (ppm) 164.3 (*C*-3), 153.4 (2C, *C*-8), 139.6 (*C*-5), 139.4 (*C*-9), 130.9 (*C*-6), 114.6 (*C*-4), 104.6 (2C, *C*-7), 67.3 (*C*-2), 60.9 (*C*-11), 56.1 (2C, *C*-10), 54.9 (*C*-1).

FT-IR (ATR): 1652 (w), 1608 (w), 1582 (w), 1505 (w), 1456 (w), 1419 (m), 1323 (m), 1234 (m), 1126 (s), 1006 (m), 996 (m), 977 (m), 959 (m), 814 (m), 629 (w), 603 (w), 470 (w) $cm^{-1}$.

EI-MS: m/z (%) 263 (29) $[M]^+$, 262 (100) $[M-1]^+$, 232 (8), 218 (7), 190 (6).

Mp: 88 °C.

### 6.2.13 2-(3,4-dimethoxybenzyl)-2-oxazoline

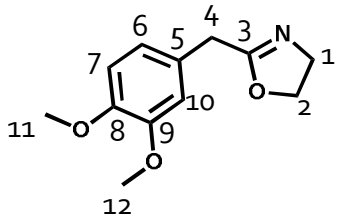


From 3,4-dimethoxyphenylacetonitrile, procedure as above (**8a**). The crude product was purified via flash chromatography (silica, ethyl acetate; $R_f$ = 0.29). Yield 3.64 g (16.47 mmol, 66 %), colorless solid.

$^{1}$H NMR (600 MHz, $CDCl_3$): δ (ppm) 6.86–6.76 (m, 3H, *H*-6, *H*-7, *H*-10), 4.23 (t, $^{3}J$ = 9.5 Hz, 2H, *H*-1), 3.90–3.79 (m, 8H, *H*-2, *H*-11, *H*-12), 3.54 (s, 2H, *H*-4).

$^{13}$C NMR (150 MHz, $CDCl_3$): δ (ppm) 167.2 (*C*-3), 148.9 (*C*-8), 148.1 (*C*-9), 127.7 (*C*-5), 121.1 (*C*-6), 112.2 (*C*-10), 111.2 (*C*-7), 67.7 (*C*-2), 55.9 (2C, *C*-11, *C*-12), 54.5 (*C*-1), 34.4 (*C*-4).

FT-IR (ATR): 2900 (w), 1662 (m), 1590 (w), 1512 (s), 1469 (w), 1444 (m), 1261 (m), 1239 (s), 1234 (s), 1160 (s), 1137 (m), 1022 (s), 984 (m), 956 (m), 921 (m), 860 (m), 822 (m), 772 (w), 761 (m), 604 (m), 543 cm (w) $cm^{-1}$.

EI-MS: m/z (%) 221 (100) $[M]^+$.

Mp: 69 °C.

### 6.2.14 *N*-*tert*-Butoxycarbonyl-(2-chloroethyl)amino)-3-(4-methoxy-*L*-tyrosin)

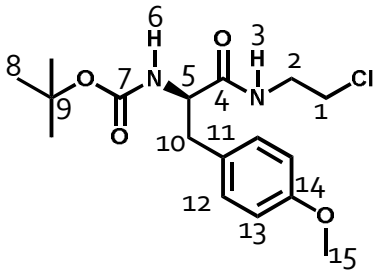


A dry flask was equipped with *N*-(*tert*-Butoxycarbonyl)-*L*-tyrosin (9.21 mmol, 2.72 g), THF (80 mL), and TEA (9.21 mmol, 1.28 mL). The solution was cooled to 0 °C and ethyl chloroformate was added dropwise within 5 min. The reaction was allowed to stir at 20 °C for 1 h. The mixture was cooled to 0 °C again and a solution of 2-chloroethylamine hydrochloride (9.21 mmol, 1.07 g), TEA (9.21 mmol, 1.28 mL), and DMF (10 mL) was added rapidly, and the reaction was stirred at 20 °C for another 1.5 h. The volatiles were removed, and the residue was dissolved in ethyl acetate (80 mL) and was washed with aqueous sodium bicarbonate solution (3 x 50 mL) and brine (3 x 50 mL). The separated organic layer was dried over magnesium sulfate, filtered, and volatiles were removed in vacuum. The crude product was used for continuing reactions without further. Yield 3.17 g (8.89 mmol, 97%), colorless solid.

$^{1}$H NMR (600 MHz, DMSO-$d_6$): δ (ppm) 8.15 (t, $^{4}J$ = 1.2 Hz, 1H, *H*-3), 7.15 (d, $^{3}J$ = 8.3 Hz, 2H, *H*-12) 6.83 (m, 3H, *H*-6, *H*-13), 4.07 (sext, $^{3}J$ = 4.3 Hz, $^{3}J$ = 5.0 Hz, $^{3}J$ = 4.5 Hz, $^{3}J$ = 9,3, 1H, *H*-5), 3.70 (s, 3H, *H*-15), 3.55 (t, $^{3}J$ = 6.1 Hz, 2H, *H*-1), 3.33 (m, 2H, *H*-2), 2.76 (m, 2H, *H*-10), 1.30 (s, 9H, *H*-8).

$^{13}$C NMR (150 MHz, DMSO-$d_6$): δ (ppm) 172.07 (*C*-4), 157.8 (*C*-14), 155.2 (*C*-7), 130.2 (2C, *C*-12), 129.9 (C-11), 113.5 (2C, *C*-13), 78.00 (*C*-9), 56.00 (*C*-5), 55,0 (*C*-15), 44.1 (*C*-1) 40.7 (*C*-2), 36.8 (*C*-10), 28.1 (3C, *C*-8).

### 6.2.15 *N-tert*-Butoxycarbonyl-(4-methoxy-*L*-tyrosin)-2-oxazoline

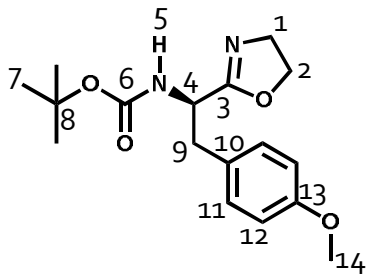


A dry flask was equipped with *N-tert*-Butoxycarbonyl-(2-chloroethyl)amino)-3-(4-methoxy-*L*-tyrosin) (8.41 mmol, 3.0 g) and dry DMF (180 mL). Subsequently, $K_2CO_3$ (16.82 mmol, 2.32 g) was added to the solution. The mixture was heated to 70 °C for 5 h. Afterwards, the volatiles were removed in vacuum, and the residue was dissolved in ethyl acetate (150 mL) and was washed with water (3 x 100 mL). The separated organic layer was dried over magnesium sulphate, filtered, and volatiles were removed in vacuum. The crude product was purified by flash chromatography (silica, ethyl acetate, $R_f$ = 0.67). Yield 2.50 g (7.48 mmol, 89%), colorless solid.

$^1$H NMR (600 MHz, DMSO-$d_6$): δ (ppm) 7.12 (d, $^3J$ = 7.7 Hz, 2H, *H*-11), 6.82 (d, $^3J$ = 8.1 Hz, 2H, *H*-12), 4.27 (m, 1H, *H*-4), 4.21 (m, 2H, *H*-1), 3.70 (m, 5H, *H*-2, *H*-14), 2.84 (m, 2H, *H*-9), 1.30 (s, 9H, *H*-7).

$^{13}$C NMR (150 MHz, DMSO-$d_6$): δ (ppm) 166.7 (*C*-3), 157.8 (*C*-13), 155.0 (*C*-6), 130.1 (2C, *C*-11), 129.7 (*C*-10), 113.5 (2C, *C*-12), 78.0 (*C*-8), 76.2 (*C*-2), 66.4 (*C*-4), 54.9 (*C*-14), 53.7 (*C*-1), 50.2 (*C*-9, 28.1 (3C, *C*-7).

FT-IR (ATR): 3331 (s), 2981 (w), 2932 (w), 1709 (m), 1685 (s), 1513 (s), 1368 (s), 1247 (s), 1165 (s), 1026, (s), 821 (m), 555 (m), 431 (w) cm$^{-1}$.

EI-MS: m/z (%) 320 (8) [M]$^+$, 264 (19), 202 (64), 121 (100).

Mp.: 77 °C.

### 6.2.16 Homopolymerization (general procedure)

All microwave vials were flame dried for 30 min in vacuum and flushed with argon. Every vial was filled with 0.5 mL of a 2.0 mM stock solution of the monomer (**1a**-**9a**) and 0.5 mL of a 0.08 mM stock solution of the initiator (MeOTos) in acetonitrile. The vials were sealed with a septum under argon atmosphere, placed one after the other in the microwave reactor (CEM Discover), heated to 100 °C, 140 °C respectively (power: 100 W), and stirred for predetermined times (see Figure 12 (140 °C) and Figure 14 (100 °C) every data point represents a separate experiment). After fast cooling to 25 °C, the crude reaction mixture was analyzed by FT-IR (ATR) spectroscopy for the determination of monomer conversion. Subsequently, 0.4 mL of a 2 M KOH solution in methanol/water 1 : 1 (v/v) was added and the mixture was stirred for another 1 h. The polymer solutions were dialyzed (using a tubing of regenerated cellulose, MWCO 3500 Da) against methanol or THF evaporated, and freeze-dried from 1,4-dioxane analysis purposes. $^{1}$H NMR spectra, SEC traces, and MALDI-TOF MS spectra of the respective homopolymers **1b**-**9b** are shown in Chapter 8, Figure S 17 - Figure S 25, Figure S 31.

### 6.2.17 Copolymerization (exemplary procedure)

All microwave vials were flame dried for 30 min in vacuum and flushed with argon. Every vial was filled with 0.3 mL of a 1.0 mM stock solution of **9a**, 0.2 mL of a 0.5 mM stock solution of **5a**, 0.25 mL of a 0.04 mM stock solution of MeOTos in acetonitrile, and filled up with 0.25 mL of acetonitrile. The vials were sealed with a septum under argon atmosphere, placed one after the other in the microwave reactor (CEM Discover), heated to 100 °C (power: 100 W), and stirred for predetermined times (see Figure 18, every data point represents a separate experiment). After fast cooling to 25 °C, the crude reaction mixture (0.05 mL) was combined with wet DMSO-$d_6$ (0.50 mL) and analyzed by $^1$H NMR spectroscopy for the determination of monomer conversions. Subsequently, 0.4 mL of a 2 M KOH solution in methanol/water 1 : 1 (v/v) was added and the mixture was stirred for another 1 h. The copolymer solution was dialyzed (regenerated cellulose, MWCO 3500 Da) against deionized water and freeze-dried. $^1$H NMR spectra and SEC traces of the respective copolymers **2b**/**9b**, **4b**/**9b**, **5b**$_x$/**9b**$_y$, and **7b**/**9b** are shown in Chapter 8, Figure S 34 - Figure S 40.

### 6.2.18 Demethylation of 5b/9b (exemplary procedure)

$AlI_3$ (408 mg, 1.00 mmol) was suspended in 4 mL of acetonitrile at 80 °C, to which were added DIC (23 mg, 0.18 mmol) and copolymer **5b**$_{10}$/**9b**$_{94}$ (1.00 g, 0.091 mmol), dissolved in 4 mL of acetonitrile. The heterogeneous reaction mixture was stirred at 80 °C for 18 h. After cooling to room temperature, the solvent was evaporated and the crude product was purified by successive dialysis (regenerated cellulose, MWCO 3500 Da) against aqueous $Na_2S_2O_3$, water, 2 M HCl, and water and freeze-drying. The copolymer **5b**$_6$/**5c**$_4$/**9b**$_{94}$ with a degree of demethylation of ~30–40%, as determined by $^1$H NMR spectroscopy, was isolated as a colorless solid, yield: 95%. $^1$H NMR spectra and SEC traces of the respective copolymers **5b**$_x$/**5c**$_{x-z}$/**9b**$_y$ are shown in Chapter 8, Figure S 41 - Figure S 43; Chapter 4.4.2 Figure 23.

### 6.2.19 Partial acidic hydrolysis of copolymers 5b$_x$/5c$_{x-z}$/9b$_y$ (exemplary procedure)

A microwave vial was filled with copolymer **5b**$_6$/**5c**$_4$/**9b**$_{94}$ (100 mg, 0.093 mmol) and 2 mL of a 16.8 wt% aqueous HCl solution. The vial was sealed with a septum, placed in the microwave reactor (CEM Discover), heated to 100 °C (power: 100 W), and stirred for 5 min. After cooling to 25 °C, the reaction mixture was neutralized with 2.5 M aqueous NaOH, dialyzed (regenerated cellulose, MWCO 3500 Da) against water, and freeze-dried. The partially hydrolyzed copolymer **5b**$_6$/**5c**$_4$/**9b**$_{86}$/**9c**$_8$ (9%, as determined by $^1$H NMR spectroscopy) was isolated as a colorless solid, yield: 92%.$^1$H NMR spectra and SEC traces of the respective copolymers **5b**$_x$/**5c**$_{x-z}$/**9b**$_{y-h}$/**9c**$_h$, **5b**$_x$/**9b**$_{y-h}$/**9c**$_h$, and the polymer **9c** are shown in Chapter 8 Figure S 32, Figure S 41 - Figure S 44; Chapter 4.4.3, Figure 24.

# 7 References


[1] J. Saiz-Poseu, J. Mancebo-Aracil, F. Nador, F. Busqué, D. Ruiz-Molina, *Angew. Chem. Int. Ed.* **2019**, *58*, 696.

[2] C. E. Brubaker, P. B. Messersmith, *Langmuir* **2012**, *28*, 2200.

[3] N. Farsad, E. D. Sone, *J. Struct. Biol.* **2012**, *177*, 613.

[4] W. Wei, L. Petrone, Y. Tan, H. Cai, J. N. Israelachvili, A. Miserez, J. H. Waite, *Adv. Funct. Mater.* **2016**, *26*, 3496.

[5] B. D. B. Tiu, P. Delparastan, M. R. Ney, M. Gerst, P. B. Messersmith, *Angew. Chem. Int. Ed.* **2020**, *59*, 16616.

[6] B. P. Lee, P. B. Messersmith, J. N. Israelachvili, J. H. Waite, *Annu. Rev. Mater. Res.* **2011**, *41*, 99.

[7] J. H. Waite, M. L. Tanzer, *Science* **1981**, *212*, 1038.

[8] A. Bdolah, P. J. Keller, *Comp. Biochem. Physiol.* **1976**, *55*, 171.

[9] H. J. Waite, *Integr. Comp. Biol.* **2002**, *42*, 1172.

[10] H. G. Silverman, F. F. Roberto, *Mar. Biotechnol.* **2007**, *9*, 661.

[11] Q. Lin, D. Gourdon, C. Sun, N. Holten-Andersen, T. H. Anderson, J. H. Waite, J. N. Istraelachvii, *J. Adhes. Sci. Technol.* **2007**, *10*, 3782.

[12] S. Das, N. R. Martinez Rodriguez, W. Wei, J. H. Waite, J. N. Israelachvili, *Adv. Funct. Mater.* **2015**, *25*, 5840.

[13] C. N. Z. Schmitt, A. Winter, L. Bertinetti, A. Masic, P. Strauch, M. J. Harrington, *J. R. Soc. Interface* **2015**, *12*, 466.

[14] C. Fant, K. Sott, H. Elwing, F. Hook, *Biofouling* **2000**, *16*, 119.

[15] G. P. Maier, M. V. Rapp, J. H. Waite, J. N. Israelachvili, A. Butler, *Science* **2015**, *349*, 628.

[16] B. K. Ahn, D. W. Lee, J. N. Israelachvili, J. H. Waite, *Nat. Mater.* **2014**, *13*, 867.

[17] W. Wei, J. Yu, C. Broomell, J. N. Israelachvili, J. H. Waite, *J. Am. Chem. Soc.* **2013**, *135*, 377.

[18] H. Lee, N. Scherer, P. Messersmith, *Proc. Natl. Acad. Sci. USA* **2006**, *103*, 12999.

[19] S. A. Mian, L. C. Saha, J. Jang, L. Wang, X. Gao, S. Nagase, *J. Phys. Chem. C* **2010**, *114*, 20793.

[20] L. Petrone, *Adv. Colloid Interface Sci.* **2013**, *195-196*, 1.

[21] S. A. Mian, X. Gao, S. Nagase, J. Jang, *Theor. Chem. Acc.* **2011**, *130*, 333.

[22] S. A. Mian, L.-M. Yang, L. C. Saha, E. Ahmed, M. Ajmal, E. Ganz, *Langmuir* **2014**, *30*, 6906.

[23] W. M. Chirdon, W. J. O´Brian, R. E. Robertson, *J. Biomed. Mater. Res.* **2003**, *66*, 532.

[24] X. Sun, H. Shao, K. Xiang, Y. Yan, X. Yu, D. Li, W. Wu, L. Zhou, K.-F. So, Y. Ren et al., *Carbon* **2017**, *113*, 176.

[25] C. Leng, Y. Liu, C. Jenkins, H. Meredith, J. J. Wilker, Z. Chen, *Langmuir* **2013**, *29*, 6659.

[26] K. L. Syres, A. G. Thomas, W. R. Flavell, B. F. Spencer, F. Bondino, M. Malvestuto, A. Preobrajenski, M. Grätzel, *J. Phys. Chem. C* **2012**, *116*, 23515.

[27] K. Syres, A. Thomas, F. Bondino, M. Malvestuto, M. Grätzel, *Langmuir* **2010**, *26*, 14548.

[28] M. J. Jackman, K. L. Syres, D. J. H. Cant, S. J. O. Hardman, A. G. Thomas, *Langmuir* **2014**, *30*, 8761.

[29] W. Lin, J. Walter, A. Burger, H. Maid, A. Hirsch, W. Peukert, D. Segets, *Chem. Mater.* **2015**, *27*, 358.

[30] A. Calzolari, A. Ruini, A. Catellani, *J. Phys. Chem.* **2012**, *116*, 17158.

[31] S. Seo, S. Das, P. J. Zalicki, R. Mirshafian, C. D. Eisenbach, J. N. Israelachvili, J. H. Waite, B. K. Ahn, *J. Am. Chem. Soc.* **2015**, *137*, 9214.

[32] A. Wislez, D. Sluysmans, N. Giamblanco, N. Willet, F. Bano, C. van de Weerdt, C. Detrembleur, A.-S. Duwez, *Biomacromolecules* **2021**, *22*, 183.

[33] A. Li, Y. Mu, W. Jiang, X. Wan, *Chem. Comm.* **2015**, *51*, 9117.

[34] M. V. Rapp, G. P. Maier, H. A. Dobbs, N. J. Higdon, J. H. Waite, A. Butler, J. N. Israelachvili, *J. Am. Chem. Soc.* **2016**, *138*, 9013.

[35] Y. Li, T. Wang, L. Xia, L. Wang, M. Qin, Y. Li, W. Wang, Y. Cao, *J. Mater. Chem. B* **2017**, *5*, 4416.

[36] X. Ou, B. Xue, Y. Lao, Y. Wutthinitikornkit, R. Tian, A. Zou, L. Yang, W. Wang, Y. Cao, J. Li, *Sci. Adv.* **2020**, *6*, 1.

[37] J. Zhou, V. Bhagat, M. L. Becker, *ACS Appl. Mater. interfaces* **2016**, *8*, 33423.

[38] J. Monahan, J. J. Wilker, *Chem. Comm.* **2003**, 1672.

[39] T. L. Coombs, P. J. Keller, *Aquat. Toxicol.* **1981**, *1*, 291.

[40] R. H. Holm, P. Kennepohl, E. I. Solomon, *Chem. Rev.* **1996**, *96*, 2239.

[41] H. Zeng, D. S. Hwang, J. N. Israelachvili, J. H. Waite, *Proc. Natl. Acad. Sci. USA* **2010**, *107*, 12850.

[42] N. Patil, C. Jérôme, C. Detrembleur, *Prog. Polym. Sci.* **2018**, *82*, 34.

[43] M. A. Rahim, S. L. Kristufek, S. Pan, J. J. Richardson, F. Caruso, *Angew. Chem. Int. Ed.* **2019**, *58*, 1904.

[44] A. M. C. Maan, A. H. Hofman, W. M. Vos, M. Kamperman, *Adv. Funct. Mater.* **2020**, *30*, 2000936.

[45] A. Muñoz-Bonilla, M. Fernández-García, *Prog. Polym. Sci.* **2012**, *37*, 281.

[46] Y. Liu, K. Ai, L. Lu, *Chem. Rev.* **2014**, *114*, 5057.

[47] D. R. Dreyer, D. J. Miller, B. D. Freeman, D. R. Paul, C. W. Bielawski, *Chem. Sci.* **2013**, *4*, 3796.

[48] A.-N. Au-Duong, C.-K. Lee, *Colloid Polym. Sci.* **2018**, *296*, 1173.

[49] O. Berberich, J. Blöhbaum, S. Hölscher-Doht, R. H. Meffert, J. Teßmar, T. Blunk, J. Groll, *J. Ind. Eng. Chem.* **2019**, *80*, 757.

[50] P. Keckeis, E. Zeller, C. Jung, P. Besirske, F. Kirner, C. Ruiz-Agudo, H. Schlaad, H. Cölfen, *Chem. Eur. J.* **2021**, *27*, 8283.

[51] J. B. P. Soares, T. F. L. McKenna, *Polyolefin Reaction Engineering*, Wiley, Weinheim, **2013**.

[52] W. Seeliger, E. Aufderhaar, W. Diepers, R. Feinauer, R. Nehring, W. Thier, H. Hellmann, *Angew. Chem. Int. Ed.* **1966**, *5*, 875.

[53] T. Kagiya, S. Narisawa, T. Maeda, K. Fukui, *J. Polym. Sci. Part B* **1966**, *4*, 441.

[54] D. A. Tomalla, D. P. Sheetz, E. C. Britton, *J. Polym. Sci. Part A* **1966**, *4*, 2253.

[55] R. Hoogenboom, H. Schlaad, *Polymers* **2011**, *3*, 467.

[56] M. O. K. Aoi, *Prog. Polym. Sci.* **1996**, *21*, 151.

[57] B. Guillerm, S. Monge, V. Lapinte, J.-J. Robin, *Macromol. Rapid Commun.* **2012**, *33*, 1600.

[58] B. Verbraeken, B. D. Monnery, K. Lava, R. Hoogenboom, *Europ. Polym. J.* **2017**, *88*, 451.

[59] B. D. Monnery, V. V. Jerca, O. Sedlacek, B. Verbraeken, R. Cavill, R. Hoogenboom, *Angew. Chem. Int. Ed.* **2018**, *57*, 15400.

[60] B. L. Rivas S. I. Ananias, *Polym. Bull.* **1987**, *18*, 189.

[61] M. W. M. Fijten, R. Hoogenboom, U. S. Schubert, *J. Polym. Sci. A Polym. Chem.* **2008**, *46*, 4804.

[62] M. Glassner, M. Vergaelen, R. Hoogenboom, *Polym. Int.* **2018**, *67*, 32.

[63] F. Wiesbrock, R. Hoogenboom, C. H. Abeln, U. S. Schubert, *Macromol. Rapid Commun.* **2004**, *25*, 1895.

[64] S. Sinnwell, H. Ritter, *Macromol. Rapid Commun.* **2005**, *26*, 160.

[65] C. Maechling-Strasser, J. C. Galin, A. Schmitt, V. Housse-Ferrari, B. Sébille, J. N. Mulvihill, J. P. Cazenave, *Biomed. Mater. Res.* **1989**, *23*, 1395.

[66] M. C. Woodle, C. M. Engbers, S. Salipsky, *Bioconjugate Chem.* **1994**, *5*, 493.

[67] S. Zalipsky, C. M. Hansen, J. M. Oaks, T. M. Allen, *J. Pharm. Sci.* **1996**, *85*, 133.

[68] S. Jana, M. Uchman, *Prog. Polym. Sci.* **2020**, *106*, 101252.

[69] D. Leibig, A. H. E. Müller, H. Frey, *Macromolecules* **2016**, *49*, 4792.

[70] J. Bernard, C. Branger, T. L. A. Nguyen, R. Denoyel, A. Margaillan, *React. Funct. Polym.* **2008**, *68*, 1362.

[71] J. Duan, W. Wu, Z. Wei, D. Zhu, H. Tu, A. Zhang, *Green Chem.* **2018**, *20*, 912.

[72] Y. Miao, F. Xie, J. Cen, F. Zhou, X. Tao, J. Luo, G. Han, X. Kong, X. Yang, J. Sun et al., *ACS Macro Lett.* **2018**, *7*, 693.

[73] Y.-K. Gong, L.-O. Liu, P. B. Messersmith, *Macromol. Biosci.* **2012**, *12*, 979.

[74] H. Wenker, *J. Am. Chem. Soc.* **1935**, *57*, 1079.

[75] W. S. H. Witte, *Liebigs Ann. Chem.* **1974**, *1974*, 996.

[76] K. Kempe, M. Lobert, R. Hoogenboom, U. S. Schubert, *J. Comb. Chem.* **2009**, *11*, 274.

[77] M. Beck, P. Birnbrich, U. Eicken, H. Fischer, W. E. Fristad, B. Hase, H.-J. Krause, *Angew. Makkromol. Chem.* **1994**, *223*, 217.

[78] H. P. C. Van Kuringen, J. Lenoir, E. Adriaens, J. Bender, B. G. De Geest, R. Hoogenboom, *Macromol. Biosci.* **2012**, *12*, 1114.

[79] A. S. Gubarev, B. D. Monnery, A. A. Lezov, O. Sedlacek, N. V. Tsvetkov, R. Hoogenboom, S. K. Filipov, *Polym. Chem.* **2018**, *9*, 2232.

[80] J. Chalmers, P. R. Griffiths, *Handbook of vibrational spectroscopy*, Wiley, **2001**.

[81] M. Hesse, H. Meier, B. Zeeh, *Spektroskopische Methoden in der organischen Chemie*. *pp 31-36*, Thieme, Stuttgart, **2005**.

[82] K. K. Kanazawa, J. G. Gordon, *Anal. Chim. Acta* **1985**, *175*, 99.

[83] B. K. M. Rodahl in *Proceedings of the International Solid-State Sensors and Actuators Conference - TRANSDUCERS '95*, IEEE, **1995**, pp. 743–746.

[84] J. T. O'Neal, E. Y. Dai, Y. Zhang, K. B. Clark, K. G. Wilcox, I. M. George, N. E. Ramasamy, D. Enriquez, P. Batys, M. Sammalkorpi, J. L. Lutkenhaus, *Langmuir* **2018**, *34*, 999.

[85] P. Schmode, A. Savva, R. Kahl, D. Ohayon, F. Meichsner, O. Dolynchuk, T. Thurn-Albrecht, S. Inal, M. Thelakkat, *Appl. Mater. & Interfaces* **2020**, *12*, 13029.

[86] G. Rudolph, A. Hermansson, A.-S. Jönsson, F. Lipnizki, *Sep. Purif. Technol.* **2021**, *254*, 117578.

[87] N. Parveen, J. P. Kumar, M. Schönhoff, *Polymers* **2019**, *11*.

[88] A. D. Easley, T. Ma,C. I. Eneh, Y. Jun, R. M. Thakur, J. L. Lutkenhaus, *J. Polym. Sci.* **2021**.

[89] M. D. Ward, D. A. Buttry, *Science* **1990**, *249*, 1000.

[90] F. R. Lack, G. W. Willard, I. E. Fair, *Bell Syst.Tech. J.* **1934**, *13*, 453.

[91] M. Rodahl, F. Höök, A. Krozer, P. Brzezinski, B. Kasemo, *Rev. Sci. Instrum.* **1995**, *66*, 3924.

[92] G. Sauerbrey, *Z. Phys.* **1959**, *155*, 206.

[93] Z. Parlak, C. Biet, S. Zauscher, *Meas. Sci. Technol.* **2013**, *24*, 85301.

[94] I. Reviakine, D. Johannsmann, R. P. Richter, *Anal. Chem. (ACS)* **2011**, *83*, 8838.

[95] M. Rodahl, F. Höök, C. Fredriksson, C. A. Keller, A. Krozer, P. Brzezinski, M. Voinova, B. Kasemo, *Faraday Discuss* **1997**, *107*, 229.

[96] M. D. Levi, N. Shpigel, S. Sigalov, V. Dargel, L. Daikhin, D. Aurbach, *Electrochim. Acta* **2017**, *232*, 271.

[97] M. V. Voinova, M. Rodahl, M. Jonson, B. Kasemo, *Phys. Scr.* **1999**, *59*, 391.

[98] S. Wang, F. Li, A. D. Easley, J. L. Lutkenhaus, *Nat. Mater.* **2019**, *18*, 69.

[99] N.-J. Cho, C. W. Frank, B. Kasemo, F. Höök, *Nat. Protoc.* **2010**, *5*, 1096.

[100] S. M. S. Schönwälder, F. Bally, L. Heinke, C. Azucena, Ö. D., *Biomacromolecules* **2014**, *15*, 2398.

[101] H. M. L. Lambermont-Thijs, M. W. M. Fijten, A. J. van der Linden, B. M. van Lankvelt, M. M. Bloksma, U. S. Schubert, R. Hoogenboom, *Macromolecules* **2011**, *44*, 4320.

[102] A. Levy, M. Litt, *J. Polym. Sci. A-1 Polym. Chem.* **1968**, *6*, 63.

[103] M. Ishihara, H. Togo, *Tetrahedron* **2007**, *63*, 1474.

[104] Kempe, K., Weber, C., Babiuch, K., Gottschaldt, M., Hoogenboom, R., U. S. Schubert, *Biomacromolecules* **2011**, *12*, 2591.

[105] C. Taubmann, R. Luxenhofer, S. Cesana, R. Jordan, *Macromol. Biosci.* **2005**, *5*, 603.

[106] R. D. Puts, D. Y. Sogah, *Tetrahedron Lett.* **1994**, *35*, 5779.

[107] D. C. Palmer, *Oxazoles: Synthesis, Reactions, and Spectroscopy*. *Part B*, Wiley, Hoboken N.J., **2003-2004**.

[108] T. G. Gant, A. I. Meyers, *Tetrahedron* **1994**, *50*, 2297 - 2260.

[109] Z. Hell, A. Cwik, Z. Finte, Z. Horváth, *J. Mil. Catal. A (Chem.)* **2002**, *184*, 191.

[110] A. Cwik, Z. Hell, A. Hegedüs, Z. Finta, Z. Horváth, *Tetrahedron Lett.* **2002**, *43*, 3985.

[111] H. Lundberg, F. Tinnis, H. Adofsson, *Synlett* **2012**, *23*, 2201.

[112] A. Butler, C. D. Davies, M. C. Elliot, N. M. Galea, M. S. Long, D. J. Willock, J. L. Wood, *Eur. J. Org. Chem.* **2005**, *17*, 3791.

[113] W. H. Binder, H. Gruber, *Macromol. Chem. Phys.* **2000**, *201*, 949.

[114] Y.-Q. Cao, Z. Zhang, Y.-X. Guo, *J. Chem. Technol. Biotechnol.* **2008**, *83*, 1441.

[115] R. Ding, Y. Liu, M. Han, W. Jiao, J. Li, H. Tian, B. Sun, *J. Org. Chem.* **2018**, *83*, 12939.

[116] D. Cartigny, A. D. Santos, L. El Kaim, L. Grimaud, R. Jacquot, P. Marion, *Synthesis* **2014**, *46*, 1802.

[117] L. Vanoye, A. Hammoud, H. Gérard, A. Barnes, R. Phillippe, P. Fongarland, C. de Bellefon, A. Favre-Réguillon, *ACS Catal.* **2019**, *9*, 9705.

[118] N. P. Ramires, B. König, J. C. Gonzalez-Gomez, *Org. Lett.* **2019**, *21*, 1368.

[119] W. S. H. Witte, *Angew. Chem. Int. Ed.* **1972**, *11*, 287.

[120] S. C. Daubner, T. Le, S. Wang, *Arch. Biochem. Biophys.* **2011**, *508*, 1.

[121] M. Hartlieb, D. Pretzel, K. Kempe, C. Fritzsche, R. M. Paulus, M. Gottschaldt, U. S. Schubert, *Soft Matter* **2013**, *9*, 4693.

[122] N. Lüdecke, S. M. Weidner, H. Schlaad, *Macromol. Rapid Commun.* **2020**, *41*, e1900404.

[123] B. Verbraeken, K. Lava, R. Hoogenboom, *in Encyclopedia of Polymer Science and Technology*, 1.

[124] B. Brissault, C. Guis, H. Cheradame, *Europ. Polym. J.* **2002**, *38*, 219.

[125] B. D. Monnery, S. Shaunak, M. Thanou, J. H. G. Steinke, *Macromolecules* **2015**, *48*, 3197.

[126] H. I. T. Saegusa, *Macromolecules* **1973**, *6*, 808.

[127] M. Litt, A. Levy, J. Herz, *J. Macromol. Sci. A* **1975**, *9*, 703.

[128] O. Nuyken, G. Maier, A. Groß, H. Fischer, *Macromol. Chem. Phys.* **1996**, *197*, 83.

[129] R. Hoogenboom, M. W. M. Fijten, R. M. Paulus, H. M. L. Thijs, S. Hoeppener, G. Kickelbick, U. S. Schubert, *Polymer* **2006**, *47*, 75.

[130] F. Wiesbrock, R. Hoogenboom, M. A. M. Leenen, M. A. R. Meier, U. S. Schubert, *Macromolecules* **2005**, *38*, 5025.

[131] R. T. Lundquist A. Ruby, *Appl. Spectrosc.* **1966**, *20*, 258.

[132] W. T. W. Seeliger, *Liebigs Ann. Chem.* **1966**, *698*, 158.

[133] V. Percec, M. N. Holerca, S. Uchida, D. J. P. Yeardley, G. Ungar, *Biomacromolecules* **2001**, *2*, 729.

[134] D. C. Schriemer, L. Li, *Anal. Chem.* **1997**, *69*, 4176.

[135] D. C. Schriemer, L. Li, *Anal. Chem.* **1997**, *69*, 4169.

[136] J. H. Waite, *J. Exp. Bio.* **2017**, *220*, 517.

[137] T. T. Chiu, B. P. Thill, W. J. Fairchok in *Adv. in Chem.*, pp. 425–433.

[138] J. E. Glass (Ed.) *Advances in Chemistry*, American Chemical Society, Washington, DC, **1986**.

[139] G. R. Fulmer, A. J. M. Miller,N. H. Sherden, H. E. Gottlieb, A. Nudelman,B. M. Stoltz, J. E. Bercaw, K. I. Goldberg, *Organometallics* **2010**, *29*, 2176.

[140] L. Chen, L. Zhang, G. Yan, D. Huang, *Asian J. Org. Chem.* **2020**, *9*, 842.

[141] B. D. Monnery,V. V. Jerca, O. Sedlacek, B. Verbraeken, R. Cavill, R. Hoogenboom, *Angew. Chem. Int. Ed.* **2018**, *57*, 15400.

[142]B. D. Monnery, S. Shaunak, M. Thanou, J. H. G. Steinke, *Macromolecules* **2015**, *48*, 3197.

[143]E. H. Vickery, L. F. Pahler, E. J. Eisenbraun, *J. Org. Chem.* **1979**, *44*, 4444.

[144]M. G. J. Asghari, *SSP* **2003**, *90-91*, 3.

[145]D. Sang, X. Tu, J. Tian, Z. He, M. Yao, *ChemistrySelect* **2018**, *3*, 10103.

[146]D. Sang, J. Wang, Y. Zheng, J. He, C. Yuan, Q. An, J. Tian, *Synthesis* **2017**, *49*, 2721.

[147]R. C. Paul, B. R. Sreenathan, S. L. Chadha, *J. inorg. nucl. Chem.* **1966**, *28*, 1225.

[148]M.-L. Bauder, *Bachelor Thesis, University Potsdam* **2021**.

[149]M. Albrecht, M. Napp, M. Schneider, *Synthesis* **2001**, *2001*, 468.

[150]R. Morales-Cerrada, S. Molina-Gutierrez, P. Lacroix-Desmazes, S. Caillol, *Biomacromolecules* **2021**, *22*, 3625.

[151]V. Gevorgyan, M. Rubi, S. Benson, J. Liu, Y. Yamamoto, *J. Org. Chem.* **2000**, *65*, 6179.

[152]J. H. Jeong, S. H. Song,D. W. Lim, H. Lee, T. G. Park, *J. Control. Release* **2001**, *73*, 391.

[153]R. Tanaka, I. Ueoka, Y. Takaki, K. Kataoka, S. Saito, *Macromolecules* **1983**, *16*, 849.

[154]T. Saegusa, S. Kobayashi, A. Yamada, *Macromolecules* **1975**, *8*, 390.

[155]H. M. Lambermont-Thijs, F. S. van der Woerdt, A. Baumgaertel, L. Bonami, F. E. Du Prez, U. S. Schubert, R Hoogenboom, *Macromolecules* **2010**, *43*, 927.

[156]A. Beer, *Ann. Phys. u. Chem.* **1852**, 78.

[157]H. G. Silverman, F. F. Roberto, *Mar. Biotechnol.* **2007**, *9*, 661.

[158]K. Zhan, H. Ejima, N. Yoshie, *ACS Sustain. Chem. Eng.* **2016**, *4*, 3857.

[159]D. N. Simavilla, W. Huang, P. Vandestrick, J.-P. Ryckaert, M. Sferrazza, S. Napolitano, *ACS Macro Lett.* **2017**, *6*, 975.

[160]R. P. L. Largitte, *Chem. Eng. Res.Des.* **2016**, *109*, 495.

[161]T. Tadros, *Encyclopedia of Colloid and Interface Science*, Springer Berlin Heidelberg, Berlin, Heidelberg, **2013**.

[162]N. Patil, C. Falentin-Daudré, C. Jérôme, C. Detrembleur, *Polym. Chem.* **2015**, *6*, 2919.

[163]Q .Wei, K. Achazi, H. Liebe, A. Schulz, P.-L. M. Noeske, I. Grunwald, R. Haag, *Angew. Chem. Int. Ed.* **2014**, *53*, 11650.

[164] Q. Wei, T. Becherer, R.-C. Mutihac, P.-L. M. Noeske, F. Paulus, R. Haag, I. Grunwald, *Biomacromolecules* **2014**, *15*, 3061.

[165] L. Yu, C. Cheng, Q. Ran, C. Schlaich, P.-L. M. Noeske, W. Li, Q. Wei, R. Haag, *ACS Appl. Mater. interfaces* **2017**, *9*, 6624.

[166] M. Fixman, *J. Chem. Phys.* **1962**, *36*, 306.

[167] F. Zhang, M. Sababi, T. Brinck, D. Persson, J. Pan, P. M. Claesson, *J. Colloid Interface Sci.* **2013**, *404*, 62.

[168] J. L. Harding, M. M. Reynolds, *Trends Biotechnol.* **2014**, *32*, 140.

[169] I. Banerjee, R. C. Pangule, R. S. Kane, *Adv. Mater.* **2011**, *23*, 690.

[170] C. V. Bonduelle, W. M. Lau, E. R. Gillies, *ACS Appl. Mater. interfaces* **2011**, *3*, 1740.

[171] R. Konradi, B. Pidhatika, A. Mühlebach, M. Textor, *Langmuir* **2008**, *24*, 613.

[172] J. Zhong, H. Ji, J. Duan, H. Tu, A. Zhang, *Colloids Surf. B* **2016**, *140*, 254.

[173] S. I. Jeon , J. H. Lee , J. D. Andrade , P. G. De Gennes, *J. Colloid Interface Sci.* **1991**, *142*, 149.

[174] R. Kun, M. Szekeres, I. Dékány, *J. Therm. Anal. Calorim.* **2009**, *96*, 1009.

[175] O. Sedlacek, B. D. Monnery, S. K. Filippov, R. Hoogenboom, M. Hruby, *Macromol. Rapid Commun.* **2012**, *33*, 1648.

[176] C. E. Hoyle, C. N. Bowman, *Angew. Chem. Int. Ed.* **2010**, *49*, 1540.

[177] J. L. Vicario, D. Badía, L. Carrillo, J. Etxebarria, E. Reyes, N. Ruiz, *Org. Prep. Proced. Int.* **2005**, *37*, 513.

[178] M. Nigam, B. Rush, J. Patel, R. Castillo, P. Dhar, *J. Chem. Educ.* **2016**, *93*, 753.

[179] H. S. N. Lüdecke, *Polym. Chem.* **2021**, *12*, 5310.

[180] M. N. Holerca, V. Percec, *Eur. J. Org. Chem.* **2000**, *2000*, 2257.

[181] A. Beutler, C. D. Davies, M. C. Elliott, N. M. Galea, M. S. Long, D. J. Willock, J. L. Wood, *Eur. J. Org. Chem.* **2005**, *2005*, 3791.

# 8 Appendix

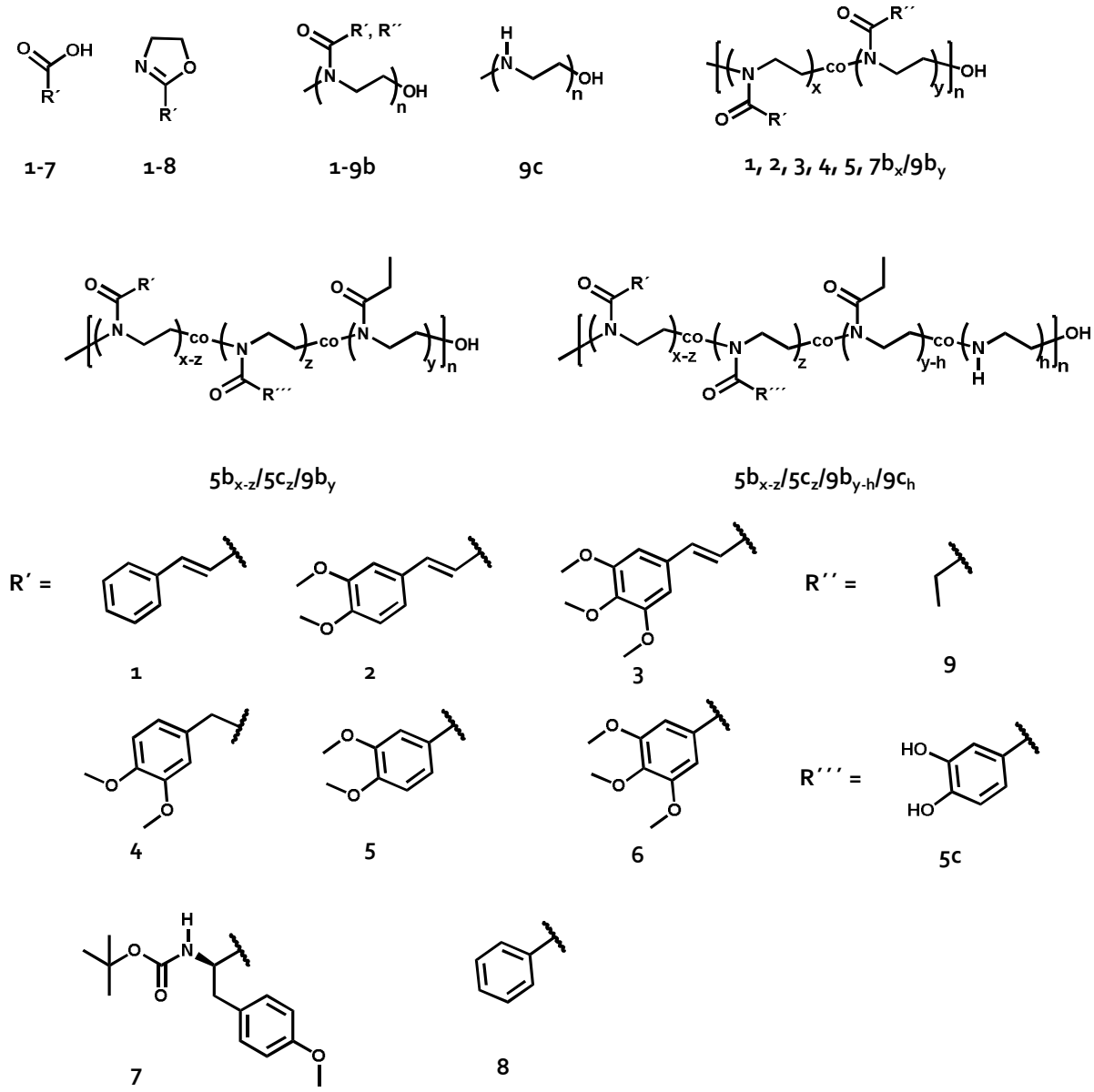


*Figure S 1: Overview of the developed nomenclature of the molecules, synthesized and used in this work.*

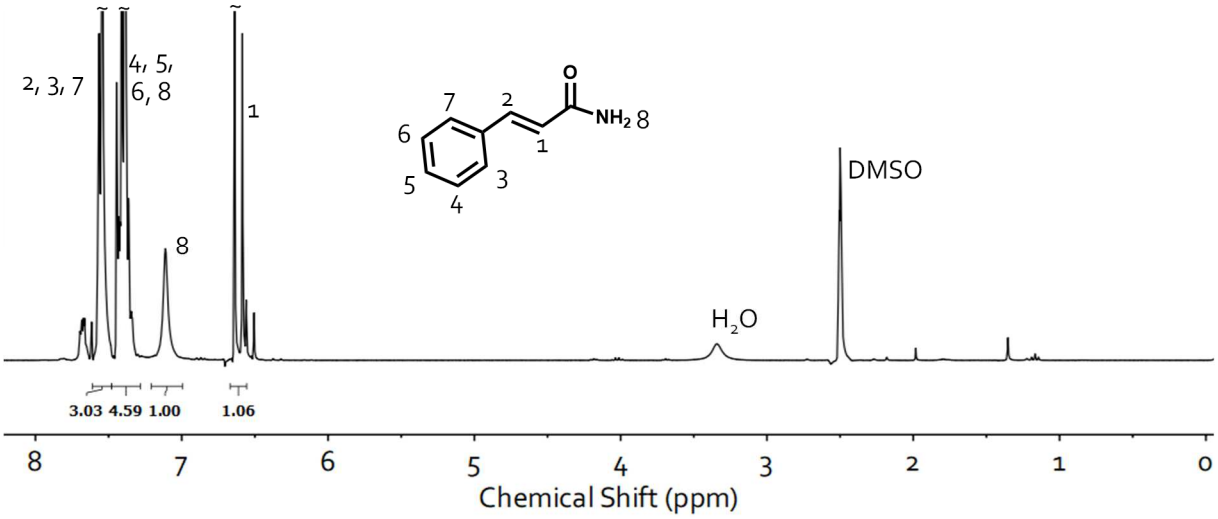


*Figure S 2: $^1$H-NMR (300 MHz) of cinnamyl amide in DMSO-$d_6$.*

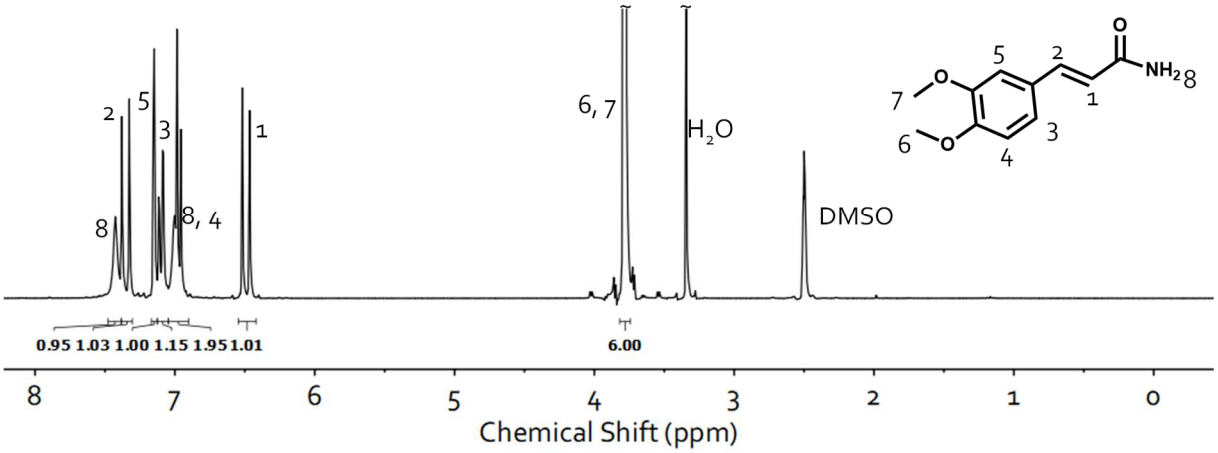


*Figure S 3: $^1$H-NMR (300 MHz) of 3,4-dimethoxycinnamyl amide in DMSO-$d_6$.*

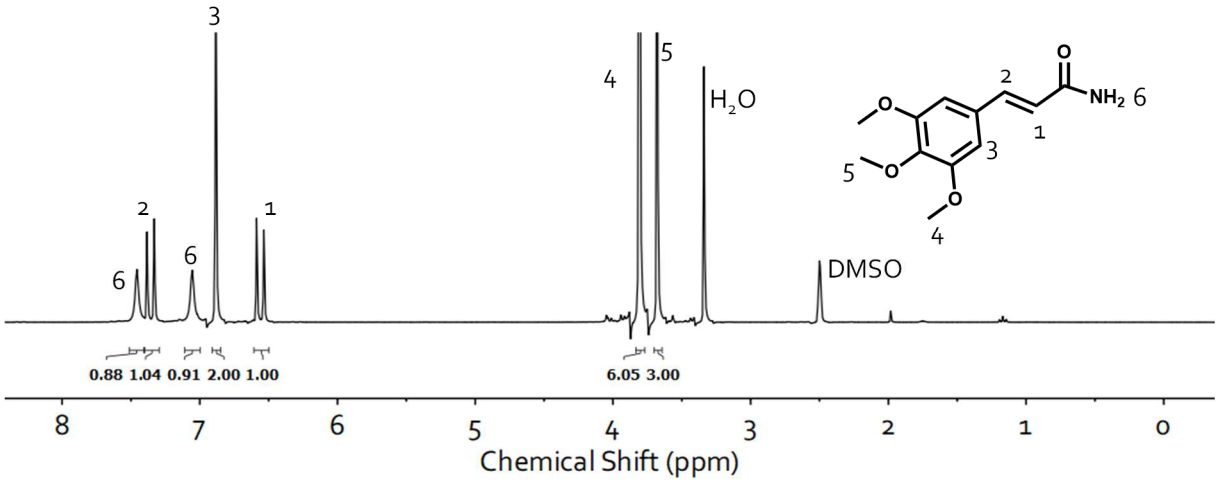


*Figure S 4: $^{1}$H-NMR (300 MHz) of 3,4,5-trimethoxycinnamyl amide in DMSO-$d_6$.*

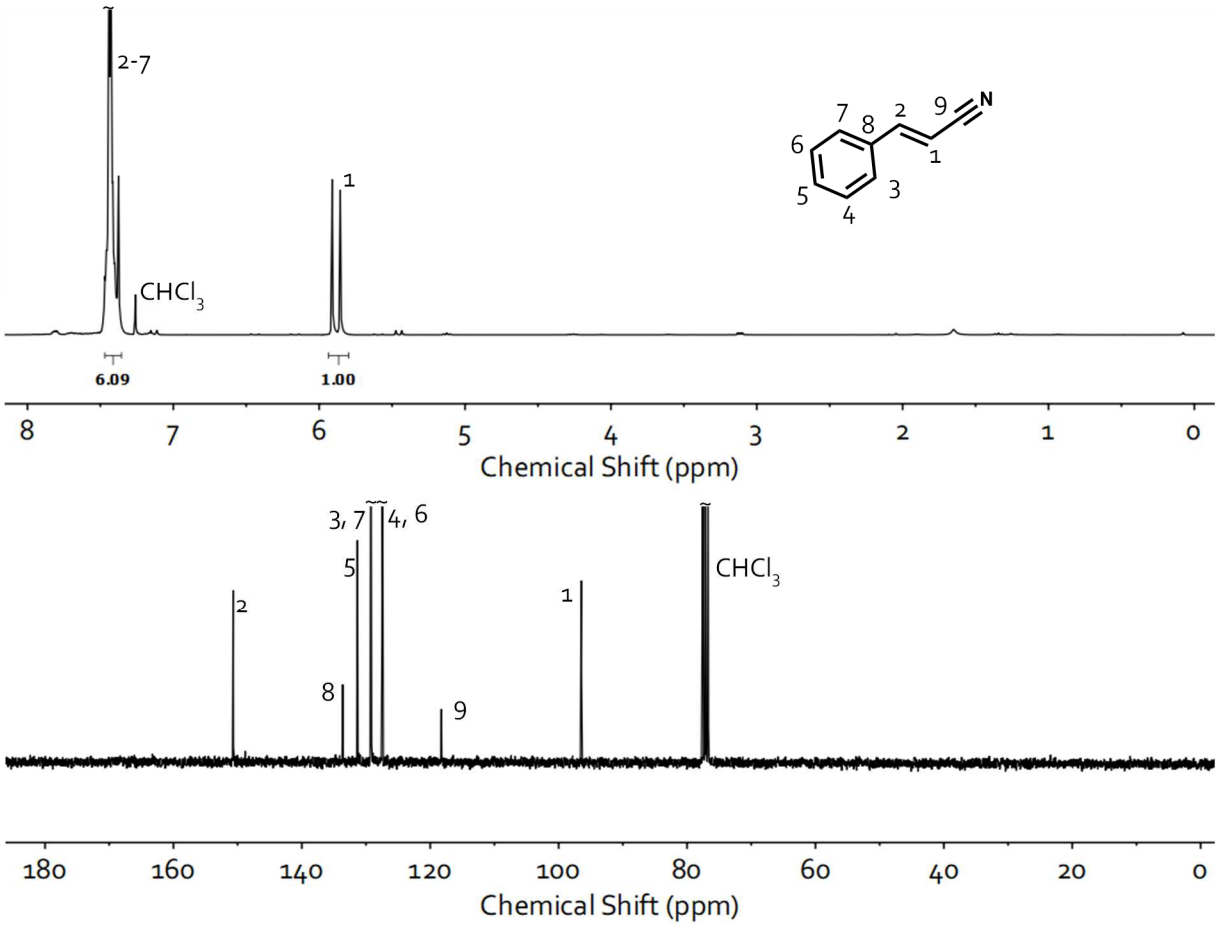


*Figure S 5: $^{1}$H- and $^{13}$C-NMR (300 MHz) of cinnamyl nitrile in $CDCl_3$.*

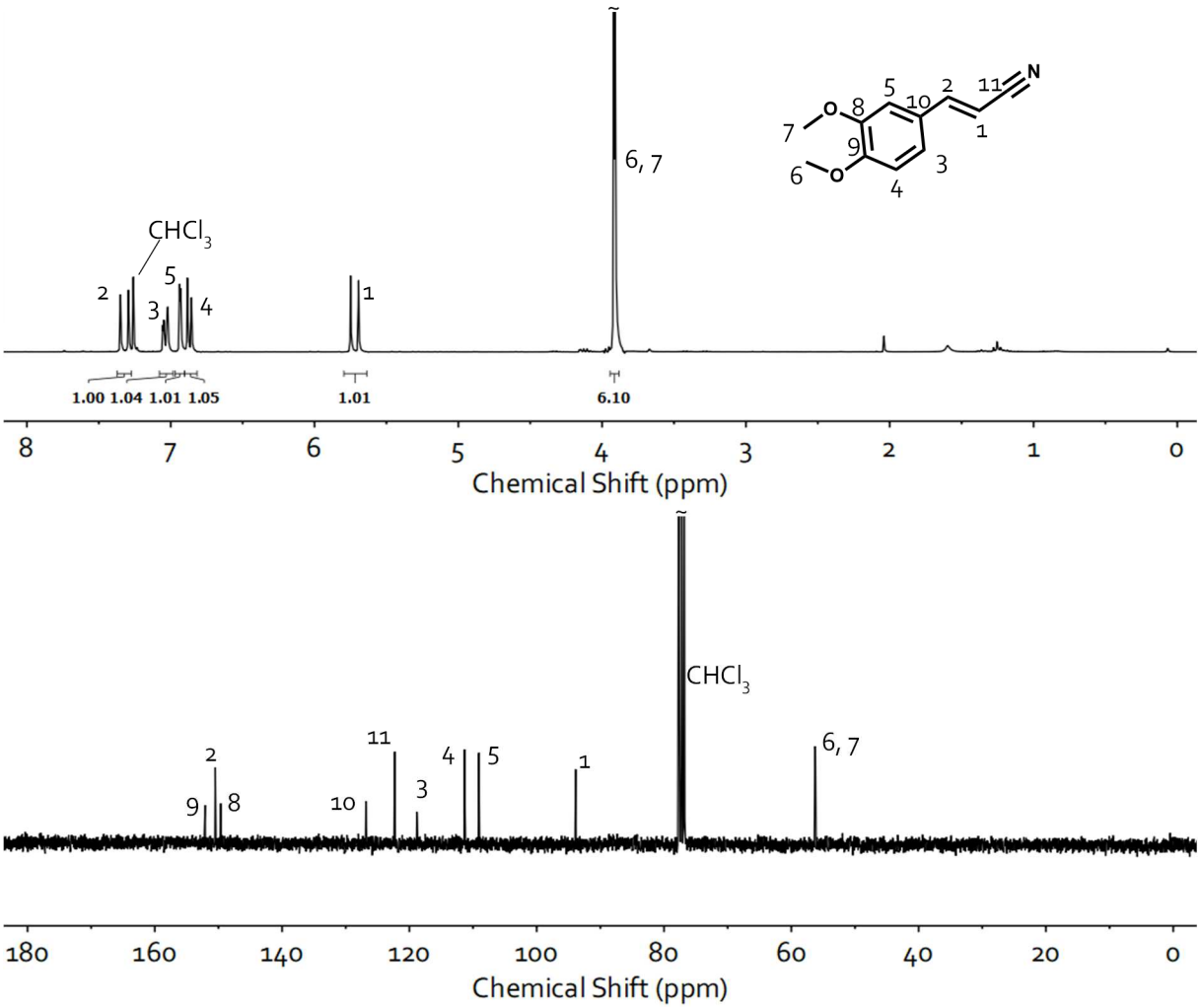


*Figure S 6: $^{1}H$- and $^{13}C$-NMR (300 MHz) of dimethoxy cinnamyl nitrile in $CDCl_3$.*

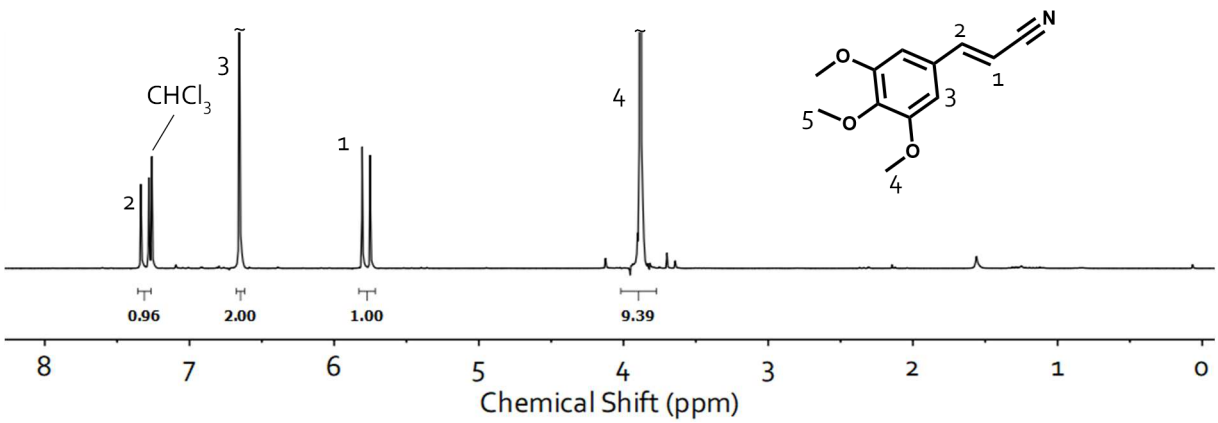


*Figure S 7: $^1$H-NMR (300 MHz) of trimethoxy cinnamyl nitrile in $CDCl_3$.*

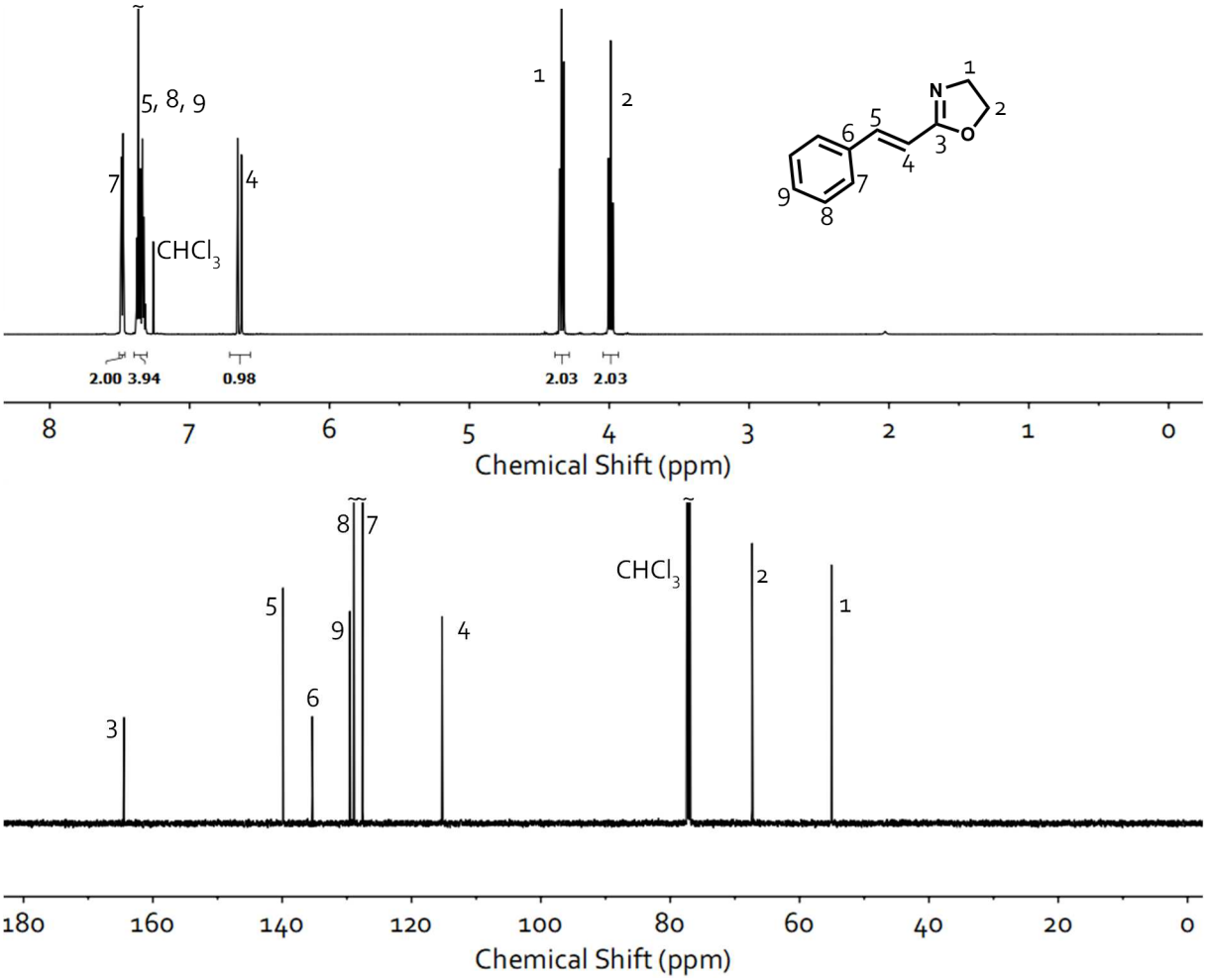


*Figure S 8: [1]H- and [13]C-NMR (500 MHz) of **1a** in $CDCl_3$.*

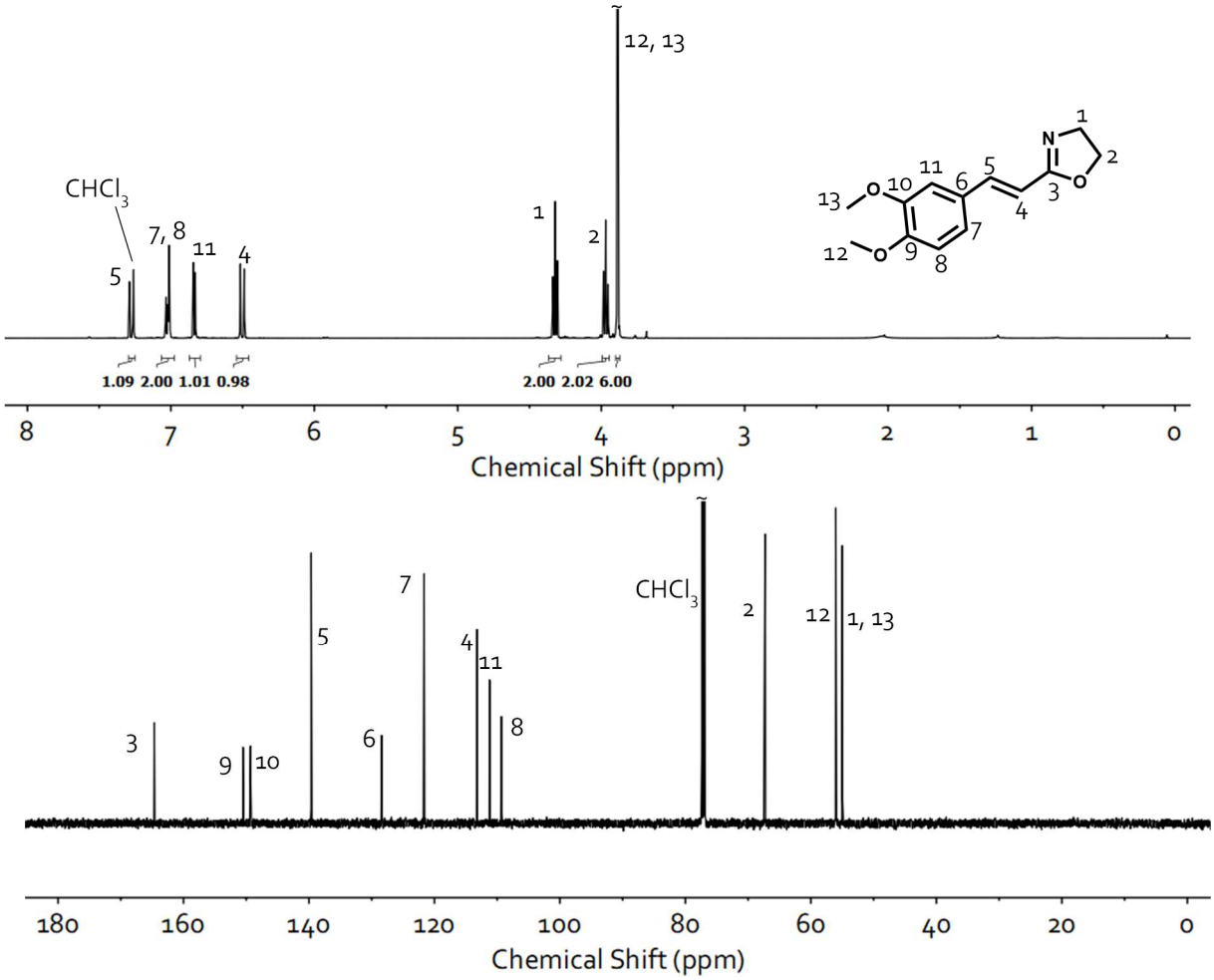


*Figure S 9: $^{1}H$- and $^{13}C$-NMR (500 MHz) of **2a** in $CDCl_3$.*

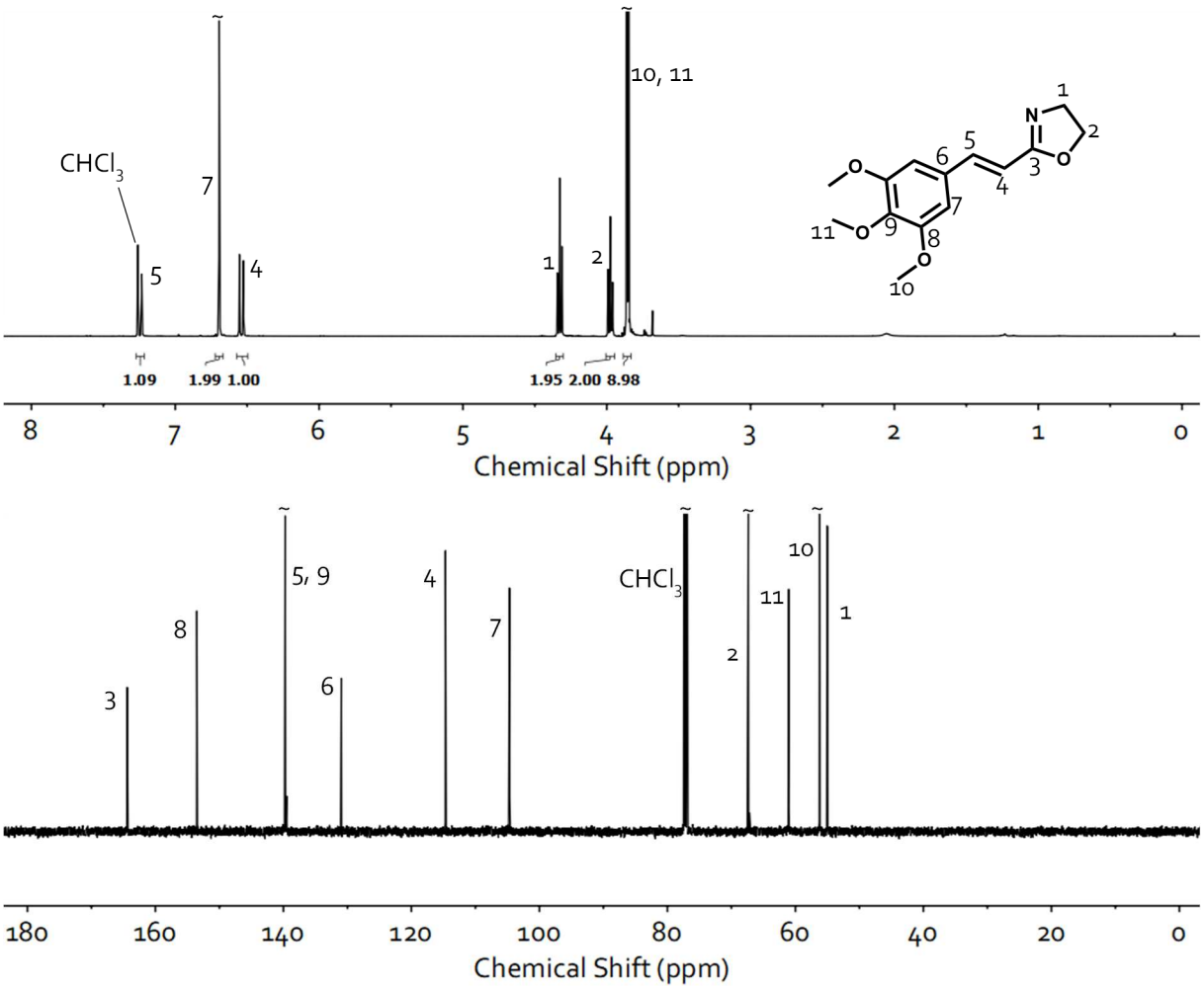


*Figure S 10: $^{1}$H- and $^{13}$C-NMR (500 MHz) of **3a** in $CDCl_3$.*

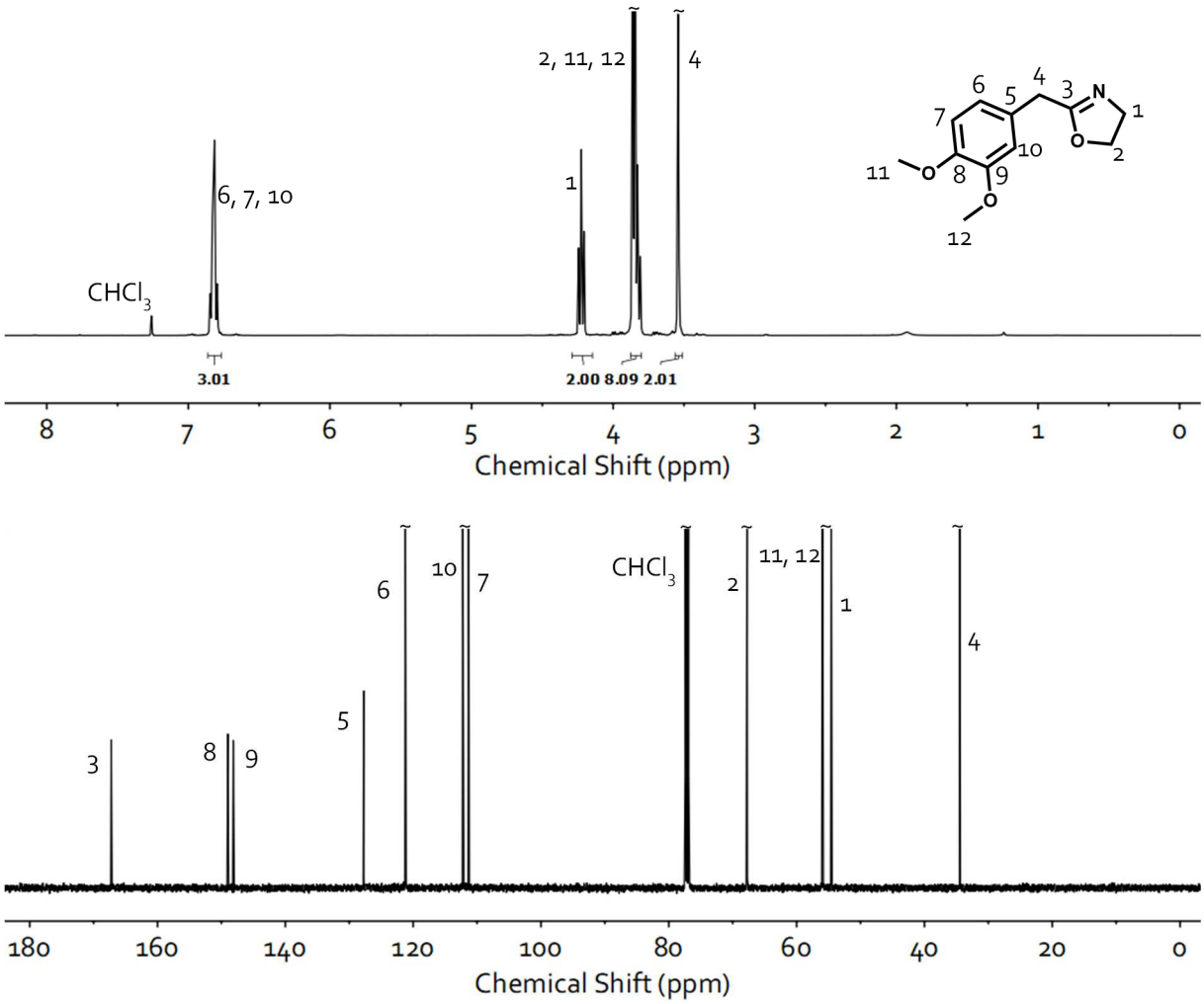


*Figure S 11: $^{1}$H- and $^{13}$C-NMR (500 MHz) of **4a** in $CDCl_3$.*

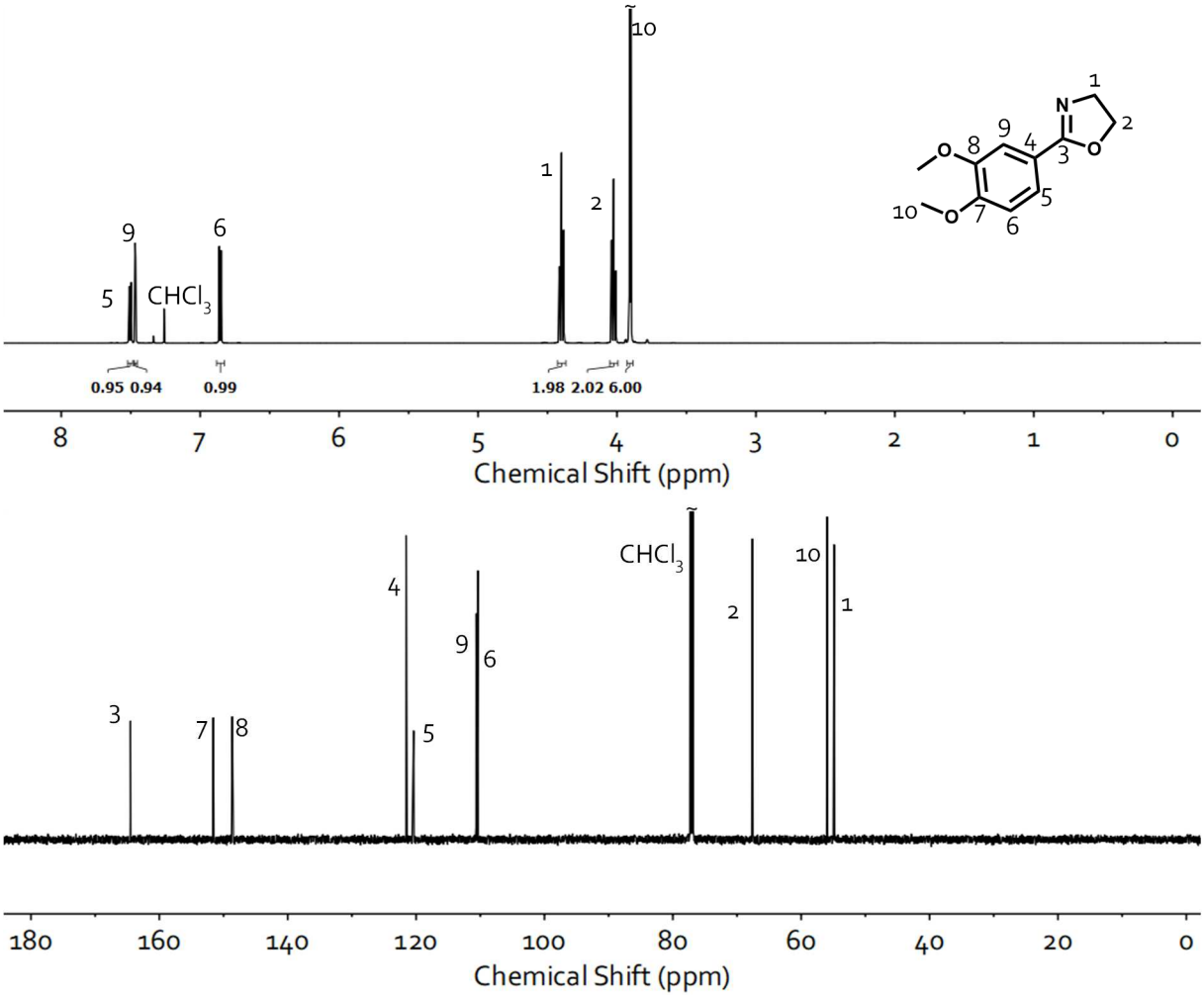


*Figure S 12: $^{1}$H- and $^{13}$C-NMR (500 MHz) of **5a** in $CDCl_3$.*

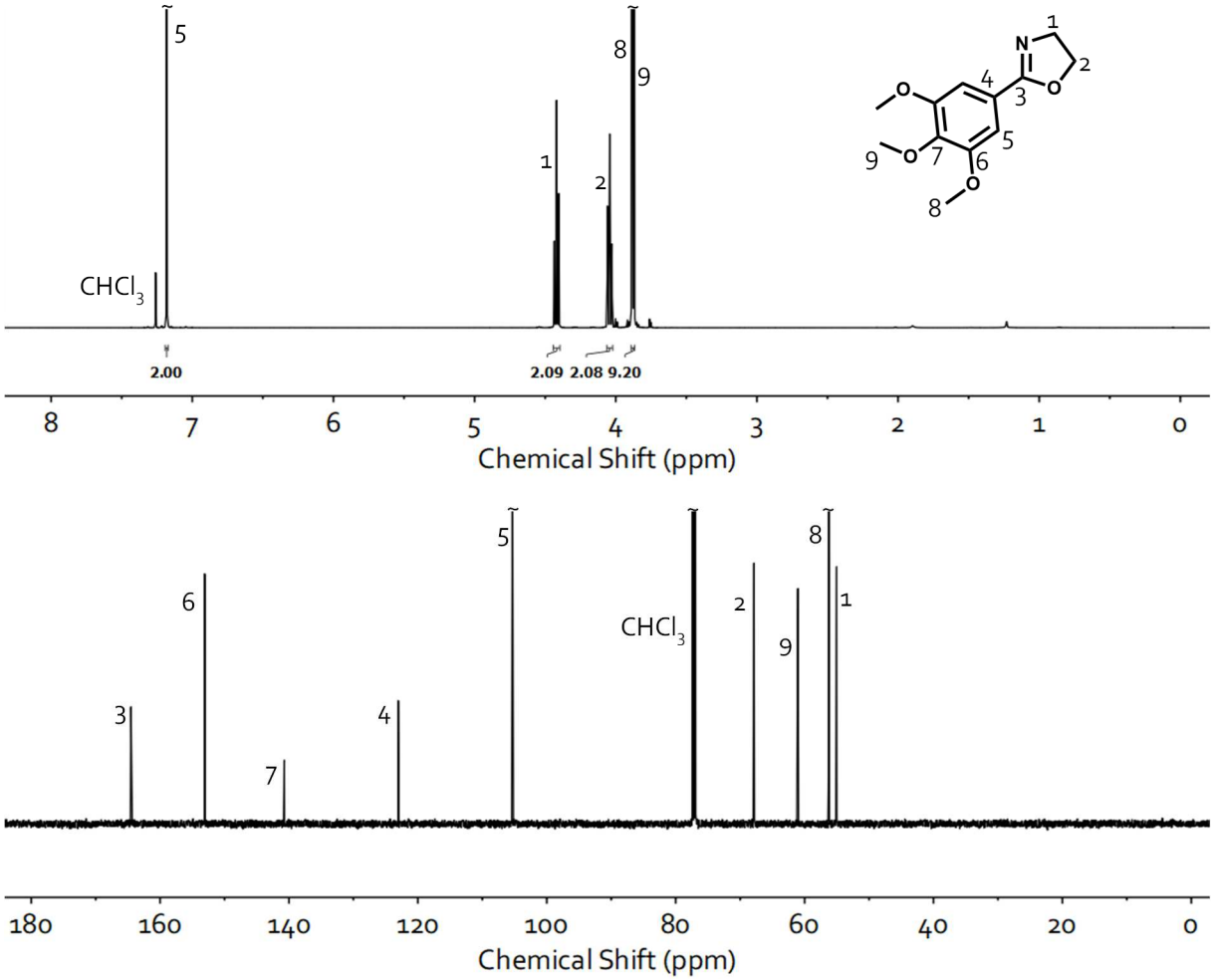


*Figure S 13: $^{1}H$- and $^{13}C$-NMR (500 MHz) of **6a** in $CDCl_3$.*

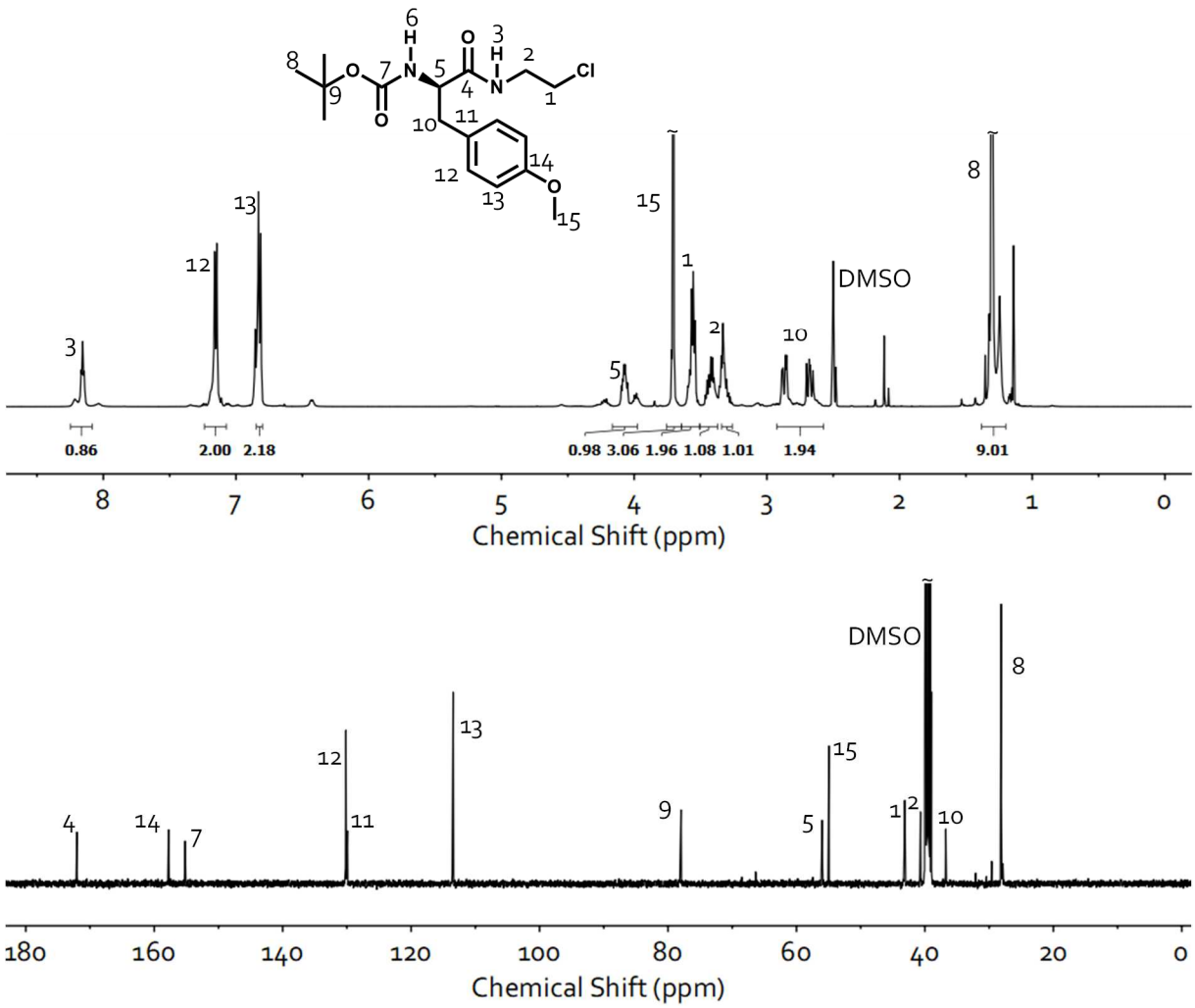


*Figure S 14: $^{1}$H- and $^{13}$C-NMR (500 MHz) of N-tert-Butoxycarbonyl-(2-chloroethyl)amino)-3-(4-methoxy-L-tyrosin) in DMSO-$d_6$.*

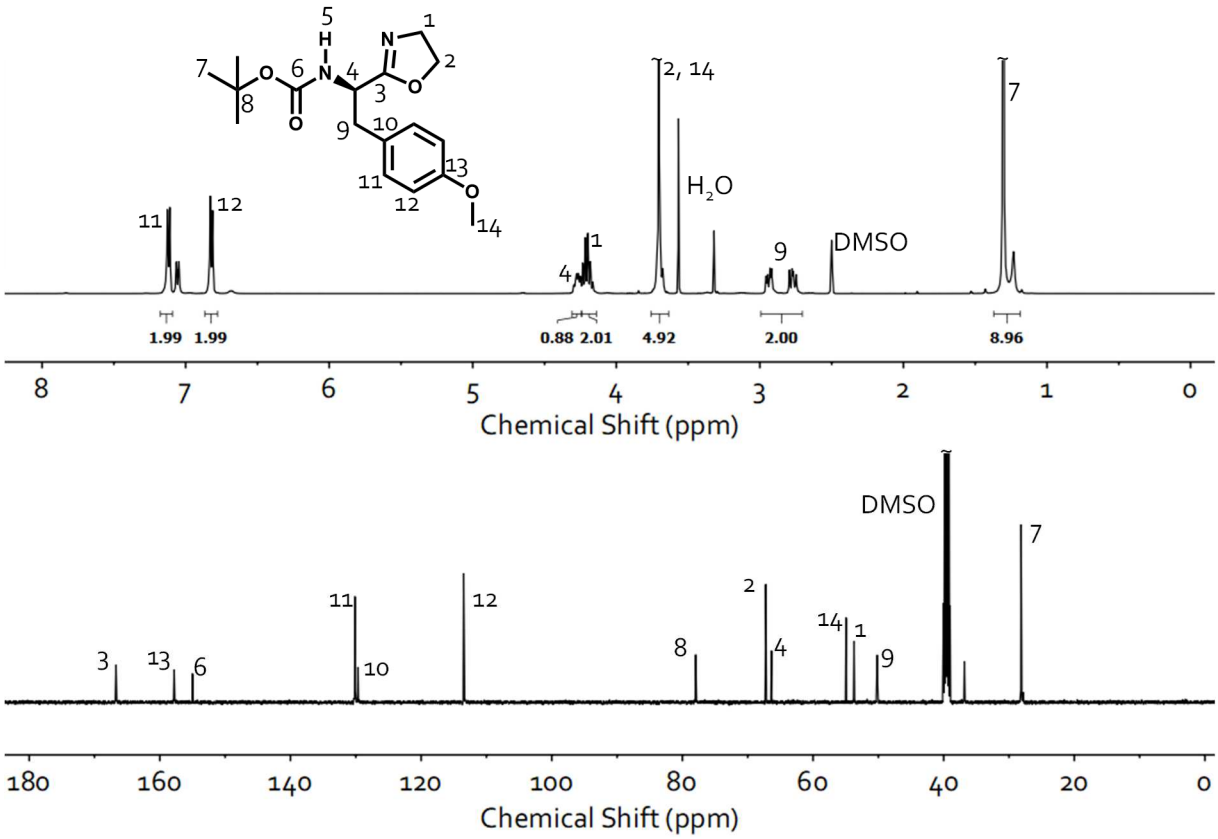


*Figure S 15: $^{1}$H- and $^{13}$C-NMR (500 MHz) of **7a** in DMSO-$d_6$.*

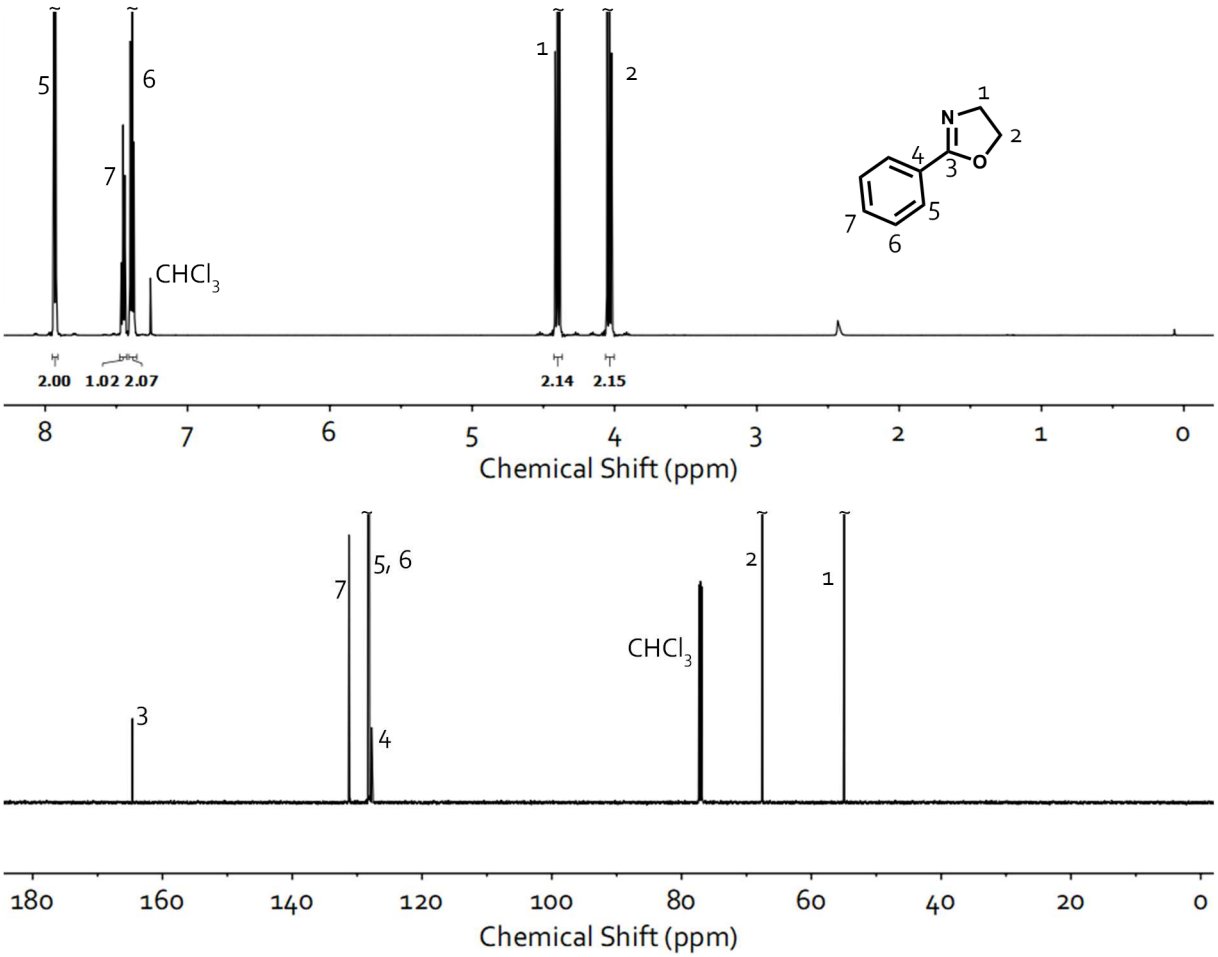


*Figure S 16: $^{1}$H- and $^{13}$C-NMR (500 MHz) of **8a** in $CDCl_3$.*

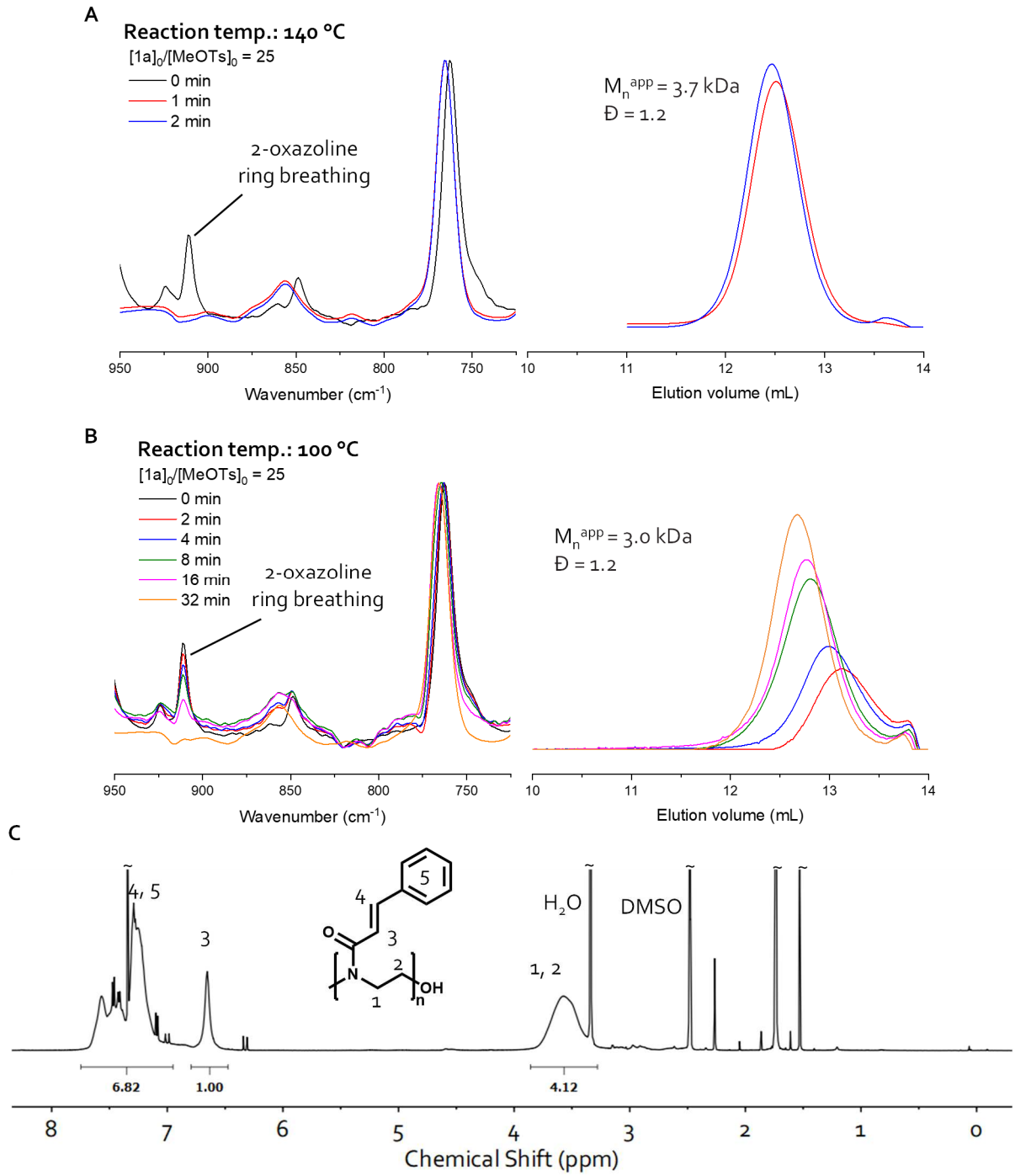


*Figure S 17: FT-IR kinetic graphs and relating SEC-RI-traces in NMP of the microwave-assisted CROP for two reaction temperatures (100 °C, A; 140 °C B) of the homopolymerization from* ***1a*** *to* ***1b****. C) The homopolymer* ***1b*** *$^1$H-NMR spectrum (300 MHz) in DMSO-$d_6$.*

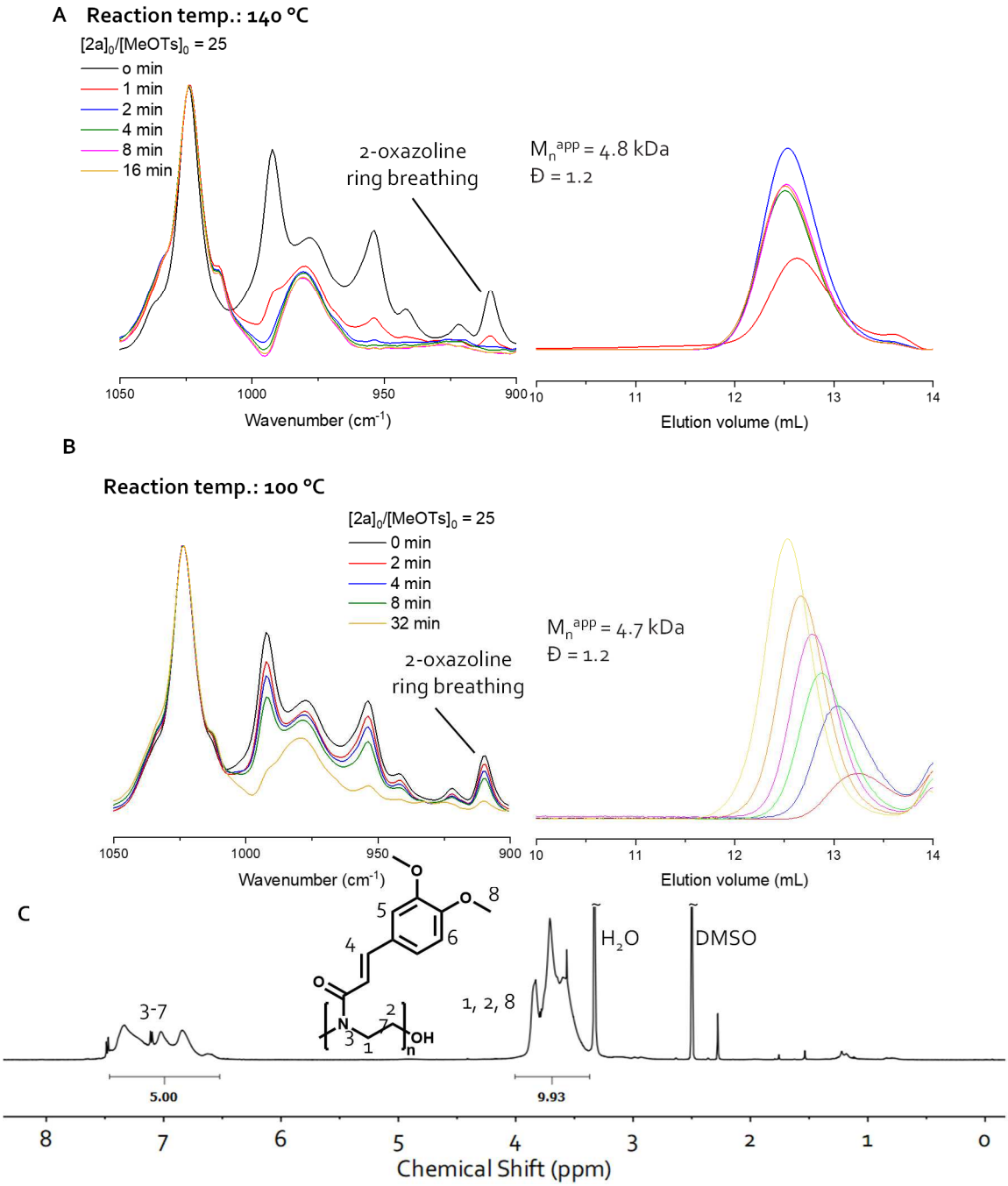


*Figure S 18: FT-IR kinetic graphs and relating SEC-RI-traces in NMP of the microwave-assisted CROP for two reaction temperatures (100 °C, A; 140 °C B) of the homopolymerization from **2a** to **2b**. C) The homopolymer **2b** $^1$H-NMR spectrum (300 MHz) in DMSO-$d_6$.*

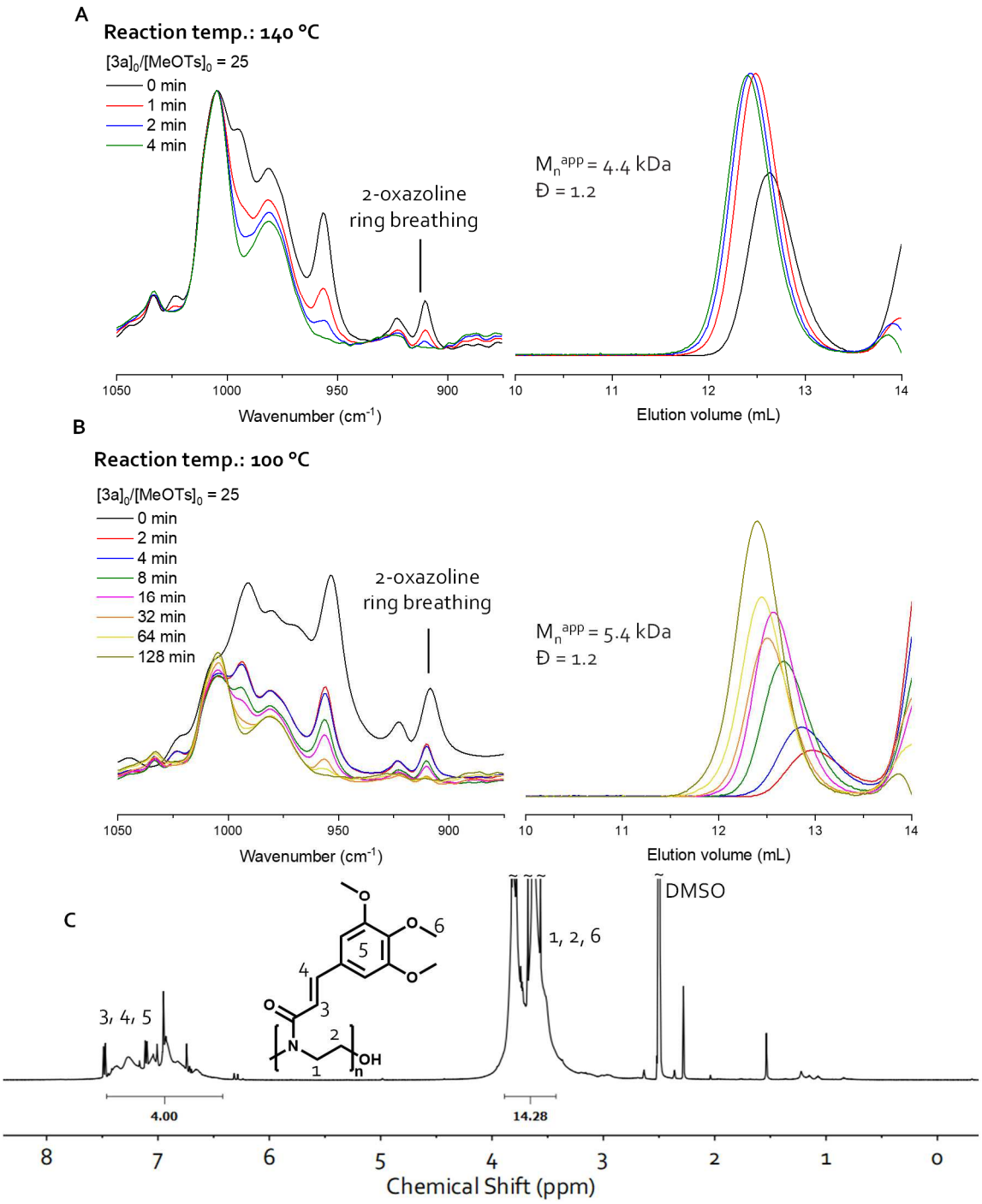


*Figure S 19: FT-IR kinetic graphs and relating SEC-RI-traces in NMP of the microwave-assisted CROP for two reaction temperatures (100 °C, A; 140 °C B) of the homopolymerization from **3a** to **3b**. C) The homopolymer **3b** $^1$H-NMR spectrum (300 MHz) in DMSO-$d_6$.*

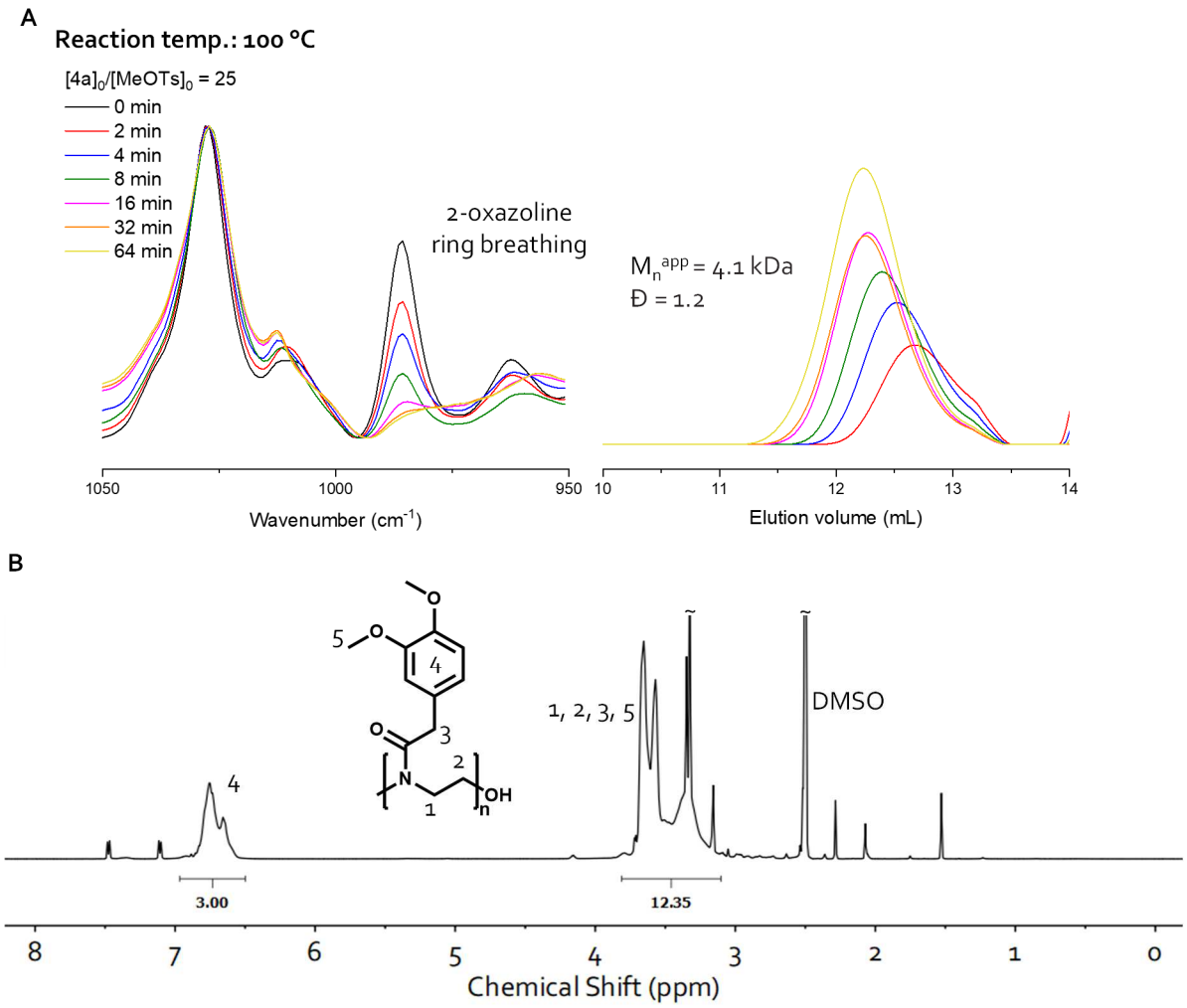


*Figure S 20: FT-IR kinetic graphs and relating SEC-RI-traces in NMP of the microwave-assisted CROP for the reaction temperature 100 °C (A) of the homopolymerization from* ***4a*** *to* ***4b****. B) The homopolymer* ***4b*** *$^1$H-NMR spectrum (300 MHz) in DMSO-$d_6$.*

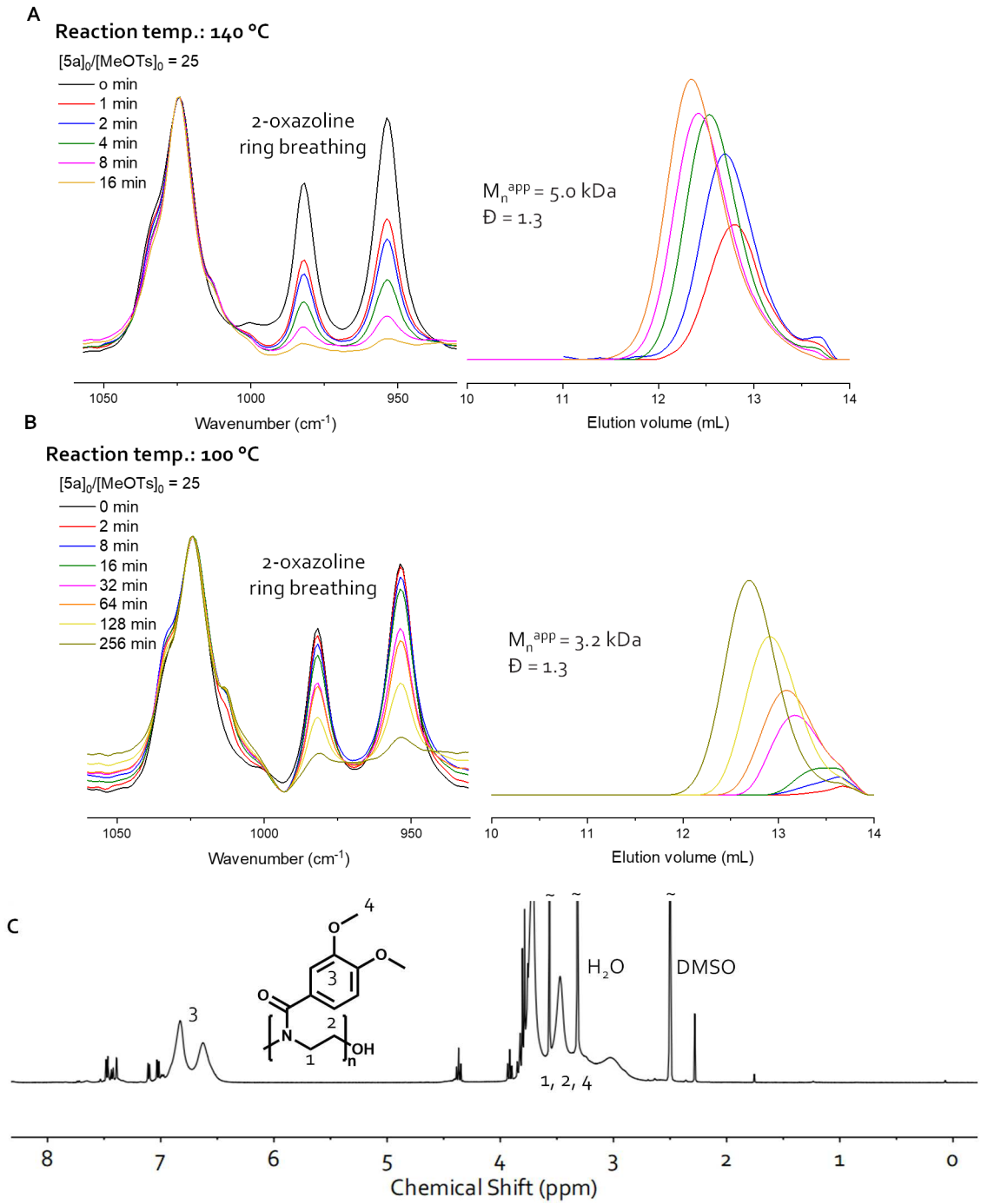


*Figure S 21: FT-IR kinetic graphs and relating SEC-RI-traces in NMP of the microwave-assisted CROP for two reaction temperatures (100 °C, A; 140 °C B) of the homopolymerization from **5a** to **5b**. C) The homopolymer **5b** $^1$H-NMR spectrum (300 MHz) in DMSO-$d_6$.*

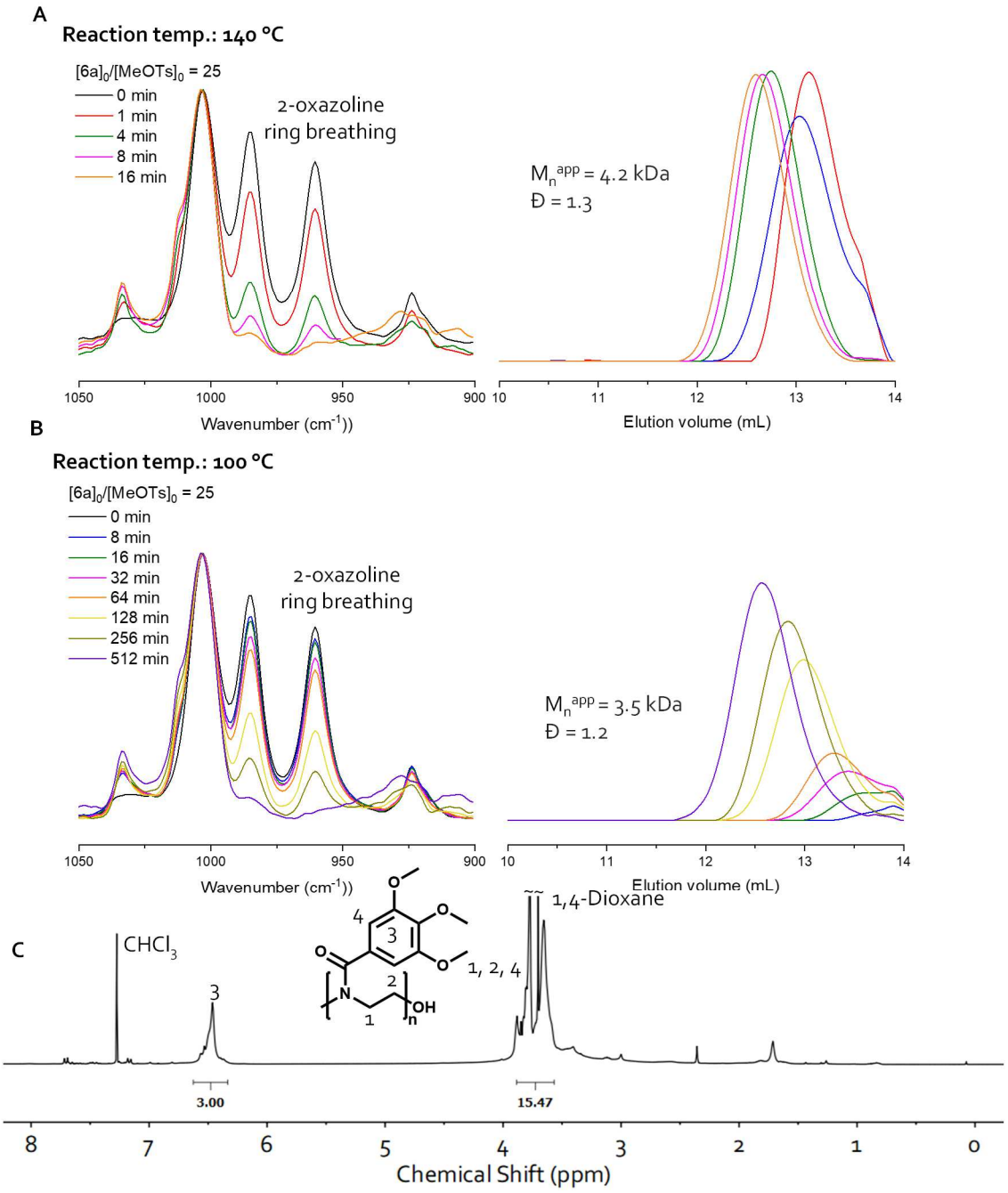


*Figure S 22: FT-IR kinetic graphs and relating SEC-RI-traces in NMP of the microwave-assisted CROP for two reaction temperatures (100 °C, A; 140 °C B) of the homopolymerization from **6a** to **6b**. C) The homopolymer **6b** $^1$H-NMR spectrum (300 MHz) in $CDCl_3$.*

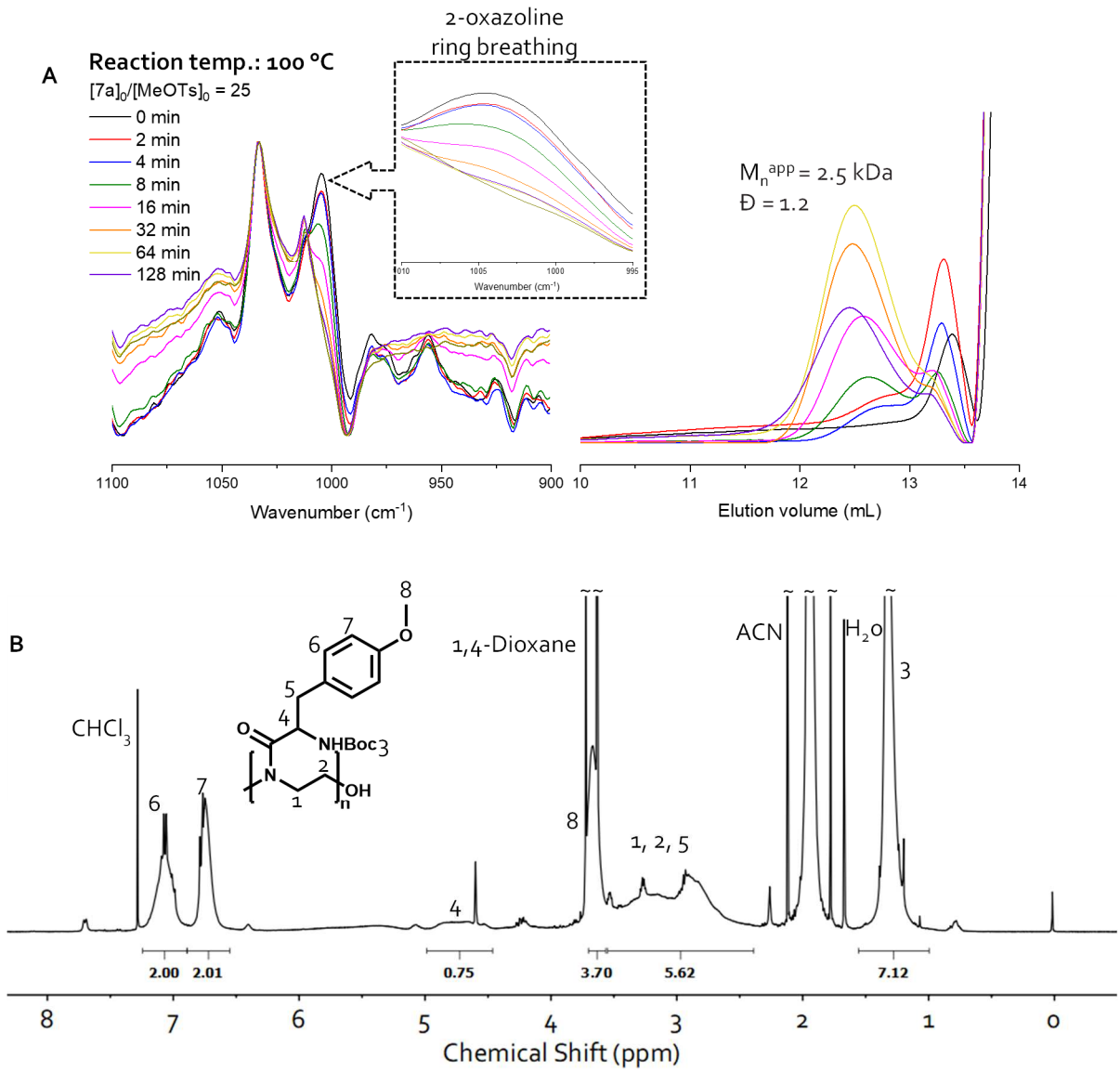


*Figure S 23: A) FT-IR kinetic graphs and relating SEC-RI-traces in NMP of the microwave-assisted CROP for the reaction temperature 100 °C of the homopolymerization from **7a** to **7b**. B) The homopolymer **7b** $^1$H-NMR spectrum (300 MHz) in $CDCl_3$.*

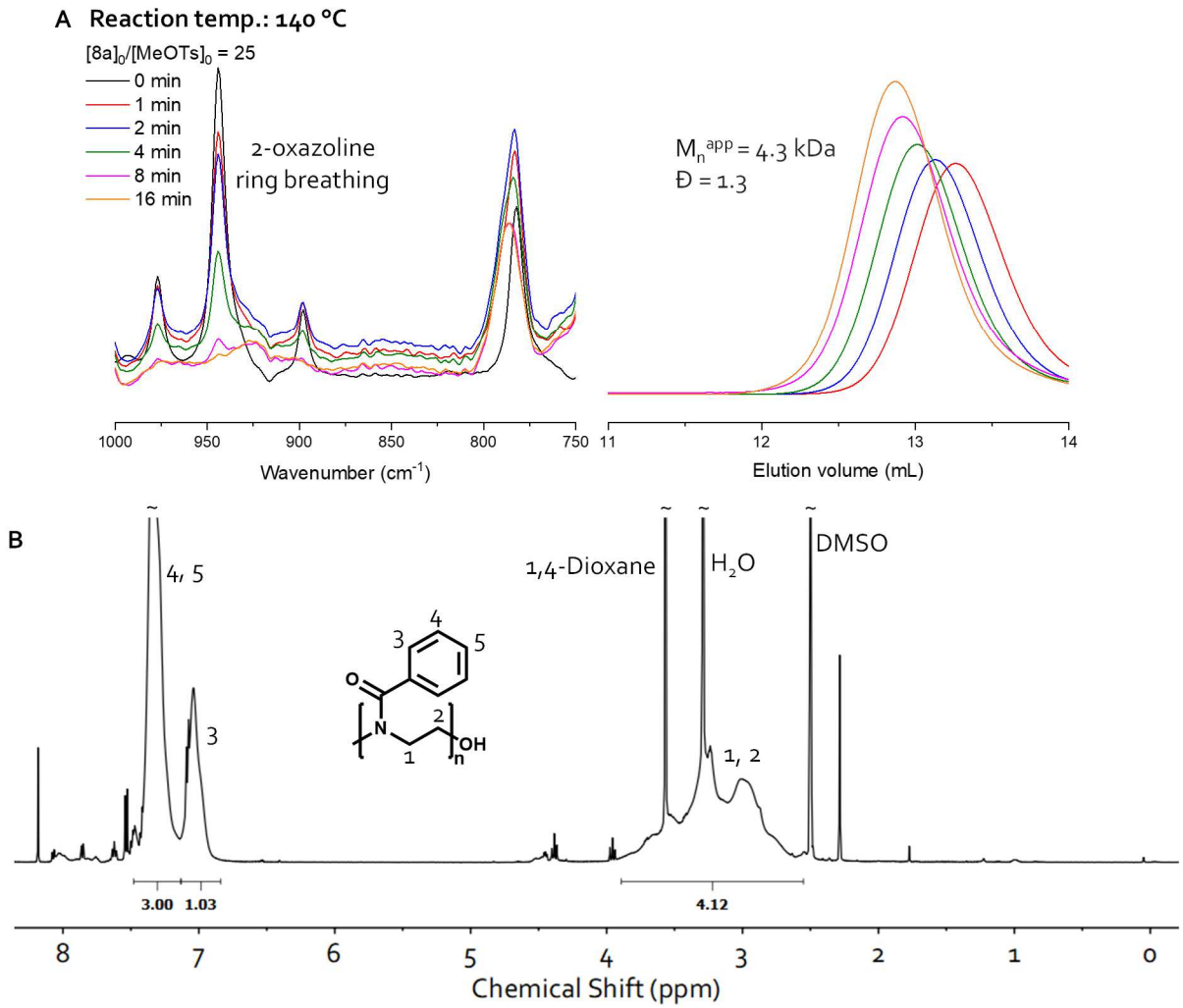


*Figure S 24: A) FT-IR kinetic graphs and relating SEC-RI-traces in NMP of the microwave-assisted CROP for the reaction temperature 140 °C of the homopolymerization from **8a** to **8b**. B) The homopolymer **8b** $^1$H-NMR spectrum (300 MHz) in DMSO-$d_6$.*

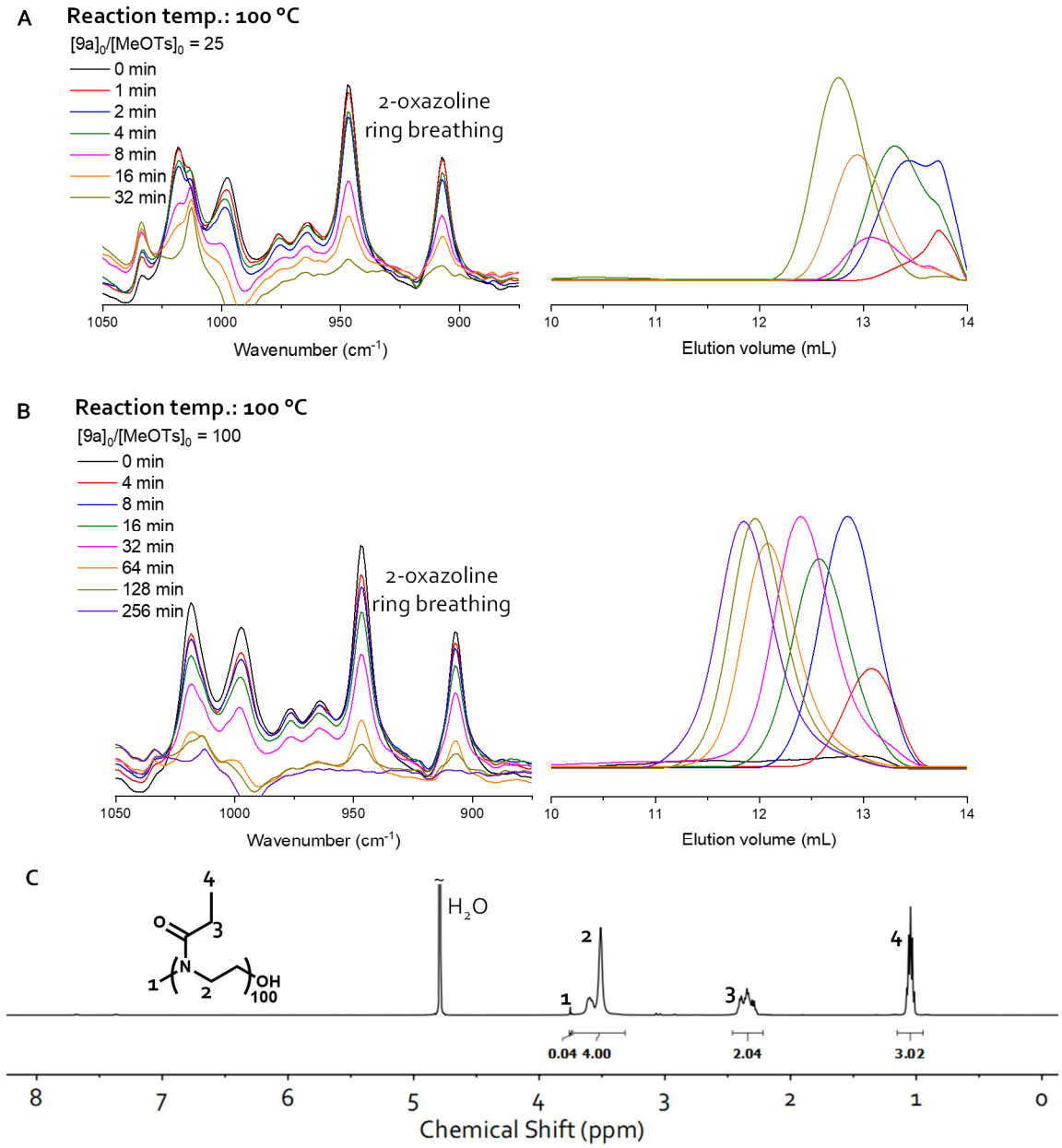


*Figure S 25: FT-IR kinetic graphs and relating SEC-RI-traces in NMP of the microwave-assisted CROP for the reaction temperature 100 °C of the homopolymerization from **9a** to **9b** with a targeted DP of 25 (A) and 100 (B). C) The homopolymer **9b** $^1$H-NMR spectrum (300 MHz) in $D_2O$.*

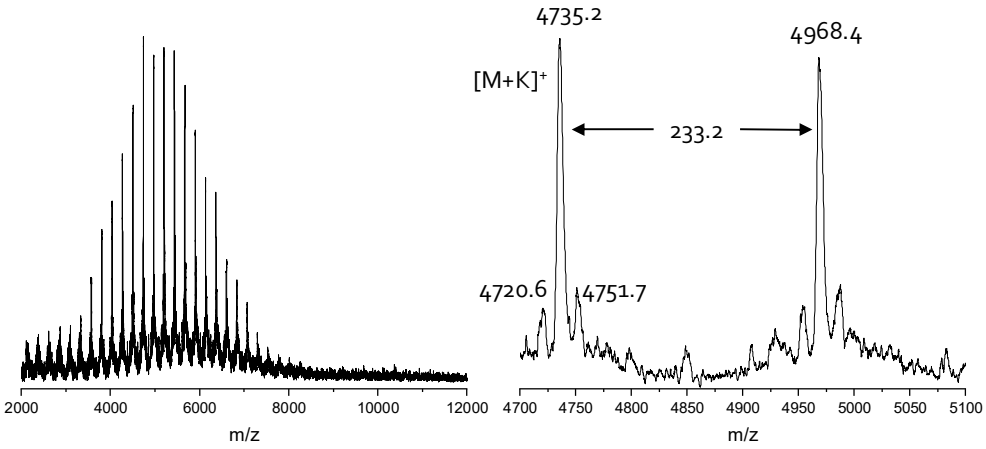


*Figure S 26: MADLI-TOF mass spectrum of polymer **2b** showing the homologous series of the corresponding repeating unit as potassium adduct [M+K]⁺. This spectrum is related to the microwave-assisted CROP of **2a** to **2b** at 140 °C.*

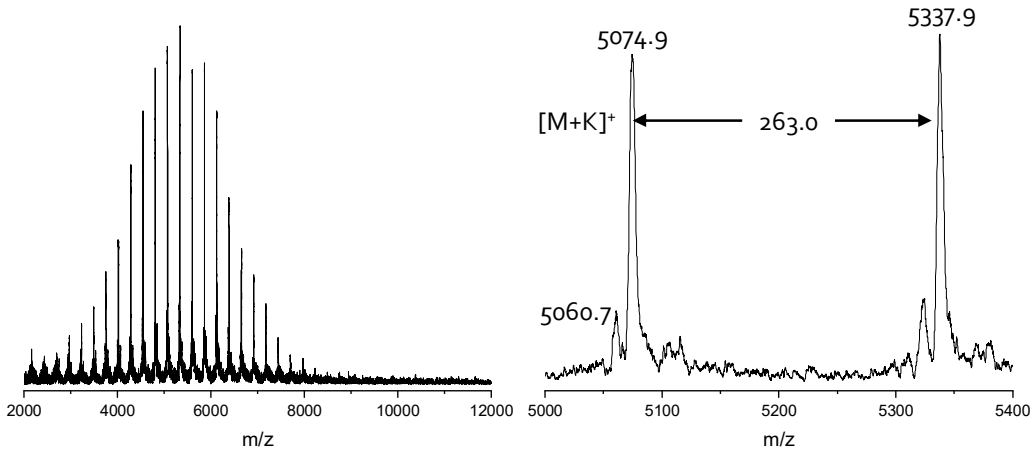


*Figure S 27: MADLI-TOF mass spectrum of polymer **3b** showing the homologous series of the corresponding repeating unit as potassium adduct [M+K]⁺. This spectrum is related to the microwave-assisted CROP of **3a** to **3b** at 140 °C.*

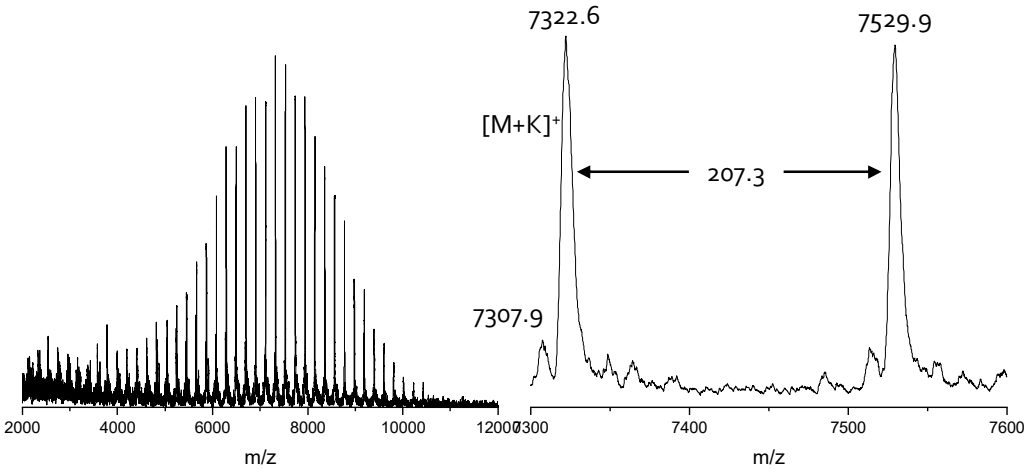


*Figure S 28: MADLI-TOF mass spectrum of polymer **5b** showing the homologous series of the corresponding repeating unit as potassium adduct [M+K]⁺. This spectrum is related to the microwave-assisted CROP of **5a** to **5b** at 140 °C.*

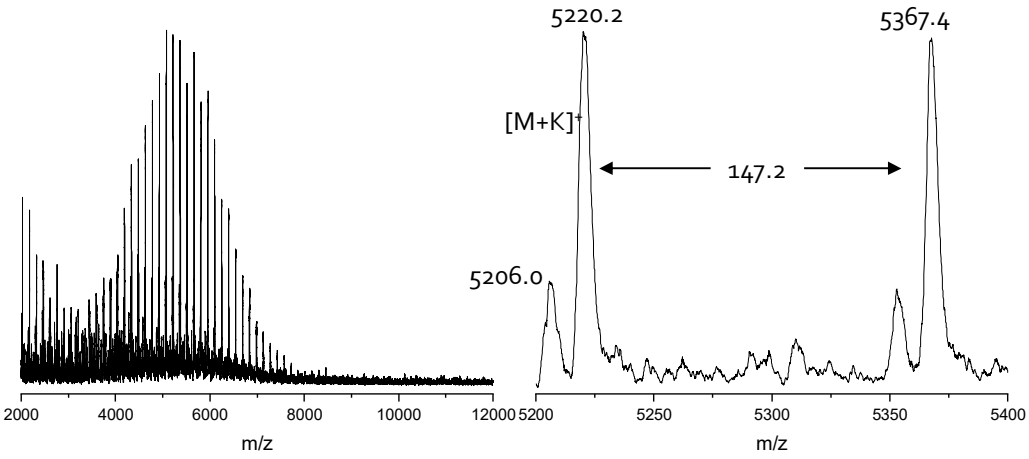


*Figure S 29: MADLI-TOF mass spectrum of polymer **8b** showing the homologous series of the corresponding repeating unit as potassium adduct [M+K]⁺. This spectrum is related to the microwave-assisted CROP of **8a** to **8b** at 140 °C.*

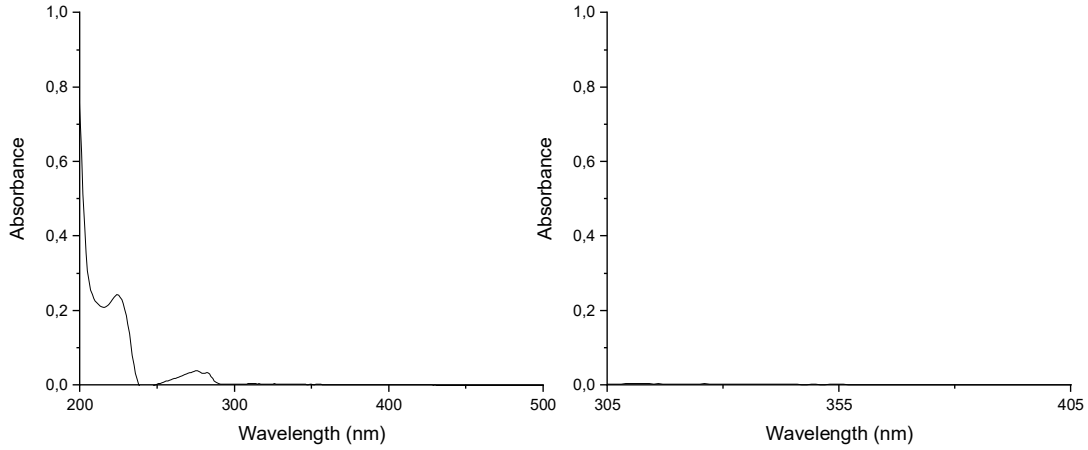


*Figure S 30: UV-spectrum of the polymer **7b** to review the absorbance at the laser's wavelength of 355 nm. Yet no absorbance in the region was measured for **7b**.*

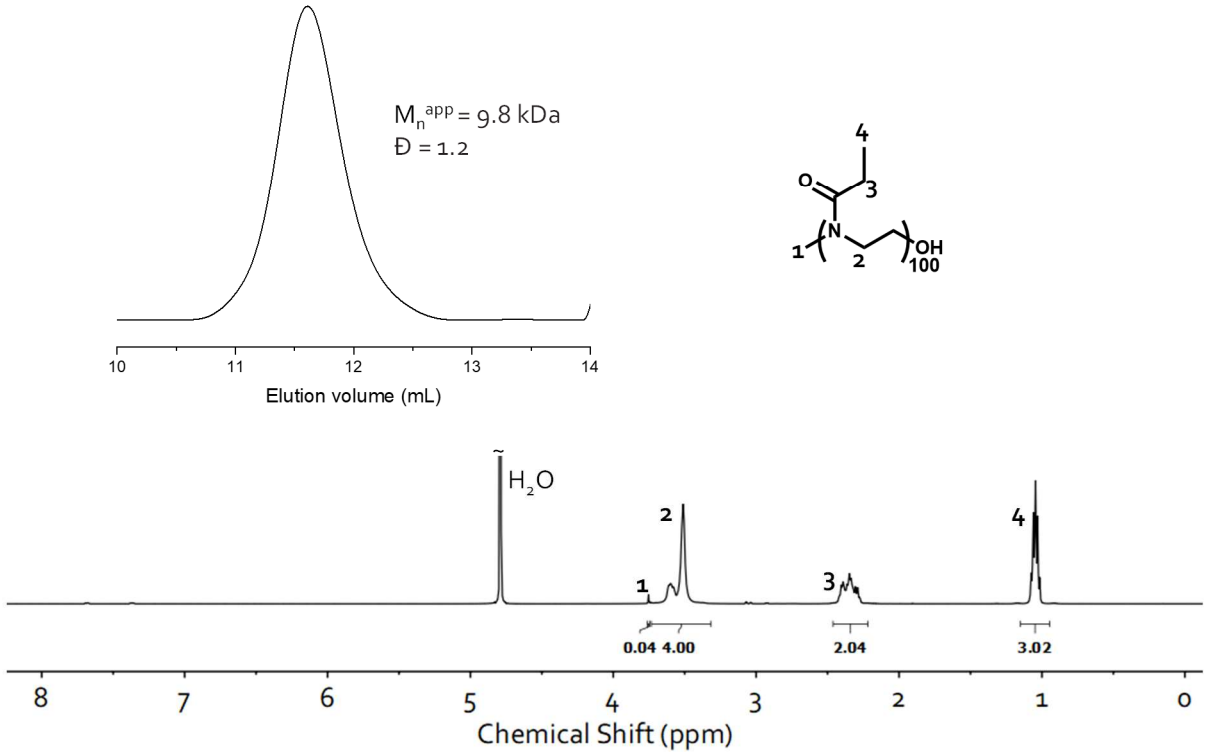


*Figure S 31: $^1$H-NMR spectrum (500 MHz) of **9b** in $D_2O$ and the corresponding SEC-RI-trace in NMP.*

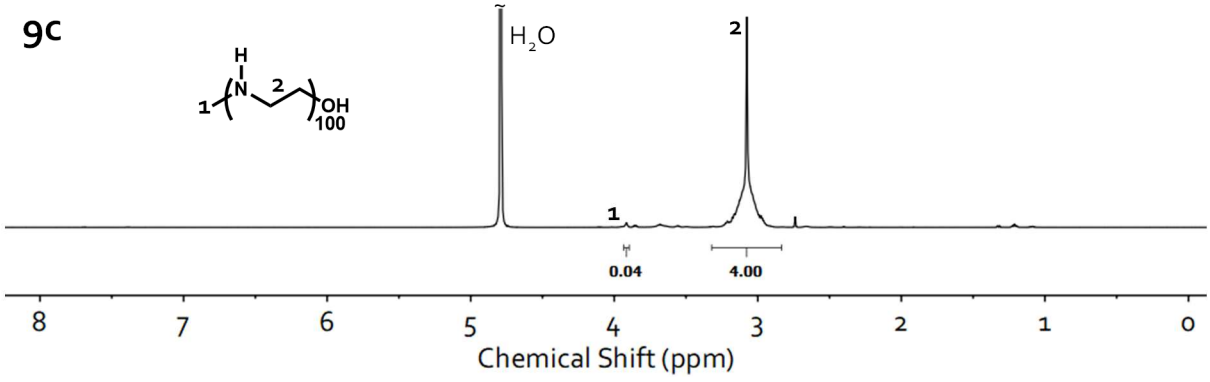


*Figure S 32: $^1$H-NMR spectrum (500 MHz) of **9c** in $D_2O$.*

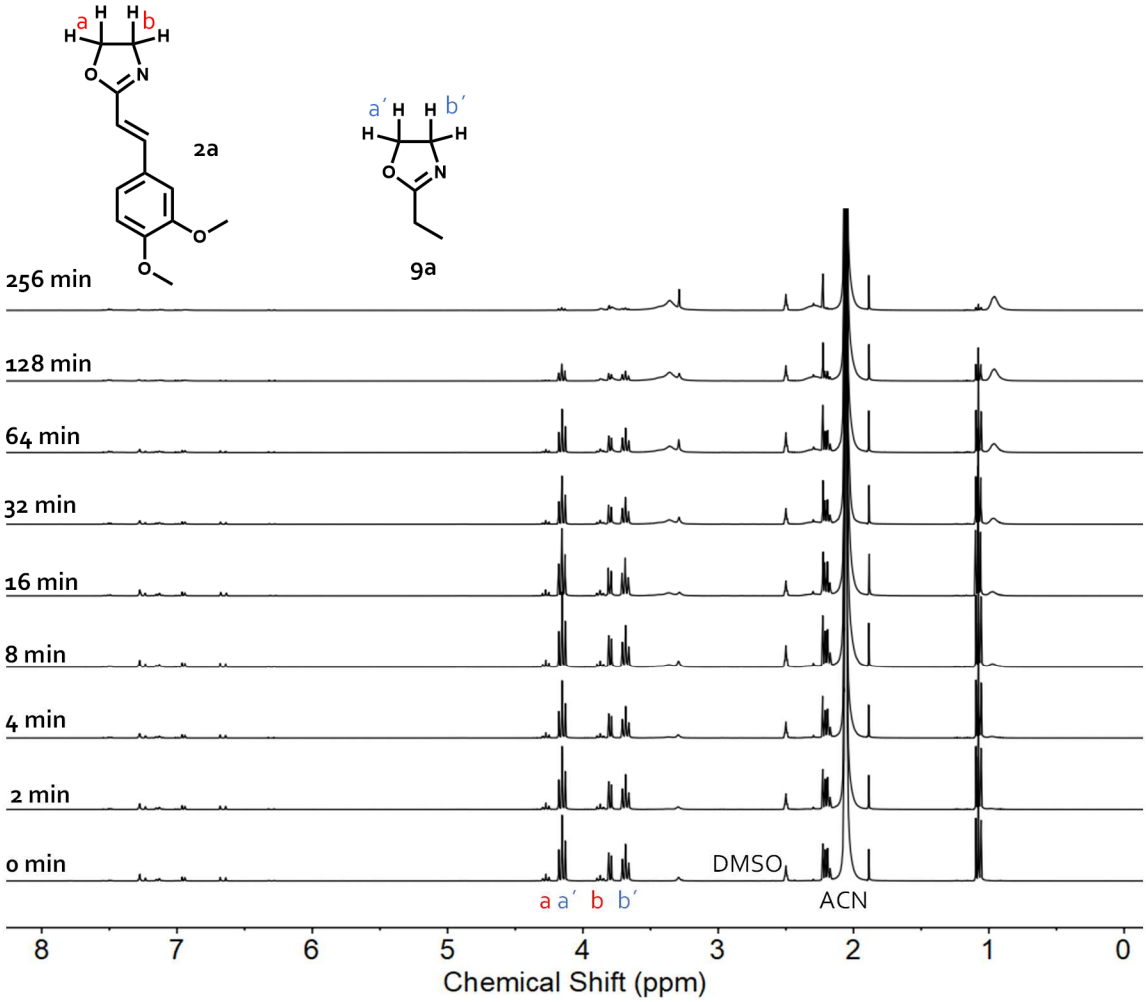


*Figure S 33: $^1$H-NMR (300 MHz) spectra in DMSO-$d_6$ of the microwave-assisted copolymerization kinetic study of **2a** and **9a** to **2b**/**9b**.*

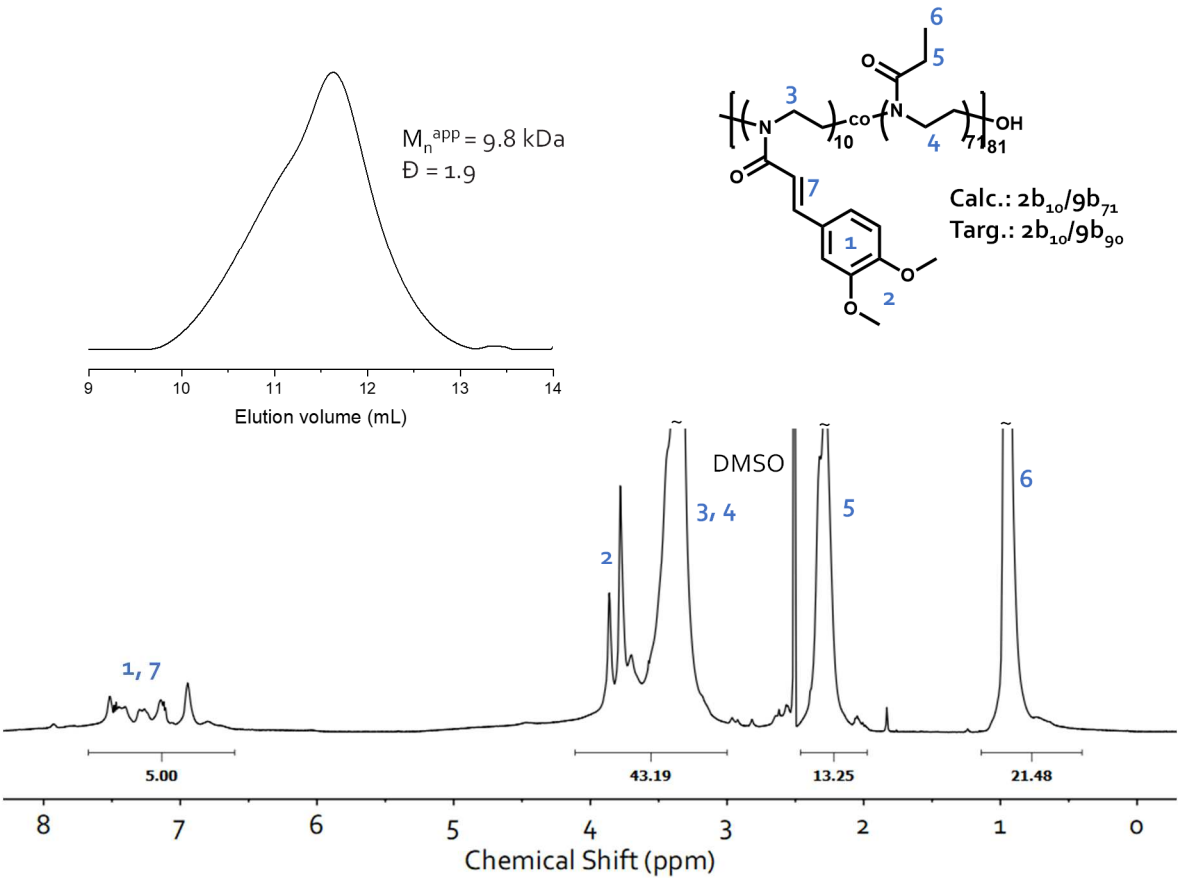


*Figure S 34: $^1$H-NMR (500 MHz) spectrum in DMSO-$d_6$ of **2b**$_{10}$/**9b**$_{71}$ and the corresponding SEC-RI trace in NMP. The number of repeating units was approximated by the proportion of the integrals concerning the signals "a, e" and "c" under the assumption that **2a** was used in the targeted amount.*

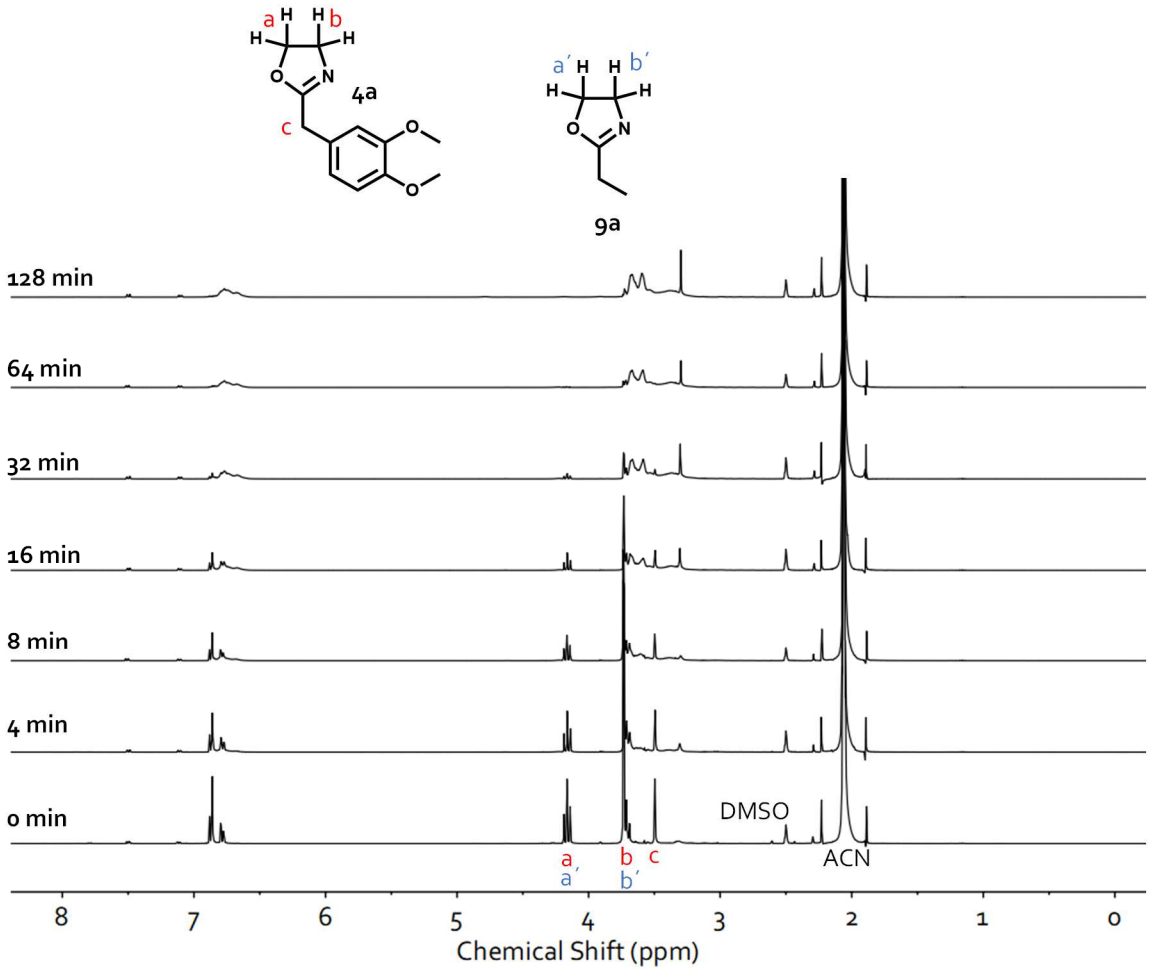


*Figure S 35: $^1$H-NMR (300 MHz) spectra in DMSO-$d_6$ of the microwave-assisted copolymerization kinetic study of **4a** and **9a** to **4b**/**9b** with the 2-oxazoline ring protons a(´) and b(´) and the benzyl proton c.*

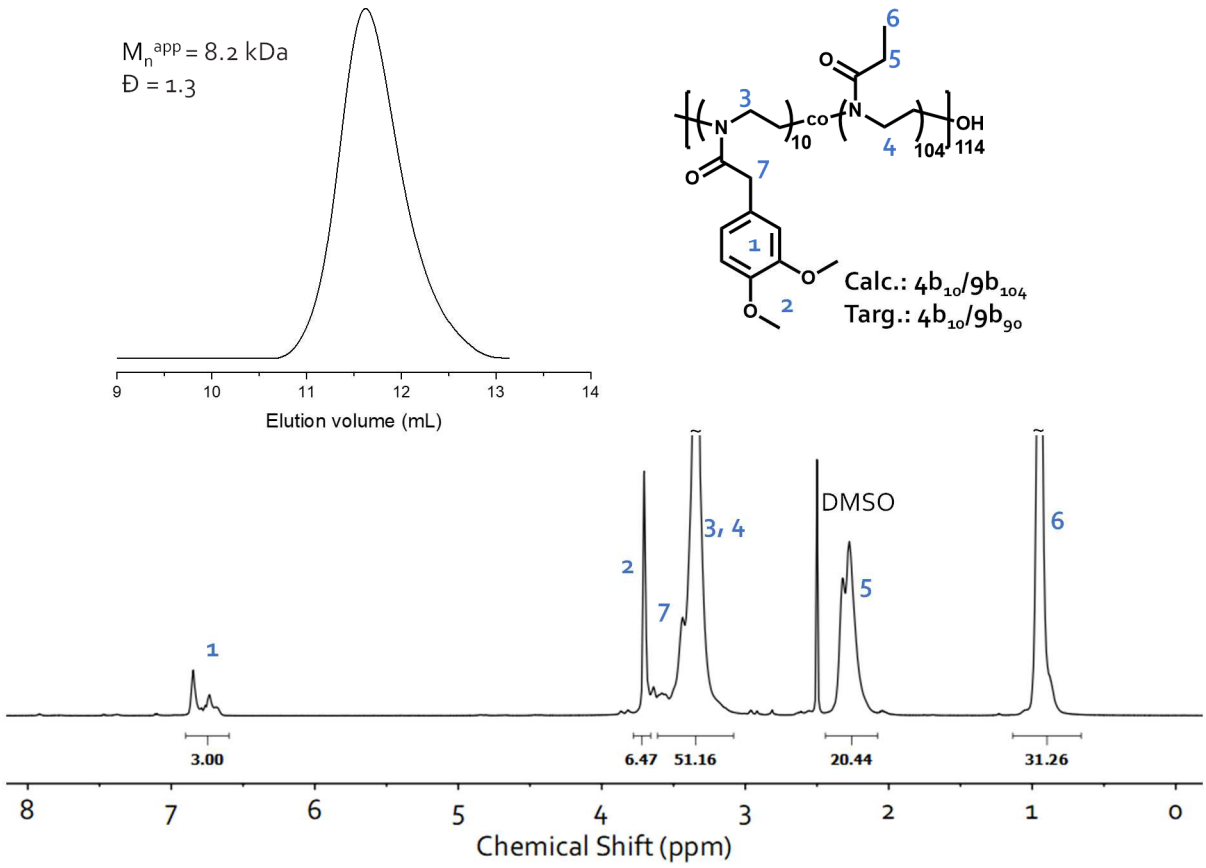


*Figure S 36: $^1$H-NMR (500 MHz) spectrum in DMSO-$d_6$ of **4b**$_{10}$/**9b**$_{104}$ and the corresponding SEC-RI trace in NMP. The number of repeating units was approximated by the proportion of the integrals concerning the signals "a" and "c" under the assumption that **4a** was used in the targeted amount.*

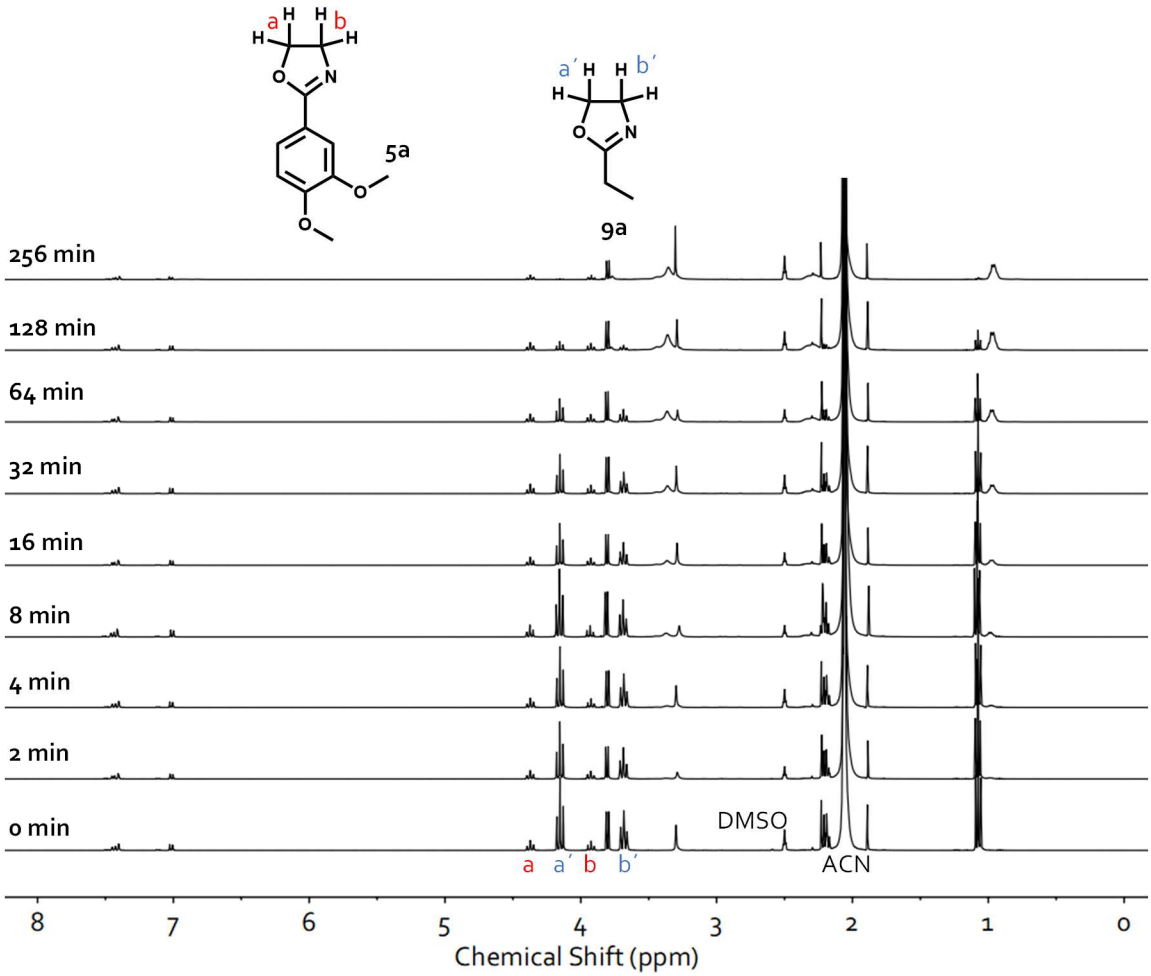


*Figure S 37: $^{1}$H-NMR (300 MHz) spectra in DMSO-$d_6$ of the microwave-assisted copolymerization kinetic study of **5a** and **9a** to **5b**/**9b** with the 2-oxazoline ring protons a(´) and b(´).*

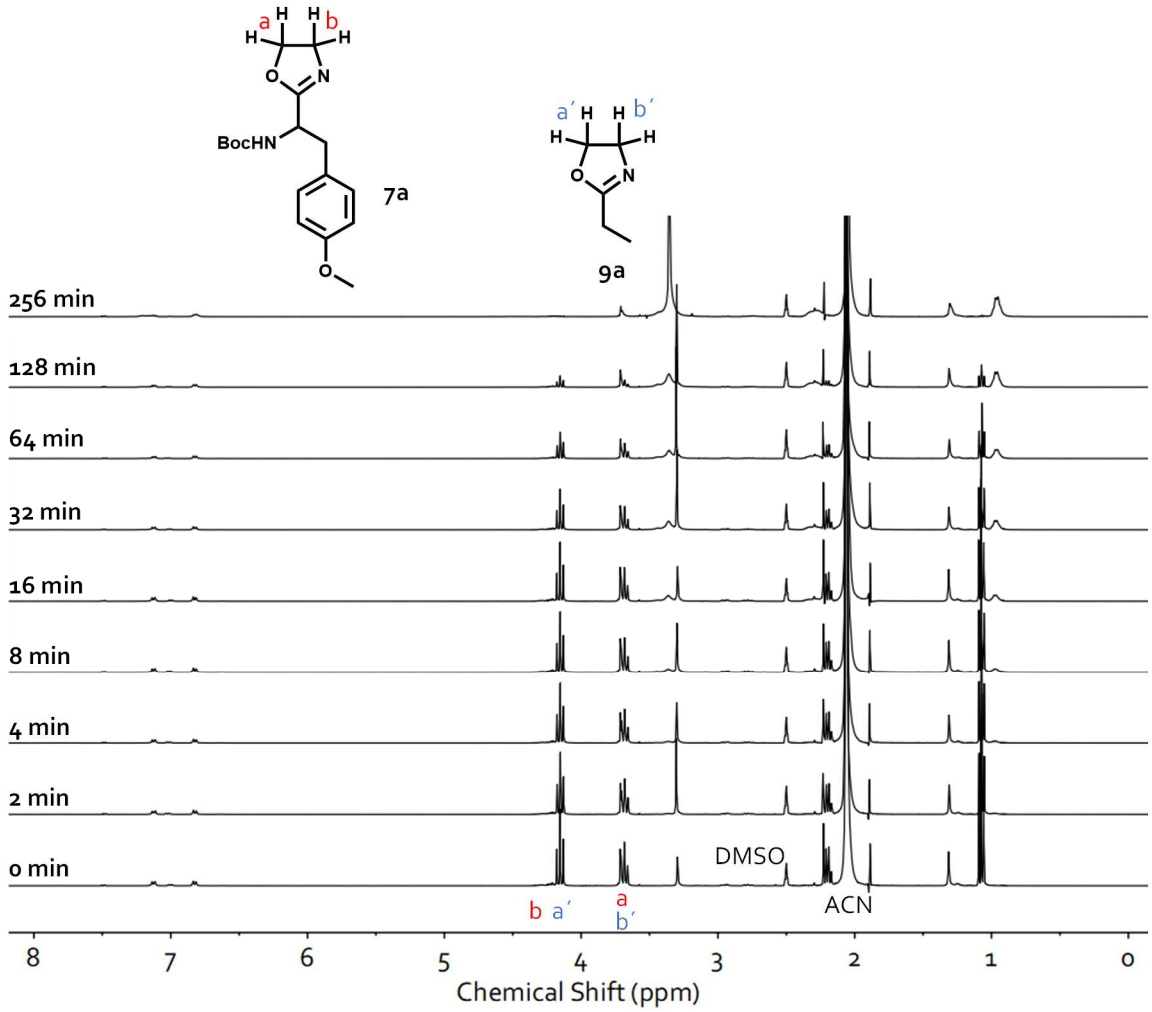


*Figure S 38: $^1$H-NMR (300 MHz) spectra in DMSO-$d_6$ of the microwave-assisted copolymerization kinetic study of **7a** and **9a** to **7b**/**9b** with the 2-oxazoline ring protons a(′) and b(′).*

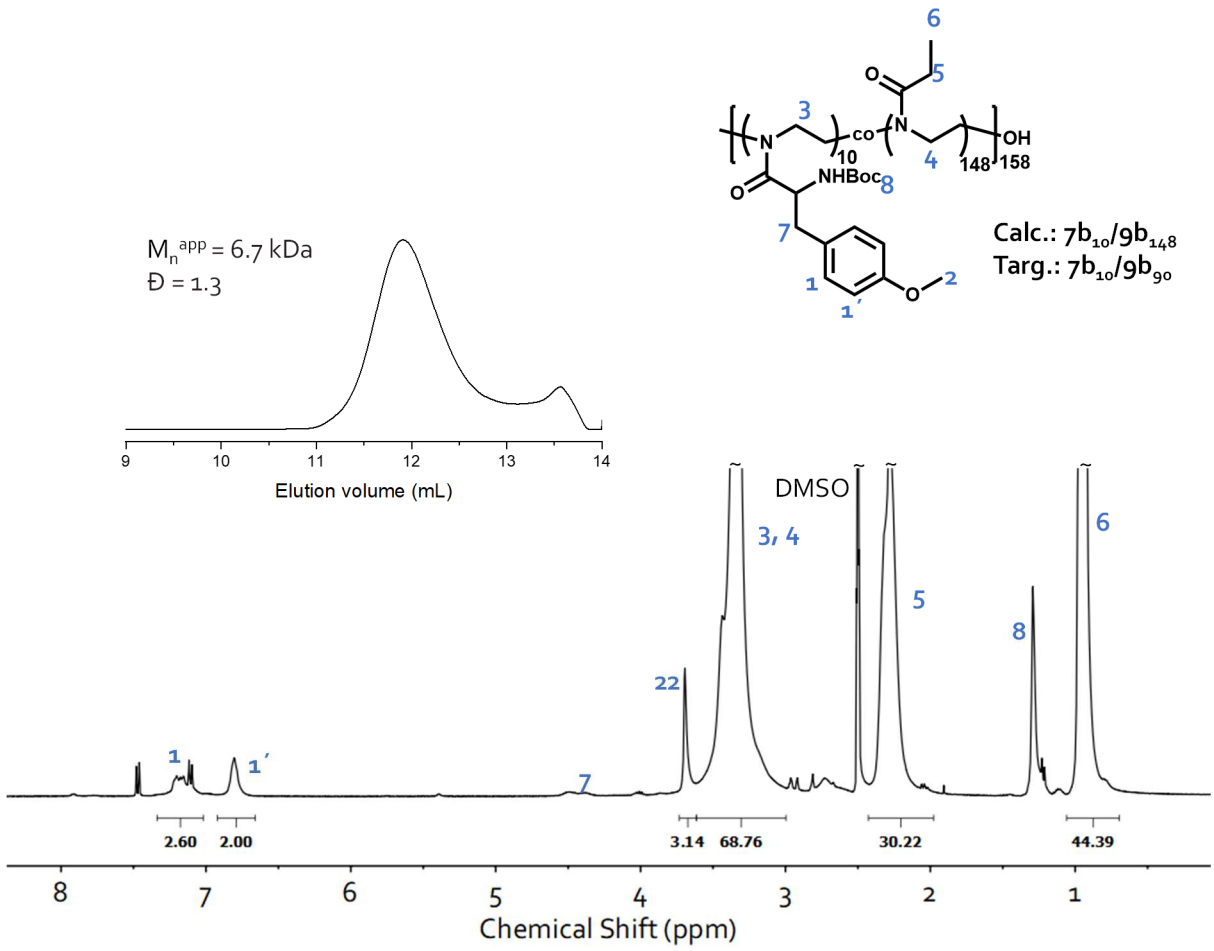


*Figure S 39: $^1$H-NMR (500 MHz) spectrum in DMSO-$d_6$ of **7b**$_{10}$/**9b**$_{148}$ and the corresponding SEC-RI trace in NMP. The number of repeating units was approximated by the proportion of the integrals concerning the signals "a´" and "c" under the assumption that **7a** was used in the targeted amount.*

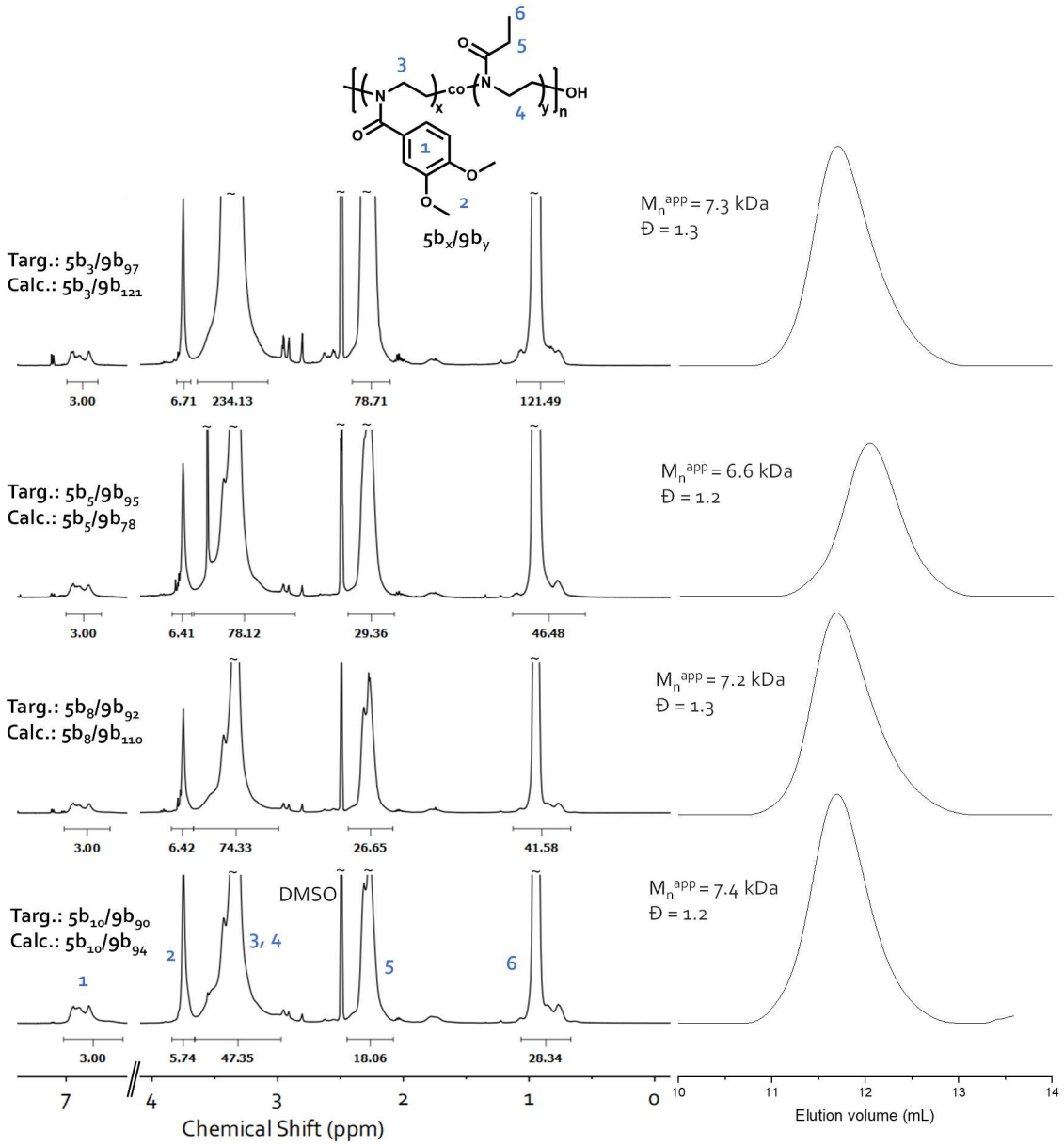


*Figure S 40: $^1$H-NMR (300 MHz) spectra in DMSO-$d_6$ of **5b$_x$/9b$_y$** and the corresponding SEC-RI traces in NMP. The number of repeating units was approximated by the proportion of the integrals concerning the signals "a" and "c" under the assumption that **5a** was used in the targeted amount.*

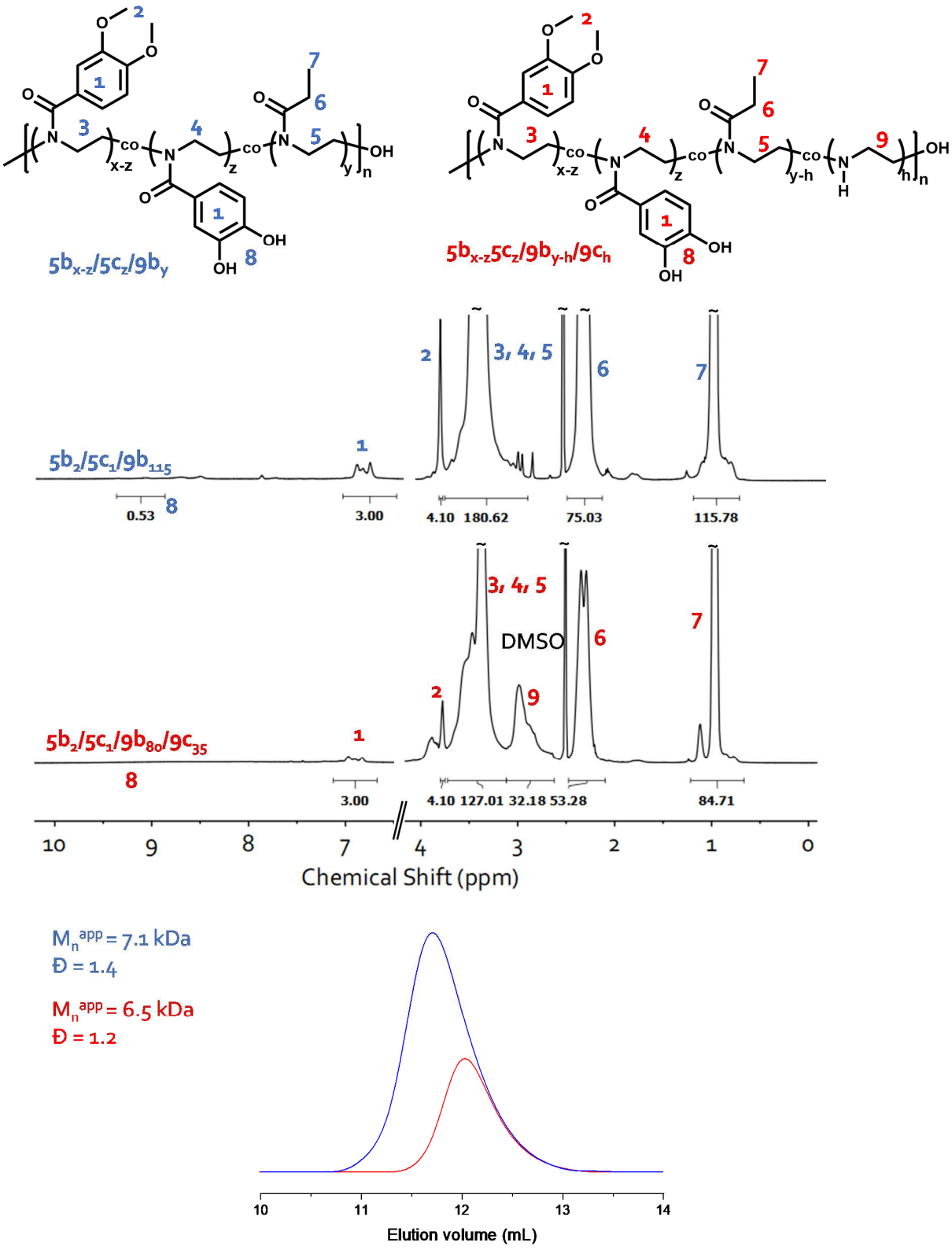


*Figure S 41: $^1$H-NMR (300 MHz) spectra of* ***5b$_2$/5c$_1$/9b$_{115}$*** *and* ***5b$_2$/5c$_1$/9b$_{80}$9c$_{35}$*** *in DMSO-d$_6$and the corresponding SEC-RI traces in NMP.*

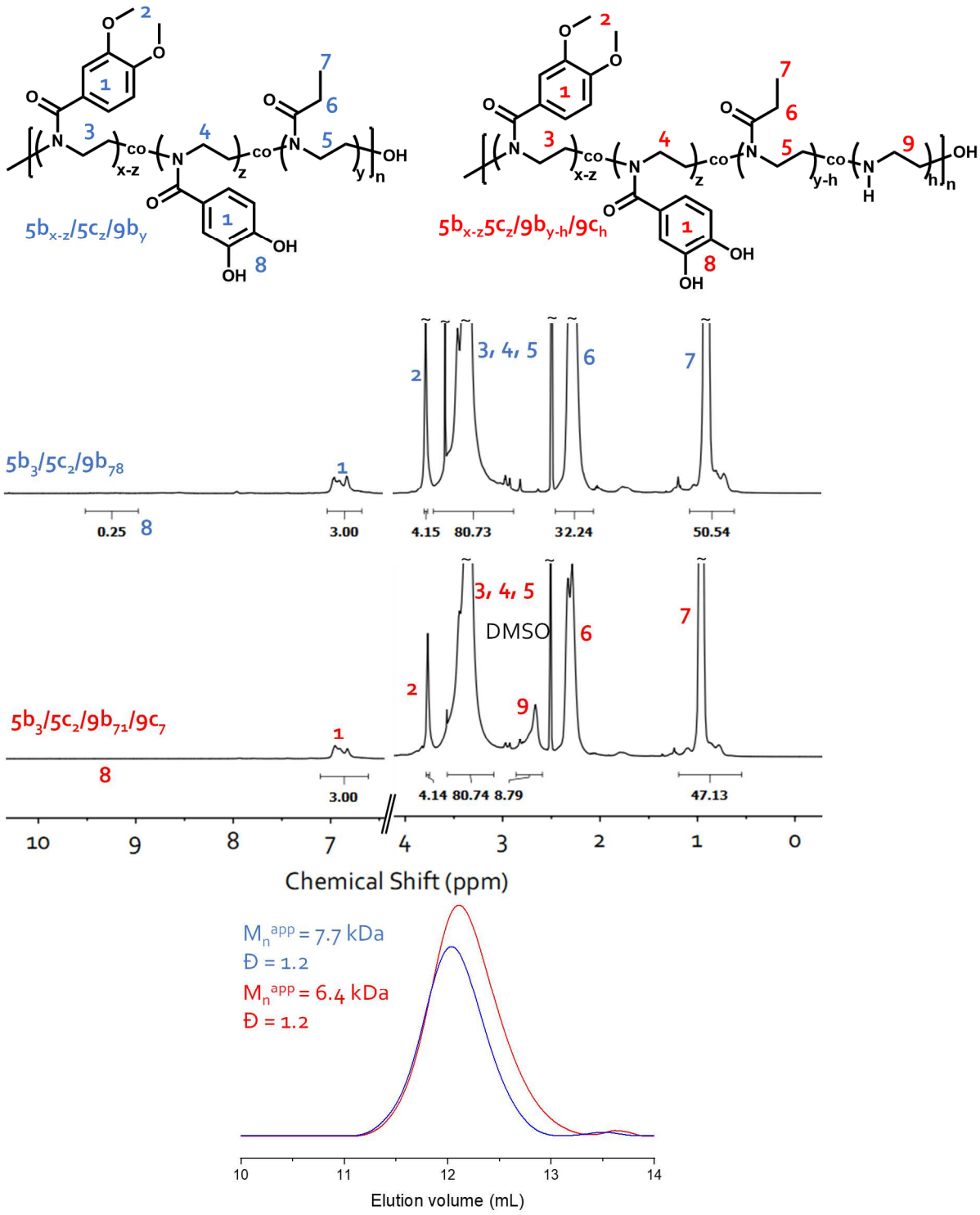


*Figure S 42: $^1$H-NMR (300 MHz) spectra of **5b$_3$/5c$_2$/9b$_{78}$** and **5b$_3$/5c$_2$/9b$_{71}$9c$_7$** in DMSO-d6 and the corresponding SEC-RI traces in NMP.*

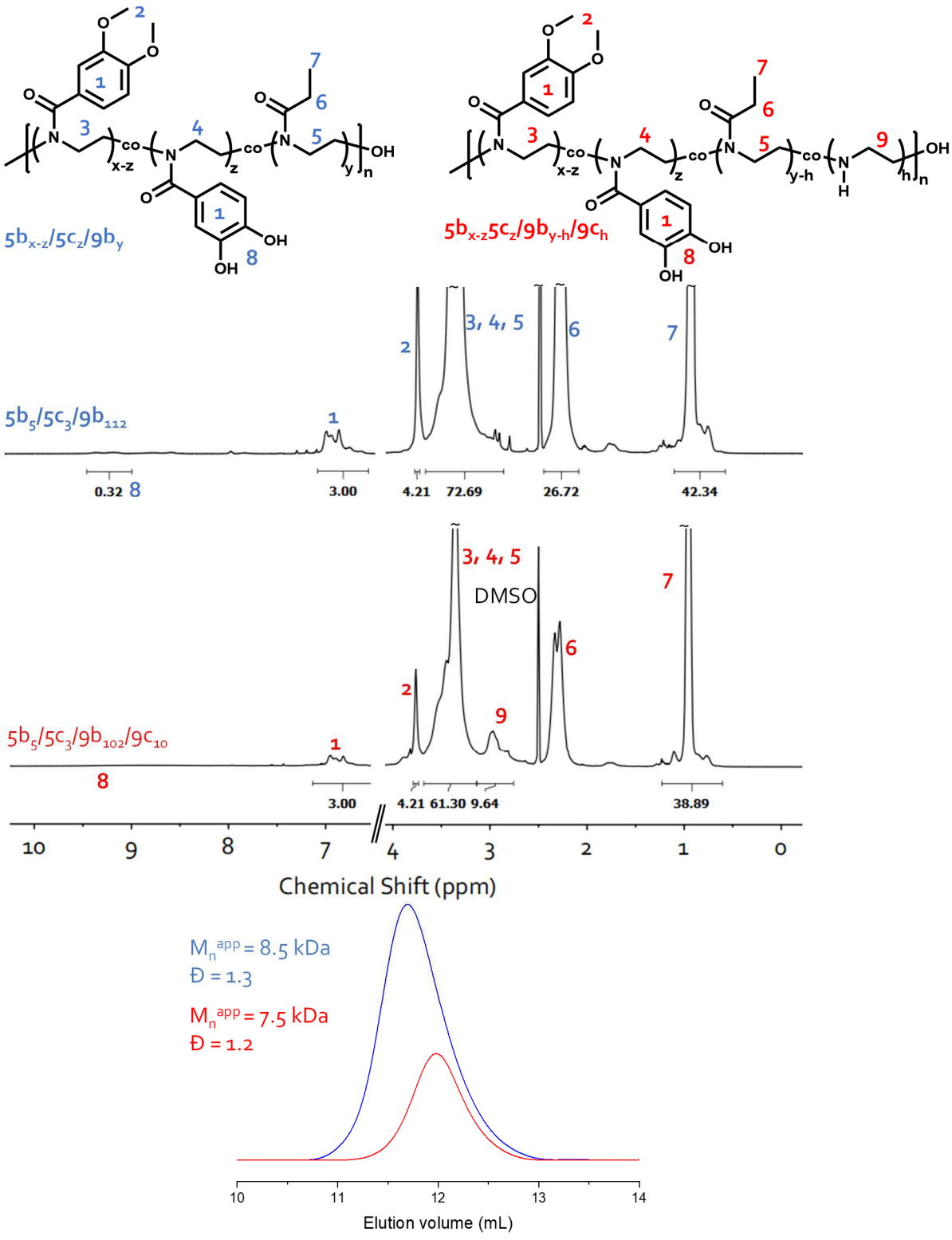


*Figure S 43: $^1$H-NMR (300 MHz) spectra of* ***5b$_5$/5c$_3$/9b$_{112}$*** *and* ***5b$_5$/5c$_3$/9b$_{102}$9c$_{10}$*** *in DMSO-d$_6$ and the corresponding SEC-RI traces in NMP.*

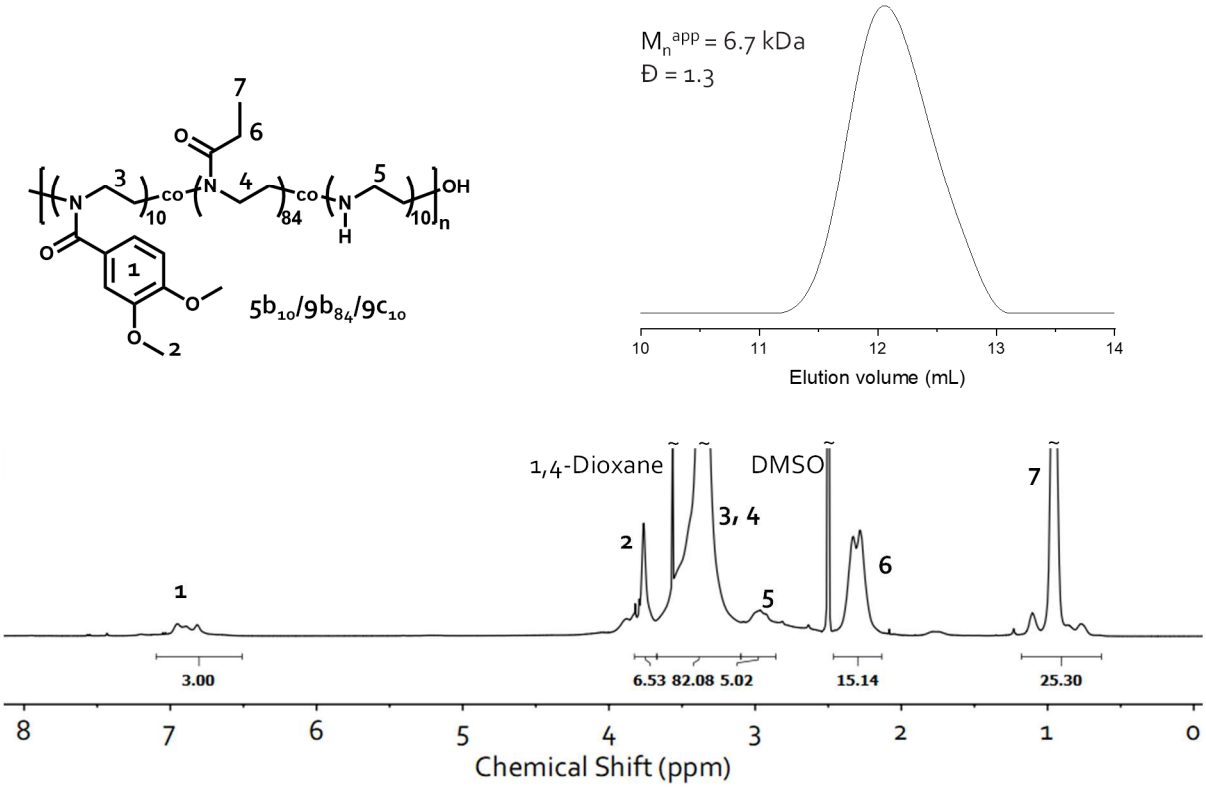


*Figure S 44: $^1$H-NMR spectrum (500 MHz) of **$5b_{10}/9b_{84}/9c_{10}$** in DMSO-$d_6$ and the corresponding SEC-RI-trace measured in NMP.*

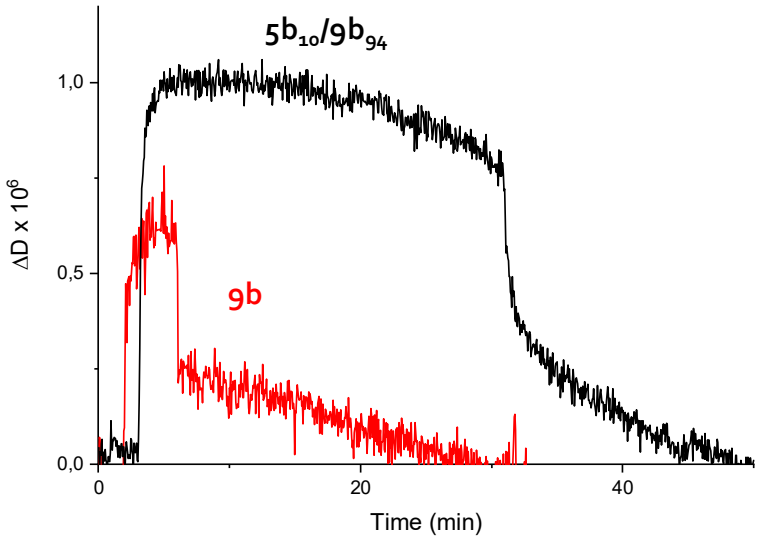


*Figure S 45: ΔD shifts on Au surfaces of the polymers* ***9b*** *and* ***5b*****$_{10}$****/****9b****$_{94}$**.

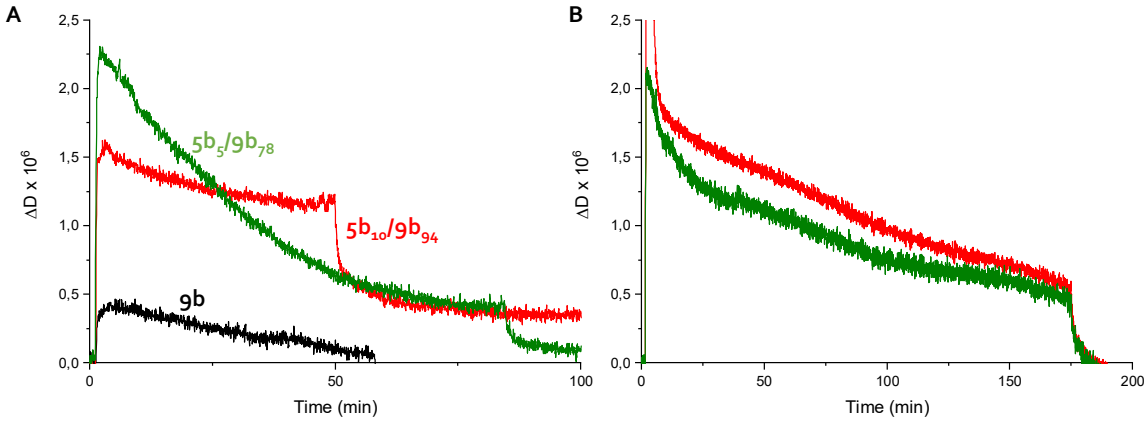


*Figure S 46: ΔD shifts on PS (A) and BS (B) surfaces of the polymers* ***9b****,* ***5b*****$_{10}$****/****9b****$_{94}$**, *and* ***5b*****$_{5}$****/****9b****$_{78}$**.

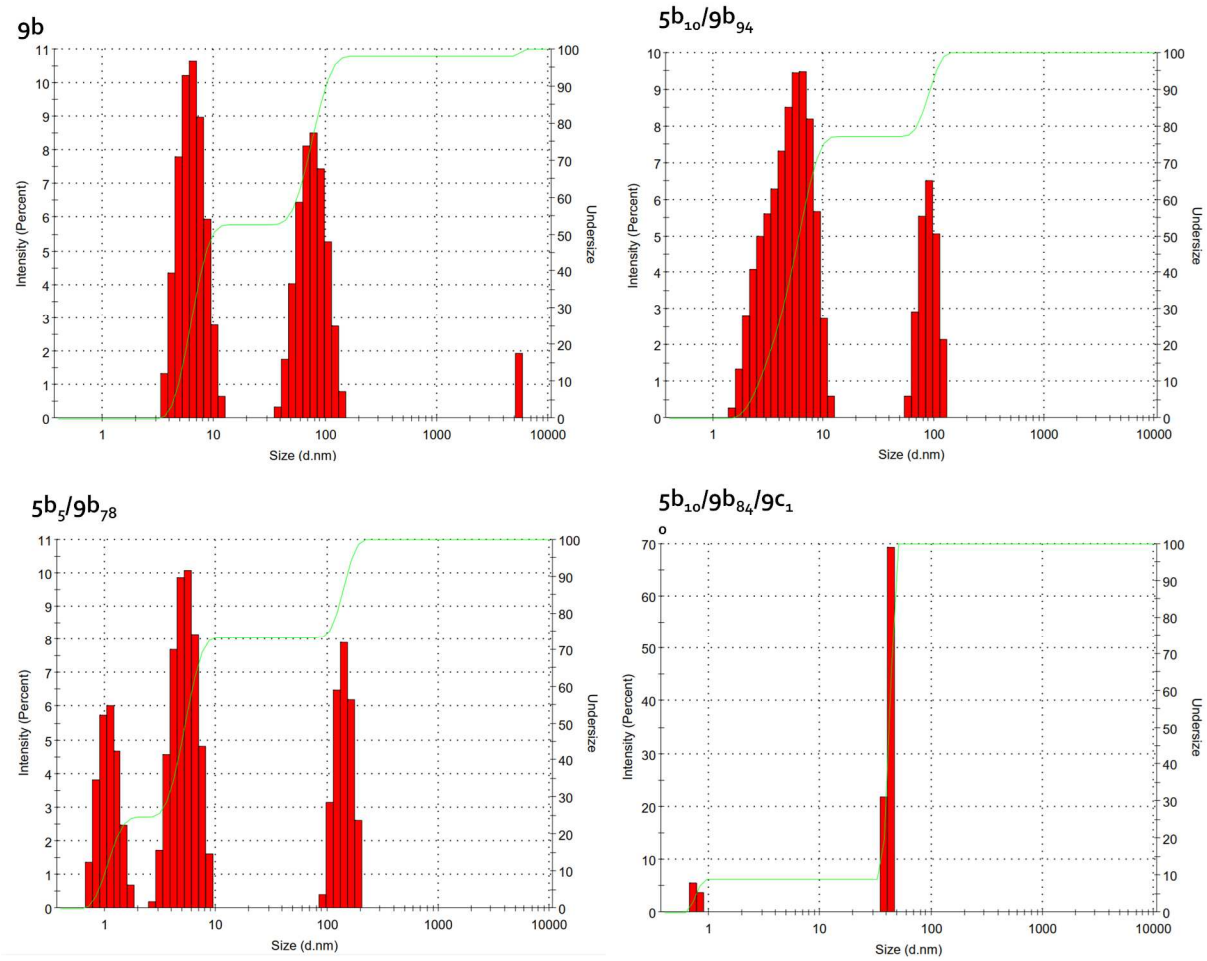


*Figure S 47: DLS measured size distribution by number with a polymer concentration of 0.1 mg/mL in water.*

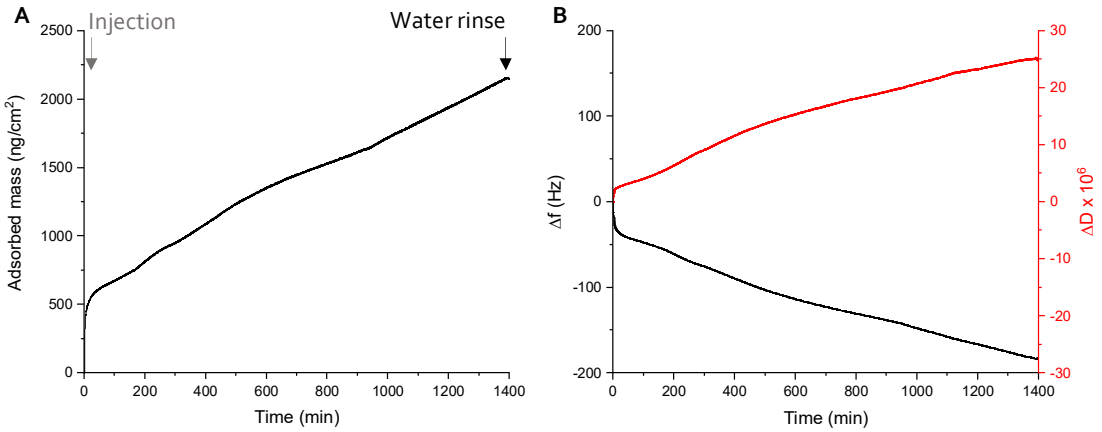


*Figure S 48: A) Adsorption graph of the 24 h QCM-D experiment of* ***5b***$_3$*/****5c***$_2$*/****9b***$_{78}$ *on an Au surface showing not any indication of reaching a state of saturation. B) The respective frequency and dissipation shifts.*

## 8.1 Journal publications

**Poly(2-oxazoline)s Based on Phenolic Acids**

N. Lüdecke, S. M. Weidner, H. Schlaad, *Macromol. Rapid Commun.* **2019**, 1900404.

**Inspired by mussel adhesive protein: Hydrophilic cationic copoly(2-oxazoline)s carrying catecholic side chains**

N. Lüdecke, H. Schlaad, *Polym. Chem.*, **2021**, 12, 5310.

## 8.2 Conference Contributions

**Tag der Chemie (TDC), Online, 2021 (Poster and Presentation)**

N. Lüdecke, H. Schlaad, Mussel-inspired Polymer Adhesives Based on Copoly(2-oxazoline)s